



Schloetel, Jan-Gero (2011) *Single-molecule FRET studies of the mechanism of strand-exchange in site-specific recombination by Tn3 resolvase*. PhD thesis.

<http://theses.gla.ac.uk/2428/>

Copyright and moral rights for this thesis are retained by the author

A copy can be downloaded for personal non-commercial research or study, without prior permission or charge

This thesis cannot be reproduced or quoted extensively from without first obtaining permission in writing from the Author

The content must not be changed in any way or sold commercially in any format or medium without the formal permission of the Author

When referring to this work, full bibliographic details including the author, title, awarding institution and date of the thesis must be given

Single-molecule FRET studies of the mechanism of strand-exchange in site-specific recombination by Tn3 resolvase

Jan-Gero Schloetel
B.Sc. M.Res

Submitted in fulfilment of the requirements for the Degree of
Doctor of Philosophy

University of Glasgow
Faculty of Biomedical and Life Sciences
Department of Molecular and Cellular Genetics

March 2011

© J.G. Schloetel

Summary

The mechanism of strand exchange by Tn3 resolvase was studied using FRET based methods. For this purpose Cy3 dye and a Cy5 dye were attached to modified thymines within Tn3 *res* site I, the DNA substrate of Tn3 resolvase. The dyes formed a FRET pair and followed the movements of the substrates, resulting in changes of the distance between both dyes and therefore changes in the FRET efficiency of the FRET pair which were monitored using fluorescence spectroscopy. A library of short, double-stranded substrates containing one copy of Tn3 *res* site I and Cy3 and/or Cy5 dyes attached to at different positions within site I was generated. Fluorescent substrates which do not interfere with the formation of synapses and with the recombination process were selected using gel-based assays. Fluorescent dyes attached at positions about five bases from the centre of site I were found to allow uninhibited recombination.

Short double-stranded substrates with dyes attached at the selected positions within site I were studied in ensemble FRET experiments. Recombination of substrates containing a FRET pair with an excess of non-fluorescent substrates resulted in a strong decrease of the FRET efficiency due to the formation of recombinant products containing one dye each. This observation suggested that recombination and strand exchange could indeed be studied using FRET-based methods.

The ensemble FRET experiment and FRET based experiments showed that the short substrates are usually recombined in both parallel and anti-parallel orientation. The lack of control over the orientation of the substrates in the synapses motivated the development of U-shaped substrates which consisted of two double-stranded arms, each containing one copy of site I, and a single stranded linker which connected both arms. In gel based assays, the U-shaped substrates were found to prefer the intramolecular recombination of both sites in one defined orientation.

A U-shaped substrate containing a Cy5 and a Cy3 dye was studied in a single-molecule FRET experiment. In the presence of an activated Tn3 resolvase mutant, several specific FRET states and transitions between FRET states had been observed. The FRET states and transitions differed in the presence and absence of MgCl₂ allowing the identification of a FRET state transition potentially corresponding to the conformational changes during ligation and several transitions corresponding to intermediate steps during strand exchange.

Table of Contents

Summary	2
Acknowledgements	6
Abbreviations	8
1 Biological Introduction	9
1.1 Summary	9
1.2 Recombination of DNA	9
1.2.1 Non-homologous end joining.....	9
1.2.2 Homologous recombination.....	12
1.2.3 Transposition.....	14
1.2.4 Site specific recombination.....	17
1.2.4.1 Tyrosine recombinases.....	20
1.2.4.2 Serine recombinases.....	23
1.3 Tn3 resolvase and related serine recombinases	27
1.3.1 Tn3 and related transposons.....	27
1.3.2 Resolvase binds and recombines res sites.....	29
1.3.3 Recombination requires a full res site and a specific DNA topology.....	29
1.3.4 Modular domain structure of resolvases	30
1.3.5 Hyperactive resolvase mutants.....	34
1.3.6 The mechanism of strand exchange by resolvases.....	34
1.3.7 Other serine recombinases: Hin, Gin and Sin	40
1.3.8 Design of hybrid serine recombinases	41
2 Introduction to Biophysical Methods.....	44
2.1 Summary	44
2.2 Fluorescence resonance energy transfer.....	44
2.3 FRET analysis according to Clegg.....	47
2.4 Single molecule FRET	51
2.5 Single-molecule FRET using TIR fluorescence microscopy.....	52
3 Materials and Methods	58
3.1 Chemicals.....	58
3.2 Bacterial growth media	58
3.3 Bacterial strains.....	58
3.4 Plasmids	59
3.5 Oligonucleotides	59
3.5.1 Oligonucleotides for single-site substrates	59
3.5.2 Oligonucleotides for U-shaped substrates.....	60
3.6 Molecular graphics.....	61
3.7 Preparation of chemically competent cells	61
3.8 Transformation of chemically competent cells.....	61
3.9 Purification of Tn3 resolvase	62
3.9.1 Overexpression of Tn3 resolvase.....	62
3.9.2 Buffers for the extraction and purification of Tn3 resolvase	63
3.9.3 Extraction and purification of Tn3 resolvase	63
3.9.4 Photometric determination of the concentration of resolvase.....	65
3.9.5 Gel-based determination of the concentration of resolvase	65
3.9.6 Nuclease activity assay for resolvase preparations	66
3.10 Oligonucleotide methods	66
3.10.1 Conjugation of fluorophores to amino-modified oligonucleotides.....	66
3.10.2 Radioactive labelling of single-site substrates	67
3.10.3 Purification of non-fluorescent oligonucleotides	67
3.10.4 Purification of fluorescent oligos.....	68
3.10.5 Photometric determination of the concentration of oligonucleotide solutions	68

3.10.6	Photometric estimation of the purity of fluorescent oligonucleotides	69
3.11	“Crush and soak” extraction of DNA from polyacrylamide gel pieces	69
3.12	Ethanol precipitation of DNA	70
3.13	Measurement of absorption spectra	70
3.14	Annealing of single-site substrates	71
3.15	Annealing of U-shaped substrates	71
3.16	Purification of U-shaped substrates	72
3.17	Gel electrophoresis methods	72
3.17.1	Agarose gel electrophoresis	72
3.17.2	Polyacrylamide gel electrophoresis (PAGE)	73
3.17.3	Native PAGE	73
3.17.4	SDS-PAGE	74
3.17.5	Discontinuous SDS-PAGE	74
3.17.6	Denaturing PAGE	75
3.17.7	Ethidium bromide staining of polyacrylamide gels	75
3.17.8	“Stains-all” staining of polyacrylamide gels	75
3.17.9	Visualisation of fluorescent DNA in polyacrylamide gels	76
3.17.10	Quantification of bands on polyacrylamide gels	76
3.18	Gel-based in vitro recombination assay for single-site substrates	76
3.19	Gel-based in vitro recombination assay for U-shaped substrates	77
3.20	Ensemble FRET experiments with single-site substrates	78
3.21	Single-molecule FRET experiments	80
3.21.1	Single-molecule FRET setup	80
3.21.2	Preparation of reaction chambers	80
3.21.3	Functionalisation of the reaction chamber surface and sample preparation	81
3.21.4	Acquisition of single-molecule FRET data	83
3.21.5	Data analysis	83
4	Preparation and purification of Tn3 resolvase mutants	85
5	Development of fluorescent single-site substrates	90
5.1	Requirements for fluorescent substrates	90
5.1.1	Fluorophore properties	90
5.1.2	Fluorophore positions optimal for FRET experiments	93
5.1.3	Fluorophore positions ideal for the recombination system	96
5.1.4	Design of fluorescent single-site substrates	100
5.2	Conjugation of fluorophores to single-site substrates	103
5.3	Purification of fluorescent single-site substrates	103
5.4	Selection of fluorescent single-site substrates that allow synapse formation	107
5.4.1	Results	108
5.4.2	Discussion	114
5.5	Recombination of single-site substrates without fluorophores within site I	115
5.5.1	Effect of the resolvase concentration on recombination	117
5.5.2	Combined effects of the concentrations of resolvase, the substrates and non-specific DNA analogues	119
5.5.3	Kinetics of recombination and the effect of magnesium ions	123
5.6	Selection of fluorescent single-site substrates that allow recombination	132
5.6.1	Results	132
5.6.2	Discussion	143
6	Ensemble FRET studies of the recombination of single-site substrates	144
6.1	Results	147
6.1.1	Recombination of substrate B50R5C5L6C3 with an excess of the competitor substrate 80LR	147
6.1.2	Recombination of a mixture of the substrates B50R5C5 and 50L6C3	150
6.1.3	Gel-based analysis of recombination products in the ensemble FRET experiment samples	152

6.2	Discussion	157
7	Development of U-shaped substrates.....	159
7.1	Limitations of single-site substrates.....	159
7.2	Design of U-shaped substrates.....	162
7.3	Preparation of U-shaped substrates.....	170
7.3.1	Results	170
7.3.2	Discussion	172
7.4	Effect of the linker length on recombination	174
7.4.1	Results	177
7.4.2	Discussion	182
7.5	Timescale of the recombination of U-shaped substrates and the effect of the resolvase concentration	183
7.5.1	Results	183
7.5.2	Discussion	186
7.6	Recombination of U-shaped substrates with Cy dyes attached within Tn3 res site I	187
7.6.1	Results	192
7.6.2	Discussion	196
8	Single-molecule fluorescence experiments with U-shaped substrates.....	198
8.1	Substrate choice for single-molecule FRET experiments.....	198
8.2	Conduction of the single molecule experiment.....	200
8.3	Data acquisition and transformation into hel files	201
8.4	Results	202
8.4.1	Analysis of single-molecule traces	202
8.4.2	Filtering of traces and statistical analysis of the observed FRET states	210
8.4.3	Analysis of the transitions between FRET states.....	216
8.5	Discussion	224
9	Conclusions and general discussion.....	226
9.1	Development and testing of suitable fluorescent substrates	226
9.2	Ensemble FRET experiments.....	228
9.3	U-shaped substrates.....	229
9.4	Single-molecule FRET experiments	231
10	Bibliography.....	234

Acknowledgements

I would like to thank everyone who supported me whilst preparing this thesis. My special thanks go to Caroline who supported me with lots of love, patience and food. I thank my friends Marko and Sarah for providing me with a home and support while I was writing this thesis. I thank my parents, Jan and Doris, and my family for always supporting me. I would like to thank Marshall, Martin, Sally, Marko, Femi, Sean, Arlene, Chris, Anne Cécile, Jonathan and David for advice, inspiring discussions and reagents while I was working in the laboratory. I would also like to thank the Wellcome Trust who made this work possible through their generous funding.

The research reported in this thesis is my own and original work except where stated otherwise and has not been submitted for any other degree.

Jan-Gero Schloetel

Abbreviations

Units

k	10^3	g	grams
c	10^{-2}	m	metres
m	10^{-3}	l	litres
μ	10^{-6}	$^{\circ}\text{C}$	degrees Celsius
n	10^{-9}	mol	moles
p	10^{-12} M	molar	
A	Ampères	rpm	revolutions per minute
V	Volts	hr	hours
W	Watts	min	minutes

Chemicals/Reagents

APS	ammonium persulphate
BSA	bovine serum albumin
ddH ₂ O	double-distilled water
DMSO	dimethyl sulfoxide
DNA	deoxyribonucleic acid
DTT	dithiothreitol
EDTA	ethylenediaminetetra-acetic acid (disodium salt)
EtBr	ethidium bromide
IPTG	Isopropyl β -D-1-thiogalactopyranoside
MQH ₂ O	filtered and de-ionised water
PAA	polyacrylamide
PAGE	polyacrylamide gel electrophoresis
SDS	sodium dodecyl sulphate
TBE	tris-borate-EDTA (electrophoresis buffer)
TMED	<i>N,N,N',N'</i> -tetramethylethylenediamine
Tn3R	Tn3 resolvase
Tn3R NM	catalytically activated Tn3 resolvase mutant NM
	contains mutations R2A, E56K, G101S, D102Y, M103I and Q105L
Tn3R NM-S10A	Inactive version of Tn3R NM with the additional mutation S10A
Tris	tris(hydroxymethyl)aminomethane

Other

A	adenine
C	cytosine
G	guanine
T	thymine
FRET	fluorescence resonance energy transfer
TIR	total internal reflection
UV	ultraviolet

1 Biological Introduction

1.1 Summary

In this introduction I will describe different recombination types, their role, mechanisms and applications in genetic engineering. The focus will be on the structural and mechanistic basics of recombination by serine recombinases, top candidates for use in genetic engineering. Furthermore I will introduce the current rotation model of DNA strand exchange by serine recombinases which was studied by biophysical techniques in this thesis. A detailed description of the biophysical approaches can be found in chapter 2.

1.2 Recombination of DNA

Recombination is the process of cutting the sugar-phosphate backbone of two DNA molecules, rearranging the DNA double-strands and subsequently ligating the DNA. As a result, regions of DNA molecules can be exchanged, removed or rearranged in multiple ways (see following chapters). Recombination of DNA is essential in major biological processes including DNA repair, gene shuffling for differentiation, horizontal gene transfer for mobilisation of antibiotic resistances in pathogens (Heffron *et al.* 1979) and insertion of viral DNA into host genomes (Shapiro 1979). Today rational use of natural recombination systems provides a means of genome modification and has yielded precious tools in reverse and forward genetics (Nagy 2000; Nagy *et al.* 2003). However, details of the reaction mechanism and kinetics of the site-specific recombination, the recombination system studied in this thesis, are still being investigated.

Several different types of recombination of DNA operate in organisms, including non-homologous end joining, homologous recombination, transposition and site-specific recombination.

1.2.1 Non-homologous end joining

Non-homologous end joining (NHEJ) is a mechanism of repairing double-strand breaks (DSB) in DNA by simply joining two DNA ends, without checking if they originated from one contiguous DNA double-strand. The DNA ends are captured by proteins (Ku70/80 in eukarya), further proteins are recruited and a complex is formed, which brings both DNA ends together (figure 1.1A). Blunt or matching DNA ends can be ligated directly, but there are many DSB variations with non compatible single strands or damaged DNA. The NHEJ system can deal with damaged and incompatible ends by DNA processing. Processing involves nucleases (Artemis) which cut single stranded areas, mainly removing 5'-

overhangs and shortening 3'-overhangs. Gaps can be filled by polymerases, possibly polymerases μ and λ . The DNA ends are then ligated by a specialised ligase (Lig4 in eukarya) with a very broad substrate range, which can include non-complementary DNA and single stranded DNA. Ligation does not occur strictly after DNA processing, since the broad substrate range of the ligase can allow even the ligation of non-compatible ends before DNA processing (figure 1.1B). This enables the repair of a wide range of DSB configurations by NHEJ in an iterative cycle of DNA processing and ligation (figure 1.1B-D) (Weterings and Chen 2008; Mahaney *et al.* 2009; Lieber 2010).

NHEJ is a very efficient but error prone way of repairing dangerous DSBs and can result in the loss of nucleotides, introduction of mutations, or gross chromosomal rearrangements. Eukaryotes employ NHEJ throughout the cell cycle (Weterings and Chen 2008) and related pathways have recently been found in bacteria (Pitcher *et al.* 2007; Shuman and Glickman 2007). The vertebrate immune system relies on NHEJ for the diversification of immunoglobulins and T-cell receptors by introducing DSB between gene segments which are then rejoined in myriad combinations through NHEJ (Weterings and Chen 2008). In eukaryotes, NHEJ also plays a role in the length regulation and end protection of telomeres (Riha *et al.* 2006).

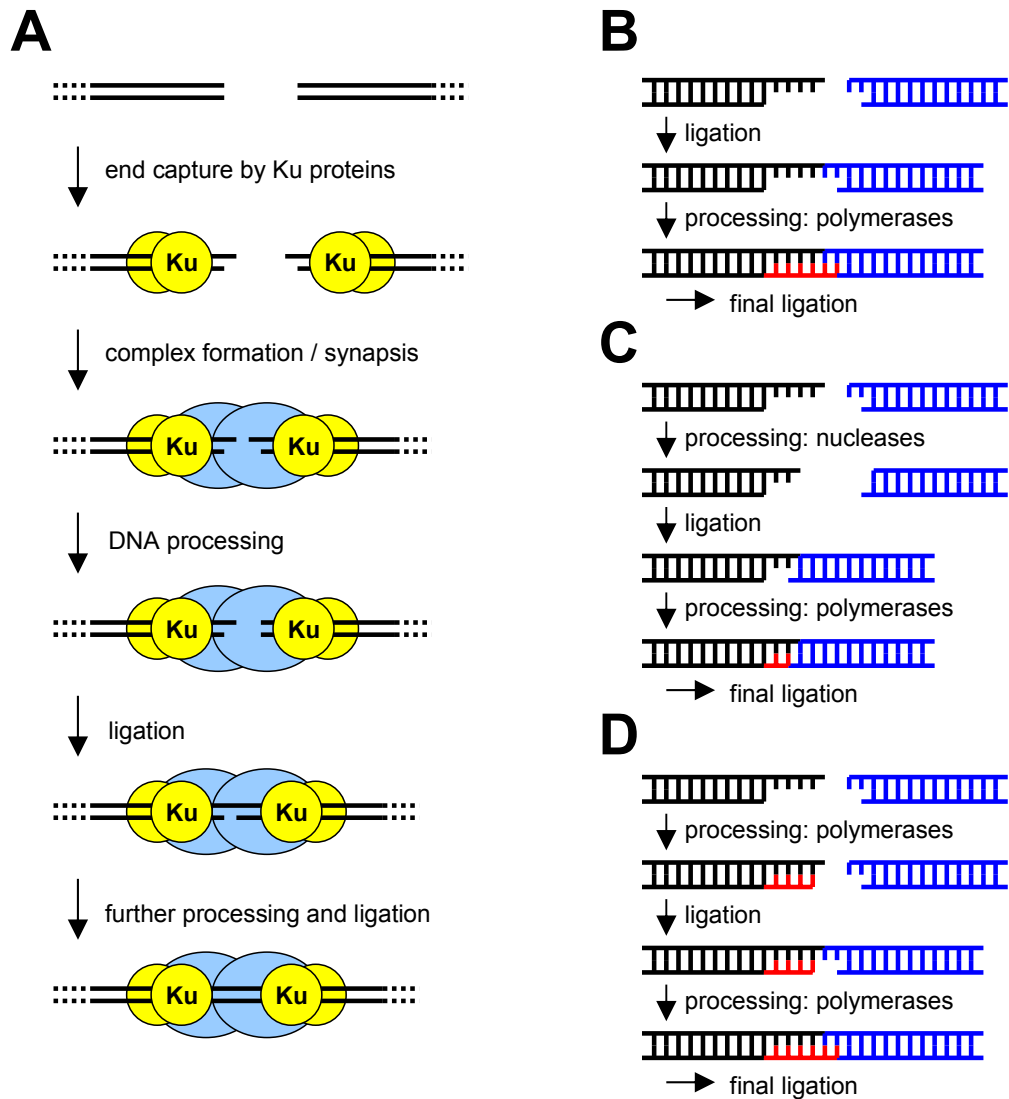


Figure 1.1. Non-homologous end joining. (A) To initiate the repair of a DSB by NHEJ, Ku proteins (yellow spheres) capture the DNA ends (black lines = DNA single strand). Further proteins are recruited and form a complex, bringing two DNA ends together. Damaged and incompatible DNA often may to be processed by nucleases and/or polymerases before the ends are ligated. Finally, further rounds of processing and ligation can be required to finish repair. (B-D) Examples of a multitude of possible DSB configurations are shown, each pictured with only one of many possible paths of repair. (B) Even incompatible DNA ends may be ligated before processing due to the broad substrate specificity of the ligase. (C) DSB processed by nucleases before ligation. (D) DSB processed by polymerases before ligation.

1.2.2 Homologous recombination

In homologous recombination (HR), a DNA DSB is repaired with high fidelity using the alignment to DNA with identical or similar sequence over an extended region. In this process the 5'-ends at the DSB are degraded and one 3'-end invades the double-strand of the homologous DNA molecule forming a loop (figure 1.2). This loop may then capture the second 3'-end. Subsequently DNA is synthesised, starting from the annealed 3'-end, and a typical intermediate, the Holliday junction, is formed. The Holliday junction is resolved by cleaving, exchanging and re-ligating two single strands. If two 3'-ends invade the homologous DNA molecule, two Holliday junctions are formed and their resolution can result in cross-over products.

Multiple HR pathways are used by eukaryotes and prokaryotes to repair dangerous DSBs in DNA and to deal with stalled replication forks (Wyman and Kanaar 2006; Huertas 2010). Eukaryotes prefer high fidelity DSB repair via HR when homologous DNA is quickly available from sister chromatids or homologous chromosomes during G2-, M- and late S-phase. During meiosis, eukaryotes increase genetic diversity by HR between homologous non-sister chromatids, initiated by generating DSBs using the Spo11 protein (Longhese et al. 2009). In genetic engineering, HR is used to replace genes in vivo with high sequence specificity but at rather low efficiency (Zhang *et al.* 1998).

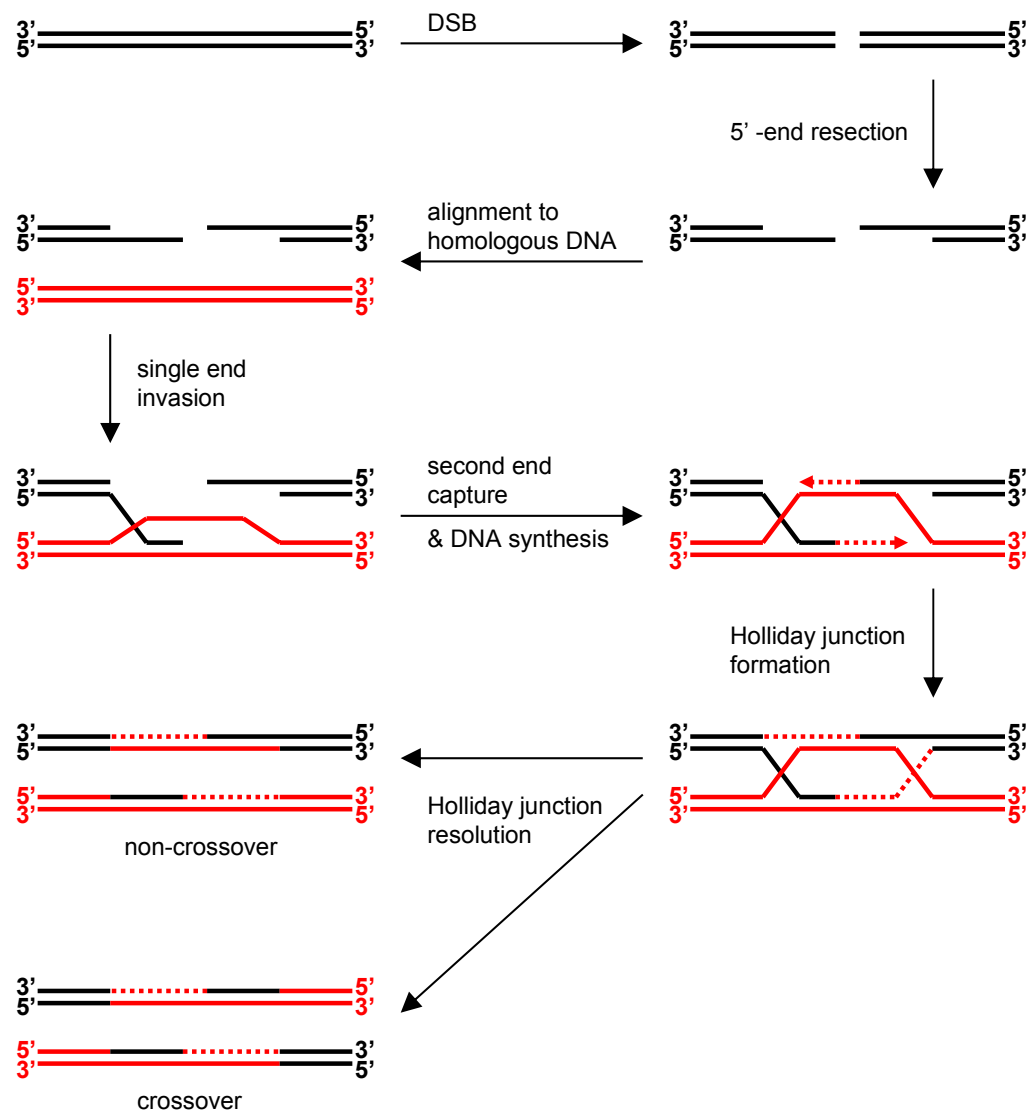


Figure 1.2: Homologous recombination. Repair of a DSB by homologous recombination can be initiated by the resection of single strands (black and red lines) from the 5' ends. When the ends of the DSB (black) are aligned to homologous DNA, a single strand with a 3'-end can invade the homologous DNA which produces a loop. If a second end is captured by the loop, homologous recombination can follow the pathway depicted here. Subsequently, DNA is synthesised using the homologous sequences as a template. Two Holliday junctions are formed and their resolution results in crossover or non-crossover products, depending on the isomerisation of the Holliday junctions.

1.2.3 Transposition

Transposons are genetic elements capable of moving or copying themselves from one locus into non-homologous loci in the genome of their host or of a targeted new host. The process is facilitated by transposases, which bind two short sequences towards the transposon ends (figure 1.3B), cut the DNA backbone at the ends, transfer the ends into the target DNA and rejoin the DNA backbone (Gill et al. 1979) (figure 1.3A). Transposases may choose these target sequences at random or prefer certain sequences. Since many transposases carry out a staggered insertion of the transposon, short single-stranded regions are left to be repaired by the host, resulting in typical short inverted repeats flanking the transposable element (figure 1.3C).

Simple transposons can encode for the transposase alone or even rely on transposases available in the host, as seen in the Ac/Ds element, the first transposon to be discovered (McClintock 1950). More complex elements feature additional genes, which, in prokaryotic transposons, are often resistance genes, like the lactamase gene in the Tn3 transposon (Heffron et al. 1979) (figure 1.3B). Bacterial transposons, especially when coupled to conjugative elements, can enable the horizontal transfer of these genes, aiding the emergence of new resistant strains. Retroviruses (HIV-1, ASV) and phage (bacteriophage Mu) are transposable elements encoding proteins necessary for virulence, such as envelope proteins. In higher eukaryotes, transposon derived sequences constitute a high proportion of the genome, over 40% in humans. The majority of these sequences are inactive remains or are repressed to maintain genomic stability. However, transposons can cause chromosome and gene rearrangements, activate or deactivate genes, and have contributed to the evolution of higher eukaryotes. A eukaryotic transposon, the P element, gained importance as a tool for disruption or introduction of genes in fruit flies.

Various types of transposition have been identified (reviewed extensively by (Curcio and Derbyshire 2003)), some of them using RNA intermediates and some relying solely on DNA intermediates (figure 1.3D). Retrotransposons and retroviruses use RNA intermediates simply to synthesise a DNA copy, subsequently proceeding similarly to transposons without RNA intermediates. In contrast, target-primed transposons reverse transcribe their RNA intermediate directly into the target sequence. Further, transposition can be divided into conservative transposition, where the transposon is cut out and inserted it into the target, and replicative transposition, where a copy of the transposon is inserted into the target. Replicative transposition requires a mechanism of copying the transposon, which retrotransposons achieve through transcription/reverse transcription, while DNA

transposons form DNA intermediates that can be replicated by the host. For this purpose, transposases like IS3 isolate and circularise one DNA single-strand of the transposon, creating a substrate for DNA polymerases. The transposases of the bacteriophage Mu and of the Tn3 family of bacterial transposons insert the transposon creating a replication fork. Subsequent replication produces a cointegrate comprising both the donor and target DNA linked by two copies of the transposon in direct repeat (Gill et al. 1978; Shapiro 1979). Specialised recombination enzymes can resolve the cointegrate into the original donor and target DNA, each carrying a copy of the transposon now (Arthur and Sherratt 1979; Sherratt et al. 1981).

Transposition may also be categorised according to their transposase families (Curcio and Derbyshire 2003; Hickman *et al.* 2010) (figure 1.3D). DDE transposases share the common motif of a catalytic amino-acid triad (DDE) for cutting the transposon out of the donor DNA and rejoining the DNA backbone. Y-transposases and S-transposases, as found in conjugative transposons, use a tyrosine or serine residue to cleave, covalently bind and rejoin the DNA backbone and are related to site-specific recombinases. Y2-transposases share two conserved tyrosine residues and may employ a “rolling-circle” mechanism for transposition similar as in bacteriophage ϕ X174. Target primed transposons (see above), do not require a transposase. Instead, they encode an endonuclease to nick the target DNA and a reverse-transcriptase to reverse-transcribe their RNA into the target starting from the nick.

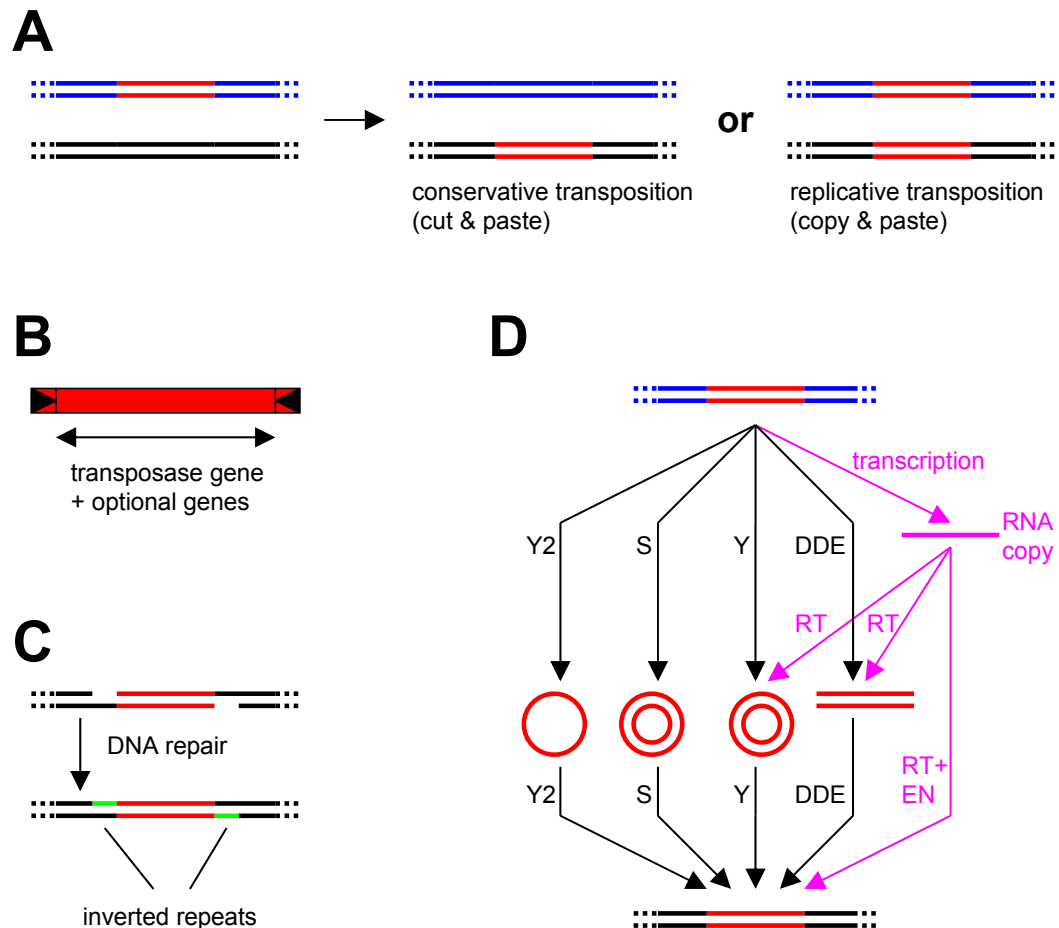


Figure 1.3: Transposition. **(A)** In conservative transposition a transposon (red) is cut out of the donor DNA (blue) and inserted into the target DNA (black) while the transposon is copied into the target DNA during replicative transposition. **(B)** Transposons usually comprise a transposase gene and optionally other genes, flanked by binding sites for the transposase (black triangles). **(C)** Many transposons perform staggered insertion into the target (black), producing short inverted repeats after repair of the resulting gaps (green). **(D)** This scheme illustrates various transposition pathways, using different transposases, including DDE, tyrosine (Y), serine (S) and Y2 transposases. The transposons (red, top) are cut or copied from the donor DNA and form a DNA intermediates (red, middle), ranging from single or double-stranded circular DNA to linear DNA. Many transposition systems proceed via a RNA intermediate (pink), which can be used by reverse transcriptases (RT) to produce DNA intermediates, which then are processed by transposases. Alternatively, the RNA intermediate is directly reverse transcribed into the target DNA, which is nicked by an endonuclease (EN).

1.2.4 Site specific recombination

Site-specific recombination enables highly efficient recombination between short (30-200 bp) specific sequences in two DNA partners. These specific sequences are often, but not necessarily, identical and resemble imperfect inverted repeats (Stark and Boocock 1995; Lilley 1997). The proteins involved, site-specific recombinases, bind to the specific recognition sequences in the DNA and bring them together to form higher order complexes, mainly through protein-protein contacts. Subsequently, the site-specific recombinases cleave, exchange and religate the DNA strands. The phosphodiester bonds of the DNA backbone are directly attacked by a catalytic residue of the site-specific recombinase, cleaved by phosphoryl transfer to the residue's side chain and religated by the reverse process. This conserves the energy of the phosphodiester bonds and eliminates the need for high energy co-factors or DNA synthesis during recombination (Grindley *et al.* 2006). Most site-specific recombinases can be divided into two families, named according to their conserved catalytic residue attacking the DNA backbone: tyrosine and serine recombinases (see following chapters).

Both families of site-specific recombinases can promote various DNA manipulations of target sequences, including inversion, integration and excision (Grindley *et al.* 2006) (figure 1.4). Each natural recombination system shows a high selectivity for one particular type of DNA manipulation, depending on the substrate topology and the location and orientation of the recombination sites (Stark *et al.* 1989). Integration describes the recombination of a single site in a circular DNA molecule with another site in a distinct target DNA, producing one recombinant DNA molecule consisting of both original DNA molecules linked by two recombination sites in direct repeat. Bacteriophage λ and various other phage use integrases, specialised site-specific recombinases, to integrate into the genome of their hosts in this way (Azaro and Landy 2002). Inversion can be mediated when a target sequence is flanked by two recombination sites, usually forming an inverted repeat. The target sequence stays in the same location within the surrounding DNA, but its direction is reversed via recombination of the flanking sites. The expression of various genes can be regulated using inversion, as seen in *Salmonella*, which uses the Hin recombinase in the regulation of flagellar phase variation (Johnson 2002). Excision is the reverse process of insertion. A target DNA sequence is circularised by recombination of two sites, flanking the targeted sequence in direct repeat. This removes the target sequence from the surrounding DNA, leaving one site in each product. In many bacteria, chromosome or plasmid dimers can be reduced by excision. Excision is important for various replicative transposons, such as the Tn3 transposon family, which can confer

antibiotic resistances to bacteria. These transposons encode site-specific recombinases to resolve the cointegrate, an intermediate of replicative transposition, by excision (Arthur and Sherratt 1979; Sherratt *et al.* 1981; Grindley 2002).

High selectivity for short DNA sequences and for defined DNA re-arrangements lends site-specific recombinases potential as precise tools for genetic engineering. However, a drawback to their application *in vivo* has been the requirement to introduce specific recombination sites in the target genome first (Liu *et al.* 2003). To work on unmodified genomes, hybrid site-specific serine recombinases recognising new DNA sites are currently being designed (Akopian *et al.* 2003; Gordley *et al.* 2007; Gordley *et al.* 2009).

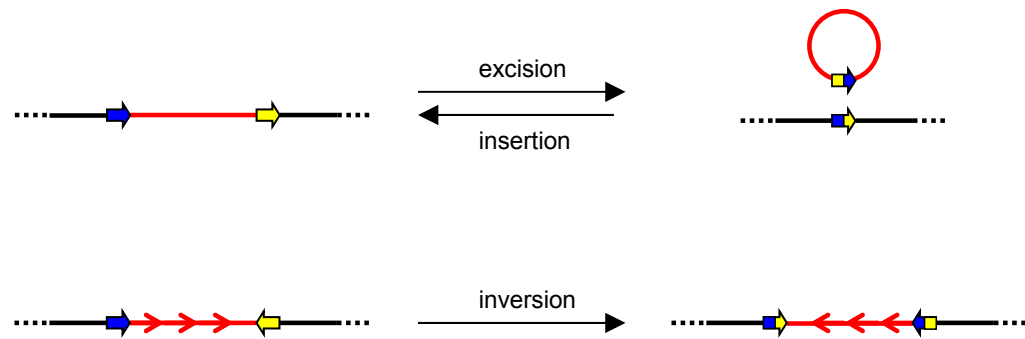


Figure 1.4: Rearrangement of DNA sequences by site-specific recombination. Excision of DNA sequences is facilitated by the recombination of two sites flanking a DNA region in direct repeat (same direction), circularising the DNA region and resulting in its removal from the surrounding DNA. In the reverse process of excision, insertion, two DNA molecules are joined by recombination of one site in each DNA molecule. Inversion describes the reversal of the direction of a DNA sequence within the surrounding DNA and is achieved by recombination of two sites flanking the DNA sequence in inverse repeat (opposing direction).

1.2.4.1 Tyrosine recombinases

Tyrosine recombinases, formerly called the phage λ integrase family, evolved separately from serine recombinases but are related to the eukaryotic IB topoisomerases and share with them a motif of five residues (RKHRH), clustered near the active site. During catalysis, two tyrosine recombinases bind to their specific sites in each of two DNA partners. A minimal recombination site consists of a 6-8 bp inverted repeat, forming a central spacer, which is flanked by two inverted sites that are bound by one recombinase unit each. The two DNA double helices and four recombinases form a synaptic complex, with the recombinases making head to tail contacts (figure 1.5). Two tyrosine recombinases then cleave a single DNA strand at the edge of the central spacer in each double helix, forming a covalent link between a tyrosine residue and a 3'-phosphate. The two single strands are exchanged and ligated giving rise to the typical Holliday junction intermediate. This Holliday junction isomerises and the remaining pair of single strands is cleaved, exchanged and religated to form the recombined products (Stark and Boocock 1995; Grindley *et al.* 2006).

In summary, cleavage, strand exchange and religation occurs in two subsequent steps, involving a single strand in both DNA partners per step. The stepwise process prevents double-strand breaks and results from the specific activation of only two recombinases per step, termed “half-of-the-sites-activity”. This arises from the true two-fold symmetry of the tetrameric complex, allowing only two recombinases within the complex, located opposite each other, to be activated by correct protein-protein contacts and DNA bending. The approximate four-fold symmetry of the complex enables the quick isomerisation of the complex, including the Holliday junction, allowing the activation of the remaining two recombinases in the new conformation (Grindley *et al.* 2006) (figure 1.5). The process of strand exchange starts, according to the current strand swapping-isomerisation model, when the 5'-OH single strands melt 2-3 bases from their DNA double helix. Since the DNA double helices are located at the core of the complex, the melted single strands can contact the partner site easily, making only small movements and without contacting the recombinases. To enable ligation, the 5'-OH end of the swapped strand is aligned to the phosphotyrosine of the partner site, through the formation of 2-3 base pairs between the single stranded regions (figure 1.5). This base pairing explains the required homology within the central spacer of the sites of tyrosine recombinases. Previously, it was thought the site homology was necessary for branch-migration during isomerisation of the Holliday-junction. It is now considered that isomerisation requires no branch migration or migration over a far smaller range (Van Duyne 2001; Rajeev *et al.* 2009).

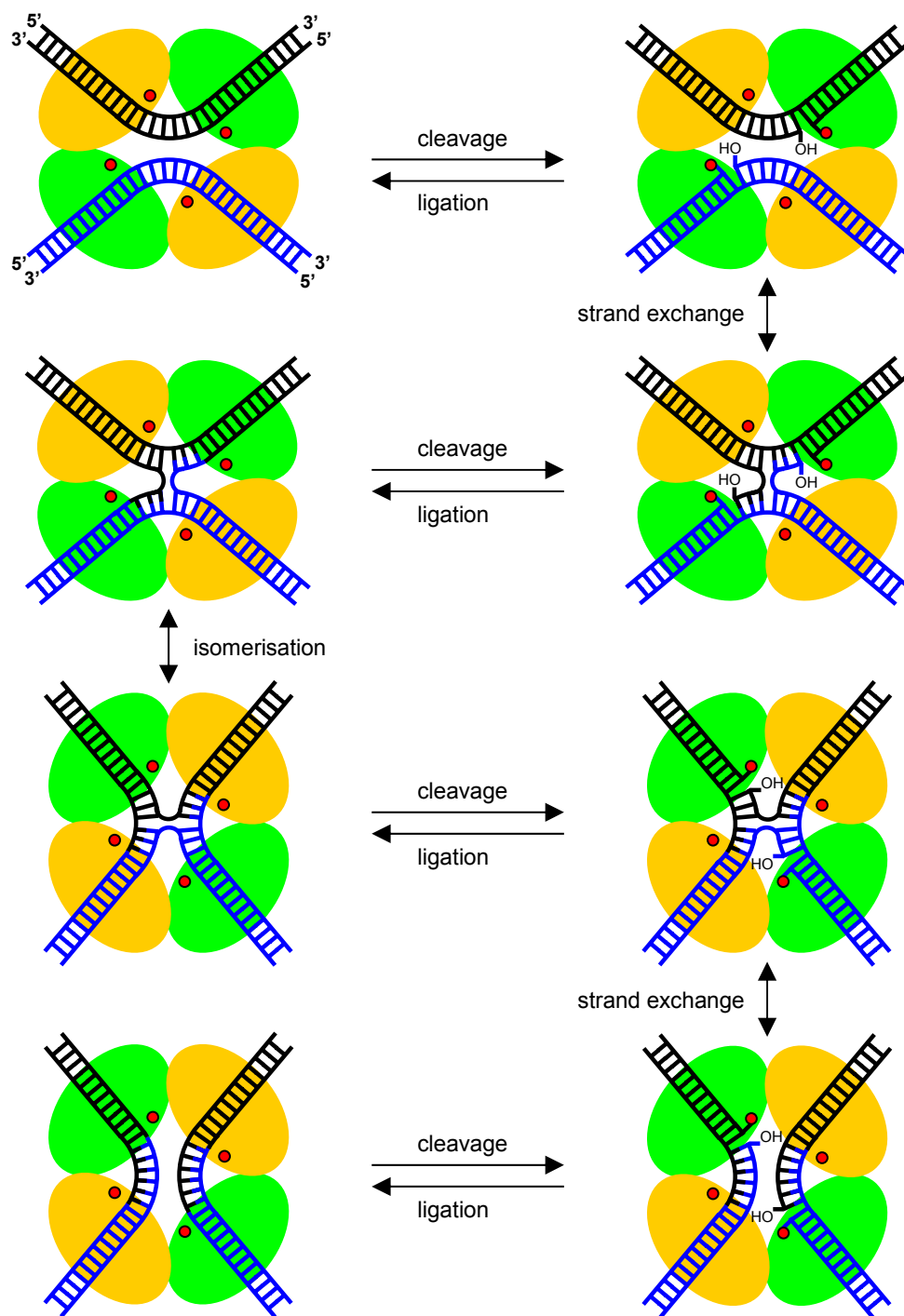


Figure 1.5: Reaction mechanism of tyrosine recombinases. Two DNA partners (black and blue) and four tyrosine recombinases (big spheres) form a recombination complex. DNA cleavage is mediated by a catalytic tyrosine residue (red dot), which becomes covalently linked to the DNA. Exchange and ligation of the two free DNA single strands produces the typical Holliday junction intermediate. Isomerisation of the Holliday junction swaps the continuity of both DNA double-strands and alternates the activity of the recombinases. Only two recombinases within the complex are active (green spheres) at the same time, while two remain inactive (yellow spheres). This enables the ordered cleavage and ligation of two DNA single strands at a time.

The outcome of the reaction (insertion, inversion excision) can be controlled at multiple levels. The recombinase dimer on each DNA site can prefer to bend the DNA into one of two conformations, selecting which recombinase unit is activated and which single strand is cleaved first. Recombination can be limited to sites in either parallel or anti-parallel orientation by the use of sites with an asymmetric central spacer (e.g. in Cre), since strand exchange one orientation results in mismatches, preventing product formation. Further, the use of accessory proteins (λ Int), specialised recombinase domains (λ Int) or hetero complexes of two different recombinases (XerC/D) can bring the DNA partners together in the correct orientation or dictate the conformation of the recombination complexes. Finally, the reversible recombination process might be biased towards substrates or products, if one is energetically favoured (Grindley *et al.* 2006).

Tyrosine recombinases are important for the integration of various phage (e.g. bacteriophage λ , see above) into the genome of their hosts (Azaro and Landy 2002). They can reduce dimers of circular DNA molecules by excision, as seen in the reduction of phage P1 plasmids by the Cre recombinase (Van Duyne 2001) and the reduction of chromosomes and various plasmids in bacteria by the XerC/D system (Barre and Sherratt 2002). Excision by tyrosine recombinases is also used by some transposons like Tn4430 to resolve cointegrate intermediates during transposition (Mahillon and Lereclus 1988). Another role of tyrosine recombinases is the inversion of DNA sequences for various purposes. Inversion can enable the regulation of genes, such as adhesin genes in *E.coli*, which are needed for the colonisation of surfaces (e.g. the human gastrointestinal tract) and regulated through the inversion of a genetic switch by the FimB and FimE recombinases (Abraham *et al.* 1985; Holden *et al.* 2007). Gene segments in the conjugative plasmid R64 can be inverted to produce variant sex pili needed for the transfer of the plasmid into other cells in different media (Komano 1999). In *Saccharomyces cerevisiae* the amplification of the 2 μ m plasmid is activated when the Flp recombinase inverts a large DNA segment during replication, reversing the direction of one replication fork (Jayaram *et al.* 2004).

The functions of tyrosine recombinases find widespread application in genetic engineering, enabling *in vivo* genome manipulations in a range of model organisms (Nagy 2000; Nagy *et al.* 2003). However, the use of tyrosine recombinases requires the introduction of their cognate sites into the genome (Liu *et al.* 2003), since the alteration of their sequence specificity had only limited success (Santoro *et al.* 2002; Saraf-Levy *et al.* 2006).

1.2.4.2 Serine recombinases

Serine recombinases bind and recombine DNA sites resembling an imperfect inverted repeat but work via a mechanism different from tyrosine recombinases. Size and domain organisation show huge variation within the family of serine recombinases, but all contain a catalytic domain, comprising the catalytic serine residue and three conserved clusters of residues. Most of the well studied recombinases, including the Hin and Gin invertases and the $\gamma\delta$ and Tn3 resolvases, also feature a DNA binding domain which contains a helix-turn-helix (HTH) motif and is usually located at the C-terminus. DNA recognition and binding is primarily mediated by the DNA binding domain, which binds to the ends of the recombination site (Rimphanitchayakit et al. 1989; Rimphanitchayakit and Grindley 1990). The catalytic domain contacts the central spacer of the site and promotes the dimerisation of recombinases through protein-protein contacts, thus enabling the cooperative binding of two recombinases to one site. Two recombination sites are brought together mainly by protein-protein interactions of the catalytic domain (Sarkis et al. 2001; Burke et al. 2004), resulting in an active protein tetramer bound to two DNA sites. In contrast to tyrosine recombinases, serine recombinases form the core of the active recombination complex, termed synapse, with the DNA on the outside (Sarkis et al. 2001; Nollmann et al. 2004; Li et al. 2005) (figures 1.6, 1.8).

Another difference to tyrosine recombinases is the concerted cleavage of all four DNA strands at the centre of the site, staggered by two base pairs (Reed 1981b; Boocock *et al.* 1995). DNA cleavage is mediated by the catalytic serine residue, forming a covalent link to the 5'-phosphate of the DNA backbone (figure 1.6). The two sides of both cleaved DNA double helices are held together by the covalently attached recombinases (Reed 1981b). The subsequent exchange of DNA double-strands is currently explained by a rotational mechanism (see section 1.3.6. for details). It is assumed that a flat protein interface in the active protein-DNA complex (Li et al. 2005) allows a 180° rotation of one half of the protein/DNA complex to exchange the DNA strands (Stark et al. 1991; Stark and Boocock 1994; McIlwraith et al. 1997), while all four recombinase units remain covalently linked to the DNA. Finally, religation yields two recombinant DNA double-stranded sites. However, despite extensive studies of the structural basis and kinetics of recombination by serine recombinases and derived hyperactive mutants (Arnold et al. 1999; Burke et al. 2004), this unique mechanism remains to be proven and is the subject of study in this thesis.

The aim of my research was to observe the movements of DNA and protein units during strand exchange and to test if these movements agree with the simple rotational model. Of further interest was the identification of intermediate states during strand exchange, the

transition between those states and the reversibility of the transitions. These movements can be observed using fluorescence spectroscopy to monitor changes in the distance between fluorescent labels attached to protein and DNA units, although only the DNA was labelled during this project. A single-molecule fluorescence setup was employed to study the movements within a single synapse in real time. This can enable the detection of transition states by avoiding the detection of a mere overlay of multiple recombination reaction.

Serine recombinases generally have a high selectivity for either inversion, insertion or excision, depending on the relative orientation and location of the recombination sites (figure 1.4). To achieve this specificity, recombination needs to be limited to sites in a parallel or anti-parallel orientation and to sites within one or two DNA molecules. Recombination can be restricted to sites in one orientation by an asymmetric overhang at the cleavage site, preventing ligation in the incorrect orientation by formation of mismatches. However, most of the well studied recombination systems readily restrict the formation and activation of recombination complexes to sites in the correct configuration. Additional DNA bending proteins (Rowland *et al.* 2006) and/or accessory recombinase sites in the DNA molecule(s) (Grindley *et al.* 1982; Kilbride *et al.* 1999) can bring the sites together in the correct configuration and induce activating protein-protein contacts between the recombinases. Further, the DNA topology can promote the correct alignment of the sites and also restrict the direction of the strand exchange (Wasserman and Cozzarelli 1985; Wasserman *et al.* 1985; Stark *et al.* 1989).

Excision by serine recombinases is important for the resolution of cointegrate intermediates during transposition of the Tn3, *gd* and related transposons, which can confer antibiotic resistances to bacteria. Serine recombinases can also reduce dimers of circular DNA molecules, such as dimers of large *staphylococcus* plasmids, which are reduced through excision by the Sin recombinase (Rowland *et al.* 2002). Inversion by serine recombinases can enable the regulation of gene expression, as seen in *Salmonella typhimurium*, where the Hin recombinase inverts a DNA region comprising a promoter to switch between the expression of two different flagellar filament proteins. Phage Mu can switch host specificity by using the Gin recombinase to invert a DNA region, which neighbours a promoter and comprises gene segments for variants of adhesion proteins at each end (van de Putte and Goosen 1992). Insertion by serine recombinases plays a role in the integration of mobile genetic elements like IS607 in *Helicobacter pylori*, which is integrated and excised by the OrfA recombinase. *Streptomyces* and myobacterial phages

can be integrated into and excised from the host genome by large serine recombinases which feature additional domains (Grindley *et al.* 2006).

Serine recombinases show high potential for applications in genetic engineering due to the modular organisation of their catalytic domain and their sequence recognising domain (Rimphanitchayakit *et al.* 1989; Rimphanitchayakit and Grindley 1990), enabling the design of hybrid recombinases with nearly completely new sequence recognition (Akopian *et al.* 2003) working in human cell lines (Gordley *et al.* 2007).

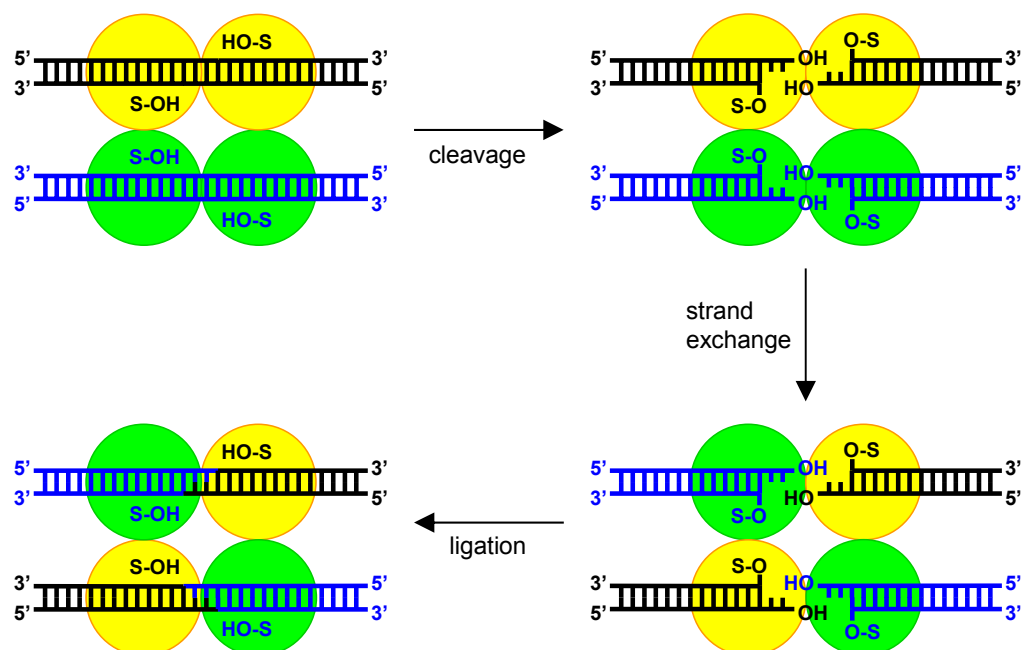


Figure 1.6: Recombination by serine recombinases. Two copies of the recombination site (black and blue) come together to form a synapse with a tetramer of serine recombinases (yellow and green spheres) at the core. The side chain of the catalytic serine residue (S) of the recombinases attacks the DNA backbone and becomes covalently attached to the 5'-phosphate, leaving a free 3'-OH group. The cleaved DNA double-strands are exchanged requiring a net rotation of one half of the complex by 180°. Finally, ligation yields the recombinant products.

1.3 *Tn3* resolvase and related serine recombinases

The following chapters will focus on serine recombinases. Their role and detailed reaction mechanisms will be described using the well studied Tn3 and $\gamma\delta$ resolvase, Sin recombinase and members of the Hin family of invertases as examples.

1.3.1 *Tn3* and related transposons

Tn3 resolvase, a serine recombinase, is encoded by the *tnpR* gene in the Tn3 transposon, along with two other genes encoding a transposase (*tnpA*) and a β -lactamase (*bla*) (Heffron et al. 1979) (figure 1.7A). The Tn3 transposon is found in *E.coli* and other gram negative bacteria and can provide the host with penicillin resistance by expression of the β -lactamase. Replicative transposition can insert a Tn3 copy from a donor DNA molecule into host plasmids DNA, including conjugative plasmids or other transferable DNA molecules, enabling horizontal transfer of the antibiotic resistance (Shapiro 1979).

The transposase effects the insertion of Tn3 (Gill et al. 1979) by binding to two inverted 38 bp sequences flanking Tn3. Tn3 is duplicated during transposition and, following the action of transposase, the donor DNA molecule is fused to the target DNA comprising one Tn3 copy at both linkage points (Gill et al. 1978; Heffron et al. 1979). This intermediate, called the cointegrate, is resolved into two distinct circular molecules, containing one Tn3 copy each (Gill et al. 1978; Arthur and Sherratt 1979) (figure 1.7B). Cointegrate resolution requires Tn3 resolvase (Arthur and Sherratt 1979; Sherratt et al. 1981), which effects site specific recombination between the *res* sites within each Tn3 copy (Heffron et al. 1979). Tn3 resolvase also has a regulatory role, repressing expression of *tnpA* and *tnpR* (Chou et al. 1979; Heffron et al. 1979).

Several transposons of the Tn3 family (or class II transposons) encode a site-specific recombinase related to Tn3 resolvase to achieve cointegrate resolution. These resolvases can be divided into several groups on the basis of their sequence specificity and ability to work on the recombination sites of the other members (Ackroyd *et al.* 1990). Members of one group show a high sequence identity ($\geq 80\%$), similar reaction mechanisms and the structural basics of each member generally apply to most of them. $\gamma\delta$ resolvase and Tn3 resolvase are within the same group and the wealth of biochemical data for Tn3 resolvase can be advantageously interpreted in conjunction with the structural data available for $\gamma\delta$ resolvase.

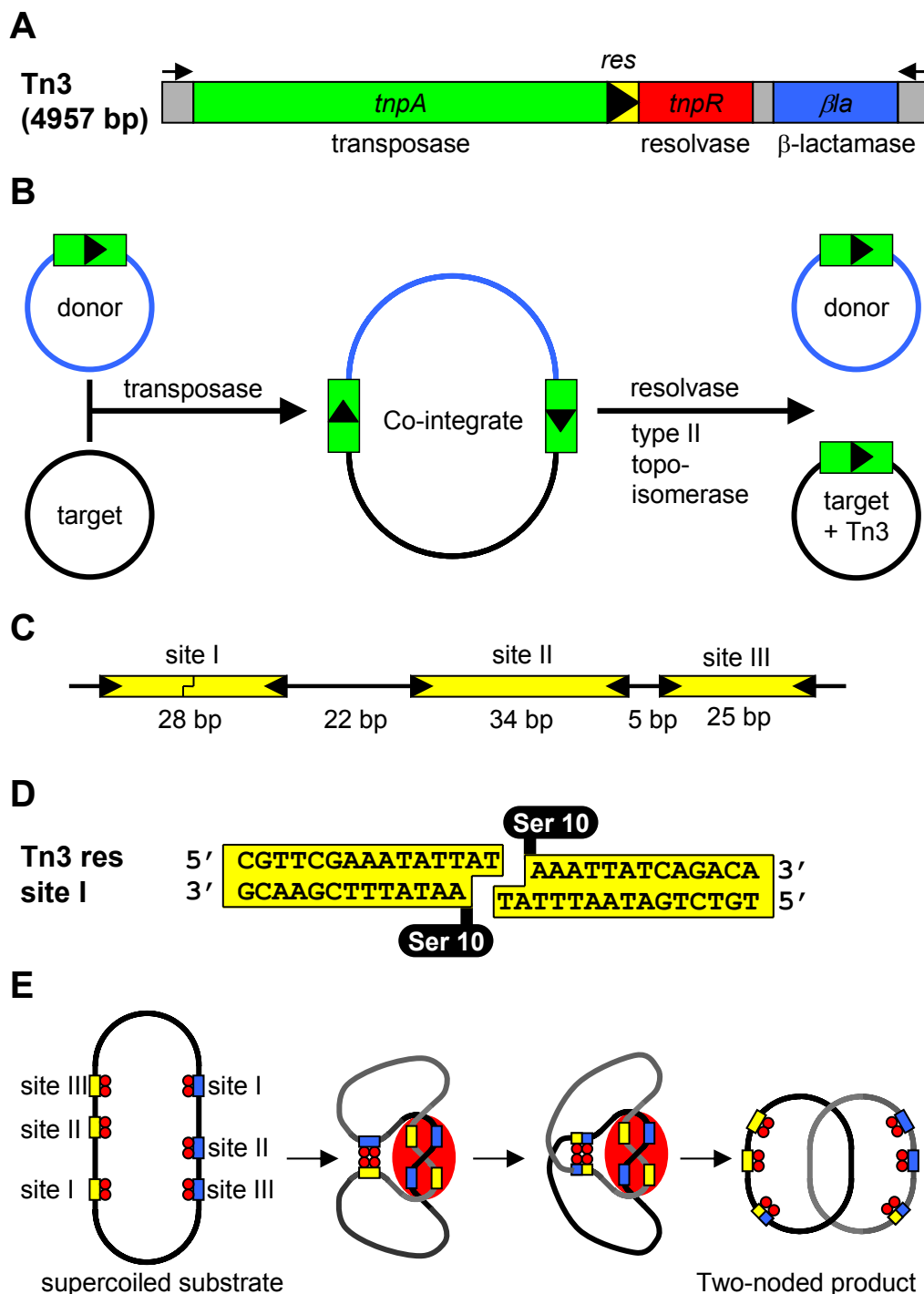


Figure 1.7: The Tn3 transposon. (A) Architecture of the Tn3 transposon encoding the transposase, Tn3 resolvase and β -lactamase. (B) The two-step process of transposition. The transposase facilitates replicative transposition of the donor plasmid, carrying one copy of the Tn3 transposon (green box), into a target plasmid, forming a co-integrate with two copies of the Tn3 transposon. Recombination of both *res* sites (black arrow) by Tn3 resolvase resolves the co-integrate into the donor plasmid and the target plasmid, now carrying a copy of the transposon. (C) Architecture of the *res* site, comprising three imperfect repeats which form sites I-III. Recombination takes place at site I, whereas sites II and III are accessory sites. (D) Sequence of site I indicating the serine 10 residue (black bubble) of Tn3 resolvase bound to the cleavage site producing a 2 bp staggered overhang. (E) Formation of the synaptosome, a superstructure on a negatively supercoiled, circular DNA substrate containing two *res* sites in direct repeat. All three sub-sites (yellow and blue boxes) are bound by two Tn3 resolvase units (red spheres) and brought together by tetramer formation. The accessory sites II-III form an unknown structure enabling recombination at site I, producing a two noded catenane.

1.3.2 Resolvase binds and recombines *res* sites

Cointegrate-like structures, negatively supercoiled plasmids containing two full *res* sites in direct repeat (same orientation) can be resolved *in vitro* using purified Tn3 resolvase (Reed 1981a; Krasnow and Cozzarelli 1983). A *res* site contains three binding sites (sites I-III) to which resolvase has been shown to bind in DNA footprinting assays (Grindley *et al.* 1982; Kitts *et al.* 1983). Each site has an imperfect inverted repeat sequence, which is cooperatively (Grindley *et al.* 1982; Hughes *et al.* 1990; Blake *et al.* 1995) bound by two resolvase subunits facing each other (Yang and Steitz 1995; Nollmann *et al.* 2005). The outer part of the inverted repeats of sites I, II and III flank central spacers of different length, giving site I, II and III a length of 28 bp, 34 bp and 25 bp (figure 1.7C).

Concerted strand cleavage takes place at the centre of site I (Grindley *et al.* 1982) when two copies of site I come together to form a synapse. The two copies of site I are held together by a resolvase tetramer at the core of the synapse (Sarkis *et al.* 2001; Nollmann *et al.* 2004) as seen in the co-crystal structure of $\gamma\delta$ resolvase and its site I (Li *et al.* 2005). The tetramer is formed mainly through interactions of the catalytic domains of the resolvase dimer bound to each site I. The nucleophilic serine residue (S10 in $\gamma\delta$ and Tn3 resolvase (Hatfull and Grindley 1986) attacks the DNA backbone and becomes covalently attached to the 5'-end of the cleaved DNA strands leaving a 2 bp staggered double-strand break (Reed and Grindley 1981) (figures 1.6, 1.7D). Following strand exchange, the DNA double-strands are religated and the resolvases detach (Reed and Grindley 1981).

Kinetic studies of recombination by Tn21 resolvase found that binding to the whole *res* site occurs within ~50 ms and complete recombination within ~500 s. Productive synapsis occurs over a wide range of times from ~10 ms to 100 s, presumably depending on the start configuration of the rather heterogeneous supercoiled DNA substrates (Oram *et al.* 1997).

1.3.3 Recombination requires a full *res* site and a specific DNA topology

Activation of the resolvase tetramer on site I of *res* requires the accessory sites II and III to be bound by resolvase dimers and to come together to form a complicated higher order complex, called the synaptosome (figure 1.7E), which restricts recombination to excision. Binding by resolvase induces DNA bends at sites I, II and III at different angles (Hatfull *et al.* 1987; Blake *et al.* 1995). The synaptosome traps three negative interdomainal supercoils and its correct formation requires the location of both *res* sites in one negatively supercoiled DNA molecule (Wasserman and Cozzarelli 1985; Wasserman *et al.* 1985).

Earlier electron micrographs had shown the three negative supercoils being trapped between the synapsed sites (Wasserman and Cozzarelli 1985; Wasserman *et al.* 1985), but the exact structure of the higher order complex has not been solved yet. Kinetic studies revealed how contact between sites I, II and III might be enhanced in supercoiled molecules (Oram *et al.* 1997). A “random collision” model (Brown *et al.* 2002) was favoured over a “slithering” model but was incompatible with the high stability of synapses (Parker and Halford 1991). A model of “unproductive complexes”, reassembling upon attack by unpaired sites, reconciled both findings (He *et al.* 2002).

The activation through a higher order complex of two *res* sites imposes a “topological filter” on recombination, preventing inversion or intermolecular recombination (insertion) and allowing only the excision reaction (Stark *et al.* 1989). Supercoiling is thought to drive recombination forward, rotating the left halves of site I by 180° (right handed) relative to the right halves and resulting in the removal of 4 negative supercoils from the substrate during resolution (Wasserman and Cozzarelli 1985; Stark *et al.* 1989). The overall linkage number change is +4. The resolution product from a supercoiled plasmid with directly repeated *res* sites is usually a two-noded catenane and other products occur only in minor quantities (Stark *et al.* 1989; Stark *et al.* 1991) (figure 1.7E). However, if an asymmetric central overlap is introduced at the cleavage site, recombination proceeding via a 180° rotation would result in mismatches and recombination proceeds mainly in multiples of 360° rotations, producing catenanes with additional nodes (Stark *et al.* 1991; Stark and Boocock 1994; McIlwraith *et al.* 1997). In catenane fusion, the reversed reaction which is possible only in substrates of low superhelical density, the linkage number change is -4 (Stark *et al.* 1989). The selectivity of the “topological filter” can be conferred to other unrelated recombinases by correct placement of sites II+III of *res* adjacent to a simple recombination site, such as *loxP*, the site for Cre recombination (Kilbride *et al.* 1999).

1.3.4 Modular domain structure of resolvases

DNA binding and catalysis are mediated by distinct domains of resolvase which are connected by a flexible linker (figure 1.8). Binding and bending of DNA by resolvase is mainly mediated by the C-terminal domain (Rimphanitchayakit *et al.* 1989), while the N-terminal domain contains all catalytic residues and the important E-helix and promotes the formation of recombination complexes through protein-protein contacts.

The C-terminal domain can bind DNA sites on its own, in contrast to the N-terminal domain, which needs to be directed towards the site (Rimphanitchayakit *et al.* 1989). If not bound to DNA, the C-terminal domain and adjacent parts of the N-terminal domain adopt

an unfolded state (Rice and Steitz 1994a). The C-terminal domain binds common 9 bp motifs, located at the outer part of sites I-III in inverted repeat, and also interacts with three more base pairs towards the centre of the site. In total the C-terminal domain spans around one third of the DNA. A helix-turn-helix (HTH) motif in the C-terminal domain enables the sequence specific DNA binding through contacts with the DNA phosphates and bases in the major groove (Rimphanitchayakit et al. 1989). DNA binding is also aided by minor groove contacts of residues in the flexible linker region (Yang and Steitz 1995) and residues in the C-terminal end of the E-helix (R125) (Li *et al.* 2005), which is part of the N-terminal domain (figure 1.8A/C).

The N-terminal domain of Tn3 resolvase (residues 1-137) can be referred to as the catalytic domain since it comprises all residues important for catalysis. It promotes the formation recombination complexes and contains the important E-helix at its C-terminus. The catalytic domain does not promote catalysis on unrelated sequences (Ackroyd et al. 1990) and contributes to DNA binding mainly through the E-helix.

The globular core of the catalytic domain (residues 1-100) comprises a 5-strand β -sheet encased by four α -helices (Rice and Steitz 1994b; Yang and Steitz 1995; Li *et al.* 2005). The conserved serine 10 residue which becomes covalently linked to the 5'-end of the cleaved DNA during catalysis is found in the core of the catalytic domain together with other residues essential for recombination (Arg8, Arg68, Arg71) (Boocock et al. 1995). Various protein-protein interfaces in the recombination complex involve residues in the globular part of the catalytic domain. The synaptic interface connects two resolvase dimers bound to the DNA site (figure 1.8D). Residues in the globular part of the catalytic domain and the beginning of the E-helix (A89, G101, D102, M103, Q105) are thought to stabilise the synaptic interface and were discovered in activated mutants (Arnold *et al.* 1999; Burke *et al.* 2004). The globular part of the catalytic domain also contains residues (R2, R32, K54, E56) that are thought to be involved in the 2-3'-interface (figure 1.8B) between resolvase units at site I and the accessory sites, which is important for the regulation of recombination in the wild system (Hughes *et al.* 1990; Sarkis *et al.* 2001). Mutation of the residues in the 2-3' interface are not directly activating, but enhance the activity of already activated mutants (Olorunniji *et al.* 2008).

The E-helix (residues 101-137) of the catalytic domain plays several important roles in recombination. The C-terminal half of the E-helix is unfolded in absence of DNA (Rice and Steitz 1994a) but forms a straight helix upon binding to the DNA site. Residues in the C-terminal part of the E-helix (especially R125) contact the minor groove of the DNA. In

the structure of the resolvase dimer at site I, the DNA close to the cleavage site is gripped by the two E-helices which are crossed at an angle of 45° (Yang and Steitz 1995) (figure 1.8A). The interlocking of the E-helices forms the majority of the dimer interface and the dimer is further stabilised by a hydrogen bond between a pair of E118 residues.

In the structure of the cleaved synapse (Li *et al.* 2005), the E-helices grip the DNA close to the 3'-ends of the cleaved DNA. The E-helices are no longer interlocked at the dimer surface and cross at an angle of 100° . This arranges the E-helices across the dimer in an anti-parallel manner, helping to form a flat interface at the core of the synapse which is thought to allow the current subunit rotation model of strand exchange (Li *et al.* 2005; Kamtekar *et al.* 2006) (figure 1.8C). Proceeding from the structure of pre-synaptic dimer to the cleaved synapse, each E-helix bends slightly and the core of the catalytic domain rotates towards the E-helix by $40-70^\circ$, using residues 101-102 as a hinge. This rotation enables DNA cleavage/ligation by moving the catalytic serine residue 11A forward into the reach of the scissile DNA phosphates (Li *et al.* 2005).

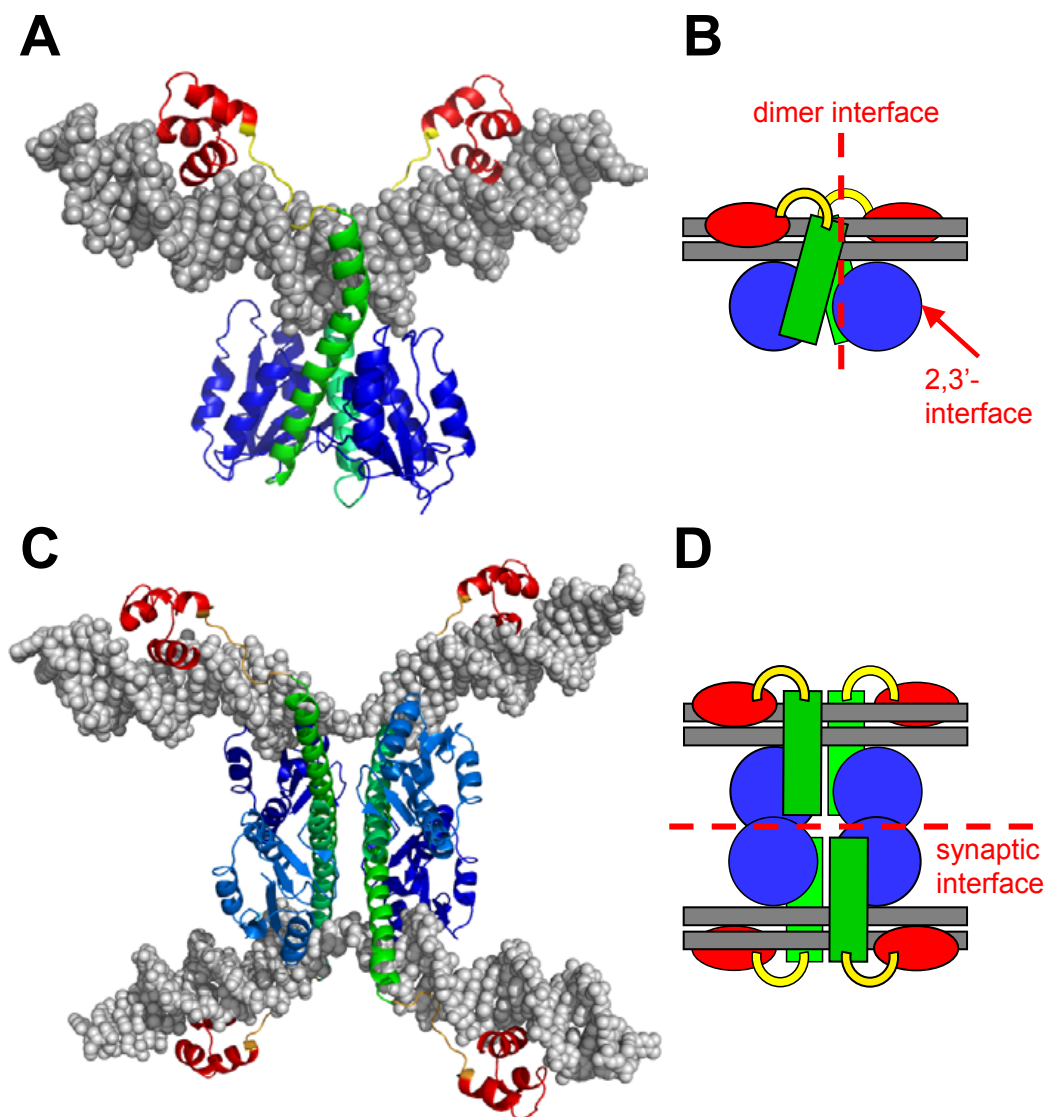


Figure 1.8: Modular domain architecture of $\gamma\delta$ -resolvase (closely related to Tn3). The C-terminal, DNA-binding domain is shown in red, the linker region in yellow, the globular part of the catalytic N-terminal domain in blue and the E-helix in green. **(A)** Co-crystal structure of a $\gamma\delta$ -resolvase dimer bound to site I (pdb: 1GDT; Yang and Steitz 1995). **(B)** Cartoon representation of the dimer co-crystal structure, highlighting the dimer and 2,3'-interface **(C)** Co-crystal structure of a $\gamma\delta$ -resolvase tetramer holding bound to two sites I forming a synapse. (pdb: 1ZR4; Li *et al.* 2005) **(D)** Cartoon representation of the site I synapse co-crystal structure, highlighting the synaptic interface.

1.3.5 Hyperactive resolvase mutants

Natural resolvases require two full *res* sites in one supercoiled DNA molecule to perform recombination (figure 1.7). Mutagenesis and *in vivo* selection of Tn3 resolvase first yielded mutants catalysing recombination between a full *res* site and a single site I in plasmids. Further mutagenesis generated double mutants working on substrates containing only two copies of site I. Those hyperactive mutants have lost their topological selectivity and recombined two sites I in direct or inverted repeat, within one or in two separate DNA molecules and even in linear DNA without the requirement of negative supercoiling (Arnold et al. 1999). For example, Tn3 resolvase NM (Tn3R NM) is a hyperactive mutant of Tn3 resolvase with the mutations R2A, E56K, G101S, D102Y, M103I and Q105L (Burke et al. 2004). Tn3R NM can bind to linear substrates containing a single copy of site I, bring two copies of the substrate together to form a synapse (Nollmann et al. 2004; Olorunniji et al. 2008) and recombine both copies of the substrate.

Analysis of the hyperactive mutants allowed identification of residues on the interfaces needed for complex formation (Burke et al. 2004) and the examination of tetramer formation on site I by native PAGE and several biophysical methods (Nollmann et al. 2005). The simplified sequence and topology requirements and selection of more active multiple mutants might lead to applications for serine recombinases in genetic engineering comparable to those of tyrosine recombinases and enabled the development of active chimeric resolvases (Akopian et al. 2003; Gordley et al. 2007).

1.3.6 The mechanism of strand exchange by resolvases

The resolvase tetramer at the site I synapse has been shown to be between the two site I DNAs (Burke et al. 2004; Nollmann et al. 2004; Li et al. 2005) forming a “DNA out” complex (figure 1.8C). In this complex, the catalytic residues within the catalytic domain of each resolvase subunit act in *cis*, meaning they make contact with the same copy of site I (Boocock et al. 1995). Similarly, both domains of each resolvase subunit act in *cis* and are bound to the same half of site I (Droge et al. 1990). The DNA strands at the centre of site I are cleaved independently, without any order, as shown in studies with $\gamma\delta$ resolvase hetero tetramers (Boocock et al. 1995). Following cleavage, the double-stranded half sites are exchanged resulting in a net rotation of 180° of both half-sites relative to each other. Evidence for the net rotation stems from measurements of the topological changes accompanying strand exchange. Recombination of supercoiled substrates by wild type resolvase induces a linkage number change of +4 and produces 2-noded catenanes, which requires a 180 degree rotation at the crossover site (Stark et al. 1989; McIlwraith et al.

1996; McIlwraith *et al.* 1997). Starting from the situation with one subunit bound to each of the four half-sites, different models may describe strand exchange:

End swapping

None of the resolvase subunits changes place and two DNA ends are detached from their resolvase subunit, exchange and re-attach to a distinct resolvase unit on one side of both sites I (figure 1.9B).

Domain swapping

The DNA-binding domain and the E-helices of all resolvase subunits stay in place. To rotate the DNA strands, the globular part of the catalytic domains of two resolvase units on the same side of site I are swapped, together with their covalently attached half-sites, using the linker region as a hinge (Grindley 2002; Li *et al.* 2005) (figure 1.9C/D).

Postulated subunit rotation model

All resolvase subunits and domains keep their position relative to the half of site I they were originally bound to. The whole protein-DNA complex is split into two parts perpendicular to the dimer-dimer interface. One half of the complex, containing two half sites and two resolvase subunits bound to it, rotates against the other half (Stark *et al.* 1989) (figure 1.9E). The half complexes are held together by a flat hydrophobic interface, which may enable smooth rotation (Li *et al.* 2005) (figures 1.8C, 1.9A).

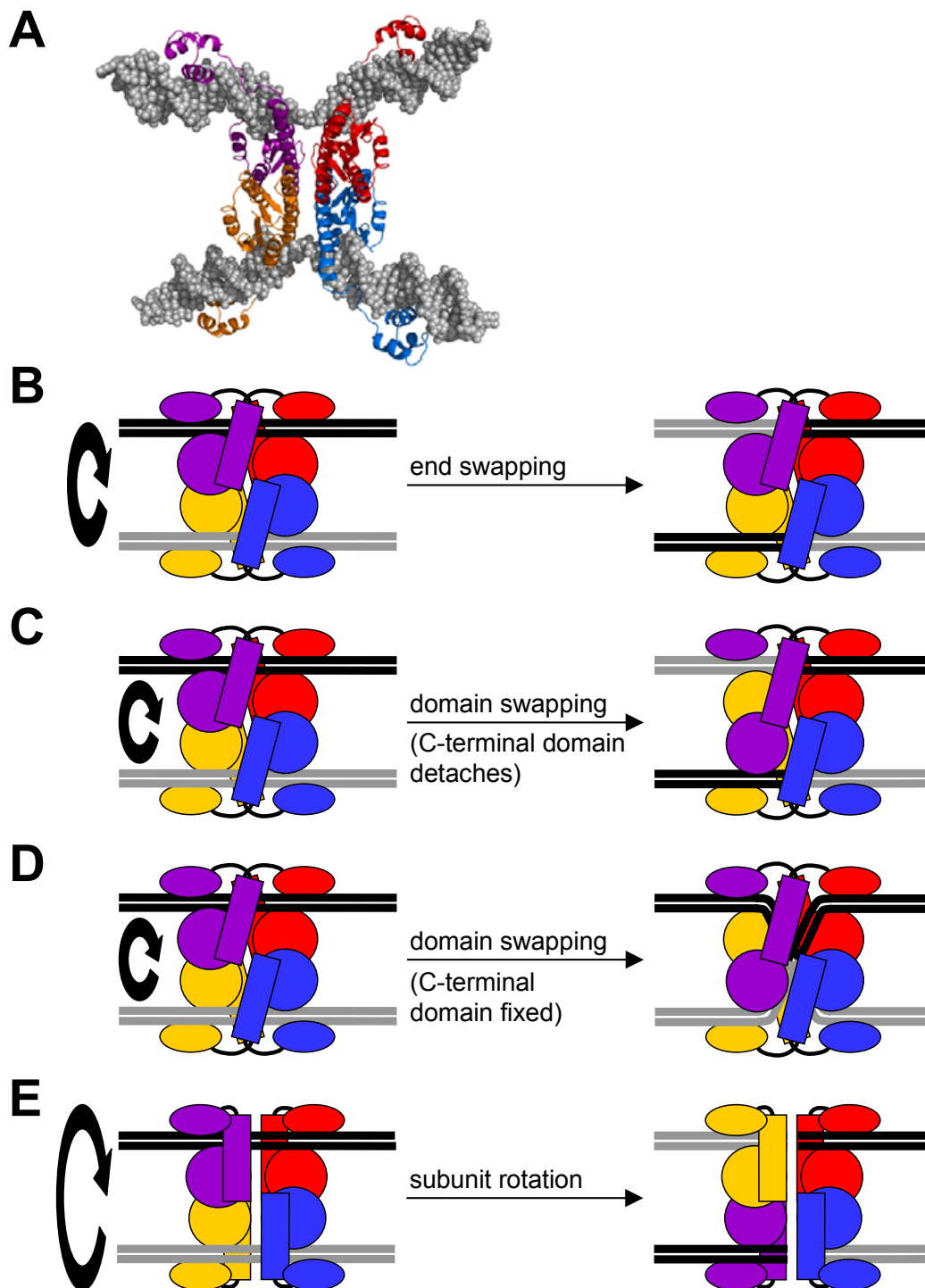


Figure 1.9: Strand exchange models for recombination by resolvase at site I. (A) Co-crystal structure of a $\gamma\delta$ resolvase tetramer bound to two copies of site I (pdb: 1ZR4; Li *et al.* 2005) comprising an extremely flat hydrophobic surface between both halves of site I. (B) End swapping model: The DNA strands on the left half of site I detach completely from the resolvase units to be exchanged (C) Domain swapping model: All E-helices and C-terminal domains stay in place. The DNA strands detach temporarily from the C-terminal domain and are exchanged by swapping the globular part of the catalytic domains on the left side of the complex. (D) Domain swapping model: Leaving the DNA strands attached to the C-terminal domains creates DNA distortion within the synapse. (E) Subunit rotation model: The whole left half of the synapse rotates by 180° relative to the right half. All resolvase subunits stay in the same position within each half.

Several earlier strand exchange models were based on a synapse with the DNA sites in its centre. These models required only small movements of the DNA and protein units. However, solution X-ray and neutron scattering (Nollmann et al. 2004) and a recent co-crystal (Li et al. 2005) structure of the synapse have shown the DNA to be on the outside of the complex.

The end swapping model was proven wrong when resolvase subunits were covalently cross-linked to their DNA sites while retaining recombination (McIlwraith et al. 1996). Both the domain swapping model and the subunit rotation model are consistent with this finding and the DNA topology shown by Stark *et al.* (1989).

When two DNA sites differing in one base of the central 2 bp overlap (AC x AT) are recombined, strand exchange proceeds in multiple rotations of 360° rather than 180°, giving rise to different knotted products (Stark et al. 1991; McIlwraith et al. 1997). This phenomenon was observed earlier on as a change from recombination activity towards topoisomerase activity due to introduction of mismatched base pairs (Falvey et al. 1988). The fact that multiple rotations can take place, without rejoining the DNA in between, suggests that strand exchange might be mediated by subunit rotation (McIlwraith et al. 1997). In the domain swapping model, rotation by more than 180° would cause the linker regions to be wrapped around each other multiple times, unless the E-helices and DNA binding domain would rotate after each rotation of the DNA strands (Grindley 2002).

In the domain swapping model the globular part of the catalytic domain moves using residues 101 to 102 as a hinge. However, in the crystal structure of a cleaved synapse, the hinges are separated by 30 Å and substantial unfolding of the E-helix or the globular part of the catalytic domain would be required for domain swapping (Li *et al.* 2005). Another weakness of the domain swapping model is that it requires the DNA to detach from the C-terminal domain due to structural restraints (Li et al. 2005) and to avoid serious distortion of the DNA within the synapse (McIlwraith et al. 1997) (figure 1.9C/D).

The co-crystal structure by Li *et al.* (2005) captures a $\gamma\delta$ resolvase tetramer bound to two cleaved DNA sites. In this state, the interface between the half sites is extraordinarily flat, contrary to what was expected from the co-crystal structure of the $\gamma\delta$ resolvase dimer bound to one DNA site, where the E-helices interlock (Yang and Steitz 1995). This suggests that strand cleavage induces a conformational change, changing the angle of the E-helix and providing the flat hydrophobic interface thought to be required for smooth movements in the subunit rotation model. Modelling showed that only minor movements

of the side-chains at the interface are required for subunit rotation and the energy has been calculated to stay constant during the process. The area covered by the flat interface should vary little during subunit rotation, since the interface has a roughly round shape. The flat interface buries about 1,760-2,400 Å² of hydrophobic surface, which is thought to establish a link strong enough to hold the cleaved synapse together (Li *et al.* 2005).

The directionality of recombination found in the wild-type system can be explained simple subunit rotation driven by the supercoiling of the plasmid substrate. The process of recombination in steps 180° is not as easily explained by subunit rotation. However, outside the hydrophobic interface, negative patches formed by D94 and D95 (in $\gamma\delta$ resolvase) interact with positive patches formed by R125 and R121 (in $\gamma\delta$ resolvase). This interaction could be established in the non-recombinant state as well as upon each 180° rotation and may align the half sites to initiate re-ligation of the DNA strands (Li *et al.* 2005).

Several cross-linking experiments can be explained best by the subunit rotation model. In $\gamma\delta$ resolvase mutant V114C disulfide bonds between cysteines at position 114 crosslink the E-helices across the flat interface. In agreement with the subunit rotation model, this crosslink allows cleavage of the DNA double-strands but does not allow recombination by preventing strand exchange via rotation along the flat interface (Li *et al.* 2005).

The K136C mutant of $\gamma\delta$ resolvase crosslinks efficiently by disulfide bond formation and permits cleavage of the substrate DNA but prevents ligation. This appears surprising since the residues at position 134 are far apart in the tetramer structure of $\gamma\delta$ resolvase. However, modelling of the subunit rotation process has shown that these residues come into close proximity after rotation by 75° (Li *et al.* 2005). Earlier, the equivalent Q134C mutant of Hin invertase had provided the same crosslinking results (Dhar *et al.* 2004). In crosslinking experiments with the $\gamma\delta$ resolvase mutant G96C or the homologous Hin invertase mutant S94C, disulfide bond formation between the introduced cysteines is incomplete, but can be explained similarly to the crosslinking of $\gamma\delta$ resolvase mutant K136C. The introduced cysteines are located in the globular part of the catalytic domain and come close after subunit rotation by 70°. An alternative explanation was offered by Kamtekar *et al.* (2006), who found these residues to be separated by only 7-9 Å in the crystal structure of a tetramer of a truncated, activated $\gamma\delta$ resolvase mutant in absence of site I. It is not clear if the globular part of the catalytic domains can, in presence of site I, assume the orientations observed in absence of site I. However, the apo structure demonstrated the flexibility of the

hinge region which is thought to be important for the structural changes necessary to proceed from an inactive dimer to the cleaved tetramer (Kamtekar *et al.* 2006).

One drawback of the interpretation of the crystal structure of the cleaved synapse is that both copies of site I are identical and symmetric. Therefore the left half (L) and right half (R) of one parental site and the half sites of the second parental site (L', R') cannot be assigned unambiguously. It is not completely clear which half sites will be joined after strand exchange or if strand exchange has already happened. However, strand exchange via subunit rotation is in agreement with the most likely configuration of the parental sites. In this configuration, the dimer at site I has the closest resemblance to the dimer in the original co-crystal structure and the distance between the 3'-OH group and phosphoserines is about 17 Å for the L-R half sites, 40.5 for L-L' half sites and 41 for the L-R' half sites (Li *et al.* 2005). The gap between the half sites also suggests that some conformational changes occur from during the transition from the unknown pre-cleavage complex to the cleaved complex.

In summary, the subunit rotation model is supported by several lines of evidence, but direct proof is still required. The aim of this project was to learn more about the mechanism of strand exchange by monitoring the relative movements of the individual components of the synapse directly. For this purpose it was planned to label specific positions in the resolvase subunits and the DNA with fluorescent dyes. Using fluorescence resonance energy transfer spectroscopy, changes in the distance between these labelled units can be measured. When a single-molecule fluorescence setup is employed, one can record the individual movements in individual synapses instead of detecting a mere average of the movements in all synapses in the sample. In this project, only the DNA was labelled at specific positions. Nevertheless, experiments with fluorescently labelled substrate DNA can allow the direct observation of DNA movements during strand exchange, the identification of intermediate states and switching between the intermediate states. This approach may reveal the kinetics of steps that involve DNA movements, like strand exchange and the transition from the pre-cleavage synapse to cleaved synapse. Since recombination occurs in steps of 180°, it was planned to test if the synapse switches between recombinant, non-recombinant states and possibly other states, if the synapse tends to rest in those states and if switching occurs in a particular order. The rate of strand exchange steps, cleavage and ligation is also of interest and studying a single synapse at a time might reveal if multiple rounds of strand exchange occur before religation of the DNA.

1.3.7 Other serine recombinases: *Hin*, *Gin* and *Sin*

Apart from the complementary group of resolvases, including Tn3, Tn21 and $\gamma\delta$, there are more well studied serine recombinases.

Hin, *Gin* and *Cin* belong to the complementing family of invertases which catalyse the inversion of DNA sequences flanked by their cognate sites. *Hin* changes gene expression in *Salmonella typhimurium* by inverting a promoter region and *Gin* alters host specific gene expression in phage MU by inverting of a region containing gene segments at its ends. The recombinases of this family invert DNA sequences flanked by two different binding sites in inverse repeat, each analogous to a Tn3 *res* site I. The wild type systems include an enhancer sequence which needs to be bound by the protein FIS to promote recombination (Johnson *et al.* 1986). However, FIS-independent mutants of *Hin* (Haykinson *et al.* 1996), *Gin* (Klippel *et al.* 1988) and *Cin* (Haffter and Bickle 1988) have been identified. Recently, hybrid recombinases using the catalytic domain of activated *Hin* and *Gin* mutants have been developed to recognise new sequences (Gordley *et al.* 2007).

Sin is a resolvase which has been particularly interesting to study, since it forms a very compact complex on its short recombination site (86 bp), called *resH*. A *resH* site contains sites I and II, each bound by a *Sin* dimer, and a discrete binding site between sites I and II which is bound by Hbsu. Hbsu can be replaced by other DNA bending proteins like IHF or Hu (Rowland *et al.* 2002). Site I is the crossover site and resembles an inverted repeat, analogous to site I in the Tn3 and $\gamma\delta$ resolvase systems. Two copies of site I come together to form synapse containing a *Sin* tetramer. The structure of the site I synapse has been modelled based on the structure of the site I synapse of the homologous $\gamma\delta$ resolvase (Rowland *et al.* 2006). Site II is an accessory site and resembles a direct repeat. Two copies of site II come together to form a synapse which is structurally different from the site I synapse. A recent crystal structure of the *Sin* site II synapse shows the DNA is located at the core and contacts between the DNA binding domains of *Sin* help to keep the tetramer together (Mouw *et al.* 2008). With the co-crystal structure of IHF bound to its DNA site (Rice *et al.* 1996), the structures of the protein complexes at all three sites in *resH* are available, enabling the construction of a model for the whole synaptosome. In this model, the *Sin* recombinase tetramers at sites I and II are adjacent to each other and IHF introduces a strong bend in the DNA that allows the DNA wrapping needed for formation of the synaptosome. The synaptosome model has been found to agree with the location and effects of regulatory mutants of *Sin* (Rowland *et al.* 2009).

Interestingly, Sin can be activated by a single mutation to catalyse recombination of substrates with two copies of site I lacking any accessory sites (Rowland et al. 2005). This is encouraging for their application in genetic engineering and hybrid Sin recombinases have been successfully developed (unpublished data).

1.3.8 Design of hybrid serine recombinases

The modular architecture of serine recombinases allowed exchange of the C-terminal domain, which naturally provides most of the sequence specificity (Rimphanitchayakit and Grindley 1990), by a zinc finger protein with different DNA-binding specificity (figure 10D). The first working hybrid (Akopian et al. 2003) consisted of the catalytic domain of a hyperactive Tn3 resolvase mutant fused to the zinc finger domain of the murine transcription factor Zif268 (Pavletich and Pabo 1991; Elrod-Erickson *et al.* 1996) by a flexible linker. Fusion to different zinc fingers, which can be readily engineered to specifically recognise many DNA sequences, can yield recombinases with new sequence specificity (Elrod-Erickson and Pabo 1999; Moore *et al.* 2003; Gordley *et al.* 2007).

The DNA site recombined by hybrid “zinc finger recombinases” consist of a central spacer (~22 bp) flanked by zinc finger binding sites (ZBS). The catalytic domain of the hybrid recombinase contacts the central spacer of the site. The central spacer contains a central sequence of about 16 base-pairs which resemble the natural site I. The ends of the central spacer do not require a specific sequence and form a randomised linker between the ZBS and the central sequence. The zinc finger recognition sequences are bound by the zinc finger domain of the hybrid recombinase, analogous to the natural C-terminal domain (figure 1.10A-D). The length of the central spacer is critical for recombination by hybrid recombinases (Akopian et al. 2003). This might be due to the catalytic domain being directed to more or less correct positions on the hybrid site. The required length of the central spacer is independent from the length or sequence of the linker between the catalytic domain and the zinc finger domain of the hybrid recombinase.

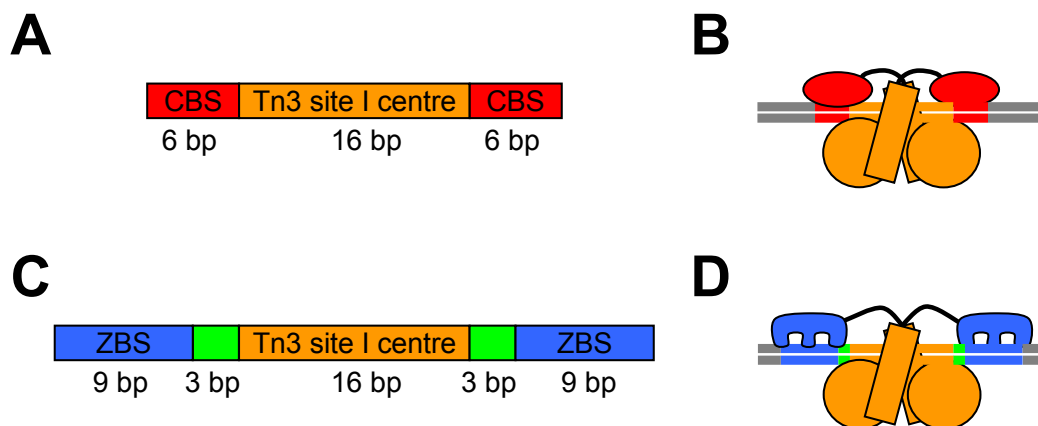


Figure 1.10: Hybrid recombinases and their DNA sites. (A) DNA sites recombined by natural recombinases comprise a 16bp central sequence (orange) flanked by inverted repeats (CBS, red). (B) Cartoon representation of a natural recombinase bound to its site. The C-terminal domain (red sphere) binds to the flanking DNA repeats (red bars) while the catalytic domain (orange sphere) contacts the central sequence (orange bars). (C) In sites for hybrid resolvases the inverted repeats are exchanged by a zinc finger binding site (ZBS) separated by a random linker sequence (green). (D) Cartoon representation of a hybrid recombinase bound to its site. The C-terminal domains are replaced by zinc finger DNA binding domains (blue fingers) binding the zinc finger binding site (blue bars).

The need of the catalytic domain for a conserved central sequence in order to recombine biases the potential substrate spectrum of hybrid serine recombinases towards site I-like sequences. Mutagenesis has yielded hybrids with somewhat broader sequence recognition (Gersbach *et al.* 2010). A more systematic approach in our laboratory focuses on the patterns in the relationship between certain amino acids in related serine recombinases and the contacted base pairs in the centre of their specific sites. Preliminary unpublished results promise hybrid recombinases with high specificity for new central sequences.

Important for the use of hybrid serine recombinases in unmodified genomes is the ability to target non-palindromic sequences. This requires differently designed recombinases to work together to form a hetero dimer on a single site in order to recombine. This has already been achieved (unpublished data).

New hybrids of zinc finger proteins and different serine recombinases, including invertases, show the general applicability of this concept and even have been shown to work in human cell lines (Gordley *et al.* 2007; Gordley *et al.* 2009). Since some recombinases can readily be activated for use in hybrids by a single mutation (Rowland *et al.* 2005), new generations of more efficient and specific hybrid recombinases will emerge and open the gate for applications in genetic engineering.

2 Introduction to Biophysical Methods

2.1 Summary

This thesis originally set out to test the validity of the subunit rotation model for strand exchange by serine recombinases by following the movements of protein subunits relative to the DNA sites. This was thought to be achievable by applying fluorescence resonance energy transfer (FRET) spectroscopy on single synapses. FRET enables the measurement of distances between fluorophores with overlapping absorption and emission spectra. Suitable fluorescent dyes were bound to various defined positions in the DNA. However, fluorescent dyes have not been bound to the protein units during the course of this project. Therefore only changes in the distance between defined positions in the DNA were followed during strand exchange. Nevertheless, these experiments can provide detailed information about the process of strand exchange when single-molecule fluorescence spectroscopy is applied (see chapter 1.3.6.). Single-molecule fluorescence spectroscopy can facilitate the direct observation of DNA motions in one synapse at a time, including fast switching between different states. In comparison, standard solution experiments can only track average distances and the overall reaction progress in an ensemble of synapses.

2.2 Fluorescence resonance energy transfer

FRET and other fluorescence-based methods are well suited to study molecular biological processes such as binding and conformation changes. FRET enables direct and non-invasive observation of biological reactions without the need to separate the products subsequently. FRET measurements are rapid (nanoseconds), highly sensitive to extremely small spatial changes (nanometres) and can be carried out at relatively low concentrations (nanomolar) without the need for radioactivity.

FRET describes the fast radiationless transfer of energy from one excited fluorophore to second fluorophore, giving rise to detectable fluorescence of the second fluorophore. The efficiency of this transfer depends, amongst other factors, on the distance between the fluorophores. When the distance between both fluorophores is close to the characteristic Förster radius (figure 2.1), small distance changes result in large measurable changes in the FRET efficiency. Labelling the substrate DNA of Tn3 resolvase with a fluorophore pair featuring a Förster radius of approximately 50-60 Å, DNA movements within the synaptic complex of ~80-100 Å can be analysed efficiently. In the following I will establish the physical basis of FRET and calculations needed for analysis.

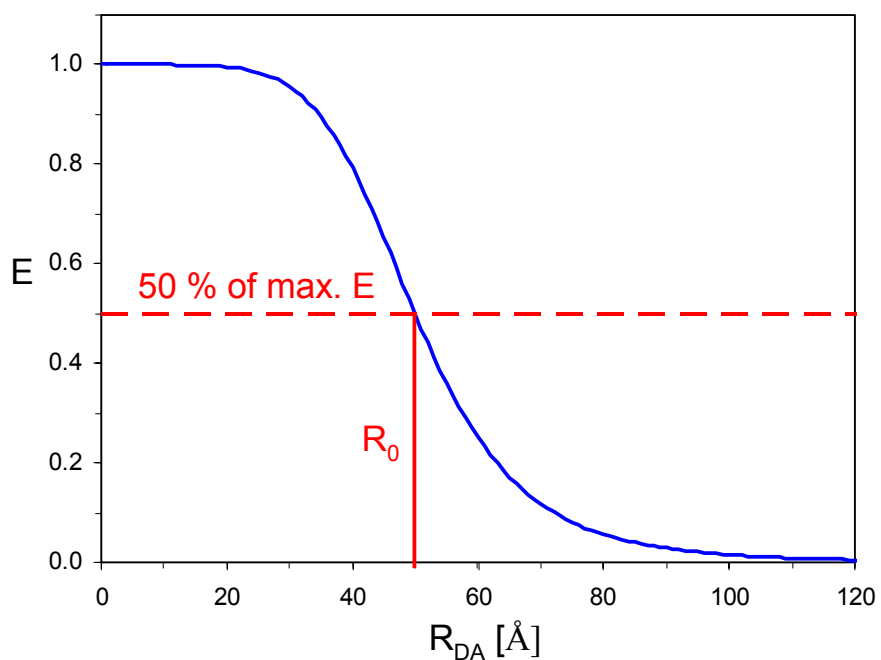


Figure 2.1: FRET efficiency and donor-acceptor distance. The efficiency of the fluorescence resonance energy transfer from the donor to the acceptor is plotted against the distance between the donor and acceptor fluorophore. The Förster radius R_0 is the donor-acceptor distance at which the FRET efficiency reaches 0.5.

Dipole-dipole interactions between the singlet states of a fluorophore pair can enable FRET, the transfer of energy from one excited fluorophore (donor) to another fluorophore (acceptor), without emission of radiation and within nanoseconds. The efficiency of FRET (E) describes the fraction of the donor excitation energy which is transferred to the acceptor. Competing decay processes of the excited state of the donor lower the FRET efficiency. Depending on the rate of energy transfer (k_{FRET}), direct fluorescence emission of the donor (k_f) and other competing decay processes (k_i), the FRET efficiency can range from 0 to nearly 1.

$$E = \frac{\text{energy transfer}}{\text{donor excitation}} = \frac{k_{\text{FRET}}}{k_{\text{FRET}} + k_f + \sum k_i} \quad (2.1)$$

The distance between the donor and acceptor fluorophore (R_{DA}) affects the rate of energy transfer and therefore the FRET efficiency. The Förster radius (R_0) describes the characteristic distance between the fluorophores at which the FRET efficiency reaches 50%. If the distance between donor and acceptor is close to the Förster radius, small changes of this distance result in big changes of the FRET efficiency, since the FRET efficiency is a sigmoid function of the distance between the fluorophores (figure 2.1). In this situation FRET measurements are at their most sensitive for relative changes of the separation of two fluorophores, and are well suited for studies of binding or conformational changes in biological systems.

$$E = \frac{1}{1 + \left(\frac{R_{\text{DA}}}{R_0} \right)^6} \quad (2.2)$$

One can determine the absolute distance between the fluorophores by measuring the FRET efficiency if the Förster Radius is known for the particular pair of fluorophores. However, the Förster radius depends on the overlap (J) of the donor's emission spectrum and the acceptor's excitation spectrum, the refractive index (n) of the solvent between the fluorophores, the fluorescence yield of the donor (Φ^D) and the orientation of the fluorophores.

$$R_0^6 = 8,8 \cdot 10^{-28} \cdot J \cdot \kappa \cdot n^{-4} \cdot \Phi^D \quad (2.3)$$

The orientation factor κ in equation 2.3 can be fixed to 2/3 if the fluorophores are isotropically oriented (Stryer 1978). This value is derived from the averaged orientations of

freely rotating fluorophores. It is often assumed that fluorophores can rotate freely if they are connected to biological molecules via a flexible linker. The overlap J in equation 2.3 is calculated from the integral of the donor's emission spectrum $f_{em}^D(\lambda)$ (normalised to 1 in its maximum) and the acceptor's excitation spectrum $f_{exc}^A(\lambda')$ (normalised to 1 in its maximum multiplied by the maximal extinction coefficient of the acceptor) over the complete range of wavelengths λ .

$$J = \int_0^\infty f^D(\lambda) \cdot \varepsilon^A(\lambda) \cdot \lambda^4 d\lambda \quad \left[\frac{nm^4}{cm \cdot M} \right] \quad (2.4)$$

Equation 2.3 is complicated by the fact that the local environment of fluorophores attached to biological molecules can be different from the remaining solution. This can result in an altered quantum yield of the donor and a changed local refractive index. It is crucial to determine all components of the Förster radius accurately for a reliable calculation of the distance between both fluorophores. Therefore this thesis and many applications of FRET focus on relative changes of the separation of fluorophores by studying the changes in FRET efficiency (Lilley and Wilson 2000). For this purpose, it can be sufficient to excite the donor fluorophore while simply using the ratio of the acceptor and donor fluorescence, separated by a dichroic mirror, as an indicator for the FRET efficiency. Another method is based on the quenching of the donor fluorescence due to energy transfer to the acceptor. Both methods can enable very quick measurements. However, the calculation of FRET efficiency from full fluorescence spectra according to Clegg (Clegg et al. 1992) provides more accurate results by eliminating various sources of inaccuracy.

2.3 FRET analysis according to Clegg

In the following I will introduce the analysis of FRET data according to Clegg (Clegg *et al.* 1992). This type of analysis separates the FRET induced fluorescence emission of the acceptor from fluorescence induced by direct excitation of the acceptor and from trailing donor fluorescence. In addition, factors such as the quantum yield of the acceptor, the concentration of labelled molecules and incomplete labelling of the biological molecules with the acceptor fluorophore are eliminated. It is helpful to measure full fluorescence spectra over a range of the emission wavelengths, λ , and the excitation wavelengths λ' . In contrast to point measurements, full spectra allow simple base-line corrections, reveal peak shifts and facilitate the normalisation and fitting of spectra required for data analysis.

Two fluorescence emission spectra of the sample of interest need to be taken at each point during the experiment (figure 2.2C). This sample typically contains biological molecules linked to the donor and acceptor fluorophores and is referred to as sample DA. For the first fluorescence emission spectrum, $f_{em}^{DA}(\lambda, \lambda'_D)$, sample DA is excited at wavelength λ'_D , the excitation wavelength of the donor. The value of λ'_D can be shifted to minimise excitation of the acceptor, but should allow for strong excitation of the donor. For the second fluorescence emission spectrum, $f_{em}^{DA}(\lambda, \lambda'_A)$, the acceptor in sample DA is directly excited at wavelength λ'_A , at which only the acceptor is excited.

Furthermore, spectra of two additional reference samples, sample D with the donor alone and sample A with the acceptor alone, need to be recorded once and are used for the data analysis of each FRET measurement (figure 2.2A). Ideally, the conditions in the reference samples should match those of sample DA during the experiment. Sample A is excited at any suitable wavelength and the fluorescence emission spectrum $f_{em}^D(\lambda)$ is taken.

Furthermore, the fluorescence excitation spectrum $f_{exc}^D(\lambda')$ of sample D is taken at a suitable emission wavelength. Similarly, the emission spectrum $f_{em}^A(\lambda)$ and excitation spectrum $f_{exc}^A(\lambda')$ of a sample A are recorded. Alternatively, absorption spectra of the reference samples can be used instead of the fluorescence excitation spectra.

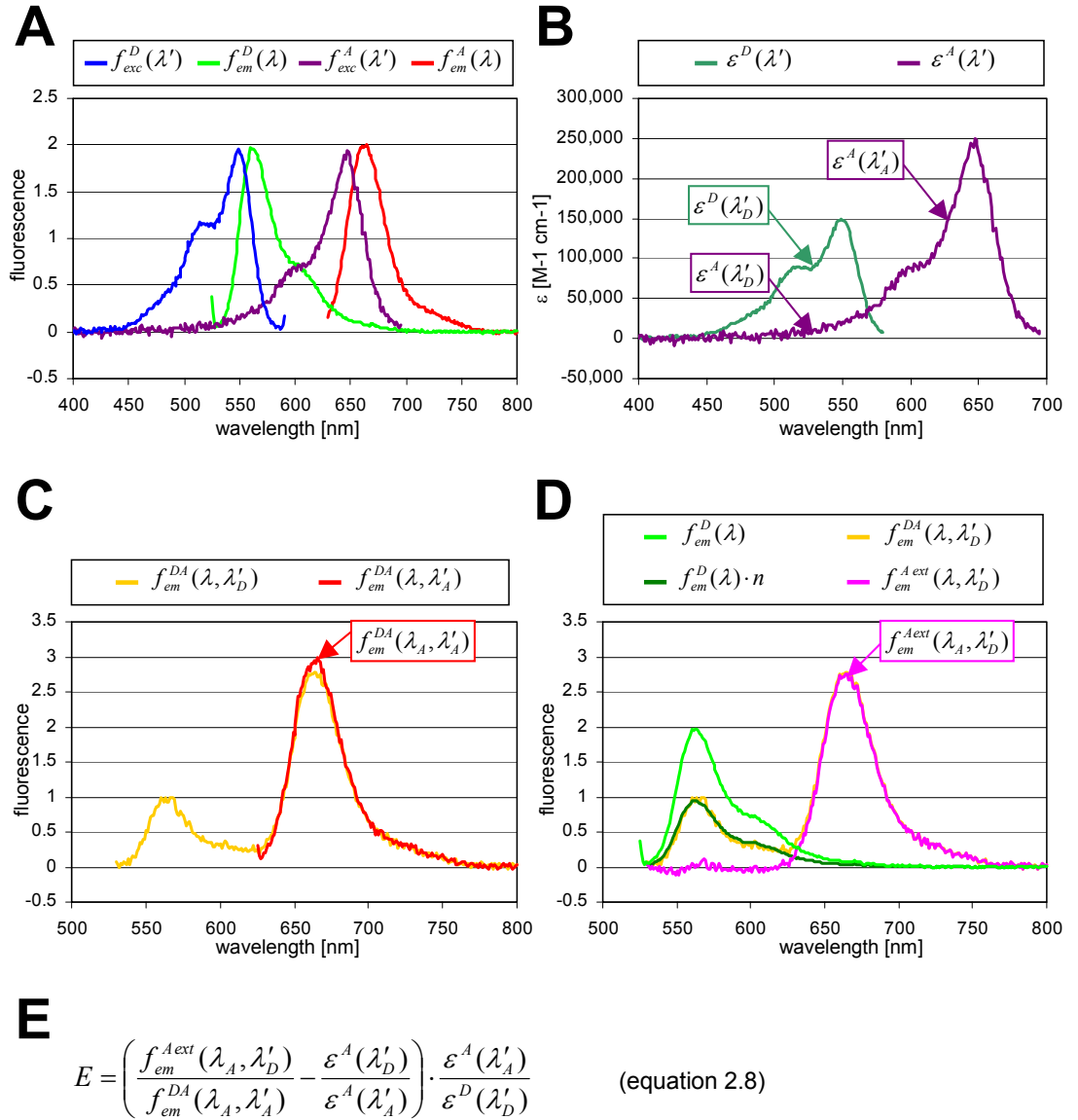


Figure 2.2: FRET analysis according to Clegg. Clegg *et al.* (1992) developed this approach to analyse data from FRET measurements. **(A)** The excitation spectrum $f_{exc}^D(\lambda')$ and emission spectrum $f_{em}^D(\lambda)$ of the sample with the donor only is recorded. Similarly, the excitation spectrum $f_{exc}^A(\lambda')$ and emission spectrum $f_{em}^A(\lambda)$ of the acceptor only sample is taken. The reference spectra in this example were generated by measuring the fluorescence of double-stranded DNA substrates with attached fluorophores as described in the materials and methods section. A Cy3 dye acted as donor (substrate B50R1C3) and a Cy5 dye as acceptor (substrate B50L1C5). Here, spectra were normalised to 2 at the maximum for visual comparison. **(B)** Spectra of the extinction coefficient of the donor $\epsilon^D(\lambda')$ and the acceptor $\epsilon^A(\lambda')$ are calculated from excitation spectra of the reference samples. **(C)** Spectra of the FRET sample of interest: The emission spectrum $f_{em}^{DA}(\lambda, \lambda'_D)$ is taken while exciting the donor. The second emission spectrum $f_{em}^{DA}(\lambda, \lambda'_A)$ is taken while exciting the acceptor only. The spectra were taken using a double-stranded DNA substrate containing a Cy3/Cy5-FRET pair (substrate B50R1C3-L1C5) under standard conditions as described in the materials and methods section. **(D)** Calculated spectra for FRET analysis: The emission spectrum $f_{em}^D(\lambda)$ of the donor only reference sample is multiplied by n to be fitted to the emission spectrum of the FRET sample $f_{em}^{DA}(\lambda, \lambda'_D)$ under donor excitation. Subtracting $f_{em}^D(\lambda)$ from $f_{em}^{DA}(\lambda, \lambda'_D)$ yields the extracted acceptor emission spectrum $f_{em}^{A, ext}(\lambda, \lambda'_D)$ of the FRET sample. **(E)** The FRET efficiency is calculated according to equation 2.8. The values are taken from the spectra in figure 2.2A-D (indicated by arrows).

In the first step of data analysis, the fluorescence excitation spectra of the reference samples are normalised through division by the fluorescence intensity at λ'_{\max} , where the excitation of the particular fluorophore peaks. Subsequently, the normalised spectra are multiplied by the molar extinction coefficient ε of the respective fluorophore. The resulting spectra, $\varepsilon^D(\lambda')$ and $\varepsilon^A(\lambda')$ (figure 2.2B), indicate the molar extinction coefficient of the fluorophore at a given wavelength:

$$\varepsilon^D(\lambda') = [f_{exc}^D(\lambda') / f_{exc}^D(\lambda'_{\max})] \cdot \varepsilon^D \quad (2.5)$$

$$\varepsilon^A(\lambda') = [f_{exc}^A(\lambda') / f_{exc}^A(\lambda'_{\max})] \cdot \varepsilon^A \quad (2.6)$$

Next, the fluorescence emission spectrum of the donor alone, $f_{em}^D(\lambda)$, is fitted to each emission spectrum $f_{em}^{DA}(\lambda, \lambda'_D)$ of sample DA measured in the experiment (figure 2.2D). The fitting factor n is found by scaling the emission peak in $f_{em}^D(\lambda)$ to the corresponding emission peak in spectrum $f_{em}^{DA}(\lambda, \lambda'_D)$. Subsequently, the normalised emission spectrum of the donor alone is subtracted from spectrum $f_{em}^{DA}(\lambda, \lambda'_D)$, yielding the extracted emission spectrum of the acceptor, $f_{em}^{A\text{ext}}(\lambda, \lambda'_D)$:

$$f_{em}^{A\text{ext}}(\lambda, \lambda'_D) = f_{em}^{DA}(\lambda, \lambda'_D) - [n \cdot f_{em}^D(\lambda)] \quad (2.7)$$

Finally the FRET efficiency E is calculated for each measurement. Equation 2.8 includes the extinction coefficients of the donor and acceptor at specific excitation wavelengths, which are derived from the reference spectra $\varepsilon^D(\lambda')$ and $\varepsilon^A(\lambda')$. Next, the fluorescence intensity values at the emission peak of the acceptor at λ_A are taken from two spectra of sample DA: $f_{em}^{A\text{ext}}(\lambda, \lambda'_D)$ and $f_{em}^{DA}(\lambda, \lambda'_A)$. With these, the intensity ratio of the extracted acceptor emission spectrum, $f_{em}^{A\text{ext}}(\lambda, \lambda'_D)$, and the emission spectrum under direct acceptor excitation, $f_{em}^{DA}(\lambda, \lambda'_A)$, is calculated at λ_A . Using this ratio corrects the calculated FRET efficiency for the concentration of labelled molecules, the quantum yield of the acceptor and incomplete labelling of the biological molecules with the acceptor fluorophore (Clegg et al. 1992).

$$E = \left(\frac{f_{em}^{A\text{ext}}(\lambda_A, \lambda'_D)}{f_{em}^{DA}(\lambda_A, \lambda'_A)} - \frac{\varepsilon^A(\lambda'_D)}{\varepsilon^A(\lambda'_A)} \right) \cdot \frac{\varepsilon^A(\lambda'_A)}{\varepsilon^D(\lambda'_D)} \quad (2.8)$$

If the fluorescence emission of the acceptor in spectra $f_{em}^{A\ ext}(\lambda, \lambda'_D)$ and $f_{em}^{DA}(\lambda, \lambda'_A)$ is taken at two different wavelengths, λ_{A1} and λ_{A2} , another factor needs to be introduced to correct for the quantum yield of the acceptor at two different wavelengths. This correction factor is the ratio of the fluorescence intensity at λ_{A2} and λ_{A1} in spectrum $f_{em}^A(\lambda)$ of reference sample A:

$$E = \left[\left(\frac{f_{em}^{A\ ext}(\lambda_{A1}, \lambda'_D)}{f_{em}^{DA}(\lambda_{A2}, \lambda'_A)} \cdot \frac{f_{em}^A(\lambda_{A2})}{f_{em}^A(\lambda_{A1})} \right) - \frac{\varepsilon^A(\lambda'_D)}{\varepsilon^A(\lambda'_A)} \right] \cdot \frac{\varepsilon^A(\lambda'_A)}{\varepsilon^D(\lambda'_D)} \quad (2.9)$$

2.4 Single molecule FRET

The motions in the synapse were analysed in single molecules to avoid the detection of a mere average of the overlaid distances and movements in all synapses in solution.

Previously, single molecule FRET techniques have enabled the direct observation of motions in biological complexes, such as protein subunit rotation in the F_0F_1 -ATP synthase (Diez et al. 2004), which shows similarities to the motions in the proposed strand exchange model of serine recombinases.

There are several approaches to studying single molecules using FRET. One method employs a confocal setup to excite and detect fluorescence only from a very small volume (~ 10 fl) within a liquid sample. Statistically, it is most likely to detect only a single molecule at a time if the solution is very dilute. However, a freely diffusing single molecule stays for too short of a time (~ 1 -25 ms) (Eggeling *et al.* 1998) in this volume to observe the relatively slow recombination reaction, which is expected to take up to 500 s. Other methods avoid diffusion by using molecules bound to the surface of a buffer filled reaction chamber. Again, a confocal setup can be used to excite and detect the molecules by moving the focal point and scanning along the surface. This method has a high temporal resolution but bleaches the fluorophores too quickly to follow the complete recombination process. Alternatively, a total internal reflection (TIR) fluorescence microscope setup can be used to excite only an extremely thin layer of molecules on a surface (100-200 nm), reducing background fluorescence dramatically (Roy et al. 2008). These molecules can be analysed using a sensitive CCD camera coupled to the microscope. TIR fluorescence microscopy can enable the simultaneous observation of about 100 molecules for up to two minutes and appears suitable for studying recombination.

For the detection of single molecules, all FRET techniques require the use of bright fluorescent dyes with a high extinction coefficient ($> 50,000 \text{ M}^{-1} \text{ cm}^{-1}$) and high quantum

yield (>0.1) (Roy et al. 2008). Since the fluorophores experience excitation at high light intensities during single-molecule experiments, they need to be very photostable. Additionally, buffer systems have been developed to reduce photobleaching and blinking in popular fluorescent dyes (Aitken et al. 2008). Apart from a spectral overlap of the donor emission and the acceptor excitation which is required for FRET, both dyes should show well separated spectra to reduce crosstalk. Therefore, the acceptor excitation should be minimal at the wavelength of the light source used for donor excitation. Well-separated fluorescence emission spectra of both dyes enable the splitting of donor and acceptor fluorescence using filters and dichroic mirrors. Regarding the biological aspects of single-molecule FRET, the dyes should be water-soluble and be available with chemical groups for conjugation to biological molecules. Several commercial dyes, including Cyanine, Alexa and Atto dyes meet those requirements well (Roy et al. 2008).

2.5 Single-molecule FRET using TIR fluorescence microscopy

TIR fluorescence microscopy utilises an evanescent field of light to excite fluorophores in the sample. The evanescent field decays exponentially with the distance from the reaction vessel's surface and extends only 100-200 nm into the sample. This allows selective excitation of molecules near the surface, including labelled biological molecules attached to the surface, while eliminating fluorescent background from the bulk of the sample solution. To create the evanescent field, the refractive index n_1 of the reaction chamber wall, typically a quartz slide or glass cover slip, needs to be higher than the refractive index n_2 of the sample solution (figure 2.3C). A laser beam is directed through the reaction chamber wall and strikes the sample solution at a large angle θ_1 , i.e. nearly parallel to the interface. Equation 2.10 describes how θ_2 , the angle of the refracted light, depends on the angle of the incident light and the refractive indexes:

$$n_1 \cdot \sin(\theta_1) = n_2 \cdot \sin(\theta_2) \quad (2.10)$$

When the angle of the incident light is increased, the refracted light enters the sample at a greater angle and a higher proportion of the light is reflected. If the angle θ_1 is greater than the critical angle θ_c , the light is refracted at an angle θ_2 greater than 90° , therefore does not enter the sample and is reflected back into the wall of reaction chamber completely:

$$n_1 \cdot \sin(\theta_c) = n_2 \cdot \sin(90^\circ) \Leftrightarrow \theta_c = \arcsin\left(\frac{n_2}{n_1}\right) \quad (2.11)$$

However, an evanescent wave or field extends into the sample medium, since the electromagnetic field has to be continuous at the boundary between both media (figure 2.3C). The wavelength of the evanescent wave is identical to that of the incident light and the evanescent field is strongest within one third of this wavelength from the boundary, decreasing exponentially with distance.

In practice, the evanescent field can be created by directing a laser onto the sample boundary at a large angle using a prism (PTIR) or a high numerical aperture objective (OTIR). For OTIR, a laser beam is focused at the rear focal plane of the microscope objective, exits from the periphery of the objective front lens into immersion oil, passes through a cover slip and strikes the sample boundary at the correct angle (figure 2.3A). The fluorescence light is collected through the same objective, freeing the other side of the reaction chamber for other accessories. In PTIR, a prism is connected to the top side of a thick quartz slide (1-1.5 mm) by immersion oil of a matching refractive index (figure 2.3B). On the bottom side of the quartz slide, the sample is sealed by a cover slip. The prism guides a focused laser beam through the immersion oil and quartz slide onto the sample boundary at a suitable angle. Fluorescent light, emitted by fluorophores on the quartz surface, can exit through the cover slip and is collected from below, through the water immersion objective of an inverted microscope. If desired, buffer injection can be used with PTIR since the quartz slide does not bend under pressure, avoiding loss of the focus during injection.

All experiments in this thesis used a PTIR fluorescence microscope setup based on that of Tan *et al.* (2003). The reaction chambers used in this setup can be built on quartz slides, which need to go through an extensive cleaning process to reduce the fluorescent background (see Material and Methods). The reaction chamber between the quartz slide and glass cover slip can be sealed by sandwiching a cut layer of thermoplastic film or double-sided tape (figure 2.3D/E). Coating the whole reaction chamber with BSA can prevent non-specific binding of molecules, though some proteins might require alternative surface treatment such as polyethylene coating. Using streptavidin, biotinylated biological molecules can be linked to the quartz surface via biotinylated BSA. The sample solution can be filled in or replaced manually through holes in the quartz slides or gaps in the chamber seal. Alternatively, a fluid injection system may enable buffer exchange during the experiment in the PTIR fluorescence microscope.

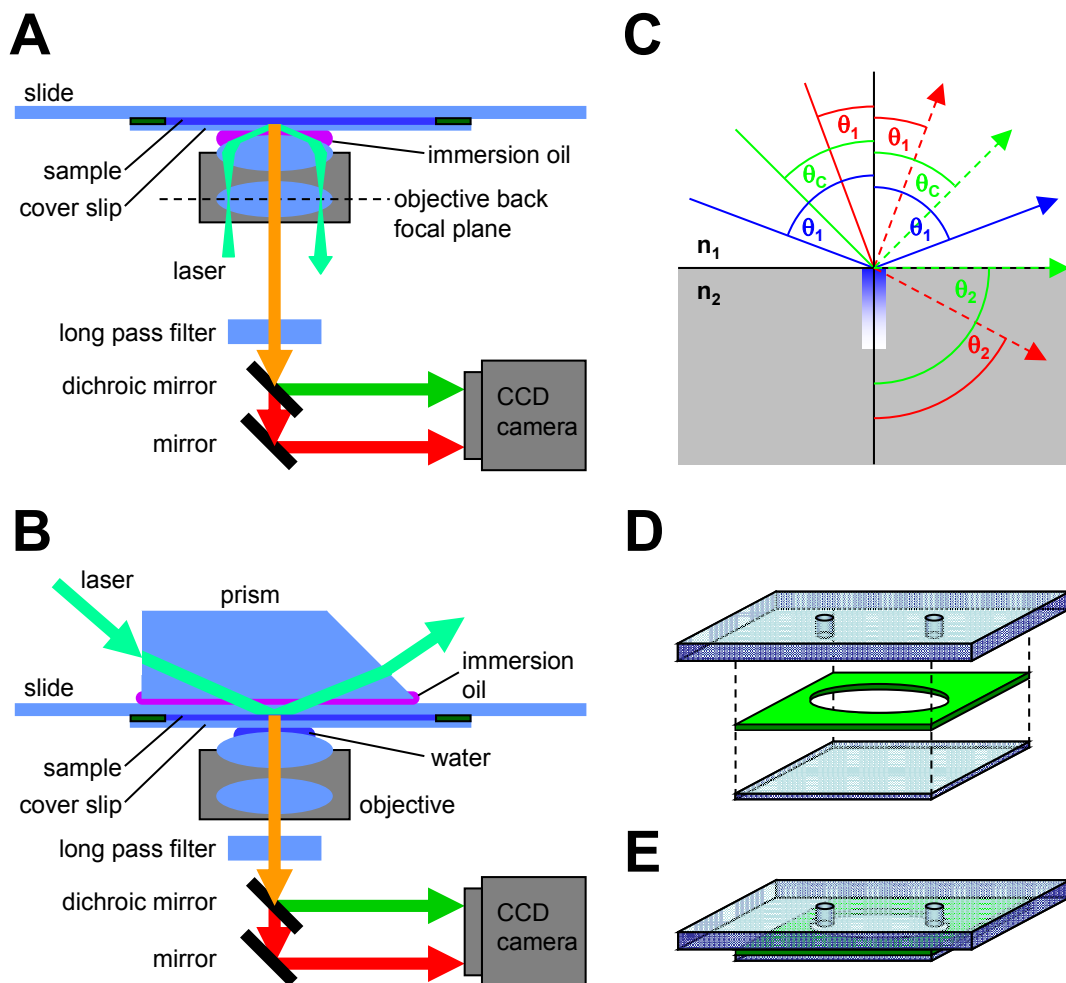


Figure 2.3: Single-molecule fluorescence using TIR setups. (A) OTIR setups use the same objective to collect the fluorescence (orange) and to guide the excitation laser to the interface between the sample and the cover slip at a great angle. An evanescent field extends 100-200 nm from the interface into the sample, allowing selective excitation of fluorescent molecules bound to the surface of the cover slip. A dichroic mirror splits separates donor (green) and acceptor (red) fluorescence before detection with a CCD camera. (B) PTIR setups use a prism to guide the laser at a great angle to the interface between the sample and the quartz slide. The evanescent field extends ~100-200 nm from the interface into the sample, allowing the selective detection of fluorescent molecules bound to the quartz surface. The fluorescence is collected through an objective below the chamber and detected as in OTIR setups. (C) Light passing from a medium with a low refractive index (n_1) into a medium with high refractive index (n_2) at the angle θ_1 is refracted at the angle θ_2 . At a low angle θ_1 (red), the light is partially reflected at the same angle and partially enters the second medium at a lower angle θ_2 . Light striking the interface at the critical angle θ_c (green) is refracted at 90° , does therefore not enter the second medium and is reflected. Light striking the interface at an angle greater than θ_c (blue) is reflected completely. However, an evanescent field (blue gradient) with the same wavelength extends into the second medium, decaying exponentially with the distance from the interface. (D) A typical reaction chamber for PTIR setups is formed by sandwiching a cut layer of thermoplastic film or double-sided tape (green) between a quartz slide (top) and a cover slip (bottom). (E) The assembled reaction chamber can be filled with samples via two holes in the quartz slide.

After collection of the fluorescence light through the objective of a TIR setup, any scattered laser light needs to be removed by a long pass filter, which allows only light of wavelengths longer than that of the laser to pass (figure 2.3A/B). The remaining fluorescence light is masked by a slit, selecting a small region of the imaged area. A dichroic mirror then splits the fluorescence into light of the spectral range of the donor and acceptor. Finally, a CCD camera detects the image of donor and acceptor fluorescence on two neighbouring areas of the camera's chip. By doing this, the same area on the reaction chamber surface is filmed twice with the same chip, resulting in a movie with the image of the donor fluorescence next to the image of acceptor fluorescence (figure 2.4A). Modern, cooled CCD cameras are sensitive enough to detect single fluorophores and can acquire the fluorescence images at rates up to 125 Hz with low effective readout noise (Roy et al. 2008).

The fluorescent molecules in the recorded movies are located using specialised software and their locations in the donor and acceptor images are matched (figure 2.4B). This can be facilitated by calibrating the software with the positions of extremely bright fluorescent micro-spheres. For every identified fluorescent molecule in the image area, the donor and acceptor fluorescence intensity is taken from each frame of the donor and acceptor images. After background subtraction, the molecules' donor fluorescence intensity, I_D , and acceptor fluorescence intensity, I_A , is traced over time (figure 2.4C). With these data, a time trace of the apparent FRET efficiency E_{app} can be calculated according to equation 2.12 (Roy et al. 2008):

$$E_{app} = \frac{I_A}{I_A + I_D} \quad (2.12)$$

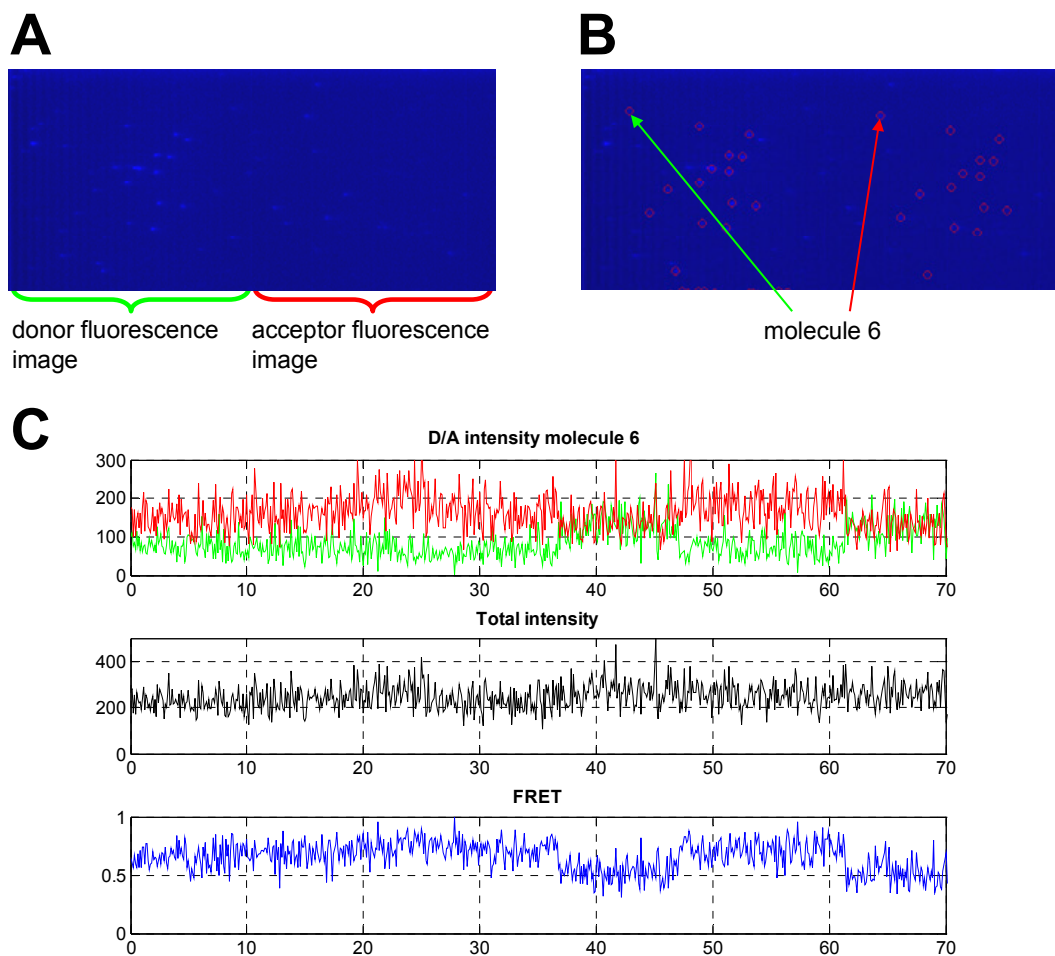


Figure 2.4: Single-molecule FRET traces. (A) Two images of the same area of the quartz surface are recorded side by side. The left half of the frame is the image of the filtered donor fluorescence, the right half is the image of the filtered acceptor fluorescence. For these images, a movie of surface bound complexes with Cy3 and Cy5 dyes was recorded and all frames were averaged over time. (B) Single molecules are identified automatically using software. Their position in the donor and acceptor images is matched and marked with red circles. (C) The intensity of the donor (green) and acceptor (red) fluorescence within the circled area of each molecule, in each frame of the movie, is traced over time. This trace can be converted into traces of the total fluorescence intensity (black) or apparent FRET efficiency (blue).

The trace of the FRET efficiency and a trace of the total fluorescence intensity can be used to identify genuine single molecules with both one donor and one acceptor fluorophore. Software can be used to filter out suspicious molecules with extremely high or low fluorescence or without any acceptor fluorescence in the first frames (~10 frames). Further manual inspection of the traces can check for constant total fluorescence intensity until blinking or photo-bleaching occurs. For example, photo-bleaching of the acceptor towards the end of the trace should reduce the acceptor fluorescence completely to the baseline. At the same time the donor fluorescence, due to the lack of a FRET acceptor, should reach the maximum, keeping the total fluorescence at a stable level. For all genuine single molecules, different FRET states may be identified. Eventually, analysis of the life-time of those states and the changes from one state to another can be used to characterise the heterogeneous population and dynamics of the biological molecules being studied.

3 Materials and Methods

3.1 Chemicals

Double-distilled water (ddH₂O) was used to prepare all solution unless stated otherwise. Chemicals were purchased from the companies listed below.

Chemicals	Source
General chemicals, biochemicals, organic solvents	Sigma/Aldrich, Invitrogen, GE Healthcare (including Amersham Biosciences),
Media	Difco, Oxoid
Agarose, Acrylamide	FMC, Biorad, Flowgen, Sigma/Aldrich
Restriction enzymes and buffers	NEB

Table 3.1: Chemicals

3.2 Bacterial growth media

Liquid cultures of *E. coli* were grown in L-Broth (10 g bacto-tryptone, 5 g bacto-yeast extract and 5 g NaCl ad 1litre ddH₂O, pH adjusted to 7.5 with NaOH). On solid medium, *E. coli* was cultured on L-agar (L-Broth with 15 g/l agar). All growth media were sterilised at 120 °C for 15 minutes.

3.3 Bacterial strains

The bacterial strain used in this project was a derivative of *Escherichia coli* K12. The strain is called BL21 (DE3) pLysS and is sourced from Studier et al. (1990). The genotype of the strain is: hsd, gal, (lcl ts 857, ind1, Sam7, ini5, lacUV5-T7 gene-1), T7 lysozyme-expressing plasmid pLysS. This strain is resistant to chloramphenicol.

3.4 Plasmids

Following plasmids were used in this project:

plasmid name	antibiotic resistance	description	source
pSA1101	kanamycin	Wild-type Tn3 resolvase overexpression plasmid, T7 promoter	(Arnold <i>et al.</i> 1999)
pFO102	kanamycin	Tn3 resolvase NM overexpression plasmid, T7 promoter, derived from pSA1101	(Olorunniji 2006)
pFO1	kanamycin	Tn3 resolvase NM-S10A overexpression plasmid, T7 promoter, derived from pSA1101	(Olorunniji 2006)
pMP129	chloramphenicol tetracycline	encodes a Z-resolvase mutant, contains no specific binding sites for resolvase	(Prorocic 2009)

Table 3.2: Plasmids

3.5 Oligonucleotides

Simple oligonucleotides were purchased from MWG-Biotechnology (Germany) while oligonucleotides with amino-modified thymines or fluorescein labels were purchased from the W.M. Keck Oligonucleotide Synthesis Facility (USA).

3.5.1 Oligonucleotides for single-site substrates

The following oligonucleotides were used to anneal single-site substrates. Some of these contained an amino-modified thymine used for the attachment of a Cy3 or Cy5 dye. The modifications and sequence features are represented as follows:

B = 5'-biotin
X = amino modified thymine with C2-linker
bold = Tn3 res site I sequence
blue = central overlap of Tn3 res site I

Name: B50 (top strand)
5'-BCGTGACTCAAC**CGTTTCGAAATATT**ATAAATTATCAGACATAGTGGGGCGG-3'

Name: B50L5 (top strand)
5'-BCGTGACTCAAC**CGTTTCGAAAXATT**ATAAATTATCAGACATAGTGGGGCGG-3'

Name: B50L2 (top strand)
5'-BCGTGACTCAAC**CGTTTCGAAATATX**ATAAATTATCAGACATAGTGGGGCGG-3'

Name: B50R1 (top strand)
5'-BCGTGACTCAAC**CGTTTCGAAATATT**AXAAATTATCAGACATAGTGGGGCGG-3'

Name: B50R5 (top strand)
5'-BCGTGACTCAAC**CGTTTCGAAATATT**ATAAAXTATCAGACATAGTGGGGCGG-3'

Name: 50 (bottom strand)
5'-CCGCCCCACTAT**TGTCTGATAATTT**ATAATATTT**CGAAC**GTTGAGTCACG-3'

Name: 50L16 (bottom strand)
 5'-CCGCCCCACTAT**TGTCTGATAATTT****ATA**AATATTT**CGAACG**GXTGAGTCACG-3'

Name: 50L6 (bottom strand)
 5'-CCGCCCCACTAT**TGTCTGATAATTT****ATA**AATAXTT**CGAACG**GTTGAGTCACG-3'

Name: 50L1 (bottom strand)
 5'-CCGCCCCACTAT**TGTCTGATAATTT****AX**AATATTT**CGAACG**GTTGAGTCACG-3'

Name: 50R2 (bottom strand)
 5'-CCGCCCCACTAT**TGTCTGATAATT****XATA**AATATTT**CGAACG**GTTGAGTCACG-3'

Name: 50R4 (bottom strand)
 5'-CCGCCCCACTAT**TGTCTGATAAXTT****ATA**AATATTT**CGAACG**GTTGAGTCACG-3'

Name: 70RR (top strand)
 5'-GGCAAGCTTGCGTGACTCAAC**TGTCTGATAATTT****ATAAATTATCAGACA**TAGTGGGATGGTC-
 TGCAGCGG-3'

Name: 70RR (bottom strand)
 5'-CCGCTGCAGACCATCCCACTAT**TGTCTGATAATTT****ATAAATTATCAGACA**GTTGAGTCACGCA-
 AGCTTGCC-3'

Name: 80LR (top strand)
 5'-GGCAAGCCAGCGTTGCGTGACTCAAC**CGTTCGAAATATT****ATAAATTATCAGACA**TAGTGGGA-
 TGGTCTAGGCCGAGCGG-3'

Name: 80LR (bottom strand)
 5'-CCGCTGCGGCCTAGACCATCCCACTAT**TGTCTGATAATTT****ATAAATTTT****CGAACG**GTTGAGTC-
 ACGCAACGCTGGCTTGCC-3'

3.5.2 Oligonucleotides for U-shaped substrates

The following oligonucleotides were used to anneal U-shaped substrates. Some of these contained an amino-modified thymine used for the attachment of a Cy3 or Cy5 dye while others contain a fluorescein label. The modifications and sequence features are represented as follows:

B = 5'-biotin
 X = amino modified thymine with C2-linker
 F = fluorescein (6-FAM)
bold = Tn3 *res* site I sequence
blue = central overlap of Tn3 *res* site I

Name: L30 (linker)
 5'-CGGGGCGGGATCCTGGTTTTTTTTTTTTTTTTTTTTTTTTTTTTTTTTTTGGGACGCGTTGGGGCC-3'

Name: L40 (linker)
 5'-CGGGGCGGGATCCTGGTT-
 GGGACGCGTTGGGGCC-3'

Name: L50 (linker)
 5'-CGGGGCGGGATCCTGGTT-
 GGGACGCGTTGGGGCC-3'

Name: BXT53 (X-arm top strand)
 5'-BGGGTCCGTGACTCAAC**CGTTCGAAATATT****ATAAATTATCAGACA**GTGGGGTGG-3'

Name: BXT53R5 (X-arm top strand)
 5'-BGGGTCCGTGACTCAAC**CGTTCGAAATATT****ATAAAXTATCAGACA**GTGGGGTGG-3'

Name: XB69 (X-arm bottom strand)
 5'-CCAGGATCCCGCCCGCCACCCAC**TG**CTCTGATAATTT**ATA**AATATTT**CGA**ACGGTTGAGT-CACGGACCC-3'

Name: YT57 (Y-arm top strand)
 5'-CGCC**CG**TT**CGA**AAATATT**ATA**AATTATCAGACACCTCACCCCGGCCCAACGCGTCCC-3'

Name: FYT57 (Y-arm top strand)
 5'-FCGCC**CG**TT**CGA**AAATATT**ATA**AATTATCAGACACCTCACCCCGGCCCAACGCGTCCC-3'

Name: YB41 (Y-arm bottom strand)
 5'-GGGGTGAGG**TG**CTCTGATAATTT**ATA**AATATTT**CGA**ACGGGCG-3'

Name: YB41L6 (Y-arm bottom strand)
 5'-GGGGTGAGG**TG**CTCTGATAATTT**ATA**ATAXTT**CGA**ACGGGCG-3'

3.6 Molecular graphics

Images of crystal structures were produced using the computer program PyMOL (DeLano 2006). The chemical structure of the Cy3 and Cy5 dyes was converted into the SMILE format using the computer program CS ChemDraw Std (CambridgeSoft Corporation). The formatted chemical structures were loaded into a demo version of the computer program CORINA (Sadowski *et al.* 1994; Sadowski *et al.* 2008) to compute the three-dimensional structure of the dyes. Using the program PyMOL, the three-dimensional structures of the dyes were inserted into to the crystal structure of the cleaved synapse of $\gamma\delta$ resolvase (Li *et al.* 2005) attaching the dyes to thymines in the site I substrate.

3.7 Preparation of chemically competent cells

5 ml of L-broth with 25 μ g/ml chloramphenicol were inoculated with a swab from a glycerol stock of *E.coli* BL21 (DE3) pLysS and incubated in a shaker (New Brunswick Scientific Excella E24 Incubator Shaker, 250 rpm, 37 °C, ~3 h) until slightly cloudy. The culture was then chilled on ice and divided into aliquots of 1.25 ml in plastic reaction tubes. The cells were harvested by centrifugation (9,300 g, 4 °C, 1 min) and the supernatant was removed. The pellet containing the cells was resuspended in 1 ml of chilled (on ice) 50 mM CaCl₂ and centrifugation was repeated. The supernatant was removed and the pellet was resuspended in 200 μ l of chilled 50 mM CaCl₂. The suspension of these competent cells was stored on ice and transformed on the same day.

3.8 Transformation of chemically competent cells

0.01-1 μ g of plasmid DNA was added to 200 μ l of competent cells and the sample was mixed by gentle pipetting. The samples were then stored on ice for 20 minutes before they were “heat shocked” by heating to 42 °C in a water bath for 2 minutes. The samples were

allowed to rest on ice for 5 minutes before adding 1 ml of L-broth without any antibiotics. The cell suspension was shaken (Eppendorf Thermomixer, 37 °C, 600 rpm, 1.5 h) and the cells were harvested by centrifugation (9,300 g, room temperature, 1 min). The pellet was resuspended in 100 µl of L-broth (no antibiotics) by pipetting. The cell suspension was then plated on L-agar plates containing the appropriate antibiotics.

3.9 Purification of Tn3 resolvase

Wild-type Tn3 resolvase and mutant versions were purified similarly and according to a method adapted from Olorunniji (2006).

3.9.1 Overexpression of Tn3 resolvase

Wild-type Tn3 resolvase, hyperactive Tn3 resolvase NM and inactive Tn3 resolvase NM-S10A were overexpressed in *E.coli* BL21 (DE3) pLysS.

Versions of *E.coli* BL21 (DE3) pLysS carrying the plasmid pFO102 for Tn3 resolvase NM overexpression or the plasmid pFO1 for Tn3 resolvase NM-S10A overexpression were readily available as glycerol stocks. Swabs of the glycerol stocks were incubated in 5 ml of L-broth (25 µg/ml chloramphenicol, 50 µg/ml kanamycin) in a shaker (New Brunswick Scientific Excella E24 Incubator Shaker, 250 rpm, 37 °C, overnight).

Chemically competent *E.coli* BL21 (DE3) pLysS cells were transformed with the plasmid pFO1 for the overexpression of wild-type Tn3 resolvase. The transformation samples were plated on L-agar plates (25 µg/ml chloramphenicol, 50 µg/ml kanamycin). Swabs of colonies of successfully transformed cells were taken with sterile toothpicks and incubated in 5 ml of L-broth (25 µg/ml chloramphenicol, 50 µg/ml kanamycin) in a shaker (New Brunswick Scientific Excella E24 Incubator Shaker, 250 rpm, 37 °C, overnight).

For the overexpression of each protein, two or four 2 litre flasks (2 flasks for wild-type Tn3 resolvase and Tn3 resolvase NM-S10A, 4 flasks for Tn3 resolvase NM) with 400 ml L-broth (25 µg/ml chloramphenicol, 50 µg/ml kanamycin) were pre-warmed to 37 °C. Each flask was inoculated with 4 ml of an overnight culture (see above) of the appropriate strain and the cultures were incubated in a flat-bed shaker (225 rpm, 37 °C, 2 h). Subsequently, expression was induced by adding 400 µl of 1M Isopropyl β-D-1-thiogalactopyranoside (IPTG) to each flask and incubation was continued for three more hours. The cells were harvested by centrifugation (Beckman Coulter JA-14 rotor, 9,000

rpm, 4 °C, 5 min), the supernatant was removed and the cell pellets were stored at -20 °C until extraction.

3.9.2 Buffers for the extraction and purification of Tn3 resolvase

The buffers used during the extraction and purification of Tn3 resolvase and its mutant versions are listed below. All stock solutions for the preparation of the buffers were filtered. DTT and PMSF were added to the buffers immediately before use.

protein purification buffer	ingredients
resuspension buffer	20 mM Tris-HCl pH 7.5, 10 mM MgCl ₂ , 1 mM DTT, 0.1 mM EDTA, 1.2 mM PMSF, 1.2% v/v ethanol
wash buffer	20 mM Tris-HCl pH 7.5, 10 mM MgCl ₂ , 1 mM DTT, 0.1 mM EDTA, 1.2 mM PMSF, 1.2% v/v ethanol, 100 mM NaCl
solubilisation buffer	20 mM Tris-HCl pH 7.5, 1 mM DTT, 0.1 mM EDTA, 1.2 mM PMSF, 1.2% v/v ethanol, 1 M NaCl
refolding buffer I	20 mM Tris-HCl pH 7.5, 1 mM DTT, 0.1 mM EDTA, 1.2 mM PMSF, 1.2% v/v ethanol, 2 M NaCl
precipitation buffer	20 mM Tris-HCl pH 7.5, 10 mM MgCl ₂ , 1 mM DTT, 0.1 mM EDTA, 1.2 mM PMSF, 1.2% v/v ethanol
buffer A	50 mM sodium phosphate pH 7.2, 0.1 mM DTT, 0.1 mM EDTA, 6 M Urea, 25 mM NaCl
buffer B	50 mM sodium phosphate pH 7.2, 0.1 mM DTT, 0.1 mM EDTA, 6 M Urea, 1 M NaCl
refolding buffer II	20 mM Tris-HCl pH 7.5, 1 mM DTT, 0.1 mM EDTA, 2 M NaCl
resolvase dilution buffer (RDB)	10 mM Tris-HCl pH 7.5, 5 mM DTT, 0.2 mM EDTA, 50% v/v glycerol, 1 M NaCl

Table 3.3 Protein purification buffers

3.9.3 Extraction and purification of Tn3 resolvase

The purification of Tn3 resolvase and its mutant versions utilises the fact that the solubility of resolvase is different from many other proteins. Tn3 resolvase is soluble in buffers with a high NaCl concentration and insoluble in buffers with low salt concentrations while most other proteins show the opposite behaviour.

During the whole extraction and purification process, the samples were either kept on ice or at 4 °C unless stated otherwise. Small samples for were taken at various steps to assess the purification process by discontinuous SDS PAGE.

Two pellets of cells (~ 1 g/pellet) harvested from 800 ml culture (2 pellet of wild-type Tn3R, 1 pellet of Tn3R NM-S10A, 2 pellets of Tn3R NM) were resuspended in 25 ml of resuspension buffer by pipetting with a 25 ml plastic pipette. The suspension was then sonicated at 40% amplitude in three bursts of 20 seconds while cooling the suspension on

ice for two minutes between bursts. The suspension was centrifuged (Beckman Coulter JA-20 rotor, 20,000 rpm, 4 °C, 10 min) and the supernatant was removed.

To remove proteins which are soluble at low salt concentrations, the pellet was resuspended in 10 ml of wash buffer using a 25 ml plastic pipette. The resulting suspension was homogenised (~100 strokes) in a Dounce homogeniser and centrifuged (Beckman Coulter JA-20 rotor, 20,000 rpm, 4 °C, 10 min). The resuspension, homogenisation and centrifugation steps were then repeated four times.

The pellet from the wash step was resuspended in 10 ml solubilisation buffer using a 10 ml plastic pipette and homogenised in a Dounce homogeniser (~50-100 strokes). Residual insoluble debris was removed by centrifugation (Beckman Coulter JA-20 rotor, 20,000 rpm, 4 °C, 10 min). The supernatant was dialysed against 3 L of refolding buffer I overnight. No visible precipitate was formed by proteins which are insoluble at high salt concentrations and a further centrifugation step was not necessary. The solution dialysed against 3 L of precipitation buffer overnight forming a white precipitate. The precipitate was harvested by centrifugation (Beckman Coulter JA-20 rotor, 20,000 rpm, 4 °C, 15 min) and the supernatant was removed.

The pellet was resuspended in 10 ml of buffer A by pipetting, vortexing and squeezing through the wide needle of a 10 ml plastic syringe at room temperature for ~30 minutes. Residual debris was removed by centrifugation (Beckman Coulter JA-20 rotor, 20,000 rpm, 4 °C, 15 min) and the supernatant was purified by ion-exchange chromatography. A 1 ml cation exchange SP sepharose column (HiTrap SP High Performance pre-packed column, GE Healthcare) was used to remove DNA and negatively charged proteins which are repelled by the column, while retaining the positively charged resolvase which is tightly bound. The column was connected to an Äkta purifier (Amersham Biosciences) and the absorbance of the liquid exiting the column was recorded at 280, 260 and 215 nm. After equilibrating the column with 10-20 ml buffer A, 10 ml of protein solution were loaded using a super-loop. The column was then washed with 10-20 ml buffer A before eluting proteins using a linear buffer gradient from low to high salt concentrations (from 100% v/v buffer A to a 1:1 mixture of buffer A and buffer B within twenty minutes at a flow rate of 1 ml/min). Fractions of 0.5 ml were collected and stored at -20 °C. A small aliquot of each fraction was analysed by discontinuous SDS PAGE.

Suitable chromatography fractions were combined and dialysed against 3 L of refolding buffer II overnight. Finally, the solutions were dialysed against 1-3 L of resolvase dilution

buffer (RDB) overnight, transferred to nunc tubes (Thermo Scientific) and stored at -20 °C. The concentration of the purified resolvase was determined by photometric and gel-based methods.

3.9.4 Photometric determination of the concentration of resolvase

For the photometric determination of the resolvase concentration, the absorption spectrum of a small aliquot (μl) of the resolvase solution was measured and baseline corrected (see: measurement of absorption spectra). The concentration was calculated from the absorption at 280 nm using the extinction coefficient of the particular resolvase mutant as predicted by the ProtParam tool (Gasteiger *et al.* 2005).

3.9.5 Gel-based determination of the concentration of resolvase

The concentration was determined by analysing the band formed by resolvase on a discontinuous SDS polyacrylamide gel stained with Coomassie blue. The bands formed by a series of dilutions of the resolvase mutant of interest were compared to the bands of a dilution series of a resolvase with known concentration. One approach was to compare the bands by eye and estimate the concentration of the resolvase solution. In a second approach, a greyscale scan of the stained SDS gel was acquired (Epson) and a digital photograph of the stained gel on a transilluminator (white light) was taken. The red channel of the digital picture (RGB colours) of the gel on the transilluminator was extracted using the graphics program Corel PHOTO-PAINT 11 (Corel Corporation). This improved the band intensity and decreased the background since the Coomassie stain absorbs more red light than blue or green light. Then the greyscale scan and transilluminator image (red channel) were inverted and converted into the TIFF file format. The TIFF images were then analysed using the ImageGauge software (Fujifilm) and the intensity of the resolvase bands was quantified. The intensity (I) of the resolvase bands was plotted against d, the dilution of the resolvase solution.

$$d = c_{\text{diluted}}(\text{resolvase}) / c_{\text{undiluted}}(\text{resolvase})$$

For the dilution series of resolvase solutions with an unknown concentration ($c_{\text{undiluted}}$), a linear regression of the plot of the band intensity (I) against the dilution (d) yielded the factor m:

$$I = m \cdot d$$

For the dilution series of a resolvase solution with a known concentration ($c_{undiluted}$), the factor m yielded the factor f :

$$f = m / c_{undiluted} (undiluted)$$

With the factor f known, the concentration of the other resolvase solutions was calculated from the linear regression of plot of the band intensity against the dilution:

$$c_{undiluted} (resolvase) = m / f$$

3.9.6 Nuclease activity assay for resolvase preparations

The purified resolvase solution was tested for nuclease activity by incubation with the plasmid pMP129, which does not contain any parts of the Tn3 res site. The assay samples contained 50 mM Tris-HCl, ~17 µg/ml pMP129, 10 mM MgCl₂, 10% v/v resolvase dilution buffer (see: Buffers for the extraction and purification of Tn3 resolvase) and 1.85-2.3 µM purified resolvase. The samples were incubated at 37 °C for 10 hours and analysed by agarose gel electrophoresis.

3.10 Oligonucleotide methods

All purification and modification steps for oligonucleotides were performed in W. Marshall Stark's laboratory.

3.10.1 Conjugation of fluorophores to amino-modified oligonucleotides

Oligonucleotides containing amino-modified thymines were redissolved in ddH₂O at ~1-2 mM, as estimated from the synthesis reports. Organic contaminations were removed from the oligonucleotide solution by Chloroform extraction. The oligonucleotide solution was vortexed with 0.5-1 volume of neutralised chloroform. The mixture was then centrifuged (16.110 g, 2 min) and the upper aqueous phase containing the oligonucleotide was collected. Three chloroform extractions were performed before removing further contaminations (especially those containing amine groups) by two sequential ethanol precipitations. The oligonucleotide was redissolved in ddH₂O at ~1-2 mM.

The conjugation of Cy3 or Cy5 dye to the oligonucleotides was usually performed at a scale of 5 or 10 nmol of the oligonucleotide and exposure to light was minimised during the whole process. The Cy3- or Cy5 Mono NHS esters (Amersham/GE Healthcare) were dissolved in dried dimethyl sulfoxide (DMSO) at 18 mg/ml immediately before use. The

final mixture of the conjugation reaction contained, unless stated otherwise, 100-200 μM amino-modified oligonucleotide, 2.5 mg/ml dye Mono NHS ester, 75 mM tetraborate pH 8.5 and 14% v/v DMSO (from the dissolved dye Mono NHS ester). In early test reactions, the tetraborate pH 8.5 (75 mM) was replaced by either tetraborate pH 8.5 (62 mM), carbonate pH 8.5 (62 mM) or carbonate pH 9.0 (62 mM). Later conjugation reaction contained up to 5 mg/ml dye Mono NHS ester when extra amounts of the dye were available. Unless stated otherwise, the reaction mixture was incubated with shaking at (500-1,000 rpm, room temperature, overnight).

3.10.2 *Radioactive labelling of single-site substrates*

Radioactive single-site substrates were produced by labelling the bottom strand oligonucleotide with $\gamma^{32}\text{P}$ using kinase and $\gamma^{32}\text{P}$ -ATP. The bottom strand was chosen since many top strand oligonucleotides carry a 5'-biotin which prevents phosphorylation by kinase.

In each reaction, 5 or 10 pmol of an oligonucleotide were labelled with an amount of $\gamma^{32}\text{P}$ -ATP that is equivalent to 5 or 10 μCi . The reaction mixture contained the oligonucleotide (0.2 μM), $\gamma^{32}\text{P}$ -ATP (0.2 $\mu\text{Ci}/\mu\text{l}$ at 3,000 Ci/mmol), kinase (1 U/ μl), Tris-HCl pH 7.5 (50 mM), MgCl_2 (10 mM), DTT (5 mM), spermidine (0.1 mM) and EDTA (0.1 mM). The kinase was added to the reaction mixture last before the samples were incubated at 37 °C for 30-60 minutes. The labelling reaction was stopped by heating to 75 °C for 10 minutes.

The oligonucleotide was separated from excess $\gamma^{32}\text{P}$ -ATP using a Quick Spin column (Sephadex G-25, Roche) according to the instructions of the manufacturer. Subsequently the oligonucleotide was purified by phenol/chloroform extraction according to Sambrook and Russell (Sambrook and Russell 2001). The extracted oligonucleotide was then annealed with a 1.2 fold molar excess of the top strand to form a single-site substrate. Finally, the annealed radioactive substrate was concentrated and purified by ethanol precipitation.

3.10.3 *Purification of non-fluorescent oligonucleotides*

Simple oligonucleotides without amino-modified thymine were purified as follows. The oligonucleotides were dissolved in ddH₂O and purified by denaturing polyacrylamide gel electrophoresis. The bands were visualised by staining with cationic carbocyanine “stains-all” dye (Aldrich). The polyacrylamide gel was soaked in a staining solution (70 ml of ddH₂O, 20 ml isopropanol, 10 ml of 0.1% w/v ‘stains-all’ solution in formamide) for ~10 minutes until sufficient staining was observed. Subsequently the gel was destained by

rinsing it several times in ddH₂O. The bands containing the full-size oligonucleotide were cut out using a scalpel. The oligonucleotides were then extracted from the gel pieces using the “crush and soak” method.

If necessary, the solution of the extracted oligonucleotide was concentrated using a “speedy-vac” concentrator. The oligonucleotide was then purified and concentrated by ethanol precipitation and redissolved in ddH₂O or 10 mM Tris-HCl buffer (pH 7.5). If necessary, the ethanol precipitation was repeated.

3.10.4 *Purification of fluorescent oligos*

Fluorescent oligonucleotides were purified similar to non-fluorescent oligos, but exposure to light was minimised throughout the process. After the conjugation reaction, the excess of non-conjugated fluorophores was removed by ethanol precipitation unless stated otherwise. In earlier test reactions, the excess of fluorophores was removed with an illustra NAP-5 desalting column (GE healthcare) according to the manufacturer’s instructions using 5% v/v DMSO for equilibration and elution. The NAP-5 eluate was concentrated by ethanol precipitation.

The fluorescent oligonucleotides were then purified by denaturing polyacrylamide gel electrophoresis using gels with high acrylamide content (18% w/v). The full-length oligonucleotide containing a fluorophore formed the band with the highest retardation. Due to the attached fluorophore, this band could readily be seen and was cut out in low levels of ambient lighting. To check the gel purification process, the remaining bands were stained with ethidium bromide and visualised using a UV transilluminator.

The fluorescent oligo was then extracted and concentrated in the same way as non-fluorescent oligonucleotides. To assess the purity of the purified fluorescent oligonucleotides, a fraction of the oligonucleotide solution was analysed by gel electrophoresis using a denaturing polyacrylamide gel with a high acrylamide content (18% w/v) electrophoresis. The purity of the fluorescent oligonucleotide was also tested photometrically.

3.10.5 *Photometric determination of the concentration of oligonucleotide solutions*

A spectrum of the diluted or undiluted oligonucleotide solution was recorded and baseline (see: Measurement of absorption spectra). The concentration of the oligonucleotide was

then calculated from the absorption at 260 nm using the extinction coefficient predicted by the OligoCalc tool (Kibbe 2007).

3.10.6 *Photometric estimation of the purity of fluorescent oligonucleotides*

The absorption spectra of the oligonucleotide solution (see: Measurement of absorption spectra) were analysed to test if the molar ratio of the oligonucleotide and the fluorophore was 1:1, as expected for completely labelled, pure oligonucleotides.

The fluorophores absorb light strongly at their absorption maximum at relatively long wavelengths. Using the extinction coefficient of the fluorophore, its molar concentration can be calculated. However, the fluorophores also show weak absorption at 260 nm. The A_{260}/A_{max} ratio, the ratio of the fluorophore absorption at 260 nm and at the absorption maximum of the fluorophore, was determined from an absorption spectrum of the fluorophore alone. For samples of fluorescent oligonucleotides, the contribution of the fluorophore to the absorption at 260 nm was calculated by multiplying the absorption of the fluorophore at its absorption maximum with the A_{260}/A_{max} of the fluorophore. This allowed the extraction of the absorption of the DNA alone at 260 nm by subtracting the fluorophore contribution from the total absorption at 260 nm. The concentration of the oligonucleotide was then calculated using its extinction coefficient at 260 nm as predicted by the OligoCalc tool (Kibbe 2007).

Finally, the molar ratio of the oligonucleotide and the fluorophore was calculated. This ratio was indeed found to be close to one for fluorescent oligonucleotides which were found to be pure in gel based assays.

3.11 “Crush and soak” extraction of DNA from polyacrylamide gel pieces

DNA was extracted from polyacrylamide gel pieces by crushing the gel pieces from 2-5 lanes in an eppendorf tube with a glass rod. 600 μl of ddH₂O were then added to each tube. Optionally, the grain size of the crushed gel pieces was decreased in an additional step by squeezing the gel piece suspension out of a 1 ml plastic syringe while pressing the syringe against the bottom of the eppendorf tube. The suspension was shaken (Eppendorf Thermomixer, 1,400 rpm, 37 °C, overnight) and the gel pieces were removed by centrifugation (16,000 g, 2-5 min). Residual gel pieces were removed from the supernatant by centrifugation (9,300 g, 10-30 min) in Costar Spin-X tube filter (Sigma-Aldrich, cellulose acetate, 0.22 μm pore size).

Annealed U-shaped substrates were extracted using 200 mM NaCl solution instead of ddH₂O.

3.12 Ethanol precipitation of DNA

DNA was precipitated DNA solutions by adding 0.05 volumes of 4 M NaCl solution followed by thorough mixing and cooling on ice. Then 2.5 volumes of ice-cold ethanol (100% v/v) were added, followed by thorough mixing. The samples were then kept on ice for at least 30 minutes followed by cooling to -20 °C for at least one hour. The samples were then spun at in a table centrifuge at maximum speed at 0-4 °C for at least 45 minutes. The supernatant was removed and ice-cold ethanol (70-80% v/v) was added to the DNA pellet to wash it. If the DNA contained fluorophores, 70% v/v ethanol was preferred for washing the pellet since the fluorophores increased the solubility of the oligonucleotide in ethanol. The samples were then spun at maximum speed at 0-4 °C for about 10-30 minutes. The supernatant was removed and the pellet was dried at the air for 5-15 minutes or by using a “speedy-vac” for 1-2 minutes. The DNA pellet was redissolved in ddH₂O or in 10 mM Tris-HCl pH 7.5.

Annealed and gel purified U-shaped substrates were precipitated similar to other DNA. However, the pellet was washed with a solution containing 100 mM NaCl and 80% v/v ethanol to prevent melting of the double-stranded regions. After the ethanol precipitation, the substrates were redissolved in a buffer containing 20 mM NaCl and 10 mM Tris-HCl pH 7.5 to stabilise the substrate.

Radioactively labelled, double-stranded DNA was precipitated similarly as to other DNA. The only difference was the addition of 0.1 volumes of 5 M ammonium acetate solution instead of 0.05 volumes of 4 M NaCl solution to facilitate precipitation.

3.13 Measurement of absorption spectra

The absorption of sample solutions was measured using either a TrayCell (Hellma, UK) in a Lambda 45 UV/visible spectrophotometer or a NanoDrop 1000 spectrophotometer (Thermo Scientific). Both methods allow measurements using only a small sample volume. In addition, samples with a high absorbance can be measured using these methods, eliminating in most cases the need for dilution of the sample and related inaccuracies. An absorption spectrum of the sample was measured over a range of wavelengths, usually 220-800 nm or 220-1000 nm. The absorption spectrum of the sample buffer alone was measured as well. The buffer spectrum was then subtracted from the spectrum of the sample solution. Further, the baseline of the sample spectrum was corrected by subtracting

the average absorption at a suitable wavelengths range (usually 700-800 nm) from each data point.

3.14 Annealing of single-site substrates

Single-substrates were produced by annealing two oligonucleotides which may contain fluorophores. Annealing was performed in annealing buffer (50 mM NaCl, 10 mM Tris-HCl pH 7.5), typically using a final concentration of the annealed substrate of 1-5 μ M. The oligonucleotide solution was heated to about 95 °C in a heat block and allowed to cool down very slowly over several hours. To produce non-fluorescent substrates and substrates comprising two fluorescent oligonucleotides, the oligonucleotides were usually mixed at a 1:1 molar ratio. If the finished substrate contained one fluorescent oligonucleotide or one radioactively labelled oligonucleotide, the molar ratio of the fluorescent and the non-fluorescent oligo was 1:1.1 up to 1:1.5 to avoid detectable single-stranded molecules.

3.15 Annealing of U-shaped substrates

The U-shaped substrates were annealed in multiple steps since they consist of five parts that need to be annealed in the correct configuration.

First, the X-arm and the Y-arm of the U-substrate were annealed separately. The annealing mixture for each arm contained the oligonucleotide with a region complementary to the linker at a concentration of 3.4-6 μ M. The oligonucleotide without a region complementary to the linker was used at a 1.5 times higher concentration. This ensured that all DNA molecules which could anneal to the linker in later steps are properly annealed. Therefore, the finished U-substrate could only contain the correct double-stranded arms. Further, the annealing mixture for each arm contained 100 mM NaCl and 10 mM Tris-HCl pH 7.5. To anneal each arm, the mixture was heated to 90 °C and cooled very slowly in a PCR cycler (Mastercycler, Eppendorf). Following program was used to create a slow and smooth temperature gradient allowing efficient annealing:

Step 1:	90 °C for 5 min
Step 2:	90 °C for 12 sec
	Temperature increment for each cycle: -0.1 °C
	Temperature changes at 0.3 °C/sec
Step 3:	50 repeats of step 2: final temperature 85 °C
Step 4-29:	steps similar to steps 2 and 3: final temperature 20 °C
Step 30:	20 °C for 1 min
	Temperature increment for each cycle: -1 °C
	Temperature changes at 0.3 °C/sec
Step 31:	16 repeats of step 30: final temperature 4 °C

Step 32: Hold 4 °C

The final U-shaped substrate was annealed from one X-arm, one Y-arm and the linker. Unless stated otherwise, all three parts had the same concentration (1.79-2 M) in the annealing mixture. Further, the annealing mixture contained 100 mM NaCl and 10 mM Tris-HCl pH 7.5. The annealing mixture was heated and cooled in a PCR cycler (Mastercycler, Eppendorf). However, the mixture was maximally heated to 40 °C, which should allow efficient annealing of the complementary regions of the arms and linker without melting the arms. The program used to create the temperature gradient was similar to the program used to anneal each arm but the starting temperature was set to 40 °C.

3.16 Purification of U-shaped substrates

Annealed U-shaped substrates were purified by standard polyacrylamide gel electrophoresis using gels with 8% w/v acrylamide (29:1 acrylamide:bis-acrylamide). The U-substrates were fluorescent resulting in a readily visible band containing the U-substrate. This band was cut out with a scalpel. If necessary, the remaining bands were visualised directly using a fluorescence imager or on a UV-transilluminator after ethidium bromide staining. The U-shaped substrate was extracted from polyacrylamide gel pieces using the “crush and soak” method. The U-substrate was then purified by ethanol precipitation. The concentration and purity of the U-shaped substrate were determined photometrically in the same way as done with purified fluorescent oligonucleotides.

3.17 Gel electrophoresis methods

Various gel electrophoresis methods were employed during this project, depending on the nature and size of the analysed DNA, proteins or protein-DNA complexes.

3.17.1 Agarose gel electrophoresis

Plasmid DNA was analysed by agarose gel electrophoresis. To produce agarose gels, 1% w/v agarose (Biorad, “Ultrapure”) was dissolved in 1×MRT buffer (40 mM Tris-acetate pH 8.2, 1mM EDTA) by mixing and heating in a microwave oven. The hot agarose solution was cooled to ~60°C, poured into a gel mould fitted with an appropriate comb and allowed to set at room temperature. Gels were run at 150 V at room temperature for ~1.5 h. The gels were stained in ethidium bromide solution (0.6 µg/ml) for 30-60 minutes and destained in de-ionised water for ~60 minutes to remove background fluorescence. The DNA was visualised on a UV-transilluminator (254 nm) and photographed using Polaroid type 667 film.

3.17.2 Polyacrylamide gel electrophoresis (PAGE)

To analyse or purify short DNA molecules (mainly double-stranded) without covalently or non-covalently attached proteins, standard polyacrylamide gel electrophoresis was employed.

To prepare polyacrylamide gels, to glass plates were clamped together, separated by spacers (0.75-1.5 mm, Sigma) and sealed with tubing or commercial seals (Sigma). A fresh solution containing a 8-12% w/v acrylamide (29:1 acrylamide:bis-acrylamide), 1x TB buffer (89 mM Tris-HCl, 89 mM boric acid), ~0.06% w/v APS (ammonium persulfate) and ~0.05% v/v TEMED (N, N, N', N'-tetramethylethylenediamine) was poured between the plates and an appropriate spacer was inserted to form wells. The gels were left to polymerise for about one hour and used immediately or stored, wrapped in cling film, at 4 °C for a maximum of one day. After removing the seals and clamps, the gel was clamped into an electrophoresis kit. The kit was filled with running buffer (1xTB) and the comb was removed. The gel was pre-run at 200 V for 30-60 min at room temperature before loading the samples in 1x loading buffer (1x TB buffer, 4% w/v Ficoll and optionally 0.005% w/v bromophenol blue) were loaded into the wells. Electrophoresis was performed at room temperature at, starting at 100-200 V for 30-60 min followed by electrophoresis at 200-250 V for an appropriate time. DNA was visualised directly using a fluorescence imager or on a UV-transilluminator after ethidium bromide staining.

If the samples contained U-shaped substrates, pre-running and electrophoresis were performed at 4 °C.

3.17.3 Native PAGE

Native PAGE was used to analyse non-covalent protein-DNA complexes in samples of the binding-assay.

Native PAGE was performed similar to standard PAGE with following differences: The gel was prepared from a solution containing 6.5% w/v acrylamide (37:1 acrylamide:bis-acrylamide), 1x TBE buffer (89 mM Tris-HCl, 89 mM boric acid, 0.2 mM EDTA pH8.3), ~0.06% w/v APS (ammonium persulfate) and ~0.05% v/v TEMED (N, N, N', N'-tetramethylethylene-diamine). 1x TBE buffer was used as running buffer and the gel was pre-run at 4 °C and 200 V for one hour. Binding assay samples containing radioactive DNA were kept on ice before they were loaded into the wells and electrophoresis was performed at 4 °C and 200 V for four hours. The gel was then dried under vacuum at 80 °C, covered with cling film and exposed to type BAS-III imaging plates (Fujifilm). The

imaging plates were scanned in a BAS-1500 phosphor-imager (Fujifilm) or a FLA-5000 fluorescence imager and the program ImageGauge (Fujifilm) was used to analyse the gel images.

3.17.4 SDS-PAGE

SDS-PAGE was performed to analyse products from recombination reactions using Tn3 resolvase mutants and fluorescent substrates.

SDS-PAGE was performed similar to standard PAGE with the following differences: The gel was prepared from a solution containing 8-12% w/v acrylamide (29:1 acrylamide:bis-acrylamide), 1x TB buffer (89 mM Tris-HCl, 89 mM boric acid), 0.1% w/v SDS (sodium dodecyl sulfate), ~0.06% w/v APS (ammonium persulphate) and ~0.05% v/v TEMED (N, N, N', N'-tetramethylethylenediamine). A solution containing 1x TB buffer and 0.1% w/v SDS was used as running buffer and the gel was pre-run at 200 V for one hour. Samples in 1x SDS loading buffer (1x TB buffer, 0.1% w/v SDS, 1 mM DTT, 4% w/v Ficoll and optionally 0.005% w/v bromophenol blue) or in 1x SDS buffer containing 1 mg/ml protease K were loaded into the wells. Electrophoresis was performed at 50-100 V for 30-60 min followed by electrophoresis at 200-250 V for an appropriate time. DNA was visualised directly using a fluorescence imager or on a UV-transilluminator after ethidium bromide staining. If required, the gel was stained with Coomassie blue as described by Sambrook and Russell (2001) to visualise the protein bands.

If the samples contained U-shaped substrates, pre-running and electrophoresis were performed at 4 °C.

3.17.5 Discontinuous SDS-PAGE

Proteins were separated by discontinuous SDS-PAGE (Laemmli 1970). Discontinuous SDS-PAGE uses two connected gels of different acrylamide percentage and ionic strength, the stacking and separation gel, to produce sharper bands.

Discontinuous SDS-PAGE was performed similar to standard PAGE with following differences: The gel is prepared in two steps. First, the separation gel prepared from a solution containing 15% w/v acrylamide (38:1 acrylamide:bis-acrylamide, 375 mM Tris-HCl pH 8.8), 0.1% w/v SDS, 0.05% w/v APS (ammonium persulphate) and 0.05% v/v TEMED (N, N, N', N'-tetramethylethylenediamine). After adding a thin layer of isopropanol the gel was allowed to polymerise for 30-45 minutes. After removing the isopropanol, the stacking gel was prepared on top of the separation gel from a solution

containing 4% w/v acrylamide (37:1 acrylamide:bis-acrylamide), 125 mM Tris-HCl pH 6.8, 0.1% w/v SDS, 0.1% w/v APS (ammonium persulphate) and 0.2% v/v TEMED. After adding a gel comb the stacking gel was allowed to polymerise for 30-45 minutes. The wells were then rinsed with electrophoresis buffer (25 mM Tris-base, 250 mM glycine, 0.1% w/v SDS). Prior to loading, the protein samples were incubated in 1x Laemmli loading buffer (50 mM Tris-HCl pH 6.8, 2% w/v SDS, 0.01% w/v bromophenol blue, 10% v/v glycerol, 100 mM) at ~90 °C for 5-10 minutes. Electrophoresis was performed at 100 V until the bromophenol blue enters the separation gel, then at 200 V for two hours. The gel was stained with Coomassie blue as described by Sambrook and Russell (2001) to visualise the protein bands.

3.17.6 Denaturing PAGE

Single-stranded oligonucleotides were purified or analysed using denaturing PAGE, preventing the formation of double-stranded DNA or secondary structures of the DNA.

Denaturing PAGE was performed similar to standard PAGE with the following differences: The gel was prepared from a solution containing 12-18% w/v acryl amide (19:1 acrylamide:bis-acrylamide), 1x TB buffer (89 mM Tris-HCl, 89 mM boric acid), 7 M urea, ~0.05% w/v APS (ammonium persulphate) and ~0.05% v/v TEMED (N, N, N', N'-tetramethylethylenediamine). 1x TB buffer was used as running buffer and the gel was pre-run at 15-20 W for 30-60 minutes to heat the gel. One volume of 2x formamide buffer (95% v/v deionised formamide, 20 mM EDTA) was added to the samples followed by incubation at 80-90 °C for 10 minutes. The hot samples were loaded into the wells of the heated gel and electrophoresis was performed at 15-25 W for an appropriate time.

While strong bands of fluorescent oligonucleotides were directly visible, other bands were visualised by staining with “stains-all” dye or on a transilluminator after ethidium bromide staining.

3.17.7 Ethidium bromide staining of polyacrylamide gels

Polyacrylamide gels were stained in a solution of 0.5-2 µg/ml ethidium bromide in deionised water or 1x TB buffer (89 mM Tris-HCl, 89 mM boric acid) for 20-30 minutes. The gel was then destained in deionised water or 1x TB buffer for 10-20 minutes.

3.17.8 “Stains-all” staining of polyacrylamide gels

Polyacrylamide gels were stained with the cationic carbocyanine “stains-all” dye (Aldrich) by soaking the gel in a staining solution (70 ml of ddH₂O, 20 ml isopropanol, 10 ml of

0.1% w/v 'stains-all' solution in formamide) for ~10 minutes until sufficient staining was observed. Subsequently the gel was destained by rinsing it several times in ddH₂O.

3.17.9 *Visualisation of fluorescent DNA in polyacrylamide gels*

To visualise DNA with a Cy5 label, polyacrylamide gels were scanned in a FLA-5000 fluorescence imager using a 635 nm laser and 665 nm long pass filter. To visualise DNA with a fluorescein label, a 473 nm laser and a 510 nm or 575 nm long pass filter were used.

To detect the fluorescence of both Cy3 and Cy5 fluorophores or to the FRET emissions of Cy3/Cy5 FRET pairs, polyacrylamide gels were scanned in a Typhoon imager (GE healthcare) using the appropriate laser and filter settings for each dye.

3.17.10 *Quantification of bands on polyacrylamide gels*

Several types of bands were detected on polyacrylamide gel during this project. Bands of radioactive DNA and fluorescent DNA were detected using a phosphor-imager or fluorescence imager. The resulting images were loaded directly into the program ImageGauge (Fujifilm) to quantify the intensity of the bands.

Bands of proteins in SDS polyacrylamide gels with protein were visualised by Coomassie blue staining according to Sambrook and Russel (2001). The gels were scanned or photographed and the resulting images were processed (see: Gel-based determination of the concentration of resolvase) before loading them into the program ImageGauge (Fujifilm) to quantify the intensity of the bands.

3.18 *Gel-based in vitro recombination assay for single-site substrates*

Unless stated otherwise, the buffer in the recombination reactions contained 100 mM Tris-HCl pH 8.2, 0-20 mM MgCl₂, 0-100 µg/ml poly-dIdC and 10% v/v resolvase dilution buffer (10 mM Tris-HCl pH 7.5, 5 mM DTT, 0.2 mM EDTA, 50% v/v glycerol, 1 M NaCl). The samples contained varying amounts of fluorescent substrates (20-100 nM) and non-fluorescent competitor substrates (25-100 nM). 1/10 volume of Tn3 resolvase mutants in resolvase dilution buffer was added to the pre-warmed reactions resulting in final concentration of the Tn3 resolvase mutants of 100-3,200 nM and accounting for the 10% v/v resolvase dilution buffer in the reaction mixture. Resolvase dilution buffer was added to samples without Tn3 resolvase mutants. The reactions were mixed by vortexing and incubated at room temperature, exactly 20 °C or exactly 37 °C in a water bath.

Small samples were taken during the experiment to be analysed by SDS-PAGE. The reaction in the taken samples was stopped by addition of 1/3 volume of 3x SDS loading buffer containing 3x TB buffer (267 mM Tris-HCl, 267 mM boric acid), 0.3% w/v SDS, 3 mM DTT, 0.015% w/v bromophenol blue and 12% w/v Ficoll. Optionally, the reaction was stopped using 3x SDS loading buffer containing 3 mg/ml protease K, followed by incubation at 37 °C for 30-60 min. The reaction products in the taken samples were separated by SDS-PAGE using gels with 10-12% w/v polyacrylamide (29:1 acrylamide:bis-acrylamide). The bands were visualised using a fluorescence imager and quantified.

3.19 Gel-based in vitro recombination assay for U-shaped substrates

Unless stated otherwise, the buffer in the recombination reactions contained 50 mM Tris-HCl pH 8.2, 10 mM MgCl₂, 50 µg/ml poly-dIdC, 1 mM DTT, 0.1 mg/ml BSA and 10% v/v resolvase dilution buffer (10 mM Tris-HCl pH 7.5, 5 mM DTT, 0.2 mM EDTA, 50% v/v glycerol, 1 M NaCl). All samples contained 20 mM of the U-shaped substrate. To start the reaction, 1/10 volume of Tn3 resolvase NM in resolvase dilution buffer was added to the pre-warmed reactions resulting in a final concentration of Tn3 resolvase NM of 1,200 nM unless stated otherwise. The addition of resolvase accounted for the 10% v/v resolvase dilution buffer in the reaction mixture. Resolvase dilution buffer was added to samples without Tn3 resolvase NM. The reactions were mixed by vortexing and incubated at 20 °C in a water bath.

Small samples were taken during the experiment to be analysed. For analysis, 1/30 to 1/7 volumes of a restriction enzyme solutions or ddH₂O were added and the sample was mixed by vortexing followed by incubation at 37 °C in a water bath for 5 minutes. The BamHI restriction endonuclease (NEB) was used at final concentrations of 0.33 to 14 U/µl while the MluI restriction endonuclease (NEB) was used at final concentrations of 0.33 to 1.4 U/µl in the digest. The digest was stopped by the addition of 1/3 volume of 3x SDS loading buffer containing 3x TB buffer (267 mM Tris-HCl, 267 mM boric acid), 0.3% w/v SDS, 3 mM DTT, 0.015% w/v bromophenol blue and 12% w/v Ficoll. Optionally, the digest was stopped using 3x SDS loading buffer containing 3 mg/ml protease K, followed by incubation at 37 °C for 30-60 min. The reaction products in the taken samples were separated by SDS-PAGE on gels with 8% w/v polyacrylamide (29:1 acrylamide:bis-acrylamide). The bands were visualised using a fluorescence imager.

3.20 Ensemble FRET experiments with single-site substrates

Ensemble fluorescence experiments were performed in a quartz SUPRASIL ultra-micro fluorescence cell with 3x3 mm light path (105-254-QS, Hellma) in an Aminco Bowman Series 2 luminescence spectrometer (Thermo Scientific). The temperature of the cell was kept at 20 °C in a cell holder connected to a temperature controlled water bath with pump (Haake/Gallenkamp).

The sample buffer contained 50 mM Tris-HCl pH 8.2, 50 µg/ml poly-dIdC and 10% v/v resolvase dilution buffer (10 mM Tris-HCl pH 7.5, 5 mM DTT, 0.2 mM EDTA, 50 % v/v glycerol, 1 M NaCl). Optionally 20 mM MgCl₂ were added to the buffer. The samples contained either the single-site substrate B50R5C5L6C3 (20 nM) and the competitor substrate 80LR (80 nM) or the single-site substrates B50R5C5 (50 nM) and 50L6C3 (50 nM). Purified Tn3 resolvase mutants in resolvase dilution buffer were added to the pre-warmed sample, accounting for the final 10% v/v resolvase dilution buffer in the sample. The final concentration of the Tn3 resolvase mutants in the sample was 3 µM. Resolvase dilution buffer was added to samples without Tn3 resolvase mutants. Immediately after mixing, the sample was shortly centrifuged and transferred into the ultra-micro cell for FRET measurements. During the experiment, the cell was kept in the temperature-controlled cell holder of the luminescence spectrometer and only removed to take samples or add SDS. The reaction in the cell was stopped by adding 1/10 volume of 1% w/v SDS.

Small samples were taken during the experiment to be analysed by SDS-PAGE. The reaction in the taken samples was stopped by addition of 1/3 volume of 3x SDS loading buffer containing 3x TB buffer (267 mM Tris-HCl, 267 mM boric acid), 0.3% w/v SDS, 3 mM DTT, 0.015% w/v bromophenol blue and 12% w/v Ficoll. Optionally, the reaction was stopped using 3x SDS loading buffer containing 3 mg/ml protease K, followed by incubation at 37 °C for 30-60 min. The reaction products in the taken samples were separated by SDS-PAGE. The bands were visualised using a fluorescence imager and quantified.

The buffer for the required reference samples contained 20 mM Tris-HCl pH7.5, 50 mM NaCl, 0.1 mM EDTA, 10 mM MgCl₂ and 5% v/v resolvase dilution buffer (10 mM Tris-HCl pH 7.5, 5 mM DTT, 0.2 mM EDTA, 50% v/v glycerol, 1 M NaCl).

For the reference spectrum $f_{em}^D(\lambda)$, an emission spectrum of the double-stranded substrate B50R1C3 (20 nM) in presence of the non-fluorescent substrate B50LR (100 nM) was recorded from 530 to 800 nm exciting at 515 nm. The buffer spectrum was subtracted and the baseline corrected at 790-800 nm. The same sample was used to record the reference excitation spectrum $f_{exc}^D(\lambda')$ from 400-585 nm measuring the emission at 600 nm. After subtraction of the buffer spectrum, baseline correction at 790-800 nm, normalisation to 1 in the maximum and multiplication with the extinction coefficient of Cy3, the average of the values at excitation wavelengths from 514 to 516 nm was used as $\varepsilon^D(\lambda'_D)$.

For the reference spectrum $f_{exc}^A(\lambda')$, an excitation spectrum of the double-stranded substrate B50L1C5 in presence of the non-fluorescent substrate B50LR (100 nM) was recorded from 400-695 nm measuring the emission at 705 nm. The buffer spectrum was subtracted and the baseline corrected at 790-800 nm before normalising the spectrum to 1 in the maximum and multiplying with the extinction coefficient of Cy5. The average of the values at excitation wavelengths from 513 to 517 nm was used as $\varepsilon^A(\lambda'_D)$ and the average of values at excitation wavelengths from 614 to 616 nm was used as $\varepsilon^A(\lambda'_A)$.

The extinction coefficients were 150,000 M⁻¹cm⁻¹ for Cy3 and 250,000 M⁻¹cm⁻¹ for Cy5 according to the manufacturers' information.

To enable quick FRET measurements of the samples of interest, automated series of scans were performed including following scans:

scan	λ excitation	λ emission start	λ emission end
light scattering test	515	525	535
emission peak Cy3	515	555	585
emission peak Cy5	515	655	685
baseline test	515	790	800
light scattering test	615	625	635
emission peak Cy5	615	655	685
baseline test	615	790	800

Table 3.4: Automated scans for ensemble FRET measurements

Individual short scans using the same excitation wavelength were merged into one file containing data points at the relevant wavelengths. The merged scans were imported into excel files and the FRET efficiency was calculated according to Clegg *et al.* (1992) as

described in chapter 2.3. The corrected reference spectrum $f_{em}^D(\lambda)$ was fitted to the spectrum $f_{em}^{DA}(\lambda, \lambda'_D)$ of the sample by matching the emission maxima. To calculate the FRET efficiency, the values for $f_{em}^{Aext}(\lambda_A, \lambda'_D)$ and $f_{em}^{DA}(\lambda_A, \lambda'_A)$ were obtained by averaging the values in the relevant spectra at emission wavelengths from 665-667 nm.

3.21 Single-molecule FRET experiments

3.21.1 Single-molecule FRET setup

All single-molecule experiments were performed in the laboratory of Prof. David M.J. Lilley FRS at the University of Dundee. I performed the experiments as described in the materials and methods section after training and advice by Prof. David M.J. Lilley FRS, Dr Anne-Cécile Déclais and Dr Jonathan Ouellet.

Single-molecule FRET experiments were performed in a total internal reflection (TIR) microscope setup. An inverted IX70 microscope (Olympus) with a water immersion objective (60x, 1.2 numerical aperture, Olympus) was connected to an iXON EMCCD camera (Andor). The samples were bound to the quartz-surface of a buffer-filled reaction chamber (see below) and were excited using a green, ultra-stable continuous wave laser (532 nm, 50 mW, Crystalaser). The laser intensity was reduced to 25 mW due by a beam splitter and directed to the quartz surface at a large angle using a quartz prism (CBI laser). The prism was placed on top of the quartz slide of the reaction chamber separated by a thin layer of mineral immersion oil. The fluorescence emissions were collected through the microscope objective and residual light from the laser was removed using a 550 nm long pass filter (Chroma Technology). The remaining fluorescence light was split into red and green light using a dichroic mirror (645 nm, Chroma Technology) before detection with the EMCCD camera.

3.21.2 Preparation of reaction chambers

On the day of the single-molecule experiment, the reaction chamber was assembled from a quartz slide (75x25x1 mm) with two small drilled holes, a glass coverslip and thermoplastic film (NESCO) (see chapter: Single-molecule FRET using TIR fluorescence microscopy). Prior to assembly of the reaction chambers, the quartz slides were cleaned extensively as follows:

Initially the slides were scrubbed with acetone using tissues followed by scrubbing with warm water and soap using gloves. After rinsing with water and deionised water, the slides were wiped with acetone and then with ethanol using tissues. The slides were transferred

into a clean vial for the next cleaning steps. After rinsing 5x with MQH₂O (deionised and filtered water), a stripping solution (50% v/v H₂SO₄, 15% v/v H₂O₂) was added and the slides were soaked for one hour followed by 30-40 minutes sonication. Subsequently the slides were rinsed 10x with MQH₂O, sonicated 15 minutes in MQH₂O, rinsed 5x with MQH₂O, rinsed 1x with acetone, sonicated 45 minutes in acetone, rinsed 5x with MQH₂O, sonicated 15 minutes in MQH₂O, rinsed 5x with MQH₂O, sonicated 45 minutes in 1 M KOH, rinsed 5x with MQH₂O, sonicated 15 minutes in MQH₂O, rinsed 5x with MQH₂O, rinsed 1x in methanol, sonicated 45 minutes in methanol, rinsed 5x with MQH₂O, sonicated 15 minutes in MQH₂O, rinsed 5x with MQH₂O, sonicated 45 minutes in 1 M KOH, rinsed 5x with MQH₂O, sonicated 15 minutes in MQH₂O, rinsed 5x with MQH₂O and stored in MQH₂O for a maximum of one week. On the day before the experiment, the slides were rinsed 5x with MQH₂O, sonicated in MQH₂O for 15 minutes and rinsed 5x with MQH₂O. The slides were blown dry with a stream of argon and stored in a clean box overnight. On the day of the experiment, the glass cover slips were wiped with ddH₂O and ethanol. The quartz slides and glass cover slips were transferred into a plasma cleaner (Harrick Plasma) with the future inside of the reaction chamber facing up and treated at maximum power for two minutes.

The reaction chambers were assembled in a laminar flow hood to avoid contamination of the surfaces with dust. The quartz slides were placed on a clean glass plate with the clean side facing up. After cutting an elliptic hole into, the thermoplastic film was wiped with ddH₂O and placed on top of the quartz slide. The glass cover slip was placed on top of the thermoplastic film with the clean side facing down and the three layers were squeezed together. To seal the reaction chambers, they were incubated at ~150 °C for two minutes and squeezed with a pipette tip.

3.21.3 *Functionalisation of the reaction chamber surface and sample preparation*

Only reagents of high purity were used for the single-molecule experiments. Before use, all solutions were centrifuged (16,000 g, 2 minutes) and filtered by centrifugation (9,300 g, 10-30 minutes) in Costar Spin-X tube filters (Sigma-Aldrich, cellulose acetate, 0.22 µm pore size). Larger volumes of solutions were filtered through syringe filters (0.22 µm pore size). Only the final imaging buffers were centrifuged but not filtered to avoid loss of the Tn3 resolvase NM mutant. Strongly diluted solutions were prepared and stored in coated non-stick eppendorf tubes to avoid the loss of reagents due to binding to the walls of the eppendorf tubes.

Shortly before the experiment, the reaction chambers were flushed with T50 buffer (10 mM Tris-HCl pH 8.2, 50 mM NaCl) through the holes in the quartz slide and checked in the single-molecule FRET setup for fluorescent contaminations. Clean reaction chambers were functionalised. First, about 100 μ l of a solution of biotinylated bovine serum albumin (BSA) (1 mg/ml biotinylated BSA, 10 mM Tris-HCl pH 8.2, 50 mM NaCl) were passed through the chamber. Subsequently the chamber was incubated in a wet-box with a water-saturated atmosphere at room temperature for 10 minutes. After flushing with 500 μ l of T50 buffer, ~100 μ l of a neutravidin solution (0.2 mg/ml neutravidin, 10 mM Tris-HCl pH 8.2, 50 mM NaCl) were passed through the reaction chamber before incubation in the wet-box for 10 minutes. After flushing with 500 μ l of T50 buffer, the reaction chamber was stored in the wet-box for about one hour. Then, ~100 μ l of a solution containing the U-shaped substrate U3 (25 pM U3, 10 mM Tris-HCl pH 8.2, 50 mM NaCl, 0.1 mg/ml acetylated BSA) was passed through the reaction chamber. After passing the substrate U3, light exposure was kept to a minimum. The reaction chamber was incubated in the wet-box for ten minutes, flushed with 500 μ l of T50 buffer and stored in the wet-box shortly until the experiment.

For the experiment, the reaction chamber had to be flushed with different types of imaging buffer (see below). Immediately before use, the imaging buffers were prepared on ice, centrifuged (16,000 g, 2 minutes) and filtered by centrifugation. To mix the imaging buffers, several solutions were prepared and filtered on the previous two days: 50x Gloxy buffer contained 8.3 mM Tris-HCl pH 8.2, 42 mM NaCl, 217,000 U/ml catalase (Sigma-Aldrich) and 16,700 U/ml glucose oxidase (Sigma-Aldrich) and was stored at 4 °C. 50x Trolox solution contained 50 mM Trolox (6-hydroxy-2,5,7,8-tetramethylchroman-2-carboxylic acid) and 10% v/v methanol and was adjusted to pH 9.5 before storage at -20 °C. 5x glucose buffer contained 250 mM Tris-HCl pH 8.2, 0.5 mg/ml acetylated BSA, 2% w/v glucose and 25% v/v glycerol and was stored at -20 °C.

Immediately before the acquisition of single-molecule FRET data, the reaction chamber was flushed with 100-150 μ l of a freshly prepared imaging buffer providing the desired reaction conditions. Imaging buffer A contained 1x glucose buffer, 1x gloxy buffer, 1x Trolox solution, 100 mM NaCl, 50 μ g/ml poly-dIdC and 1% v/v resolvase dilution buffer (10 mM Tris-HCl pH 7.5, 5 mM DTT, 0.2 mM EDTA, 50% v/v glycerol, 1 M NaCl). Imaging buffer B contained 1x glucose buffer, 1x gloxy buffer, 1x Trolox solution, 90 mM NaCl, 50 μ g/ml poly-dIdC, 1% v/v resolvase dilution buffer (10 mM Tris-HCl pH 7.5, 5 mM DTT, 0.2 mM EDTA, 50% v/v glycerol, 1 M NaCl) and 600 nM Tn3 resolvase NM.

Imaging buffer C contained 1x glucose buffer, 1x gloxy buffer, 1x Trolox solution, 90 mM NaCl, 50 µg/ml poly-dIdC, 1% v/v resolvase dilution buffer (10 mM Tris-HCl pH 7.5, 5 mM DTT, 0.2 mM EDTA, 50% v/v glycerol, 1 M NaCl), 600 nM Tn3 resolvase NM and 20 mM MgCl₂.

3.21.4 Acquisition of single-molecule FRET data

Before the single-molecule experiment, a reaction chamber containing surface-bound beads with extremely strong fluorescence over a broad range of wavelengths had been inserted into the microscope setup and single-molecule data was recorded using a program, written in C++ by Sean McKinney. With the resulting dataset, a map of matching positions in the red and green images of the observable area was constructed using a software routine, written in IDL (ITT Visual Information Solutions) by Stephen Chu. The map was then used to identify and match single fluorescent molecules in the red and green images during the single-molecule FRET experiment.

During the single-molecule FRET experiment, single-molecule data was recorded at rates between 0.02 and 0.1 seconds per frame using a program written in C++ by Sean McKinney. First, the reaction chamber was flushed with fresh imaging buffer A to record data for the substrate U3 in absence of Tn3 resolvase NM and magnesium. In the following, time points are given as time elapsed after flushing the reaction chamber with buffer A. Data was acquired from ~26 minutes to ~70 minutes. At 1 hour 34minutes, the reaction chamber was flushed with fresh imaging buffer B and data for the substrate U3 in presence of Tn3 resolvase NM and absence of magnesium was recorded from ~1 hour 43 minutes to ~2 hours 35 minutes. At 3 hours 1 minutes, the reaction chamber was flushed with fresh imaging buffer C and data for the U3 substrate in presence of Tn3 resolvase NM and magnesium was recorded from ~3 hours 24 minutes to 4 hours 16 minutes.

3.21.5 Data analysis

After the data acquisition had finished, a software routine, written in IDL by Stephen Chu, was used to transform the recorded data into hel files accompanied by images of the fluorescence intensity in the observed area averaged of the observation time. The hel files contain a trace for each automatically identified fluorescent molecule in the observed area. The traces describe the fluorescence intensity of each identified molecule in the green and red channel over the recording time.

The hel files were analysed with the software routine UniCon, which runs within the MatLab program (The MathWorks Inc.) and was written by T. Ha, J. Ouellet and C.

Penedo in MatLab. UniCon was used to visualise the traces and calculate graphs of the total intensity (the sum of intensities in the green and red channels) and of the apparent FRET efficiency versus time.

UniCon was used to filter the traces removing unsuitable traces automatically or manually. During filtering, UniCon matched each trace to the corresponding fluorescent molecule in the image of the observed area enabling the identification of overlapping molecules. Further, UniCon was used to merge several hel files into one hel file containing all traces of the individual hel files.

UniCon was also used to export lists of the apparent FRET efficiency, averaged over the first ten frames, of all molecules within one hel file. These lists were analysed with the programs Excel (Microsoft) and OriginPro (OriginLab Corporation) to generate histograms of the initial apparent FRET efficiency of all molecules.

The traces which remained after the filtering process were visualised with UniCon and FRET states were identified by eye considering all time frames. A list of the apparent FRET efficiency and the duration of all identified FRET state was compiled for each trace. The lists for all traces were analysed with the programs Excel and OriginPro to generate histograms of all identified FRET states. All FRET states which were followed by a second FRET state were identified and compiled in a list of FRET state transitions stating the apparent FRET efficiency of the first FRET state and of the second FRET state. This list was transformed into a matrix using the program OriginPro. Each matrix ranged from apparent FRET efficiencies of 0 to 1 for the first and second FRET state with bins of 0.05 for the first and second state. The matrix provided the number of FRET state transitions falling into each bin. Two-dimensional histograms of FRET transitions were generated with the OriginPro program providing a visual representation of the frequencies of the observed FRET state transitions.

4 Preparation and purification of Tn3 resolvase mutants

The experiments described in this thesis required large quantities of purified Tn3 resolvase mutants. To ensure that all experiments were conducted with Tn3 resolvase mutants of comparable concentration, purity and activity, only one large batch of each Tn3 resolvase mutant was prepared and used in the experiments. The purified Tn3 resolvase versions included wild type Tn3 resolvase, hyperactive Tn3 resolvase NM and Tn3 resolvase NM-S10A, the catalytically inactive version of Tn3 resolvase NM.

Wild type Tn3 resolvase and the mutant versions were purified similarly and according to a method adapted from Olorunniji *et al.* (2006) (see section 3.9). The proteins were overexpressed in and extracted from *E.coli* cells. In contrast to most other proteins, Tn3 resolvase and mutant versions are soluble at high ionic strength. The purification method made use of this fact and employed a series of extraction and dialysis steps using buffers of different ionic strengths to separate Tn3 resolvase from other most other proteins. Tn3 resolvase was purified further by ion-exchange chromatography which allowed the separation of the positively charged Tn3 resolvase and mutant versions from negatively charged proteins, DNA and RNA. Finally, Tn3 resolvase was refolded in a buffer with high ionic strength and stored in resolvase dilution buffer.

Following purification, the concentration of Tn3 resolvase and mutant versions was measured using different methods. It is likely that the photometric determination of the protein concentration (see section 3.9.4) was inaccurate due to the low extinction coefficient of Tn3 resolvase and especially of the mutant versions. Therefore, the resolvase concentration was determined by a gel-based method (see section 3.9.5). A dilution series of the purified proteins and a reference dilution series of proteins with known concentration were subjected to discontinuous SDS-PAGE. The protein bands were visualised by staining with Coomassie blue, showing the high purity of the purified proteins (figure 4.1). Images of the Coomassie blue-stained gel were scanned or taken on a transilluminator (white light) using a digital camera followed by image processing. Then, the intensity of the bands was either compared by eye or quantified from the processed gel images using the computer program ImageGauge (Fujifilm). The quantified band intensities were plotted against the dilution of the protein sample allowing the determination of the resolvase concentration in the new preparation by linear regression (for details see section 3.9.5).

All variations of the gel-based determination of the resolvase concentration provided comparable results (table 4.1). Comparing the band intensities by eye was considered the most inaccurate method due to biased interpretation. After image-processing, the gel image taken on a transilluminator had the best signal-to-background ratio. Therefore, the resolvase concentrations, retrieved from this image by linear regression of the quantified band intensities, were used throughout this thesis. The photometric determination of the concentration of wild type Tn3 resolvase was in agreement with the results from the gel-based determination (table 4.1). However, the results differed substantially for the mutant versions due to their extremely low extinction coefficient and showed the inaccuracy of this method.

After the concentration had been established, the purified resolvase proteins were tested for nuclease contaminations (figure 4.2). For this purpose, a plasmid without specific sites for Tn3 resolvase was incubated with the purified proteins in the presence of magnesium overnight. Only the purified hyperactive Tn3 resolvase NM produced a slight increase of the nicked version of the plasmid. Most likely, the nicking resulted from the slight unspecific nicking activity of Tn3 resolvase NM and not from nuclease contaminations. None of the purified proteins contained detectable quantities of DNA or RNA contaminants as seen in the samples without plasmid DNA.

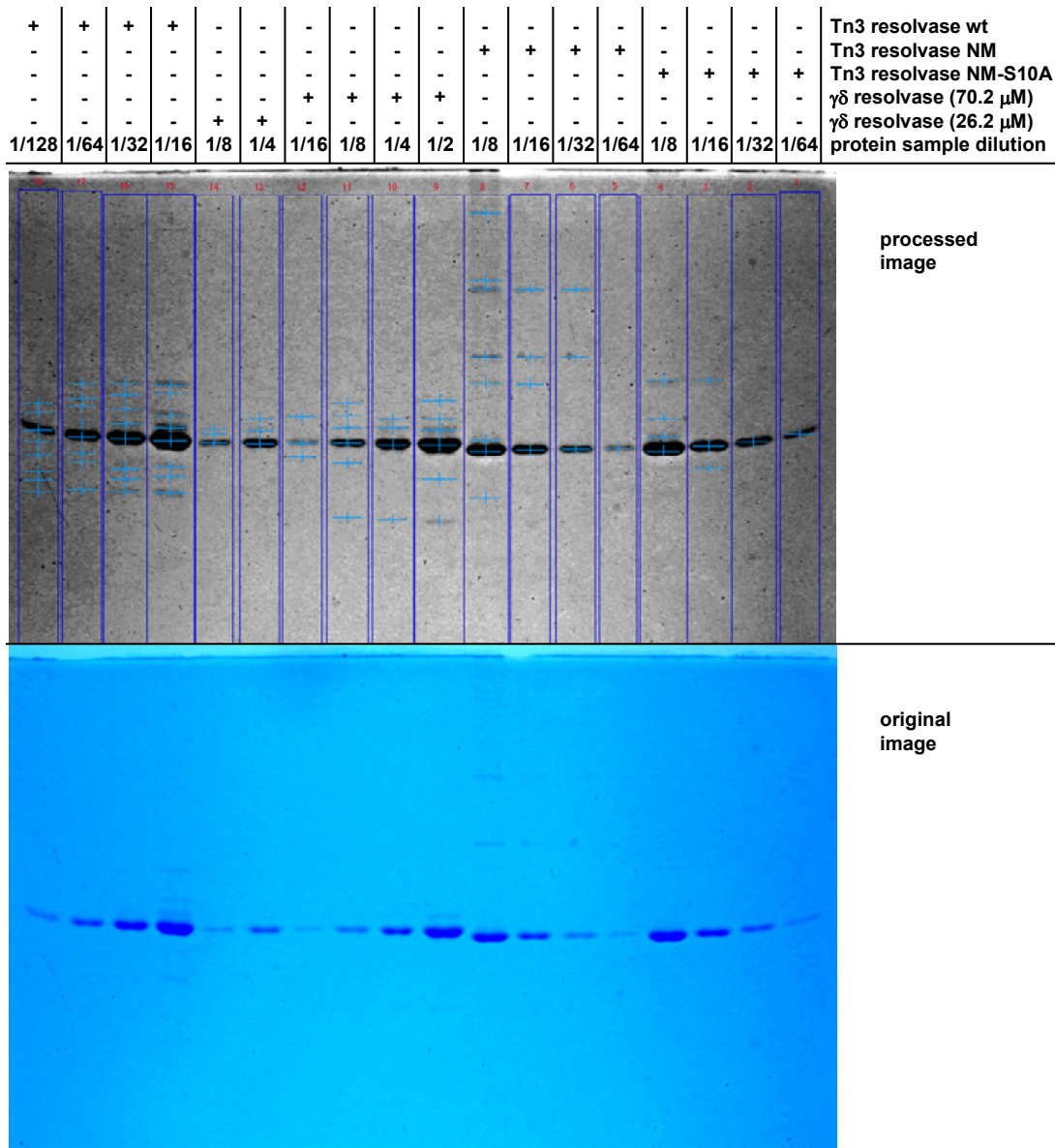


Figure 4.1: Gel-based determination of the resolvase concentration

Dilution series of the purified Tn3 resolvase mutants and of $\gamma\delta$ resolvase with known concentration were subjected to SDS-PAGE. After Coomassie blue staining, the gel was photographed on top of a transilluminator emitting white light. The main band in each lane is formed by the resolvase protein suggesting a high purity of the purified resolvase. The original picture was processed for the quantification of the protein bands. The resolvase concentration was determined by linear regression of the band intensity plotted against the dilution of the protein sample.

method used to determine the resolvase concentration	Tn3 resolvase wild type	Tn3 resolvase NM	Tn3 resolvase NM-S10A
	c [μ M]	c [μ M]	c [μ M]
gel-based: transilluminator gel image	743	230	273
gel-based: scanned gel image	731	213	267
gel based: band comparison by eye	800	200	260
UV-vis absorption	758	417	371

Table 4.1: Comparison of the resolvase concentration determined by different methods

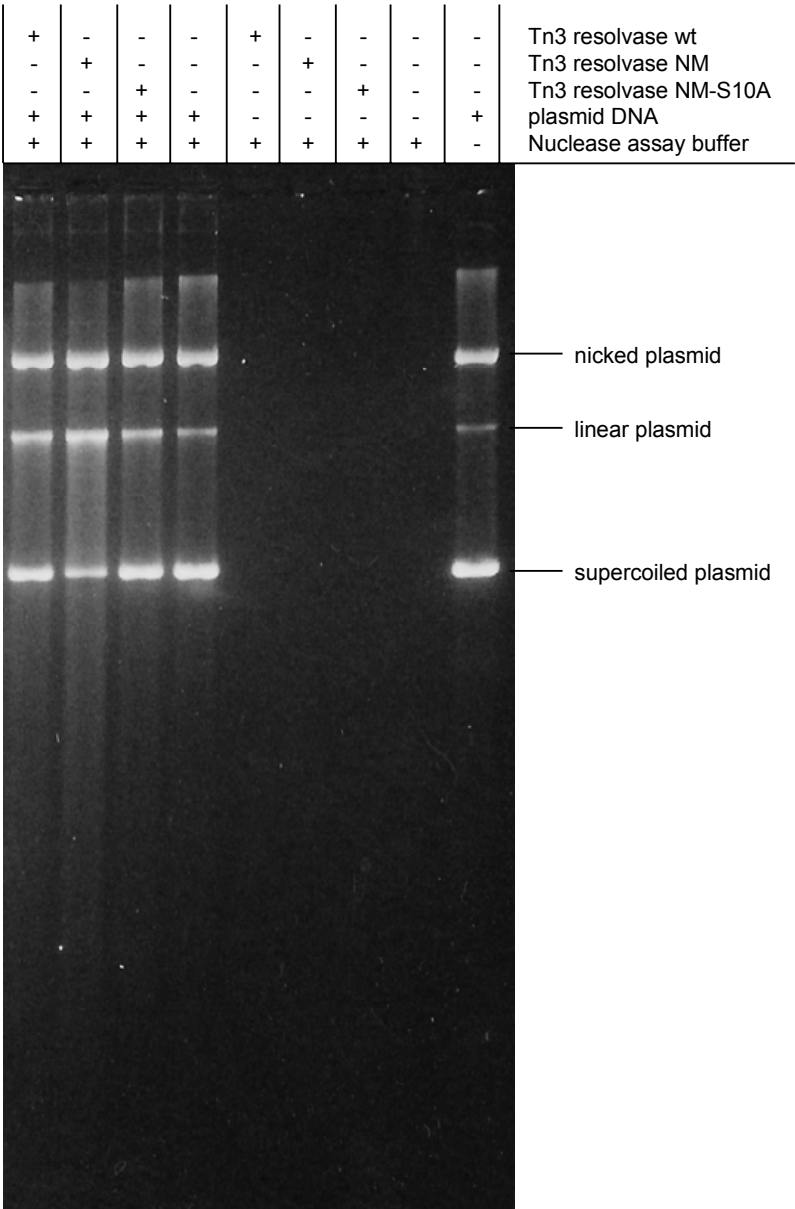


Figure 4.2: Nuclease activity assay of the purified resolvase proteins
Plasmid DNA without specific sites for Tn3 resolvase was incubated with the purified resolvase proteins in presence of magnesium at 37 °C overnight. Only the purified Tn3 resolvase NM produced an increase of nicked plasmids due to its unspecific nicking activity.

5 Development of fluorescent single-site substrates

The aim was to introduce two dyes into a synapse, comprising a resolvase tetramer and two short linear DNA substrates, each containing one copy of Tn3 *res* site I. The two dyes should form a FRET pair, enabling measurements of the distance between both dyes using fluorescence spectroscopy. By attaching the dyes to specific components of the synapse, the movements of those components relative to each other can be measured during recombination. In this project, dyes were attached only to specific positions in the linear substrate DNA. However, these fluorescent substrates needed to be designed carefully to allow detectable FRET changes during recombination without interfering with synapse formation and recombination.

5.1 Requirements for fluorescent substrates

5.1.1 Fluorophore properties

The dyes attached to the DNA substrates need to form a FRET pair. The Förster radius of this FRET pair should be somewhere around half of the expected maximal separation of the dyes within the synaptic complex. This ensures that changes in the distance between the two dyes, which can be located at any two positions in the complex, result in strong, detectable changes in the FRET efficiency. The Cy3 and Cy5 dyes, which were used throughout this project, have a Förster radius of roughly 50-60 Å, which matches the distance of ~40-80 Å between the centres of the two copies of site I in the structure of the cleaved $\gamma\delta$ resolvase synapse (depending on whether the distances are measured from the nearest or furthest parts of the DNA) (Li *et al.* 2005).

The dyes Cy3 and Cy5 were chosen because the single-molecule setup used throughout this project is optimised for Cy3 and Cy5 fluorophores. The setup was adjusted for those dyes since their properties are suited well for single-molecule FRET experiments with labelled DNA. Cy3 and Cy5 are bright with a high quantum yield (0.15 and 0.28) and a high extinction coefficient (150,000 and 250,000 M⁻¹ cm⁻¹). Several buffer additives have been developed to enhance the photo-stability of Cy3 and Cy5 to reduce blinking and bleaching during single-molecule FRET experiments, enabling sufficiently long measurement times.

In the context of biochemical experiments, the Cy3 and Cy5 dyes feature several advantageous properties. Cy dyes show little spectral variation in buffers of different pH and are commercially available with a variety of chemical groups for the covalent attachment to biological molecules. In this project, Cyanine dyes with a N-Hydroxysuccinimide (NHS) ester group were conjugated to the amine group of modified thymines at specific positions in the substrate DNA, forming a stable amide bond (figure 5.1). The DNA can be readily synthesised with amino modified thymines at specific positions and the conjugation reaction performs well under mild conditions. The dye becomes covalently attached to the modified thymine base via a short linker. In double-stranded DNA, the Cy dye will usually protrude from the major groove and can move and rotate freely in an area limited by the linker. This conjugation method preserves most properties of the DNA molecule such as base pairing and stacking, which helps to minimise inhibitory effects on synapse formation and recombination. In addition, there are many potential positions in site I to which the dyes can be attached using this conjugation method, since site I is very AT-rich.

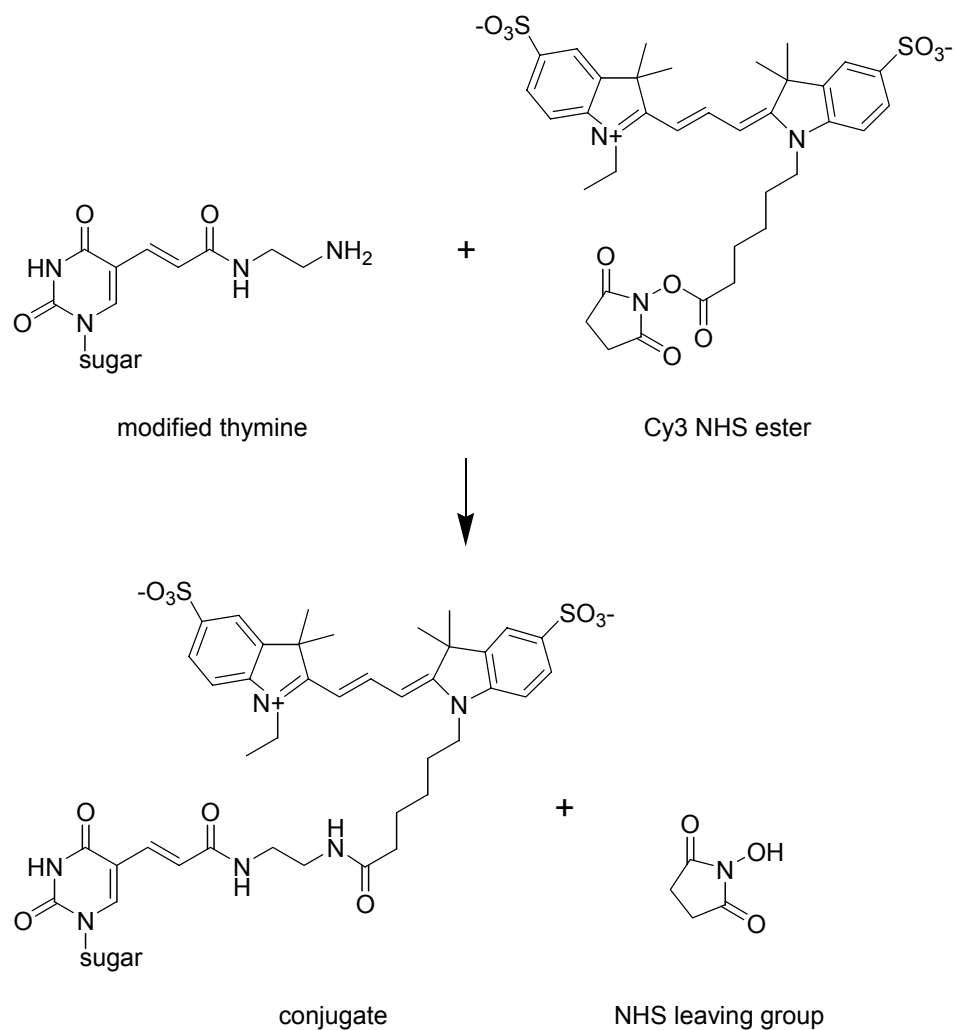


Figure 5.1: Conjugation of Cy3 NHS ester to amino-modified thymines. The modified thymine is connected to an amine through a C2 linker. The conjugative Cy3 dye features a carbon linker with a NHS ester group at its end. The NHS ester reacts selectively with the amine group, forming an amide bond and linking the dye covalently to the modified thymine via a flexible linker.

5.1.2 Fluorophore positions optimal for FRET experiments

Within the synapse, the fluorophores can be attached to the left (L) or right (R) half of one parental site I or to the left (L') or right (R') half of the second parental site. To follow the movements of the half sites during strand exchange, the fluorophores of the FRET pair should be close to each other in the non-recombinant state and far apart in the recombinant state. Alternatively, they can be far apart in the non-recombinant and close in the recombinant state. Both versions ought to provide strong changes in the FRET efficiency during strand exchange.

The simplest solution is to place the FRET pair close to the cleavage site at the centre of site I, with one fluorophore in the L-half and one fluorophore in the R-half of site I. Initially both fluorophores are close but they get separated by a large distance upon strand exchange. The distance is even larger, if one considers that the fluorophores protrude from the major grooves of the DNA on the outside of the complex (figure 5.2).

Attaching the fluorophores to L and R close to the centre of site I may also enable the detection of double-strand cleavage and ligation in the synapse, since the half sites appear to move ~ 17 Å apart upon cleavage, as seen in the crystal structure of the cleaved synapse (Li *et al.* 2005). However, for this purpose it might be advantageous to attach the fluorophores further from the cleavage site, to separate them by a distance close to the Förster radius. In this configuration, the system is more sensitive to any small changes in the separation of the fluorophores, induced by cleavage or ligation.

A model of the dyes attached to L and R directly next to the centre of site I was built with the program PyMOL (DeLano 2006) using the crystal structure of the cleaved synapse (Li *et al.* 2005) and the calculated structures of the Cy3 and Cy5 fluorophores. The chemical formulae of Cy3 and Cy5 in the SMILE format were used to compute the three-dimensional structure of the fluorophores using a demo of the CORINA program (Sadowski *et al.* 1994; Sadowski *et al.* 2008). The configuration of the synapse after strand exchange was generated without altering the structure; the identities of the half sites were simply assigned differently. In the modelled synapse, the centres of the fluorophores in L and R are initially separated by ~ 11 Å, and move ~ 80 Å apart after strand exchange (figure 5.2). However, due to the flexibility of the linker of the fluorophores, the dyes might even make direct contact when located in the same parental site.

If the fluorophores are attached to L and R several base pairs away from the centre of site I, the fluorophores will protrude from the major groove of the DNA towards the core of the synapse, due to the helical twist of the DNA. This suggests that the fluorophores may exhibit relatively high residual FRET efficiency when after strand exchange, since they have not moved apart all the way to opposing positions at the outside of the complex. This configuration could enable the detection of synapse formation by FRET, if the dyes are initially placed in two distinct copies of site I which come together in the synapse. Another consequence of the helical twist is that the distance between two fluorophores in one double-stranded DNA molecule does not grow linearly with the number of base pairs separating them. As a result, the fluorophores are surprisingly close to each other when they are attached to the DNA at positions 10 bp apart, since they are in the same helical phase.

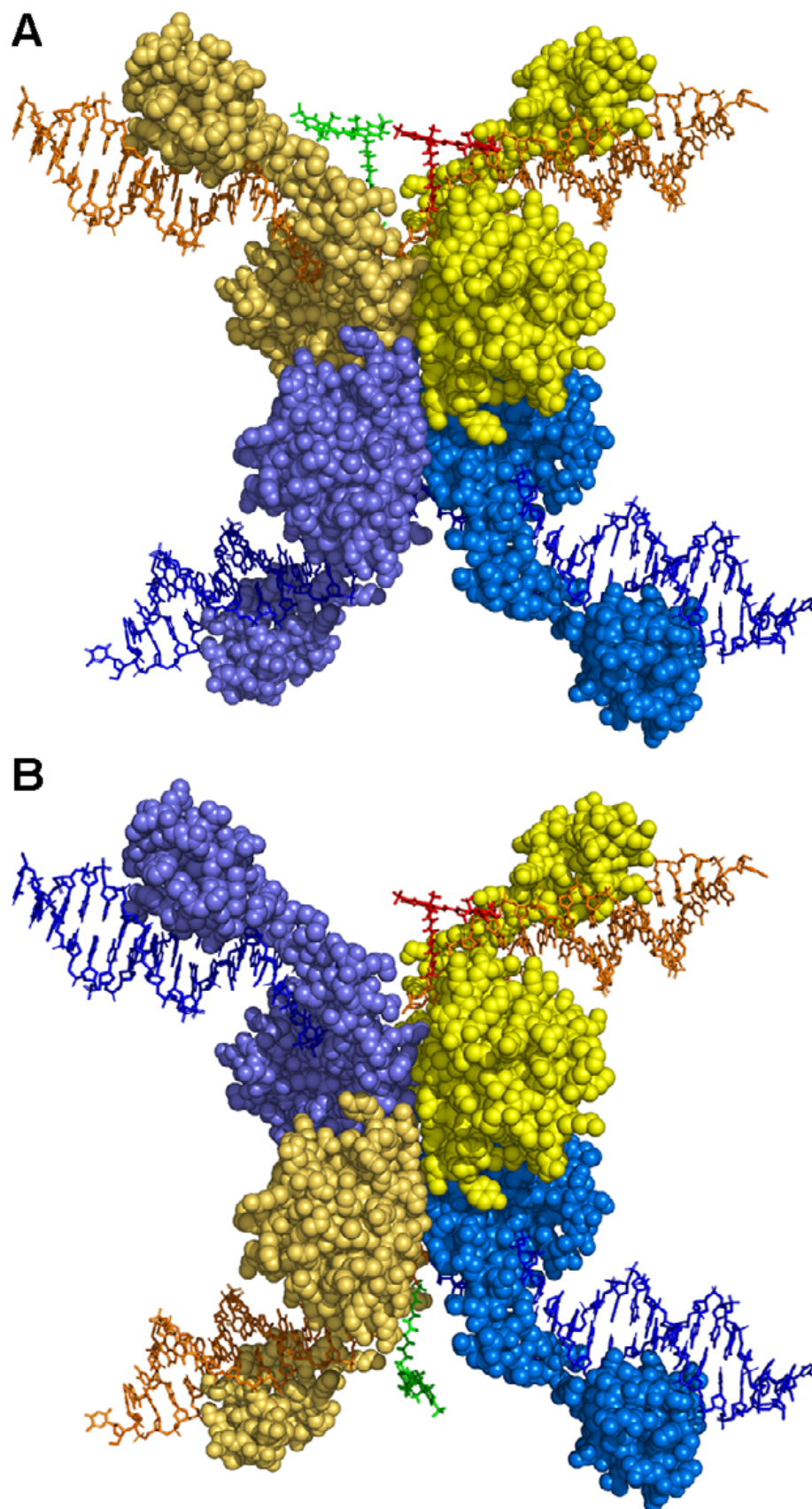


Figure 5.2: Modelled location of Cy3 and Cy5 in the site I synapse before and after strand exchange. The computed structures of Cy3 (green) and Cy5 (red) were added to the structure of a $\gamma\delta$ resolvase tetramer at site I (pdb: 1ZR4; Li *et al.* 2005). Cy3 and Cy5 are separated by ~11 Å before strand exchange (**A**) and by ~80 Å after strand exchange (**B**).

5.1.3 Fluorophore positions ideal for the recombination system

Attaching the dyes to modified thymines leaves an organic compound protruding from an unnatural base. The potentially adverse effects of this modification on synapse formation and recombination need to be minimised to study the system. For this purpose, the dye positions were selected according to which positions were predicted to tolerate modifications. Several data sets were available to find potential positions.

Mutagenesis of Tn3 *res* site I provided data on which base-pairs in site I can be altered without impairing recombination *in vivo* (Burke and Stark, unpublished work) (figure 5.3A). This data set is particularly helpful since it directly suggests which positions may be modified.

DNase I footprinting of synapsed Tn3 *res* sites indicate at which positions Tn3 resolvase makes close contact with the DNA backbone of site I (Burke and Stark 2005). A high degree of protection from cleavage indicates close contacts with resolvase. For each base in site I, the protection of the adjacent phosphodiester bonds was combined into one value (figure 5.3B). The footprinting results do not directly reveal which bases can be modified, but suggest at which positions close contacts between resolvase and the DNA might be disrupted by the introduction of a fluorophore.

Finally, the crystal structure of a $\gamma\delta$ resolvase dimer bound to site I (Yang and Steitz 1995) and the structure of a $\gamma\delta$ resolvase tetramer bound to two cleaved copies of site I (Li *et al.* 2005) can be analysed to identify positions in the DNA which do not come into close contact with resolvase. These positions were found using the program PyMOL (DeLano 2006) to calculate the distance between all nucleotides in site I and the resolvase units. All nucleotides that are separated from the resolvase units by a minimum of 4-5 Å were identified and considered more suitable for the attachment of fluorophores (figures 5.3C, 5.4). However, this approach does not indicate if the resolvase units are close to the DNA backbone or the base of a particular nucleotide. A gap around the crucial nucleotides at the central overlap, as seen in the cleaved synapse structure (Li *et al.* 2005), suggests there is space for fluorophores at the very centre of site I. This gap could result from the two half sites moving apart upon DNA double-strand cleavage though, and might not exist in the pre-cleavage synapse. Therefore it is likely that fluorophores attached to the crucial central nucleotides would interfere with recombination. In addition, substrates with fluorophores located one or two bases to the left or right of the centre of site I, might prevent access to the scissile phosphates of the DNA by catalytic residues of resolvase and inhibit cleavage

or ligation of the substrate. Nevertheless, dyes were attached to the central nucleotides and the modified substrates were tested *in vitro* since the fluorophores were expected to exhibit a high FRET efficiency at these positions.

Figure 5.3 sums up the relevant data from all three datasets and shows the chosen positions for fluorophore attachment.

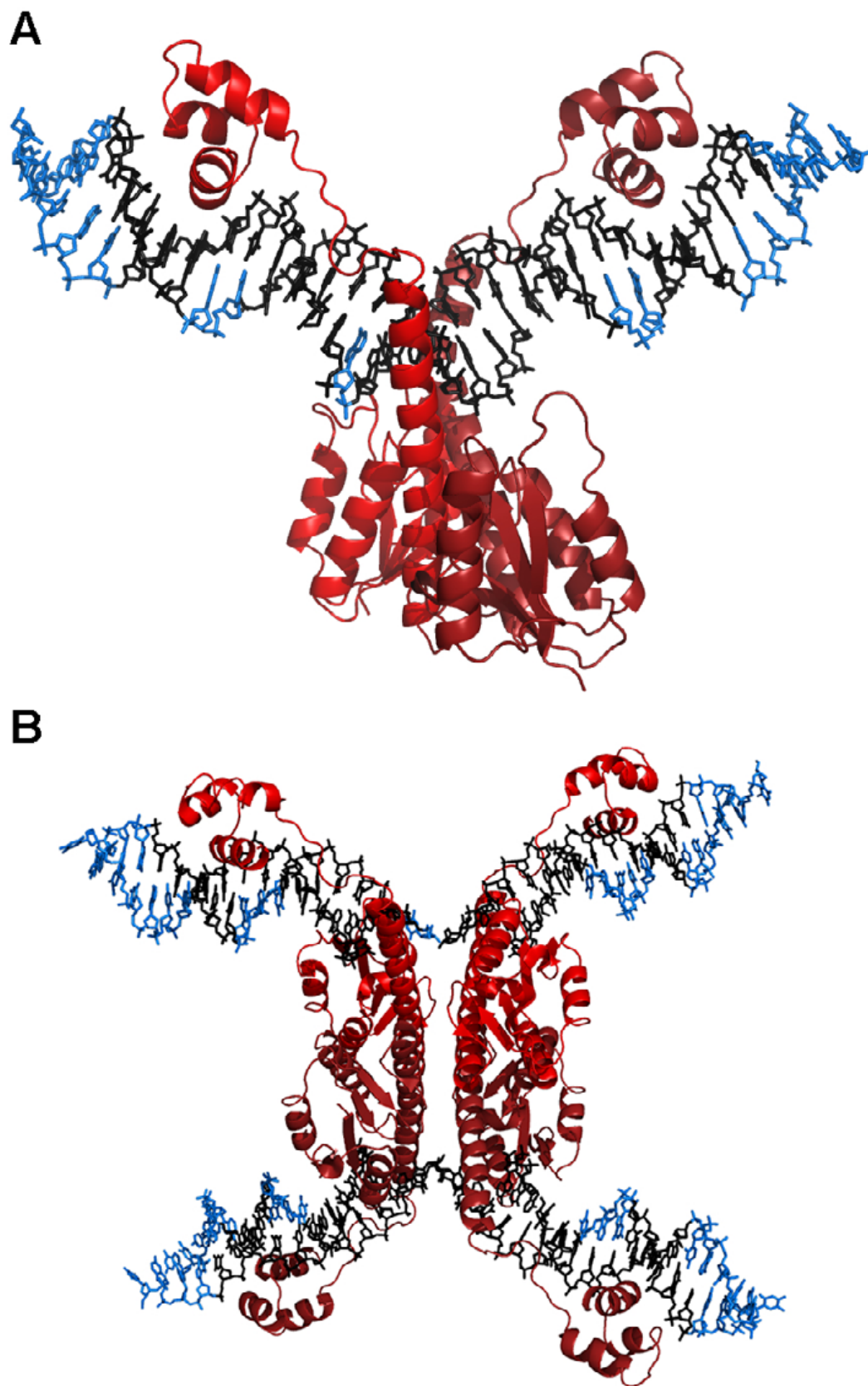


Figure 5.4: Separation of nucleotides in site I from bound resolvase units. The DNA is shown as sticks and the resolvase units as red cartoons. **(A)** In the crystal structure of a $\gamma\delta$ resolvase dimer bound to site I (pdb: 1GDT; Yang and Steitz 1995), several nucleotides of site I are separated from resolvase units by a minimum of 5 Å (highlighted in blue). **(B)** In the crystal structure of a cleaved $\gamma\delta$ site I synapse (pdb: 1ZR4; Li *et al.* 2005), several nucleotides are separated from the resolvase units by a minimum of 4 Å (highlighted in blue).

5.1.4 Design of fluorescent single-site substrates

The linear single-site substrates for *in vitro* recombination experiments are double-stranded DNA molecules, annealed from two synthesised oligonucleotides. The substrates contain one copy of Tn3 *res* site I at the centre, flanked by random GC-rich sequences which prevent fraying of the DNA. The substrates could be shorter than 50 bp without major adverse effects on binding, but the gel-based analysis of recombination products had been established in preliminary experiments with 50 bp substrates. Recombination of short substrates (50 bp) with competing long substrates (70-80 bp) had been found to give characteristic recombination products and intermediates. Locating site I at the centre of the short and long substrates simplifies the analysis of recombination products, since recombination of the sites in parallel and anti-parallel orientation results in products of the same length.

For FRET experiments, two dyes need to be introduced into the synapse. For this purpose, each of both site I substrates in the synapse can contain one fluorophore of the FRET pair. Alternatively, both dyes can be introduced into one site I substrate DNA while the second substrate remains unlabelled. Since both dyes of the FRET pair are conjugated to the DNA using the same chemical reaction, Cy3 and Cy5 need to be introduced into two different molecules in separate reactions to guarantee specific labelling (labelling reactions were performed in the W. Marshall Stark's laboratory). Therefore the oligonucleotides were synthesised with only one modified thymine for conjugation. Oligonucleotides with a single fluorophore can be annealed with an unlabelled oligonucleotide to form substrates with a single fluorophore, or they can be annealed with a second labelled oligonucleotide to form substrates with two dyes. An advantage of this approach is that oligonucleotides with fluorophores at different positions can be mixed and matched to produce a multitude of different FRET pairs.

In single-molecule experiments, the synaptic complexes are fixed to a surface via a biotin-neutravidin link. To enable this link, one of the substrates in the synapse needs to contain a biotin label. Oligonucleotides can be readily synthesised with a biotin at the 5' end. In this project, the biotinylated oligos always form the top strand of the single-site substrates.

To describe substrates with dyes attached at given positions, a nomenclature has been established (figure 5.5). Oligonucleotides with a biotin attached to the 5'-end carry a B at the start of the substrate name. This is followed by the length of the substrate in bases. Then, the letters L and R indicate if the dye is located to the left or right of the centre of

site I. The exact position of the dye is follows as a distance from the centre of site I in bases. Following the location of the dye, the dye type is given by the abbreviations C3 and C5 for Cy3 and Cy5 dyes. For example, a biotinylated oligonucleotide with a Cy5 dye attached to the right nucleotide of the central overlap is called B50R1C5. A double-stranded substrate containing this top-strand and a bottom-strand with further modifications would be called B50R1C5-50L1C3. This substrate can also be referred to B50R1C5L1C3 because it is not necessary to point out the double-stranded nature of the substrate since all substrates used in experiments during this project were double-stranded.

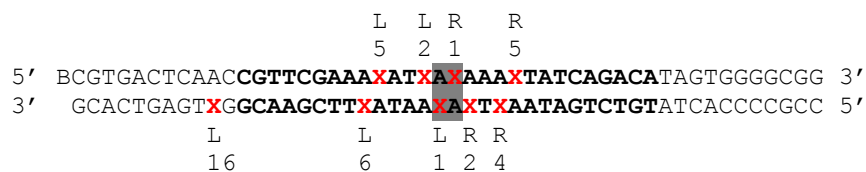


Figure 5.5: Nomenclature of linear single-site substrates. The linear substrates contain one copy of Tn3 *res* site I (bold) at the centre. The prefix “B” in the substrate name indicates that a biotin (B) is attached to the 5'-end of the top-strand. This prefix is followed by the length of the substrate in bases. Next, the letters L or R indicate if a fluorophore is located to the left (L) or right (R) of the centre of site I. The exact position of the fluorophore is then given as a distance from the centre of site I in bases. Last, the dye type is specified by C3 for a Cy3 dye and C5 for a Cy5 dye.

5.2 Conjugation of fluorophores to single-site substrates

The NHS ester group of the fluorophores reacts with the amine group of the modified thymines in the oligonucleotides to form an amide bond. Since the NHS ester group can react with other amines, any traces of contaminants containing amine groups were removed by ethanol precipitation prior to the conjugation reaction, while avoiding precipitants containing ammonium ions. The conditions of the conjugation reaction were optimised by testing the effect of the buffering agent, the pH, the percentage of dimethyl sulfoxide (DMSO) and the temperature on the efficiency of conjugation (figures 5.6, 5.7). Borate buffer at pH 8.5 improved the conjugation efficiency slightly, while the other parameters appeared to have no significant effect. In subsequent large-scale conjugation reactions, borate buffer (pH 8.5) and 14% v/v DMSO were used at room temperature. Variations between batches of the reactive dye were found to have the biggest impact on conjugation efficiency. Using dye packages with an undefined amount of dye (supplied by GE Healthcare), sold as sufficient for labelling a certain molar amount of amine groups, provided a lower labelling efficiency than using defined amounts of dye as recommended by fellow researchers (personal communication; see materials and methods).

5.3 Purification of fluorescent single-site substrates

The labelled substrates were initially pre-purified through NAP-5 gel-filtration columns to remove an excess of free dyes, but this step was later omitted in favour of ethanol precipitation, which does not dilute the sample so much and saves a concentration step. Further purification steps included denaturing gel purification, which required long polyacrylamide gels with a high polyacrylamide percentage due to the small separation between bands of labelled and unlabelled oligonucleotides (see figures 5.6, 5.7). After further ethanol precipitations, the purity of the labelled substrates was checked by gel-based analysis (figure 5.8) and by comparison of the absorbance of the dye and the DNA. Cy dyes, especially Cy5, are susceptible to damage through light exposure and oxidation, giving rise to a fraction of damaged dyes with an altered absorption spectrum. However, during the whole process of conjugation and purification, aggressive chemicals and light exposure were strictly avoided. As a result, no damaged fluorophores were detected (data not shown) and further HPLC purification of the oligos was not necessary. Subsequently, the single-site substrates were made by annealing purified oligonucleotides and required no further purification, as indicated by gel-analysis (data not shown). For details of the conjugation reaction and purification, refer to the materials and methods chapter.

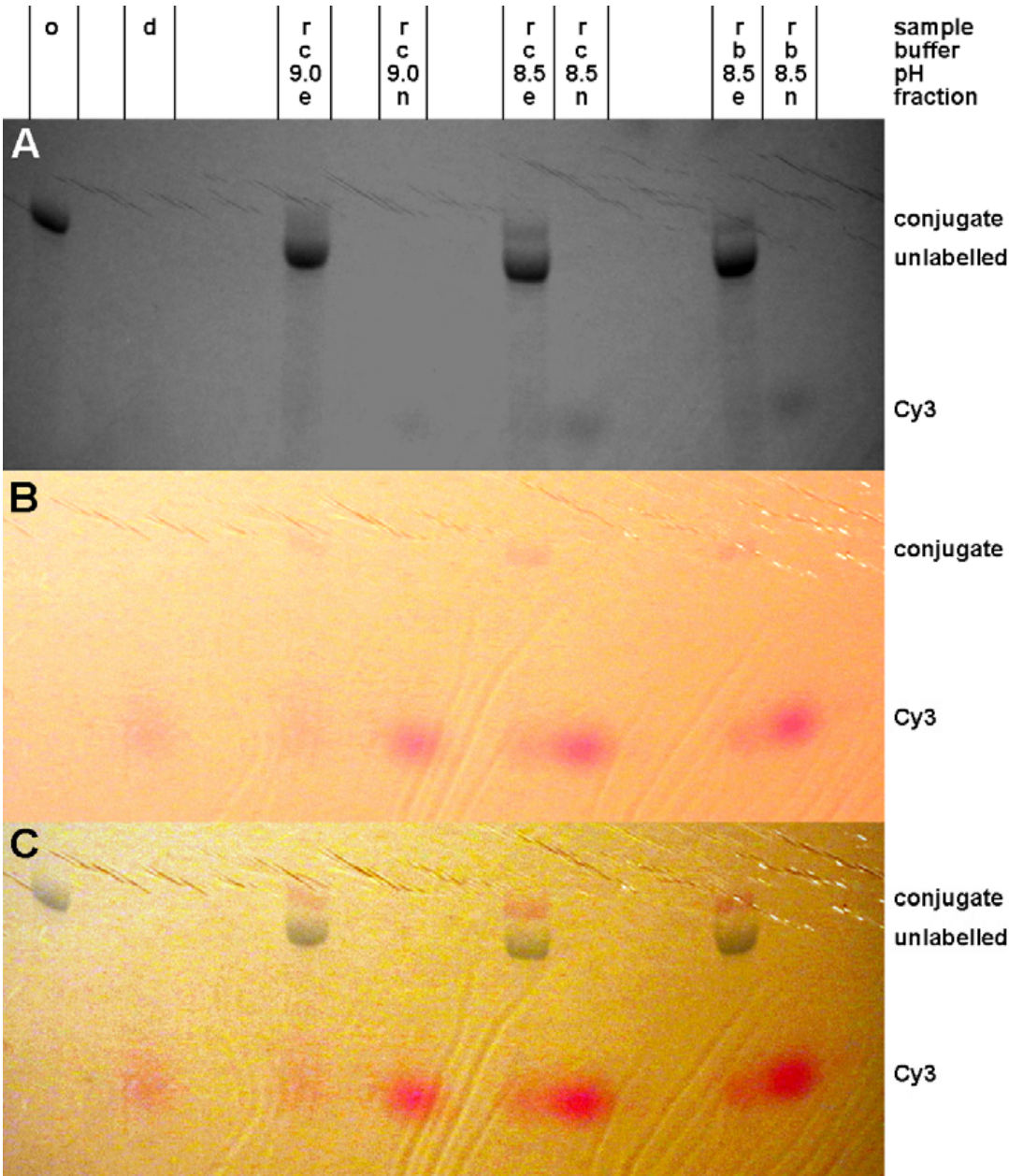


Figure 5.6: Effect of the buffering agent and pH on conjugation efficiency. Samples of the oligonucleotide B50R1 before (o) and after conjugation (r) and samples of the Cy3 dye alone (d) were run on a polyacrylamide gel (18% w/v acrylamide, TB). The bands were visualised using UV-shadowing (**A**), visible light (**B**) and an overlay of both methods (**C**) to match the bands. The conjugation reactions contained carbonate buffer (c) or borate buffer (b) at pH 9.0 or 8.5. The conjugation reactions were partly purified through a NAP-5 column. For each conjugation reaction, the elution fraction (e), containing most of the oligonucleotides, and the next fraction (n), containing mainly free Cy5, were loaded on the gel. The conjugate is slightly more retarded than the unlabelled oligonucleotide and the free Cy5 dye.

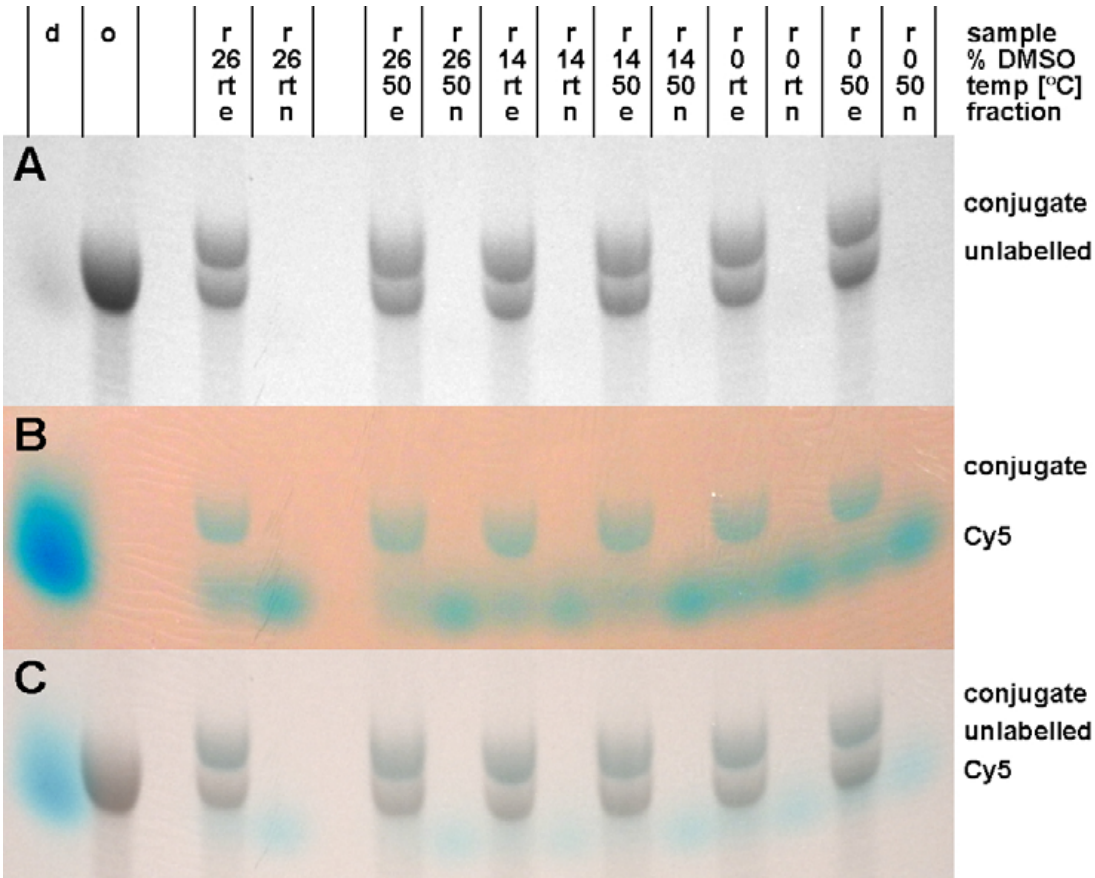


Figure 5.7: Effect of the DMSO content and temperature on the conjugation efficiency. Samples of the oligonucleotide 50L1 before (o) and after conjugation (r) and samples of the Cy5 dye alone (d) were run on a polyacrylamide gel (18% w/v acrylamide, TB). The bands were visualised using UV-shadowing (**A**), visible light (**B**) and an overlay of both methods (**C**) to match the bands. The conjugation reactions contained different percentages of DMSO and were performed at room temperature (rt) or 50 °C. The conjugation reactions were partly purified through a NAP-5 column. For each conjugation reaction, the elution fraction (e), containing most of the oligonucleotides, and the next fraction (n), containing mainly free Cy5, were loaded on the gel. The conjugate is slightly more retarded than the unlabelled oligonucleotide and the free Cy5 dye.

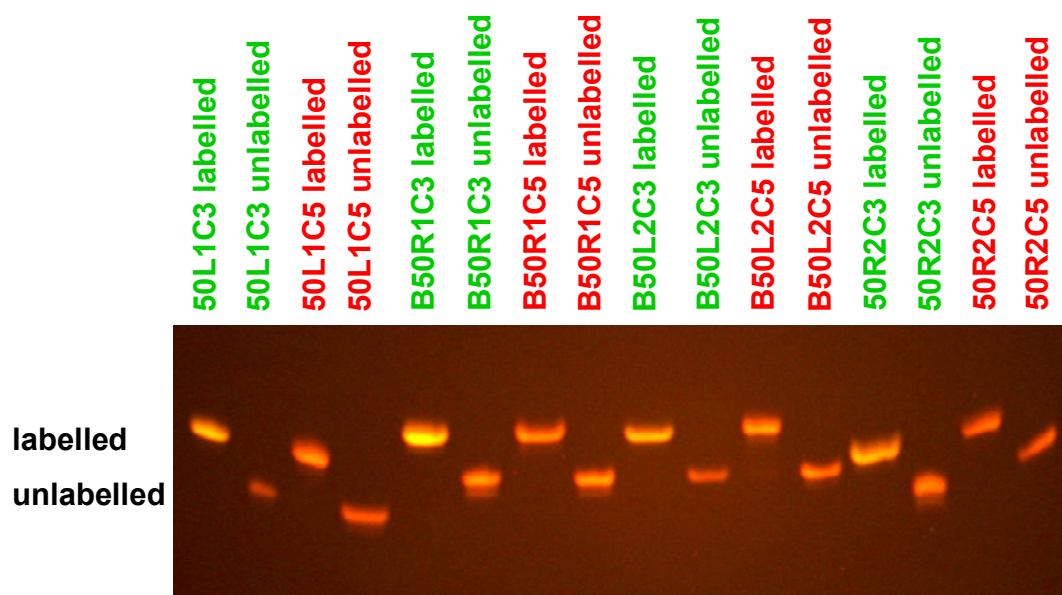


Figure 5.8: Gel-based control of the purity of labelled oligonucleotides. Oligonucleotides were labelled with Cy3 and Cy5 dyes at different positions. After the conjugation reaction, the labelled and unlabelled oligonucleotides were separated by denaturing PAGE and re-run on a denaturing polyacrylamide gel (18% w/v acrylamide, TB, thin) to check the purity. Bands are visualised on a UV transilluminator (short wavelength). In this representative example, all labelled oligonucleotides, apart from B50L2C5, were free of detectable amounts of unlabelled oligonucleotides.

5.4 Selection of fluorescent single-site substrates that allow synapse formation

Multiple single-site substrates with fluorophores in various positions were generated. To use fluorescent substrates for FRET-based experiments with Tn3 resolvase, it is necessary to select substrate variations that do not interfere with the recombination reaction. Synapse formation is a requirement for recombination. Stable synapses are also needed for single-molecule FRET experiments, which aim to follow the movements within a synapse for an extended time up to several minutes.

An established gel-based assay was employed to select fluorescent substrates which allow synapse formation. Tn3 resolvase NM (Tn3R NM) can bind to linear substrates containing a single copy of site I, bring two copies of the substrate together to form a synapse (Nollmann *et al.* 2004; Olorunniji *et al.* 2008) and recombine both copies of the substrate. Tn3R NM was added to radioactively labelled substrates and the resulting DNA-protein complexes were analysed by native PAGE. The binding reactions were performed in a standard buffer with low amounts of salt and in the absence of magnesium (see materials and methods), slowing down the ligation of cleaved intermediates and stabilising the synaptic complexes. In this native PAGE assay, the most retarded band potentially comprises synaptic complexes. To identify synaptic complexes unambiguously, Tn3R NM was bound to mixtures of a radioactive substrate and a non-radioactive substrate of a different length. This produces several distinct synaptic complexes which contain substrates of different lengths and show distinct retardation in the native gel. Specifically, a sample containing only short radioactive substrates (50 bp) and an excess of short non-radioactive substrates, can produce only a synapse with two short substrates (S50/50). If the short non-radioactive substrates (50 bp) are replaced with long non-radioactive substrates (70 bp), synaptic complexes with two short substrates (S50/50), with a short and a long substrate (S50/70) and with two long substrates (S70/70) are formed. However, only the S50/50 and the S50/70 complex contains radioactivity and so can be detected. Only the retardation of a radiolabelled synaptic complex can be altered by adding a competing, non-radioactive substrate of different length, since only the synaptic complex contains two DNA substrates. As a control, samples containing long radioactive substrates (70 bp) and long non-radioactive substrates (70 bp) produce synaptic complexes with two long substrates (S70/70). Samples with radioactive long substrates (70 bp) and short non-radioactive substrates (50 bp) produce two detectable synaptic complexes: S70/70 and S50/70. The S50/70 complexes of samples with radioactive long substrates and short non-radioactive substrates and of samples with short radioactive substrates and long non-

radioactive substrates should show the same retardation in the native gel, confirming the identity of the synaptic complexes.

Substrates with fluorophores at positions one and two bases left and right from the centre (L1, L2, R1, R2) were thought to be likely to have an adverse effect on recombination or synapse formation. Fluorophores close to the cleavage site might inhibit cleavage or ligation of the DNA and therefore inhibit the formation of covalent links between the DNA and resolvase. In addition, the pre-cleavage synapse may not provide a gap at the centre of site one to accommodate fluorophores, resulting in the destabilisation of the synapse by modifications at these positions. To test if substrates with fluorophores close to the cleavage site allow complex formation, several fluorescent substrates 50 were radioactively labelled and mixed with Tn3R NM. The resulting complexes were separated by native PAGE and visualised by phosphor-imaging.

5.4.1 Results

In native gels, the retardation of unbound short substrates with a single Cy3 or Cy5 dye attached to position L2, L1, R1 or R2 was very similar to the retardation of short non-fluorescent substrates (U50) and clearly distinct from the retardation of unbound long non-fluorescent substrates (U70) (figures 5.9, 5.10). The same is true for the monomer complexes (M50, M70), containing one DNA substrate and one resolvase subunit. Synaptic complexes containing two short fluorescent substrates (S50/50) ran at the same position as synaptic complexes containing non-fluorescent short substrates (S50/50). Adding an excess of long, non-fluorescent substrates produced an additional band with a distinct retardation (S50/70) and allowed the unambiguous identification of the synaptic complex as described above. Surprisingly, samples containing substrates with a single dye gave rise to slightly higher amounts of synaptic complexes than samples containing only non-fluorescent substrates. This was observed for samples containing only fluorescent substrates as well as for samples containing mixtures of fluorescent and non-fluorescent substrates. Samples containing only substrates with one fluorophore can only produce synapses with two fluorophores, while samples containing fluorescent and non-fluorescent DNA may produce synapses with one or two fluorophores. This suggests that the introduction of a single fluorophore or a fluorophore FRET pair does not inhibit the formation of stable synapses, even if the fluorophores are located one or two bases to the left or right of the centre of site.

Unbound short substrates with two fluorophores at any of the positions L2, L1, R1 and R2, showed a higher retardation than substrates with only one fluorophore (figures 5.11, 5.12).

However, the retardation of short substrates with two fluorophores was still similar to the retardation of short non-fluorescent substrates and clearly different from the retardation of long non-fluorescent substrates, allowing the identification of all complexes. As observed with substrates with a single fluorophore, substrates with two fluorophores produced higher amounts of synaptic complexes than non-fluorescent substrates. This effect seems appeared to be even stronger for substrates with two fluorophores. Samples containing only substrates with two fluorophores can only produce synapses with four fluorophores, while samples containing fluorescent and non-fluorescent DNA may produce synapses with two or four fluorophores. This suggests the introduction of a fluorophore FRET pair or even the introduction of four fluorophores does not inhibit the formation of stable synapses. Further, it suggests that substrates containing a FRET pair allow Tn3R NM to bind and form monomeric and dimeric complexes, which are the precursors of the synaptic complex.

In all binding experiments, Cy3 and Cy5 dyes showed the same effect on synapse formation.

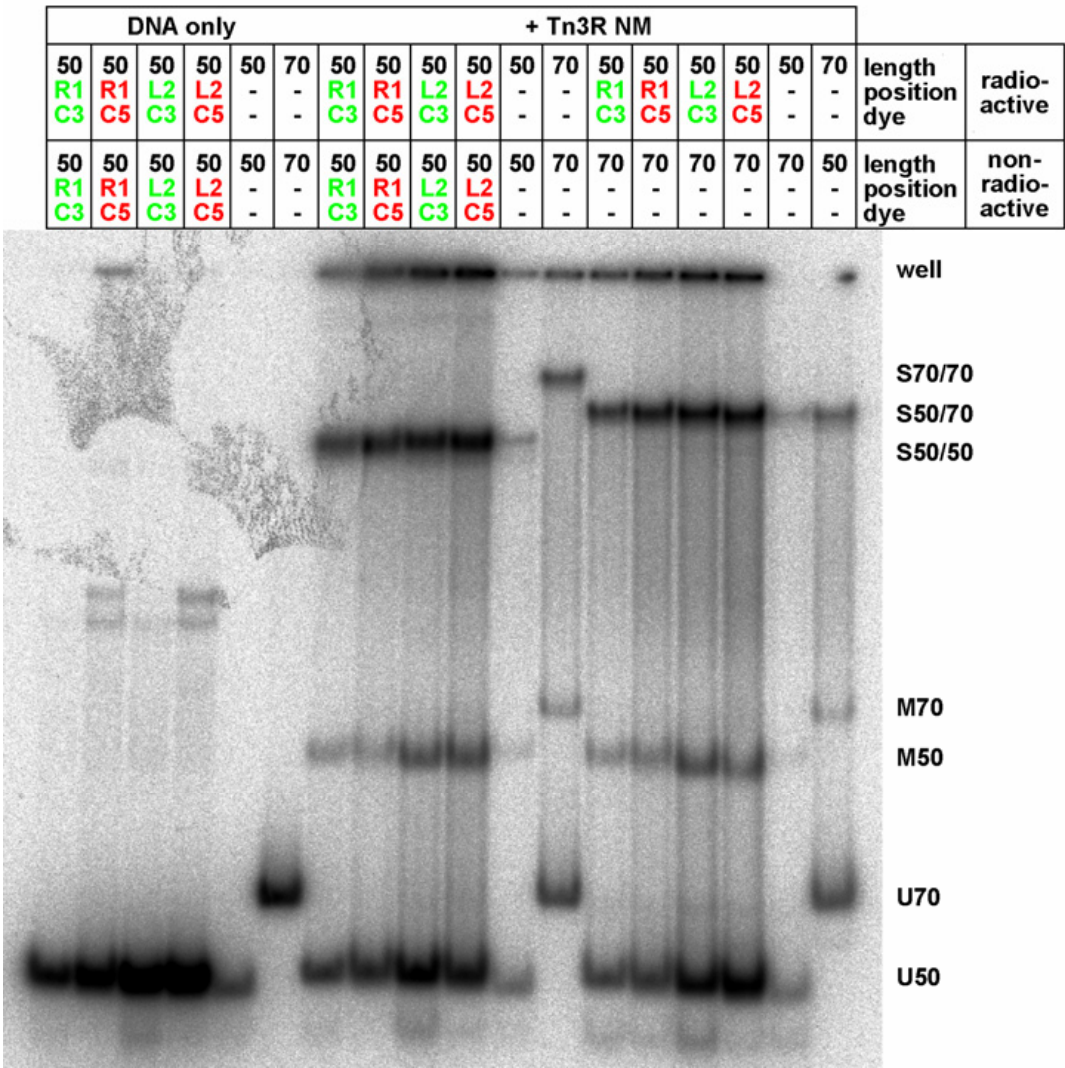


Figure 5.9: Synapsis of single-site substrates with a single fluorophore (R1, L2). Tn3 resolvase NM was bound to various mixtures of radioactive substrates and non-radioactive substrates and the resulting complexes were separated on a native polyacrylamide gel. All substrates were biotinylated at the 5'-end of the top strand. The length of the substrates is given in base-pairs and the position of fluorophores is indicated. The fluorescent substrates were found to form slightly higher amounts of synaptic complexes than non-fluorescent substrates. This experiment was performed once but is in agreement with results from earlier tests for optimisation.

Legend: U50 = unbound short substrates (50 bp), U70 = unbound long substrates (70 bp), M50 = resolvase monomer bound to short substrates, M70 = resolvase monomer bound to long substrates, S50/50 = synaptic complex with two short substrates, S50/70 = synaptic complex with one short and one long substrate, S70/70 = synaptic complex with two long substrates.

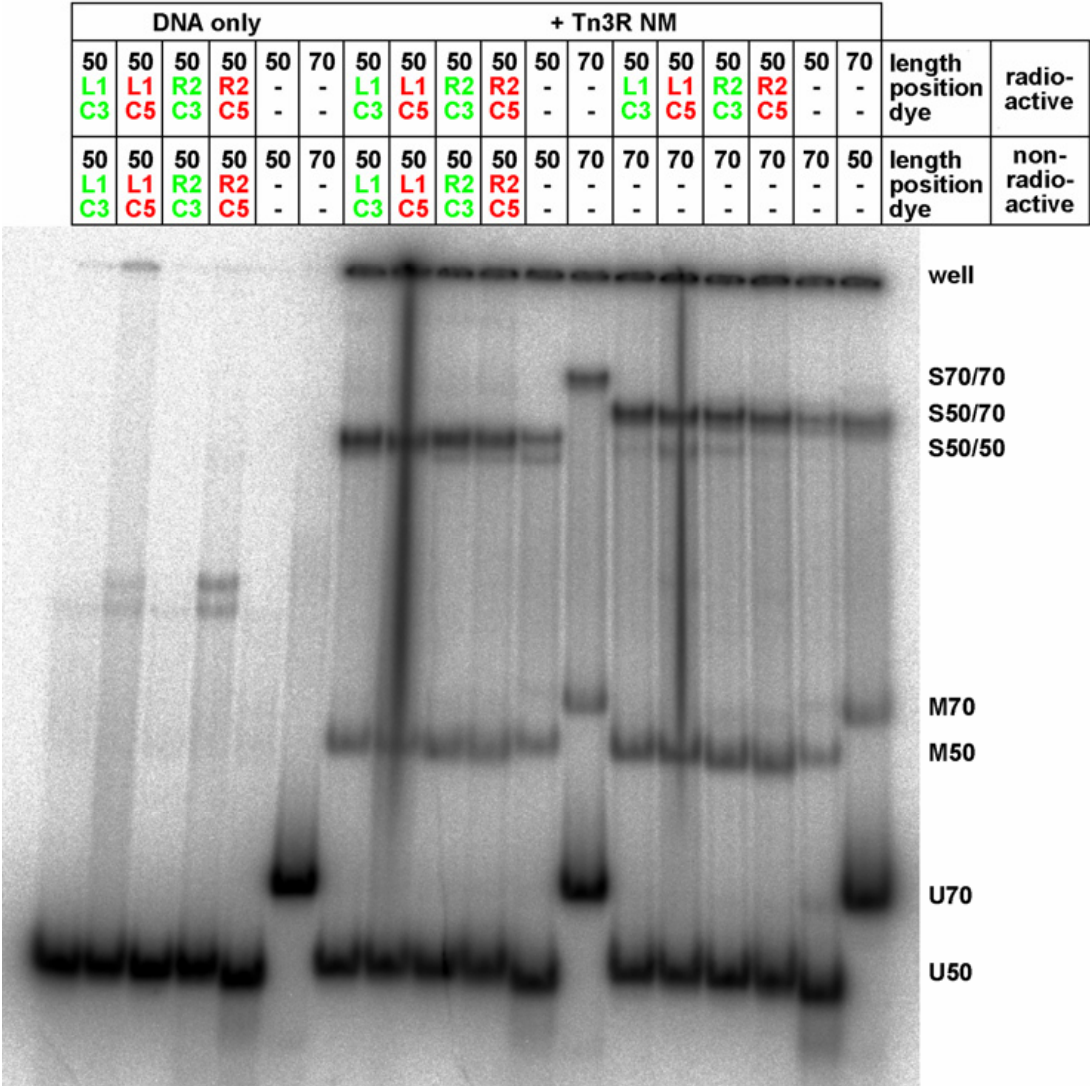


Figure 5.10: Synapsis of single-site substrates with a single fluorophore (L1, R2). Tn3 resolvase NM was bound to various mixtures of radioactive substrates and non-radioactive substrates and the resulting complexes were separated on a native polyacrylamide gel. All substrates were biotinylated at the 5'-end of the top strand. The length of the substrates is given in base-pairs and the position of fluorophores is indicated. The fluorescent substrates were found to form slightly higher amounts of synaptic complexes than non-fluorescent substrates. This experiment was performed once but is in agreement with results from earlier tests for optimisation.

Legend: U50 = unbound short substrates (50 bp), U70 = unbound long substrates (70 bp), M50 = resolvase monomer bound to short substrates, M70 = resolvase monomer bound to long substrates, S50/50 = synaptic complex with two short substrates, S50/70 = synaptic complex with one short and one long substrate, S70/70 = synaptic complex with two long substrates.

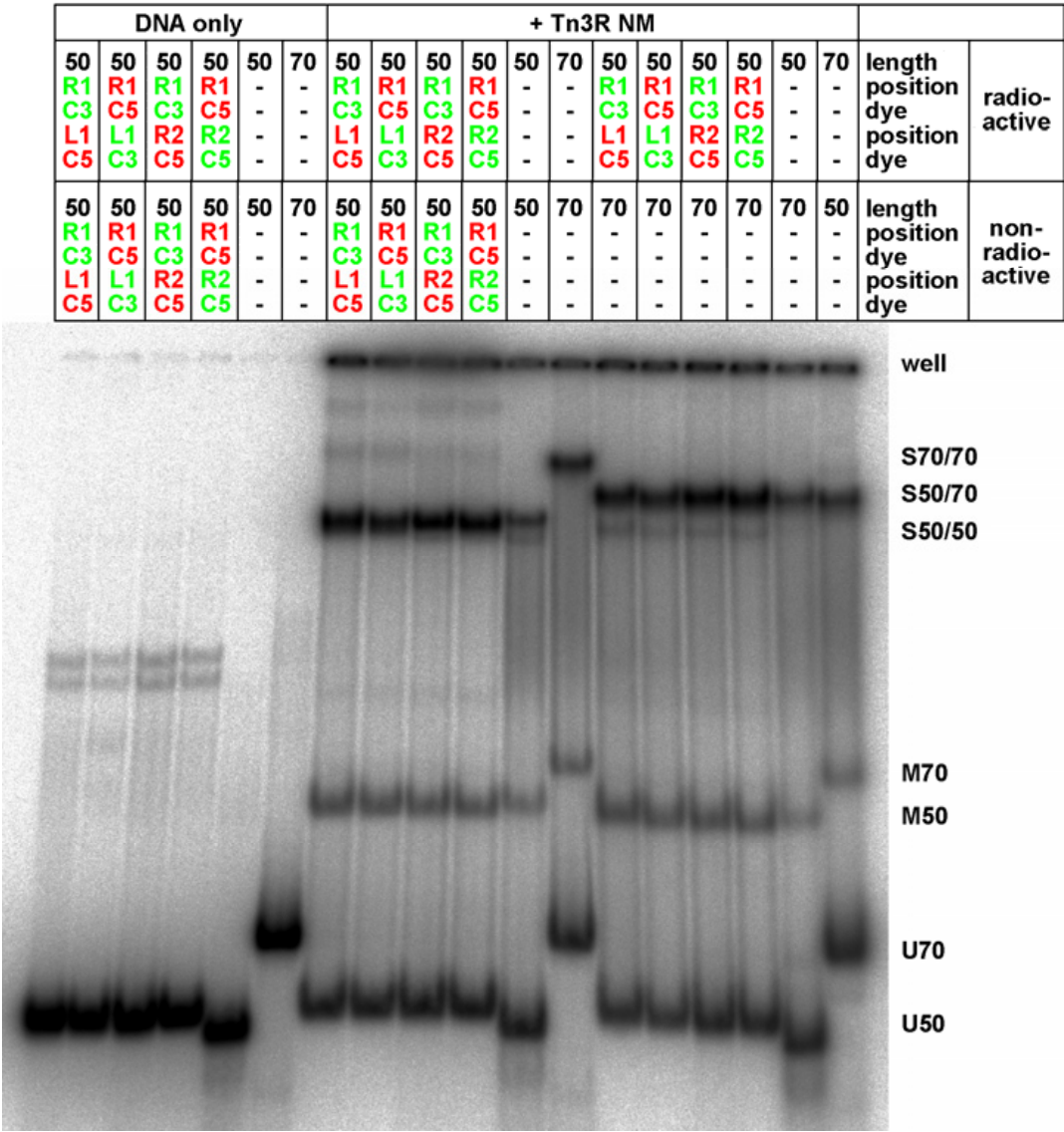


Figure 5.11: Synapsis of single-site substrates with two fluorophores (R1-L1, R1-R2). Tn3 resolvase NM was bound to various mixtures of radioactive substrates and non-radioactive substrates and the resulting complexes were separated on a native polyacrylamide gel. All substrates were biotinylated at the 5'-end of the top strand. The length of the substrates is given in base-pairs and the position of fluorophores is indicated. The fluorescent substrates were found to form slightly higher amounts of synaptic complexes than non-fluorescent substrates. This experiment was performed once but is in agreement with results from earlier tests for optimisation.

Legend: U50 = unbound short substrates (50 bp), U70 = unbound long substrates (70 bp), M50 = resolvase monomer bound to short substrates, M70 = resolvase monomer bound to long substrates, S50/50 = synaptic complex with two short substrates, S50/70 = synaptic complex with one short and one long substrate, S70/70 = synaptic complex with two long substrates.

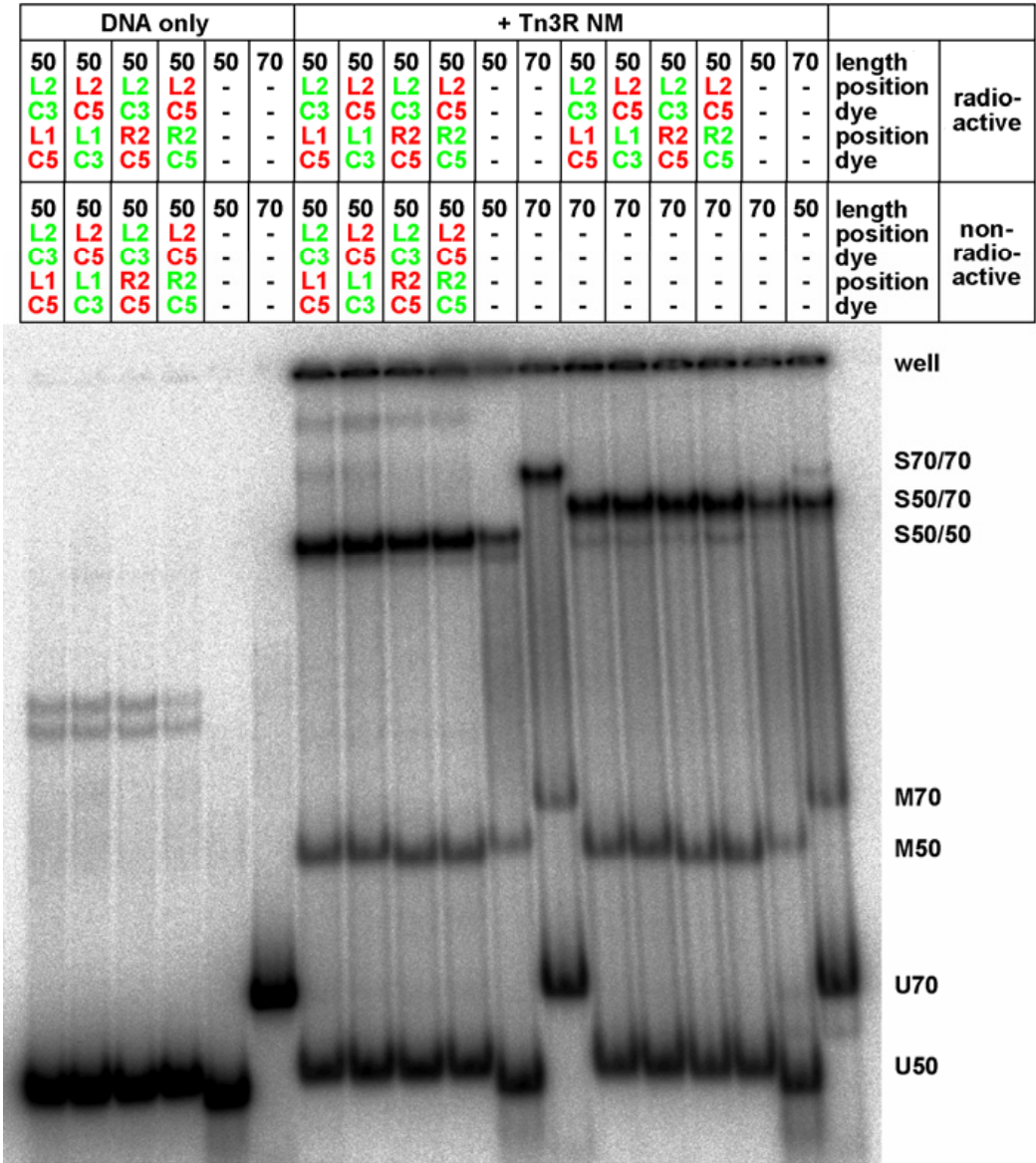


Figure 5.12: Synapsis of single-site substrates with two fluorophores (L2-L1, L2-R2). Tn3 resolvase NM was bound to various mixtures of radioactive substrates and non-radioactive substrates and the resulting complexes were separated on a native polyacrylamide gel. All substrates were biotinylated at the 5'-end of the top strand. The length of the substrates is given in base-pairs and the position of fluorophores is indicated. The fluorescent substrates were found to form slightly higher amounts of synaptic complexes than non-fluorescent substrates. This experiment was performed once but is in agreement with results from earlier tests for optimisation.

Legend: U50 = unbound short substrates (50 bp), U70 = unbound long substrates (70 bp), M50 = resolvase monomer bound to short substrates, M70 = resolvase monomer bound to long substrates, S50/50 = synaptic complex with two short substrates, S50/70 = synaptic complex with one short and one long substrate, S70/70 = synaptic complex with two long substrates.

5.4.2 Discussion

It was shown that the introduction of one, two or four fluorophores does not inhibit the formation of stable synapses, even if the fluorophores are located within or adjacent to the central overlap of site I. On the contrary, it appears the introduction of fluorophores results in the production of higher amounts of synaptic complexes. This effect is not necessarily due to a stabilising effect of the fluorophores on synapses, but may be due to the inhibition of cleavage or ligation of the substrates. The binding assay is performed at relatively low salt concentration and in the absence of magnesium with the intention of stabilising the synaptic complex. Recombination assays show that these conditions decrease the rate of ligation of cleaved intermediates, which may inhibit the dissociation of the synaptic complexes. It is therefore likely that the introduction of fluorophores does not interfere with complex formation but inhibits the cleavage and/or ligation of the substrates, therefore stabilising the synaptic complex. In future work, fluorescence anisotropy experiments it could be used to test if fluorophore stacking increases the stability of the complexes. If this was the case, the fluorescence anisotropy would be expected to increase significantly upon complex formation.

It was encouraging to know that multiple fluorophores can be attached to crucial positions at the centre of site I without inhibiting synapse formation. In addition, it has been shown that a FRET pair can be successfully introduced into the synapse either by using two substrates with one fluorophore each or by using one substrate with a FRET pair together with non-fluorescent substrates. Within a FRET pair, the position of the Cy3 and the Cy5 dye can be swapped, since both dyes had the same effect at a given position. However, the potentially adverse effects on cleavage or ligation highlighted the importance of a recombination assay to reveal the effect of fluorophores at any position on cleavage and ligation.

5.5 Recombination of single-site substrates without fluorophores within site I

The characterisation and optimisation of the recombination of non-fluorescent, linear single-site substrates by Tn3R NM should reveal if the recombination reaction can be studied by ensemble and single-molecule FRET experiments. Further, the recombination reaction needs to be optimised to allow the selection of suitable fluorescent substrates that allow unimpaired recombination by Tn3R NM. To avoid lengthy radioactive labelling, the recombination assay was optimised using a different fluorescent substrate to enable direct detection of recombination products using a fluorescence imager. In contrast to the fluorescent substrates for FRET experiments, the fluorescent substrate used for the optimisation of the recombination assay contained a Cy5 dye attached to position L16 outside site I to avoid interference with the recombination process. Comparison to previous experiments with radioactive substrates showed that substrates with a fluorophore at position L16 allow recombination rates similar to non-fluorescent substrates (data not shown).

For the recombination assay (figure 5.13), a short fluorescent substrate B50L16C5 (50 bp) is mixed with an excess of 80LR, a longer non-fluorescent competitor substrate (80 bp), and recombined by Tn3R NM under various conditions. Subsequently, non-covalent protein-DNA complexes are disrupted with SDS and the protein units of covalent complexes are digested by protease K. The reaction products are then separated on a gel containing SDS and visualised using a fluorescence imager. The competitor substrate 80LR features one copy of site I in the centre, and recombination in parallel or anti-parallel orientation results in products of similar length. The length of the original B50L16C5 substrate is 50 bp, fluorescent recombinant products from the recombination with 80LR have a length of 65 bp and fluorescent products resulting from unligated double-strand breaks (DSB) are 25 bp long. Recombination of two copies of B50L16C5 can result in products with two fluorophores, but these show the same retardation on a polyacrylamide gel as the original B50L16C5 substrate. The original competitor substrate 80LR and other recombination products without a fluorophore remain undetected using a fluorescence imager. As a control, identical samples are incubated with protein dilution buffer (RDB) only or with Tn3R NM-S10A. Tn3R NM S10A is an inactive version of Tn3R NM, in which the catalytic serine residue is replaced by an alanine.

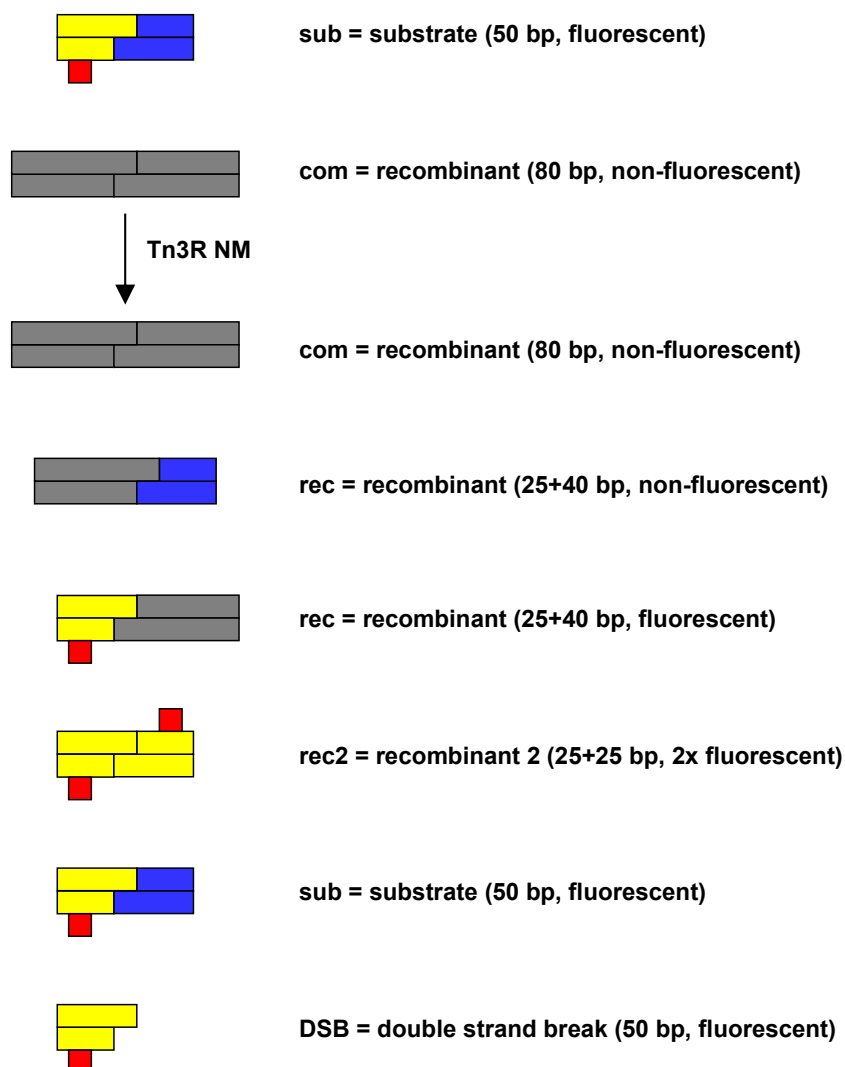


Figure 5.13: Recombination products of single-site substrates after protease K digest.

The substrate B50L16C5 features a Cy5 dye (red box) attached at position L16, a position outside site I. Recombination of B50L16C5 with the long competitor substrate 80LR (grey) can result in various products, which are depicted in the same order as they would appear after separation on a polyacrylamide gel. However, the rec and rec2 products exhibit the same retardation on a polyacrylamide gel. Only recombination products containing the left half of B50L16C5 (yellow) are detected when using a fluorescence imager. Products containing only the right half of B50L16C5 (blue) and/or one half of 80LR are not detected.

5.5.1 Effect of the resolvase concentration on recombination

There are several variables in the reaction conditions that can be optimised to allow a high degree of recombination. Initially it was confirmed that Tn3R NM works over a broad pH range around the commonly used pH of 8.2 (data not shown). However, it became clear that there was a great variation in the amount of recombination products when Tn3R NM was used at low concentrations. This suggested that the recombination reaction depends strongly on the concentration of Tn3R NM and that small inaccuracies in the added amount of protein cause big variations in the amount of recombinant products. To ensure consistent results, it needed to be established at what concentration the recombination activity of Tn3R NM reaches a plateau. Around this concentration, small inaccuracies in the added amount of Tn3R NM should have a minimal effect. Therefore, samples with 50 nM total substrate concentration were incubated with Tn3R NM at different concentrations. The concentration of the fluorescent substrate B50L16C5 was 25 nM, close to the relevant minimal concentration required for ensemble FRET experiments. The concentration of competitor substrate 80LR was 25 nM, too. All reactions were performed in the presence of 10 mM MgCl₂ to allow efficient ligation of the substrates. The recombination products were digested with protease K, analysed on a SDS gel and quantified (figure 5.14).

The recombination activity was found to reach a plateau at a Tn3R NM concentration of about 1,500 nM, which equals a molar ratio of resolvase monomers / substrate DNA of 30 (figure 5.14B). The formation of recombinant products was found to be incomplete after 5 minutes and more recombinant products were found after 60 minutes. In contrast, the amount of half-site products, resulting from unligated double-strand breaks (DSB), was the same after 5 minutes and 60 minutes. It is likely that the DSB product is derived from active synapses with a DSB in both substrates. This suggests that active, cleaved synapses are formed rapidly and remain at a constant concentration for an extended time. In the context of single-molecule experiments, this would provide a good basis to study active synapses.

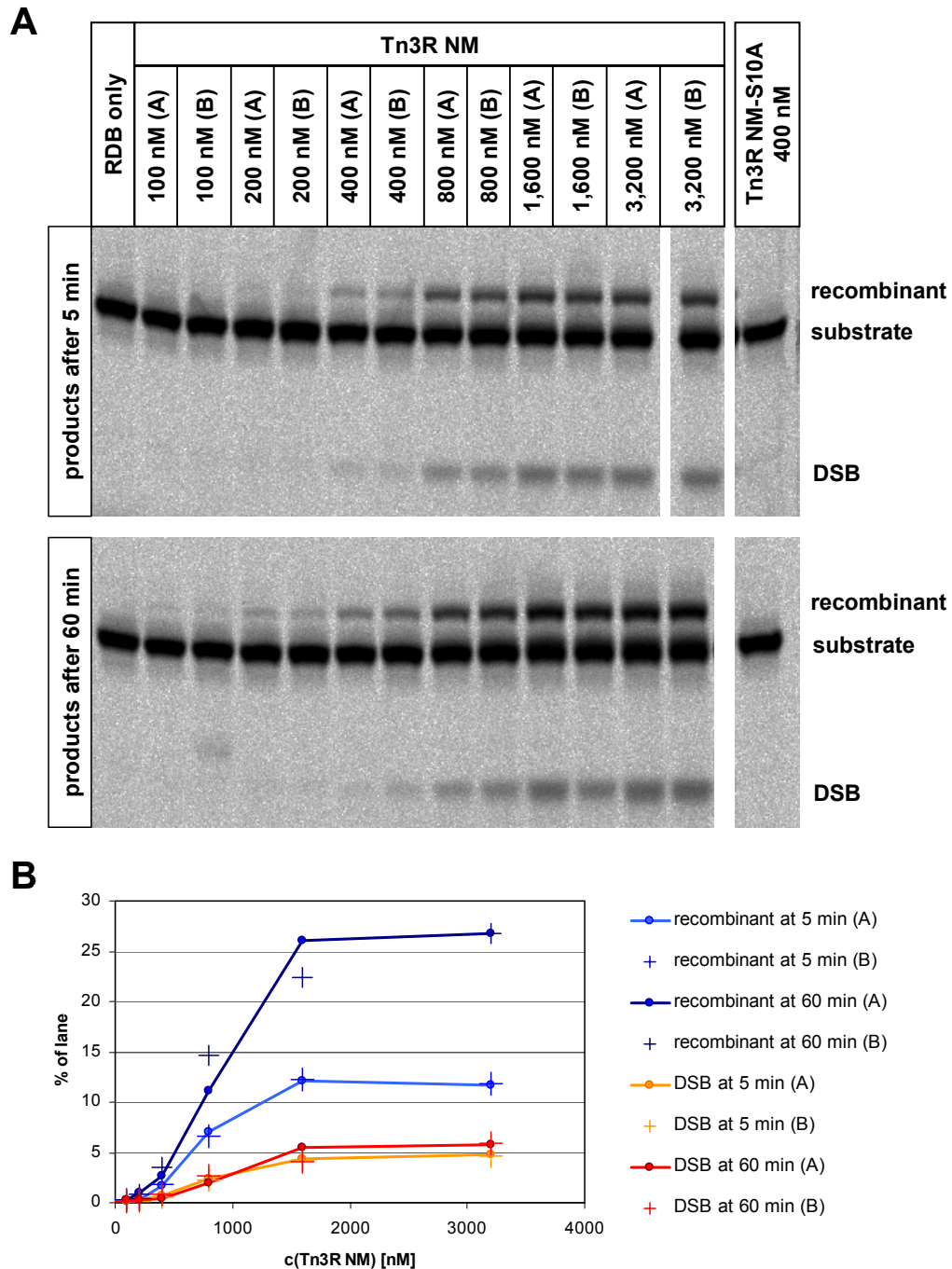


Figure 5.14: Effect of the Tn3R NM concentration on recombination efficiency. Two identical samples (A and B) containing the fluorescent substrate B50L16C5 (25 nM) and the competitor substrate 80LR (25 nM) were incubated with different concentrations of Tn3R NM at room temperature. As a control, samples were incubated with resolvase dilution buffer (RDB) only or with inactive Tn3R NM-S10A. The reaction buffer contained 100 mM Tris-HCl (pH 8.2), 10 mM MgCl₂ and 50 g/ml poly-dIdC. Samples were taken after 5 min and 60 min, stopped with SDS, digested with protease K and separated by SDS-PAGE (10% w/v acrylamide). **(A)** The separated reaction products were visualised using a fluorescence imager. **(B)** Quantification of the reaction products showed that the amount of recombinant products reaches a plateau at a Tn3R NM concentration of about 1,500 nM.

5.5.2 Combined effects of the concentrations of resolvase, the substrates and non-specific DNA analogues

To optimise the recombination reaction further, it was tested if a higher percentage of the fluorescent substrate can be recombined with the competitor substrate by increasing the concentration of the competitor substrate (figures 5.15, 5.16). This may be useful to identify fluorescent substrates that allow recombination only at low rates. It may also help to induce larger FRET changes in ensemble FRET experiments. Increasing the overall substrate concentration, without altering the ratio of the competitor substrate and the fluorescent substrate, may also have a direct effect on the recombination efficiency.

When increasing the total substrate concentration, it is likely that the resolvase concentration needs to be increased accordingly to keep the molar resolvase/substrate ratio constant. Therefore, samples containing increasing total substrate concentrations were incubated with Tn3R NM either at a fixed concentration of 1,500 nM or at concentration raised according to the substrate concentration (figures 5.15, 5.16). An increased concentration of resolvase may result in aggregation of the protein. It was tested if the recombination efficiency is influenced by addition of poly-dIdC which provides stabilising, non-specific interactions with resolvase (figures 5.15, 5.16). However, poly-dIdC may have an adverse effect at high concentrations since it may act as a competitor to the substrates.

As expected, the ratio of the competitor / fluorescent substrate had the biggest effect on the percentage of fluorescent substrates that were recombined with the competitor (figure 5.16). Increasing the total substrate concentration, without altering the competitor / fluorescent substrate ratio, enhanced the recombination efficiency only moderately. When increasing the total substrate concentration only slightly, the Tn3R NM concentration could be kept at 1,500 nM without impairing recombination strongly. However, a strong increase in total substrate concentration while fixing the Tn3R concentration to 1,500 nM resulted in decreased recombination with large variations between samples. An adjustment of the Tn3R NM concentration proportional to the total substrate concentration was required, keeping the resolvase / substrate ratio at about 30. The concentration of poly-dIdC had little influence on the recombination efficiency, as long as the resolvase / substrate ratio was sufficient. At low resolvase / substrate ratios, a high amount of poly-dIdC had a negative effect on recombination, presumably because poly-dIdC binds and removes a fraction of the available resolvase. In summary, samples with a high competitor / fluorescent substrate ratio, a resolvase / substrate ratio around 30 and about 50 µg/ml

poly-dIdC seem to provide efficient recombination between the fluorescent substrate and the competitor substrate.

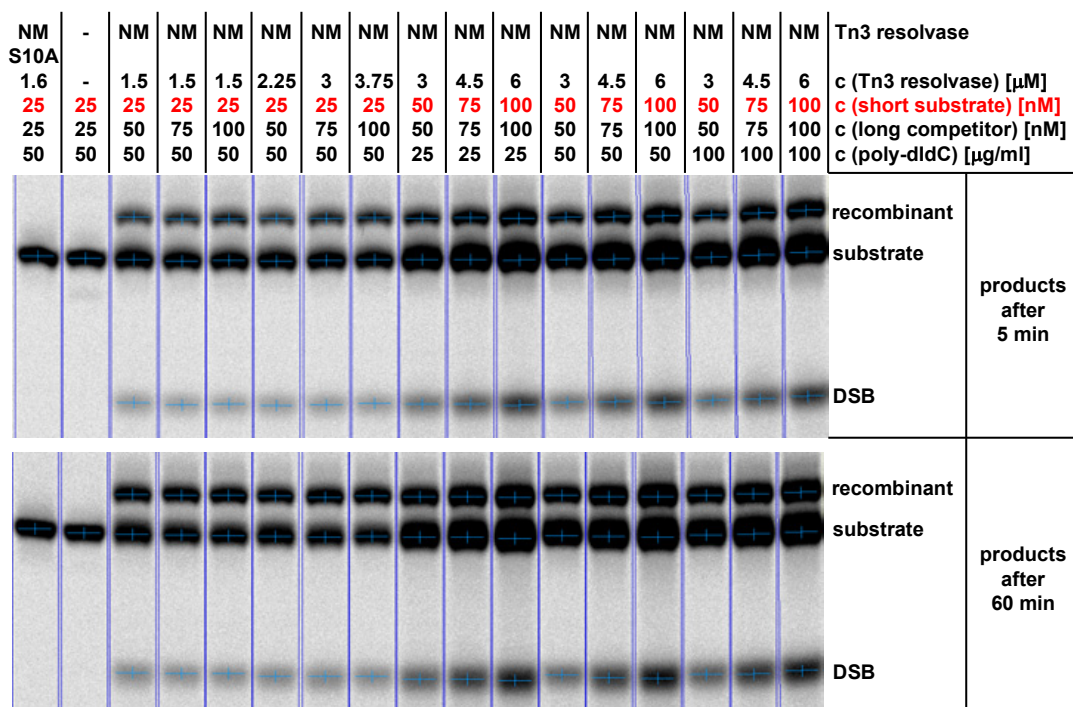
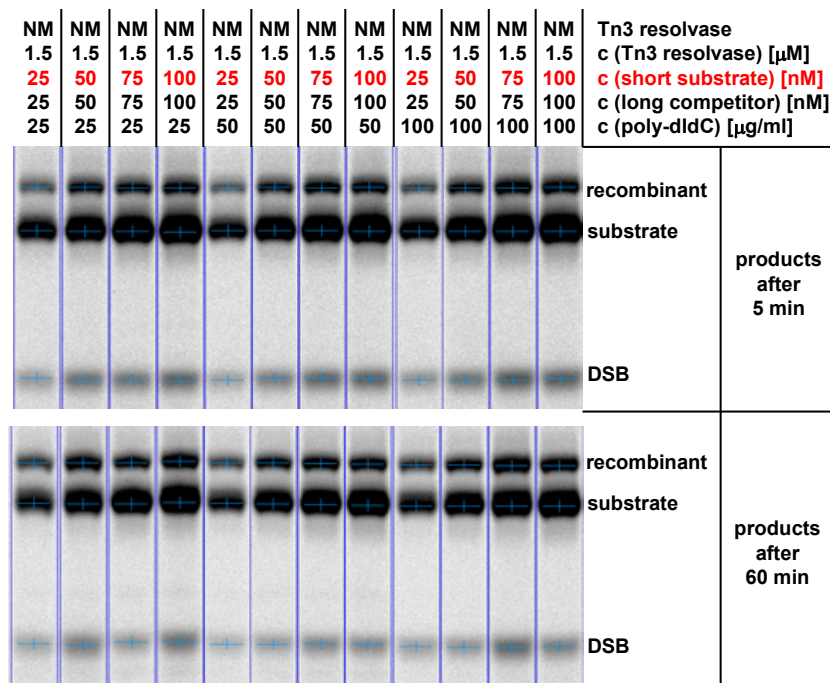


Figure 5.15: Effect of substrate, resolvase and poly-dIdC concentration on recombination efficiency (gel pictures). Samples containing different concentrations of the fluorescent substrate B50L16C5, of the competitor substrate 80LR and of poly-dIdC were incubated with different concentrations of Tn3R NM at room temperature. The reaction buffer contained 100 mM Tris-HCl (pH 8.2) and 10 mM MgCl₂. As a control, samples were incubated with resolvase dilution buffer only or with inactive Tn3R NM-S10A. Samples were taken after 5 min and 60 min, stopped with SDS, digested with protease K, separated by SDS-PAGE (10% w/v acrylamide). The reaction products were detected with a fluorescence imager and quantified. The gel pictures (exponential contrast) include lane and band markers used during quantification.

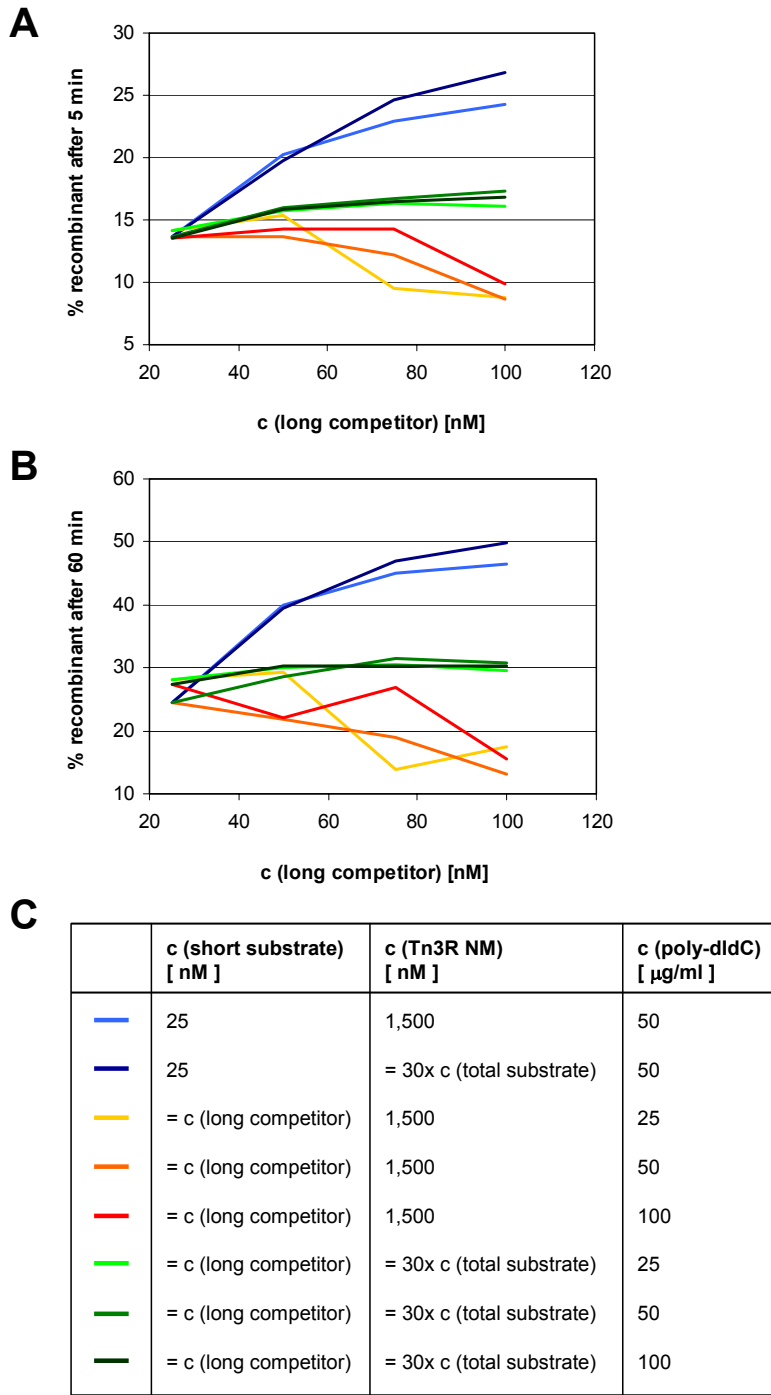


Figure 5.16: Effect of substrate, resolvase and poly-dIdC concentration on recombination efficiency. Samples containing different concentrations of the fluorescent substrate B50L16C5, of the competitor substrate 80LR and of poly-dIdC were incubated with different concentrations of Tn3R NM at room temperature. The reaction buffer contained 100 mM Tris-HCl (pH 8.2), 10 mM MgCl₂. Further reaction mixtures are described in the table (C). Samples were taken after 5 min (A) and 60 min (B), stopped with SDS, digested with protease K, separated by SDS-PAGE (10% w/v acrylamide) and quantified. The same sample was used for the data points after 5 min and 60 min. The data points in the plots (A) and (B) correspond to a single experiment which is in good agreement with previous experiments for the optimisation of the reaction conditions.

5.5.3 Kinetics of recombination and the effect of magnesium ions

It had become clear that the process of recombination is not completed after 5 minutes, but it remained unclear whether recombination had reached a plateau after 60 minutes (5.14B, 5.16A/B). Therefore, a time-course of recombination was performed under optimised reaction conditions to establish when recombination reaches a plateau and what amount of recombinant products is maximally formed. Furthermore, the effect of the concentration of magnesium ions on the formation of recombination products and intermediates was tested (figures 5.17, 5.18).

In the time-course experiment, DSB products were formed quickly and reached a stable level after about one hour (figure 5.18). The amount of DSB products was greatly increased in the absence of magnesium, suggesting that ligation was more inhibited than cleavage. DSB products formed more quickly than recombinant products and the concentration of DSB products reached a plateau while recombinant products were still being formed at high rates. This indicates that the DSB products are an intermediate of the recombination reaction rather than the "dead end" product of disrupted intermediates, which would accumulate as long as recombination proceeds. Therefore, the DSB products most likely represent synapses containing substrates with double-strand breaks, which are disrupted only after the addition of SDS. It is unclear if these synapses are in a recombinant or non-recombinant state before the addition of SDS, since this information is lost upon dissociation.

The rate of the formation of recombinant products increased with the magnesium concentration (figure 5.18). In the presence of magnesium, the amount of recombinant products reached a plateau after about 10 hours but in the absence of magnesium the plateau had not been reached within 24 hours. In the presence of 10 mM or 20 mM magnesium, about half of the final amount of recombinant products was formed already after 5 minutes while it takes longer to reach this point in the absence of magnesium.

The depletion of the substrate appeared to follow an exponential decay function, while the accumulation of recombinant products seemed to follow an exponential association function (figure 5.18). However, at least in the absence of magnesium, it appeared that initially recombinant products were formed quickly, but later the amount increased at a much slower rate, instead of reaching a plateau as quickly as expected from the initial rate. This suggests that there may be a slow and a fast process contributing to the decay of the substrate and the accumulation of recombinant products. To test this hypothesis, the

experimental data were fitted with exponential functions with one or two phases using the Prism software (figure 5.19). Since the recombination status of the DSB products is unknown, only the substrate and recombinant product quantities were fitted. Omitting the DSB products, the sum of the quantities of the substrate and the recombinant products was defined as 100%. Only the decay of the substrate needed to be fitted, since the accumulation of recombinant products is simply the reverse process. The substrate concentration was fixed to 100% at 0 minutes to improve the fits. Exponential decay functions with two phases could be fitted to the experimental data significantly better than exponential functions with one phase (figure 5.19B). Interestingly, fits using two phases provided similar plateaus of the substrate percentage at around 23-28%, equivalent to 72-77% recombinant products, in the absence and presence of magnesium. The calculated half-life of the fast decay process was similar in the presence and absence of magnesium at around 2.7 to 3.3 minutes. However, the rate of the slow decay process increased greatly with increasing magnesium. The calculated half-life of the slow decay process was 177 minutes in the absence of magnesium and only 44 minutes in the presence of 20 mM MgCl_2 . It is hard to assign a particular catalytic process to the fast and the slow processes. One possibility is that the fast process represents simple recombination, consisting of cleavage, strand-exchange and ligation of at least one single-strand per substrate, while the slow process may represent the dissociation and re-assembly of synapses which allows re-recombination of the substrates and requires complete ligation of double-strand breaks.

The theoretical maximum percentage of recombinant products can be calculated to test if re-assembly of complexes plays a role in recombination (figures 5.20, 5.21). In samples containing a 4:1 mixture of competitor and (fluorescently labelled short substrate, recombination without synapse re-assembly can result in a maximum of 40% of detectable recombinant products in the sample, while recombination with reassembly synapses can achieve a maximum of 80%. This calculation takes into account that some recombination products cannot be detected, that some products contain two fluorophores and that some products have similar retardations on a polyacrylamide gel. Assuming that reassembly of synapses takes place, recombination products from the first synapses can be recombined again with any other substrate, competitor or recombination product (figure 5.20). As a result, the left and right halves of all short and long substrates are mixed and matched. Therefore, the product mixture at equilibrium depends on the probabilities of all the possible combinations of the half substrates and competitor substrates. If no reassembly of synapses takes place, synapses stay stable once assembled and can contain only combinations of the original short substrate and the long competitor substrate (figure 5.21). Only recombination products of the original substrate and competitor can be formed. It has

to be taken into account, that there are different probabilities for any two substrates to come together. Furthermore, the substrates can come together in different orientations and recombination may proceed several times, resulting in recombinant and non-recombinant products.

Comparing the calculated maximum percentage of recombinant products (figures 5.20, 5.21) to the experimental data (figure 5.18), it becomes clear that in all samples more recombinant products had been formed than would be possible without synapse reassembly. At the plateau, the recombinant products reach, in the presence of magnesium, a percentage very close to the maximum that can be achieved with synapse reassembly (80%). The sample without magnesium did not reach a plateau and proceeded to about 55% within 24 hours. This suggests that complex reassembly takes place and that its rate might be dependent on the presence of magnesium (at least in samples with low overall salt concentrations). Visual inspection of the graph plotting the accumulation of recombinant products measured in the absence of magnesium (figure 5.18) shows the following: Before the effect of the slow component of recombination is large, the fast component appears to tend towards a plateau at a percentage of recombinant products of around 30-50%. This is in the region of the maximum of recombinant products without synapse reassembly (40%), suggesting that the slow component of recombination represents the process of synapse reassembly.

Fits using a two-phase exponential decay function calculated plateaus at similarly high percentages of recombinant products (72-77% of the sum of recombinant products and original substrates) for samples with and without magnesium (figure 5.19B). This supports the idea that synapse reassembly takes place both in the presence and absence of magnesium, only the rates differ. Furthermore, fitting two-phase exponential decay functions predicted similar half-lives of the fast component of recombination in the presence and absence of magnesium. In contrast, the half-life of the slow component decreases with increasing magnesium concentrations, suggesting that the rate of synapse reassembly increases with increasing magnesium concentrations.

In summary, it became clear that the rate of substrate ligation increases with increasing magnesium concentrations. Therefore it appears to be best to select fluorescent substrates using high magnesium concentrations that allow uninhibited recombination, including the ligation step. The time-course experiment showed that a high rate of recombination can be observed throughout the first 30 minutes of the reaction, which is promising in the context of single-molecule experiments (figure 5.18). Furthermore, in the absence of magnesium,

the sample contains a high percentage of DSB products, presumably representing active synapses with unligated substrate DNA. It is likely that those synapses perform strand exchange but ligate the substrate at a lower rate, since recombination was shown to proceed even in the absence of magnesium. Therefore, samples without magnesium may be suited for single-molecule experiments, since the probability of finding active complexes is increased. In addition, fitting the time-course data with exponential decay functions suggested that the half-life of synapse reassembly (44-177 min) is much higher than the half the fast component of recombination (2.7-3.3 min) (figure 5.19B). This indicates a high probability of finding and observing stable, active synapses within the timescale of single-molecule experiments. Again, it may be beneficial to perform single-molecule experiments in the absence of magnesium, since this appears to increase the half-life of synapse reassembly which means the synapse stability is enhanced.

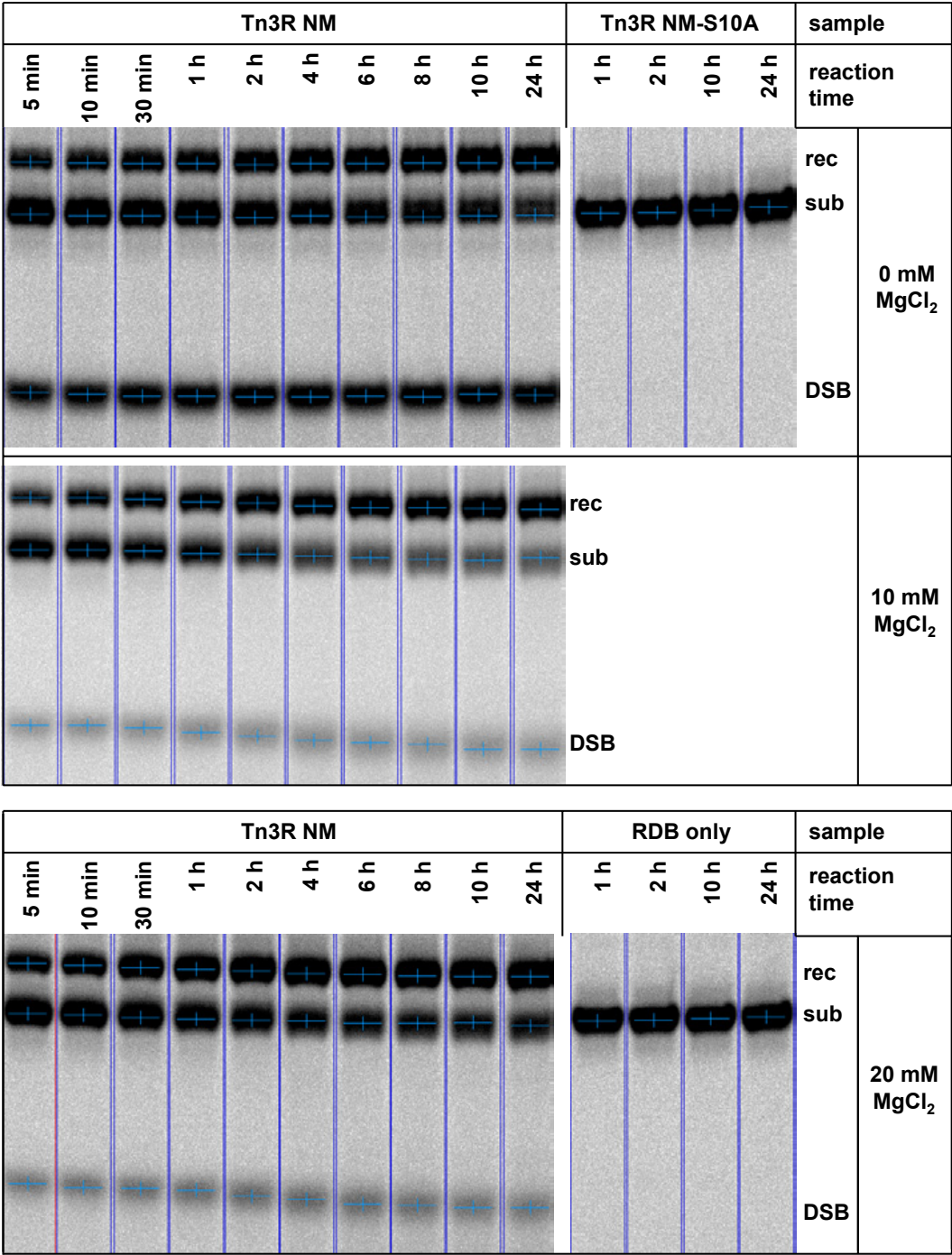


Figure 5.17: Time-course of recombination of single-site substrates (gel pictures).

Samples containing B50L16C5 (20nM) and the competitor substrate 80LR (80 nM) were incubated with Tn3R NM (3 μ M) at room temperature. The reaction buffer contained 100 mM Tris-HCl (pH 8.2), 50 mg/ml poly-dIdC and 0, 10 or 20 mM MgCl₂. As a control, samples were incubated with resolvase dilution buffer only or with inactive Tn3R NM-S10A (1.6 μ M). Samples were taken at different time points, stopped with SDS, digested with protease K and separated by SDS-PAGE (10% w/v acrylamide). The reaction products were detected with a fluorescence imager and quantified. The gel pictures (exponential contrast) include lane and band markers used during quantification.

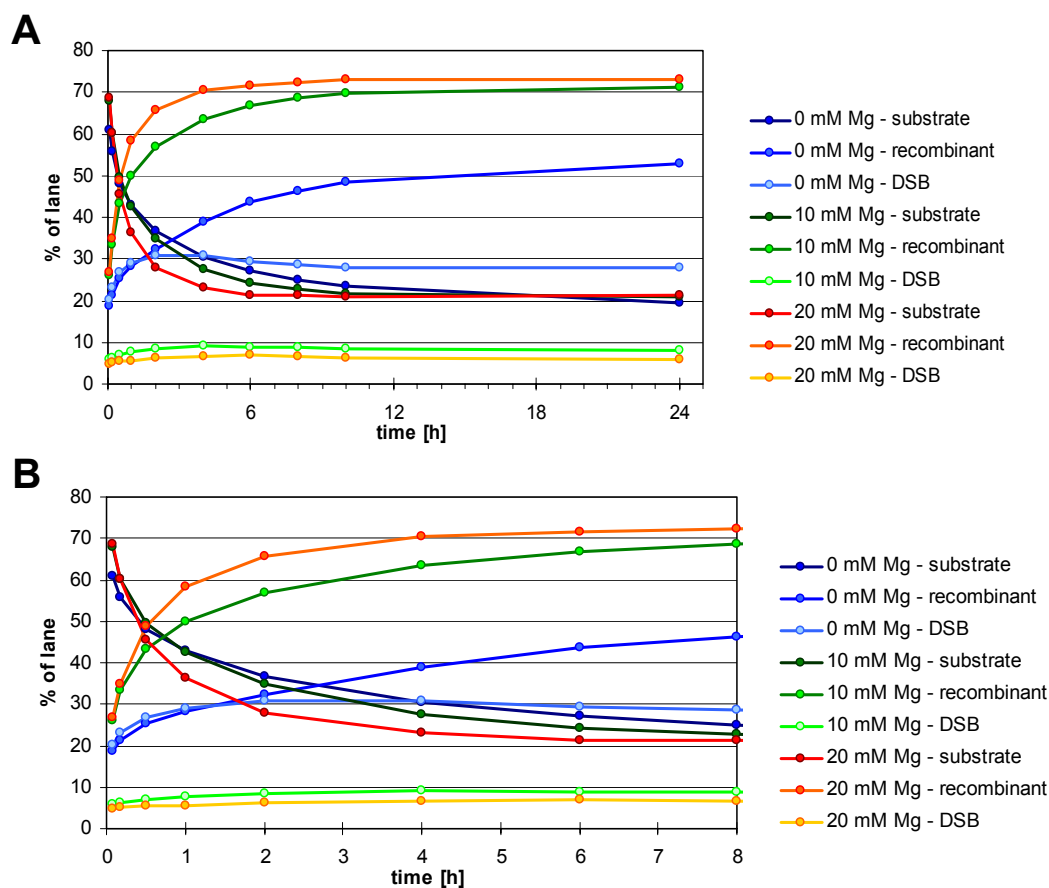


Figure 5.18: Time-course of recombination of single-site substrates. The reaction products in a time-course of recombination (figure 5.17, data corresponds to a single experiment) were quantified and plotted against time. Zooming from the full timescale (**A**) into the earlier part of the reaction (**B**), it can be seen that, in the presence of 20 mM MgCl₂, about 50% of the final amount of recombinant products is formed already after 5 min. Recombinant products are formed more slowly in the absence of magnesium ions, and an increased amount of products with double-strand breaks (DSB) is formed.

The data corresponds to a single experiment in agreement with other time-course experiments with different substrates and fewer time points (data not shown).

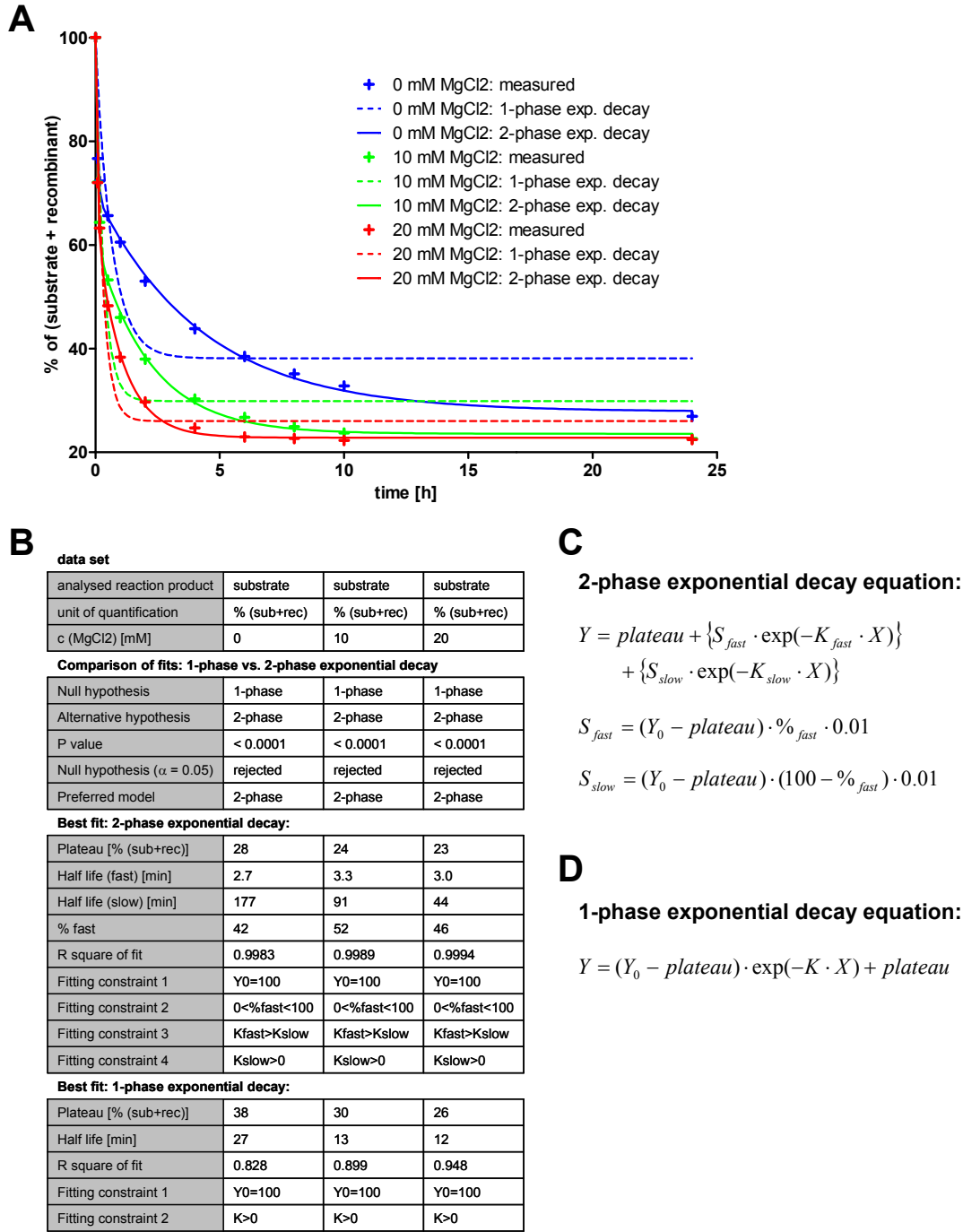


Figure 5.19: Exponential decay fits of a recombination time-course. The sum of the substrate and recombinant product in the samples of the recombination time-course (see figures 5.17, 5.18) was defined as 100%, eliminating the DSB products. **(A)** The substrate concentration was fixed to 100% at 0 min and exponential decay functions were fitted over the whole time range. **(B)** A 2-phase exponential decay function, consisting of two decays with different half-lives **(C)**, provided a significantly better fit than a 1-phase exponential decay function **(D)**. The 2-phase fits show that the fast decay is similar at all magnesium concentrations, while the slow decay increases with the magnesium concentration.

The data corresponds to a single experiment in agreement with other experiments with different substrates and fewer time points (data not shown).

A**original substrate ratio**

1x short substrate: B50L16C5



4x long competitor substrate: 80LR

B**half substrates frequencies**

10 % of total half substrates



10 % of total half substrates



40 % of total half substrates



40 % of total half substrates


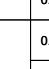
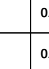
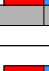
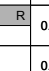
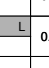

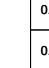
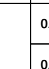
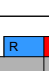
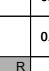
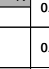
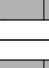
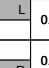
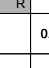
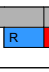
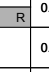
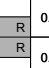
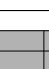
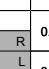
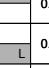
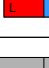
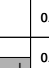
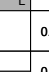

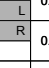
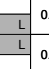


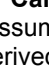
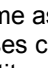
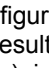
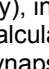
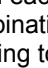
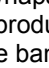
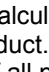
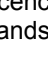
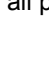



C**maximum recombination with synapse reassembly**

half sub. combination	P comb.	Cy5 dyes	fluoresc. intens.	band intens.	intens. [% total]	assigned product
	0.04	2	0.08	0.16	20	short substrate (50 bp) (ignoring recombinant products L-L & R-R)
	0.04	1	0.04			
	0.04	1	0.04			
	0.04	0	0			
	0.16	1	0.16	0.64	80	recombinant products (65 bp)
	0.16	1	0.16			
	0.16	1	0.16			
	0.16	1	0.16			
	0.16	0	0			
	0.16	0	0			
	0.16	0	0			
	0.16	0	0			
	0.64	0	0	0	0	undetected long products & substrates (80 bp)
	0.64	0	0			
	0.64	0	0			
	0.64	0	0			

Figure 5.20: Calculated product ratios after full recombination with synapse reassembly.

Assuming that synapses dissociate and reassemble during recombination, multiple cycles of recombination can take place. Given unlimited time, this results in random combinations of half substrates, derived from the original substrates by double-strand cleavage. **(A)** The ratio of the original short substrate (blue/red) and the long competitor (grey) in the sample determines the frequency of the available left (L) and right (R) halves of the substrates **(B)**. **(C)** The frequency of the half-sites was used to calculate the probability (P) of every possible combination of half-substrates in every orientation. The relative fluorescence intensity of the products of random half-site combinations was calculated by multiplying the probability of the combination with the amount of Cy5 dyes (red) in the product. The products were then grouped according to the band they form on a polyacrylamide gel. Finally, the fluorescence intensity of each band, equivalent to the sum of the fluorescence of all products in the band, was transformed into the percentage of the total intensity of all bands.

A

synapse	P each sub	P synap.	products of 1&2 rec. cycles	P product
	0.10	0.01		0.0025
	0.10			0.0025
	0.10	0.01		0.0025
	0.10			0.0025
	0.10	0.04		0.01
	0.40			0.01
	0.10	0.04		0.01
	0.40			0.01
	0.10	0.01		0.0025
	0.10			0.0025
	0.10	0.01		0.0025
	0.10			0.0025
	0.10	0.04		0.01
	0.40			0.01
	0.10	0.04		0.01
	0.40			0.01
	0.10	0.04		0.01
	0.40			0.01
	0.10	0.04		0.01
	0.40			0.01
	0.10	0.04		0.01
	0.40			0.01
	0.10	0.04		0.01
	0.40			0.01
	0.10	0.04		0.01
	0.40			0.01
	0.10	0.04		0.01
	0.40			0.01
	0.10	0.04		0.01
	0.40			0.01
	0.10	0.04		0.01
	0.40			0.01
	0.10	0.04		0.01
	0.40			0.01
	0.10	0.04		0.01
	0.40			0.01
	0.10	0.04		0.01
	0.40			0.01
	0.10	0.04		0.01
	0.40			0.01
	0.10	0.04		0.01
	0.40			0.01
	0.10	0.04		0.01
	0.40			0.01
	0.10	0.04		0.01
	0.40			0.01
	0.10	0.04		0.01
	0.40			0.01
	0.10	0.04		0.01
	0.40			0.01
	0.10	0.04		0.01
	0.40			0.01
	0.10	0.04		0.01
	0.40			0.01
	0.10	0.04		0.01
	0.40			0.01
	0.10	0.04		0.01
	0.40			0.01
	0.10	0.04		0.01
	0.40			0.01
	0.10	0.04		0.01
	0.40			0.01
	0.10	0.04		0.01
	0.40			0.01
	0.10	0.04		0.01
	0.40			0.01
	0.10	0.04		0.01
	0.40			0.01
	0.10	0.04		0.01
	0.40			0.01
	0.10	0.04		0.01
	0.40			0.01
	0.10	0.04		0.01
	0.40			0.01
	0.10	0.04		0.01
	0.40			0.01
	0.10	0.04		0.01
	0.40			0.01
	0.10	0.04		0.01
	0.40			0.01
	0.10	0.04		0.01
	0.40			0.01
	0.10	0.04		0.01
	0.40			0.01
	0.10	0.04		0.01
	0.40			0.01
	0.10	0.04		0.01
	0.40			0.01
	0.10	0.04		0.01
	0.40			0.01
	0.10	0.04		0.01
	0.40			0.01
	0.10	0.04		0.01
	0.40			0.01
	0.10	0.04		0.01
	0.40			0.01
	0.10	0.04		0.01
	0.40			0.01
	0.10	0.04		0.01
	0.40			0.01
	0.10	0.04		0.01
	0.40			0.01
	0.10	0.04		0.01
	0.40			0.01
	0.10	0.04		0.01
	0.40			0.01
	0.10	0.04		0.01
	0.40			0.01
	0.10	0.04		0.01
	0.40			0.01
	0.10	0.04		0.01
	0.40			0.01
	0.10	0.04		0.01
	0.40			0.01
	0.10	0.04		0.01
	0.40			0.01
	0.10	0.04		0.01
	0.40			0.01
	0.10	0.04		0.01
	0.40			0.01
	0.10	0.04		0.01
	0.40			0.01
	0.10	0.04		0.01
	0.40			0.01
	0.10	0.04		0.01
	0.40			0.01
	0.10	0.04		0.01
	0.40			0.01
	0.10	0.04		0.01
	0.40			0.01
	0.10	0.04		0.01
	0.40			0.01
	0.10	0.04		0.01
	0.40			0.01
	0.10	0.04		0.01
	0.40			0.01
	0.10	0.04		0.01
	0.40			0.01
	0.10	0.04		0.01
	0.40			0.01
	0.10	0.04		0.01
	0.40			0.01
	0.10	0.04		0.01
	0.40			0.01
	0.10	0.04		0.01
	0.40			0.01
	0.10	0.04		0.01
	0.40			0.01
	0.10	0.04		0.01
	0.40			0.01
	0.10	0.04		0.01
	0.40			0.01
	0.10	0.04		0.01
	0.40			0.01
	0.10	0.04		0.01
	0.40			0.01
	0.10	0.04		0.01
	0.40			0.01
	0.10	0.04		0.01
	0.40			

5.6 Selection of fluorescent single-site substrates that allow recombination

Ensemble and single-molecule FRET experiments can be used to study the mechanism of strand exchange by Tn3 resolvase only if the fluorescent substrates permit strand exchange by hyperactive mutants of Tn3 resolvase. The minimum requirement for suitable fluorescent substrates is that these allow Tn3R NM to perform double-strand cleavage and strand exchange. Optimally, the substrates can be recombined similarly to non-fluorescent substrates, including the ligation step. Further, the rate of recombination should be comparable to non-fluorescent substrates and the ratio of recombinant and non-recombinant products should be similar towards the end of the reaction. However, the binding experiments suggested that some substrates, such as those with fluorophores attached close to the centre of site I, might inhibit cleavage or ligation. Therefore, a gel-based recombination assay was used to analyse cleavage, strand exchange and ligation of fluorescent substrates. The optimal conditions for the recombination of unmodified substrates had been established and this allowed the efficient selection of suitable substrates with fluorophores attached within or outside of site I.

5.6.1 Results

It became clear that recombination of some fluorescent substrate variations gave rise to products that result in additional bands in the gel assay. These bands may represent reaction intermediates other than the DSB intermediate. It was possible that some fluorescent substrates inhibited the cleavage of particular DNA single strands, resulting in nicked intermediates with covalently attached resolvase subunits. However, the usual protease K digestion of the reaction products removes most parts of the resolvase subunits. Therefore, the retardation of digested nicked intermediates on a SDS gel and the retardation of the equivalent products without nicks can be similar yet slightly different. To identify all products and intermediates unambiguously, undigested and digested products were compared on SDS gels (figure 5.22).

The potential products of various fluorescently labelled short substrates (50 bp), when recombined with the non-fluorescent long substrate 80LR (80 bp), are shown in figures 5.23 and 5.24. Products from substrates with a single Cy5 dye or a Cy5 dye attached to the bottom strand are not shown, but their recombination products can easily be derived from figures 5.23 and 5.24.

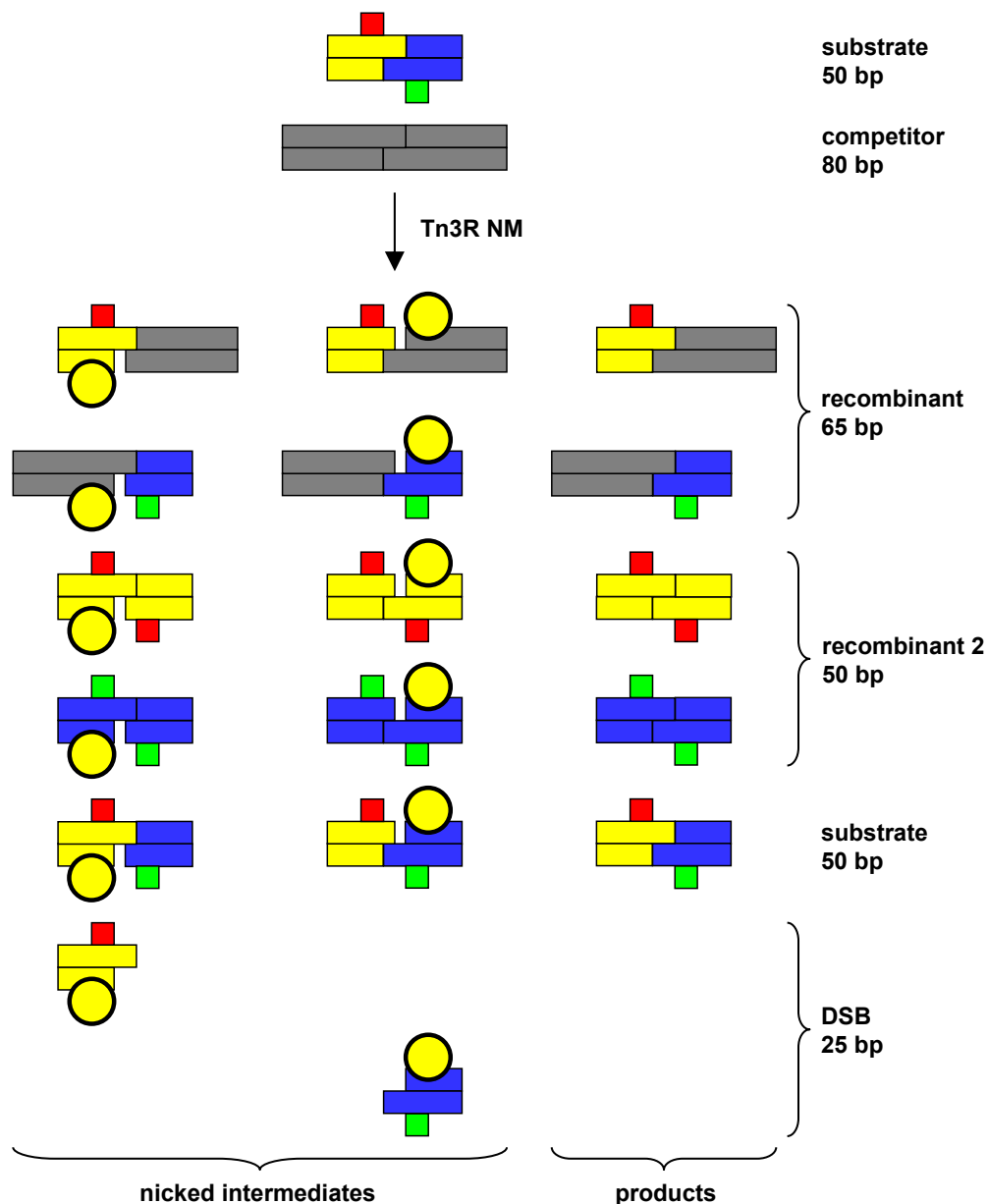


Figure 5.23: Recombination products and intermediates of various fluorescent single-site substrates. Recombination of short, fluorescent substrates (yellow and blue bars) and the long, non-fluorescent competitor substrate 80LR (grey bars) can result in a multitude of products and intermediates. Here, the potential products from fluorescent substrates with a Cy5 dye (red square) attached to the left half (yellow bars) in the top strand of the substrate and a Cy3 dye (green square) to the right half (blue bars) in the bottom strand are shown. Undigested nicked intermediates are covalently bound by a resolvase unit (yellow spheres). In the experiments in this chapter, the fluorescence scanner was set up to detect efficiently only products and intermediates with a Cy5 dye. Products containing only 80LR DNA are not shown.

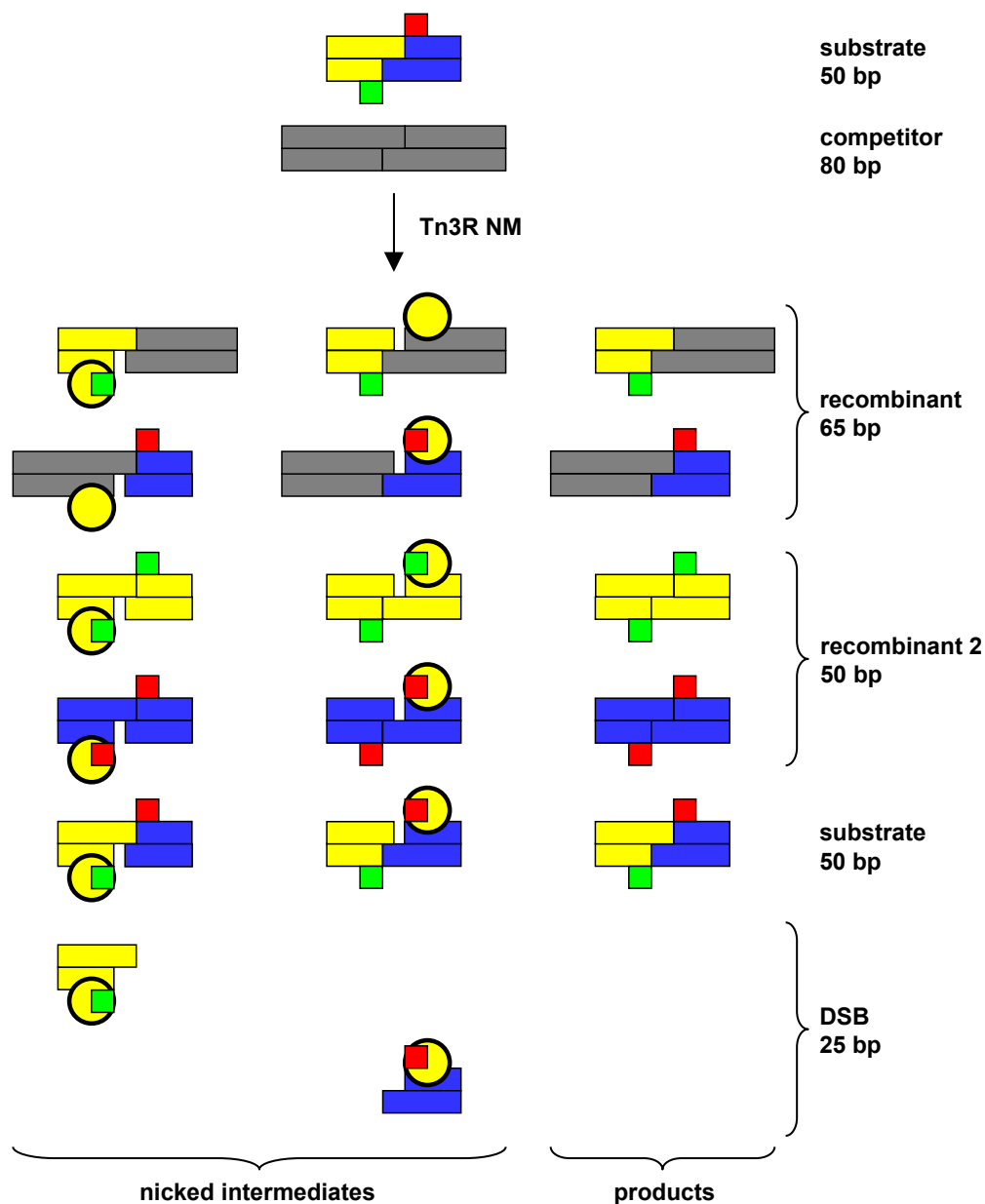


Figure 5.24: Recombination products and intermediates of various fluorescent single-site substrates. Recombination of short, fluorescent substrates (yellow and blue bars) and the long, non-fluorescent competitor substrate 80LR (grey bars) can result in a multitude of products and intermediates. Here, the potential products from fluorescent substrates with a Cy5 dye (red square) attached to the right half (blue bars) in the top strand of the substrate and a Cy3 dye (green square) to the left half (yellow bars) in the bottom strand are shown. Undigested nicked intermediates are covalently bound by a resolvase unit (yellow spheres). In the experiments in this chapter, the fluorescence scanner was set up to detect efficiently only products and intermediates with a Cy5 dye. Products containing only 80LR DNA are not shown.

The band of the original short fluorescent substrate is easily identified by comparison to samples incubated with inactive Tn3R NM-S10A or only resolvase dilution buffer (figure 5.22). However, in samples incubated with Tn3R NM, the band of the original short substrate may also include unknown quantities of recombinant products originating from recombination of two copies of the short substrate (see figures 5.23, 5.24). The retardation of products from recombination of two short substrates can be slightly altered by the presence of additional fluorophores, as seen in samples without the competitor substrate.

The recombinant product resulting from recombination between the short substrate and the long competitor should have the same retardation for samples digested with protease K and for undigested samples, since no resolvase units are covalently bound. The band of this recombinant product is, apart from the band of the original short substrate, the only band with an identical retardation for digested and undigested samples. However, this product will only be present in samples containing the competitor.

The digested double-strand break (DSB) intermediate is the smallest possible fragment found in samples incubated with Tn3R NM. Without digestion by protease K, the retardation of the DSB intermediate increases drastically due to the covalently attached resolvase unit. The band containing the undigested DSB intermediate was identified by comparing the bands of the digested and undigested sample and finding the band that matches the intensity of the band of the undigested DSB intermediate. The identification process is aided by the fact that some fluorescent substrates, for example B50L1C5, give rise to large amounts of the DSB intermediate.

This leaves us with the identification of the bands formed by nicked substrates and nicked recombinant products. The bands of the nicked recombinant product, resulting from recombination between the short substrate and the long competitor, were easily found since they are absent from samples without the long competitor. If undigested, these nicked recombinant products formed two bands that were highly retarded due to the covalently bound resolvase. There were two bands of the nicked recombinant products, corresponding to cleavage of either the top strand or the bottom strand. The two bands were strongly separated since the position of the covalently bound resolvase influences the retardation of the asymmetric recombinant product (25+40 bp) strongly. If desired, the band of these nicked recombinant products could be identified for digested samples by comparing the intensity of bands from digested and undigested samples.

Only the bands of the nicked short substrate remained to be identified. Like the nicked recombinant products, the undigested nicked substrate is covalently attached to resolvase and was therefore strongly retarded on SDS gels. The nicked substrate ran slightly faster than the longer nicked recombinant products. The undigested nicked substrate formed two bands corresponding to cleavage of the top strand or the bottom strand, as seen for the nicked recombinant products. However, the two bands of the nicked substrate were separated only slightly since the original short substrate is nearly symmetric, apart from the attached fluorophores. An alternative explanation for the two bands is that one band was formed by the nicked original substrate while the other band was formed by nicked recombinant products from recombination between two copies of the original substrate. Since the two bands can hardly be told apart, it is irrelevant which explanation is correct. In the following experiments, the two bands will be interpreted as nicked original substrates, if no other recombinant products or intermediates have been formed in the sample.

Once the identity of all the bands in the gel-based recombination assay had been established, all the fluorescent substrates were screened for efficient recombination (figures 5.25-5.28). First the effect of a single Cy5 fluorophore in the substrate, at each of the chosen positions, was tested. The control substrate B50L16C5, with a fluorophore attached outside of site I, produced very small amounts of recombination intermediates and high amounts of recombinant products. In contrast, some substrates containing a fluorophore within site I did not allow complete recombination.

Substrates with a Cy5 dye attached within the central overlap at the cleavage site of site I (B50L1C5, B50R1C5) did not allow the formation of finished recombinant products (figures 5.25-5.27). However, large amounts of the DSB intermediate accumulated and a small amount of nicked recombinant was formed. This suggests that these substrates allow double-strand cleavage and some strand exchange, but impair ligation substantially.

A Cy5 dye adjacent to the central overlap (B50L2C5, B50R2C5) allows the formation of small amounts of finished recombinant products and larger amounts of nicked recombinant products (figures 5.25-5.27). However, DSB products still accumulate. This indicates that strand exchange takes place although ligation is impaired, but not as seriously as in substrates with Cy5 attached within the central overlap. Therefore, it appears that the integrity of the base is essential for the ligation of the free OH-group but not necessarily for the attack of the phosphodiester by the S10 residue. In this context, the tolerance for attached dyes seems to be higher at position L2 than at position R2. Some nicked products

ran as multiple bands in the protease K-digested sample. This may be caused by an altered mobility of the products due to dyes at position L2 or R2. Another explanation is that the covalently attached resolvase units were only partially digested when a dye was present in close proximity to the cleavage site.

Placing the Cy5 dye further from the centre of site I results in increasing amounts of ligated recombinant products (figures 5.25-5.27). Substrate B50R4C5 provides only slightly more efficient recombination than substrate B50L2C5. A dye attached to position L5 permits the formation of much more recombinant products but the amount of DSB intermediates is still significantly increased. Finally, a Cy5 dye at position R5 or L6 allows efficient recombination very similar to the control substrate, with high amounts of finished recombinant products and only marginally increased amounts of nicked intermediates and DSB intermediates. Substrate B50R5C5 gives rise to somewhat elevated amounts of the DSB intermediate though.

As expected from the results with substrates containing one fluorophore, substrate B50R1C5L1C3, with both a Cy3 and a Cy5 dye attached within the central overlap of site I, did not allow the formation of finished recombinant products (figures 5.26-5.27). In addition, substrate B50R1C5L1C3 did not even produce nicked recombinant products. However, the substrate B50L2C5R2C3 permitted the formation of small amounts of finished recombination products, although the amount of DSB intermediates was strongly increased.

Placing both fluorophores of the FRET pair at positions further from the centre of site I generally improved the efficiency of the recombination reaction. The substrate B50R5C5L6C3, a combination of the best substrates containing one fluorophore, was recombined very similarly to the control substrate, with only marginally increased amounts of the DSB intermediate (figure 5.26). However, some substrates with two fluorophores which permitted more efficient recombination than expected from tests with substrates containing one fluorophore. One example is the substrate B50L5C5L1C3, which gives substantial amounts of recombinant products while producing very high amounts of DSB products. The results of all tested substrates are summarised in figure 5.28.

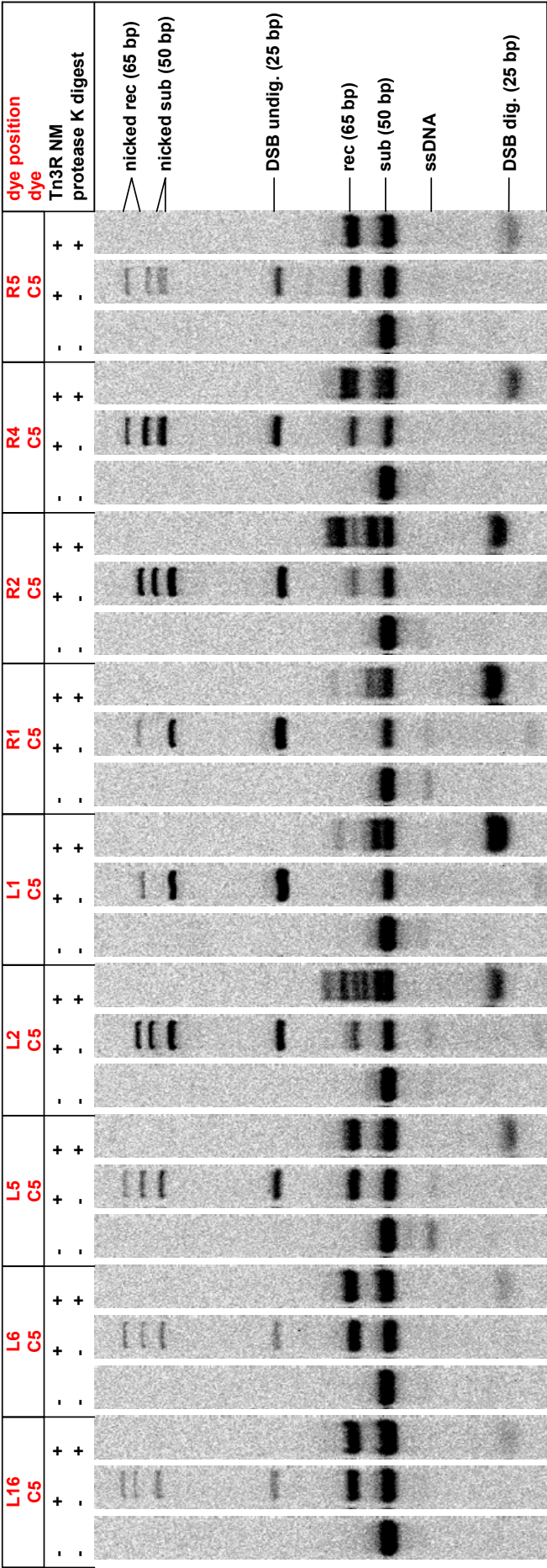


Figure 5.25: Effect of a single fluorophore at different positions on the recombination of single-site substrates. Samples containing short, fluorescent substrates (25 nM) with one Cy5 dye and the non-fluorescent competitor substrate 80LR (75 nM) were incubated with Tn3R NM (1,500 nM) under standard conditions. For control samples, 10% v/v resolvase dilution buffer was added to substrate solutions without incubation. The control samples were then treated with SDS in same way as all other samples. To identify the bands of recombination products and intermediates unambiguously, samples digested with protease K and undigested samples were compared. The potential recombination products and intermediates are shown in figures 5.23 and 5.24. Some samples contained traces of residual single-stranded DNA from the annealing process. The gel images are representative of repeat experiment under similar conditions.

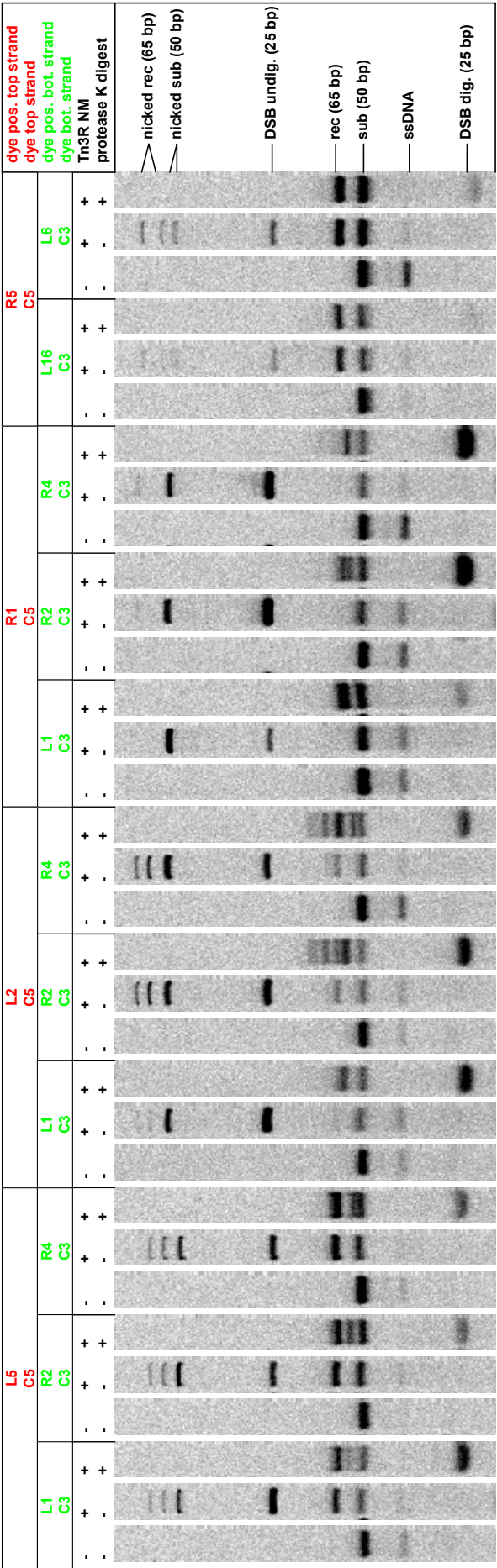


Figure 5.26: Effect of two fluorophores at different positions on the recombination of single-site substrates (FRET pairs detecting strand exchange). Short, fluorescent substrates with one Cy5 dye attached to the top strand and one Cy3 dye attached to the bottom strand were recombined with the long, non-fluorescent competitor substrate 80LR. Only fluorescent substrates with FRET pairs that can detect strand exchange, due to fluorophores in locations that can become separated through strand exchange, are shown here.

Samples with 25 nM fluorescent substrate and 75 nM competitor substrate were incubated with Tn3R NM (1,500 nM) under standard conditions. For control samples, 10% v/v resolvase dilution buffer was added to substrate solutions without incubation. The control samples were then treated with SDS in the same way as all other samples. To identify the bands of recombination products and intermediates unambiguously, samples digested with protease K and undigested samples were compared. The potential recombination products and intermediates are shown in figures 5.23 and 5.24. Some samples contained traces of residual single-stranded DNA from the annealing process. The gel images are representative of repeat experiment under similar conditions.

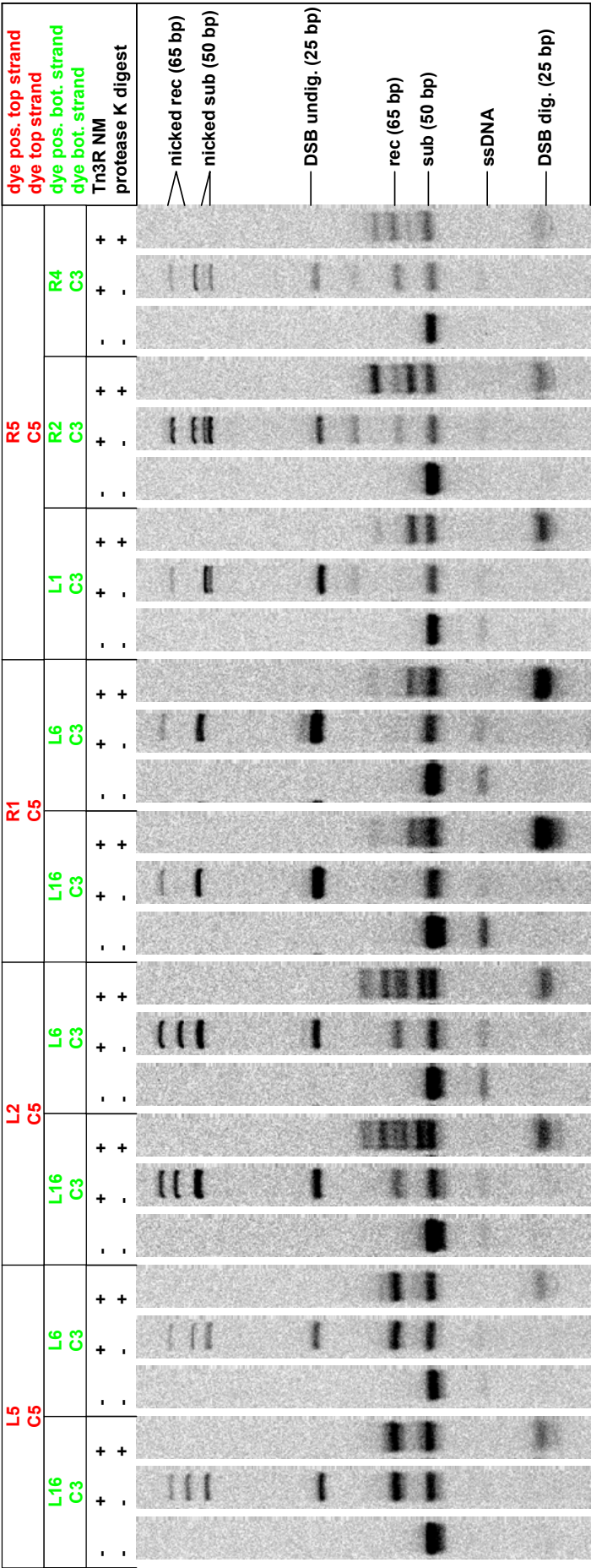


Figure 5.27: Effect of two fluorophores at different positions on the recombination of single-site substrates (FRET pairs not detecting exchange). Short, fluorescent substrates with one Cy5 dye attached to the top strand and one Cy3 dye attached to the bottom strand were recombined with the long, non-fluorescent competitor substrate 80LR. Only fluorescent substrates with FRET pairs that cannot detect strand exchange, due to fluorophores in locations that cannot become separated through strand exchange, are shown here.

Samples with 25 nM fluorescent substrate and 75 nM competitor substrate were incubated with Tn3R NM (1,500 nM) under standard conditions. For control samples, 10% v/v resolvase dilution buffer was added to substrate solutions without incubation. The control samples were then treated the same way as all other samples. To identify the bands of recombination products and intermediates unambiguously, samples digested with protease K and undigested samples were compared. The potential recombination products and intermediates are shown in figures 5.23 and 5.24. Some samples contained traces of residual single-stranded DNA from the annealing process. The gel images are representative of repeat experiment under similar conditions.

A

Cy5 position	L16	L6	L5	L2	L1	R1	R2	R4	R5
Recombinant	5	5	5	3	0	0	2	4	5
Nicked recombinant	1	1	2	5	1	1	5	4	1
Nicked substrate	1	1	2	5	5	3	5	4	1
DSB	1	1	3	4	5	5	4	3	2

B

strand exch. detection	-	-	+	+	+	+	-	-	+	+	+	+	+	-	-
Cy5 pos. top-strand	L5	L5	L5	L5	L5	L2	L2	L2	L2	L2	L2	L2	L2	R5	R5
Cy3 pos. bottom-strand	L16	L6	L1	R2	R4	L16	L6	L6	L6	L16	R1	R2	R4	L1	R2
Recombinant	5	5	3	5	5	2	2	2	0	0	0	0	0	5	2
Nicked recombinant	1	1	1	1	1	3	3	3	1	1	1	1	1	1	3
Nicked substrate	2	1	2	3	3	3	3	3	3	3	3	3	3	1	2
DSB	3	2	4	3	3	3	3	3	5	2	5	5	2	4	3

Figure 5.28: Summary of the effect of fluorophores on the recombination of single-site substrates. Short fluorescent substrates with fluorophores in various positions were recombined with the long, non-fluorescent competitor substrate 80LR using Trn3R NM (see figures 5.22-5.27). The relative amounts of the recombination products and intermediates were estimated and summarised here for fluorescent substrates containing one Cy5 dye (**A**) and for substrates containing a Cy3/Cy5 pair (**B**). For the estimation of the amounts of recombination products, the band intensities in the gel images (figures 5.25-5.27) were compared by eye. The numbers represent relative amounts of reaction products on an arbitrary scale, with "0" for no visible detection and "5" for the highest amount found in the samples. The gel images in figures 5.25-5.28 are representative of further repeat experiments, in which comparable sample mixtures were incubated under similar conditions, stopping the reactions after five minutes or one hour through the addition of 3x SDS loading buffer without protease K (data not shown).

Fluorescent substrates with fluorophores in locations that can become separated through strand exchange can potentially be employed to detect strand exchange in FRET experiments.

5.6.2 Discussion

Substrates with fluorophores attached close to the centre of site I (L1, L2, R1, R2) are promising in the context of FRET experiments but disturb the recombination reaction significantly. Dyes attached close to the centre of site I seem to have a strong inhibitory effect, especially on the ligation activity of Tn3R NM. However, substrates with a FRET pair close to the centre of site I may still be useful for FRET experiments. While substrate B50L2C5R2C3 inhibits ligation strongly, it definitely permits strand exchange at an unknown rate since small amounts of recombinant products can be found. It is not completely clear if the rate of strand exchange is impaired, since the recombinant products are ligated with low efficiency resulting in the loss of information about the recombinant or non-recombinant state. Amongst all ligated species, the fraction of recombinant products is relatively high though, indicating that strand exchange is not severely impaired. This suggests that substrate B50L2C5R2C3 is recombined similarly to unmodified substrates in the absence of magnesium. As discussed before, this may provide a good basis for single-molecule FRET experiments. Substrate B50R1C5L1C3 may provide similar advantages, but it is not clear it permits strand exchange at all, since this information is lost due to the extremely strong inhibition of ligation.

The fluorescent substrates which were recombined most efficiently contained fluorophores attached further away from the centre of site I. These substrates, such as B50R5C5L6C3 and B50L5C5R4C3, may provide a recombination system which is very similar to the unmodified system and can be studied in FRET experiments. In the substrates B50R5C5L6C3 and B50L5C5R4C3, the positions of the two fluorophores are 9-10 bases apart. However, these FRET pairs reside in the same helical phase of the DNA and may still provide a high FRET efficiency when located within the same substrate. Therefore, these substrates are promising candidates for ensemble and single-molecule FRET experiments.

6 Ensemble FRET studies of the recombination of single-site substrates

In gel based recombination assays, the fluorescent single-site substrate B50R5C5L6C3, containing a Cy5 dye at position R5 and a Cy3 dye at position L6, had been shown to allow recombination by Tn3 resolvase NM comparable to substrates without dyes within Tn3 *res* site I. This made substrate B50R5C5L6C3 a promising candidate for ensemble and single-molecule FRET experiments. However, as the fluorophores of the FRET pair are separated by 10 bases, it was not clear if this substrate could provide a high FRET efficiency. A further requirement for studying recombination using FRET spectroscopy is that recombination of the substrates results in detectable FRET changes. To test if substrate B50R5C5L6C3 meets these requirements, two ensemble FRET experiments were conducted.

In the first ensemble FRET experiment, four samples containing substrate B50R5C5L6C3 and a fourfold excess of the non-fluorescent competitor substrate 80LR were analysed (figure 6.1). One sample contained the substrates without any protein to establish the basic FRET efficiency of the substrate B50R5C5L6C3. A sample containing catalytically inactive Tn3R NM-S10A was used to reveal the effect of binding by Tn3 resolvase and of synapsis on the FRET efficiency. Catalytically activated Tn3 resolvase NM was added to two further samples to test the effect of recombination of the substrate B50R5C5L6C3 with the competitor substrate. Tn3 resolvase NM was added in absence of magnesium and in presence of 20 mM magnesium chloride to study how the accumulation of cleaved intermediates affects the FRET efficiency.

In the second ensemble FRET experiment, four samples containing equal concentration of the substrates B50R5C5 and 50L6C3 were treated in the same way as in the first experiment (figure 6.2). This second ensemble FRET experiment is in fact the reverse experiment of the first FRET experiment described above. Recombination of both substrates in the correct orientation should yield the original substrate B50R5C5L6C3. This experiment should reveal the FRET efficiency of the FRET pair in substrate B50R5C5L6C3 after recombination with both dyes in separate substrate molecules.

During the FRET experiments, samples were taken and the reaction products were analysed in a gel based assay to support the FRET data.

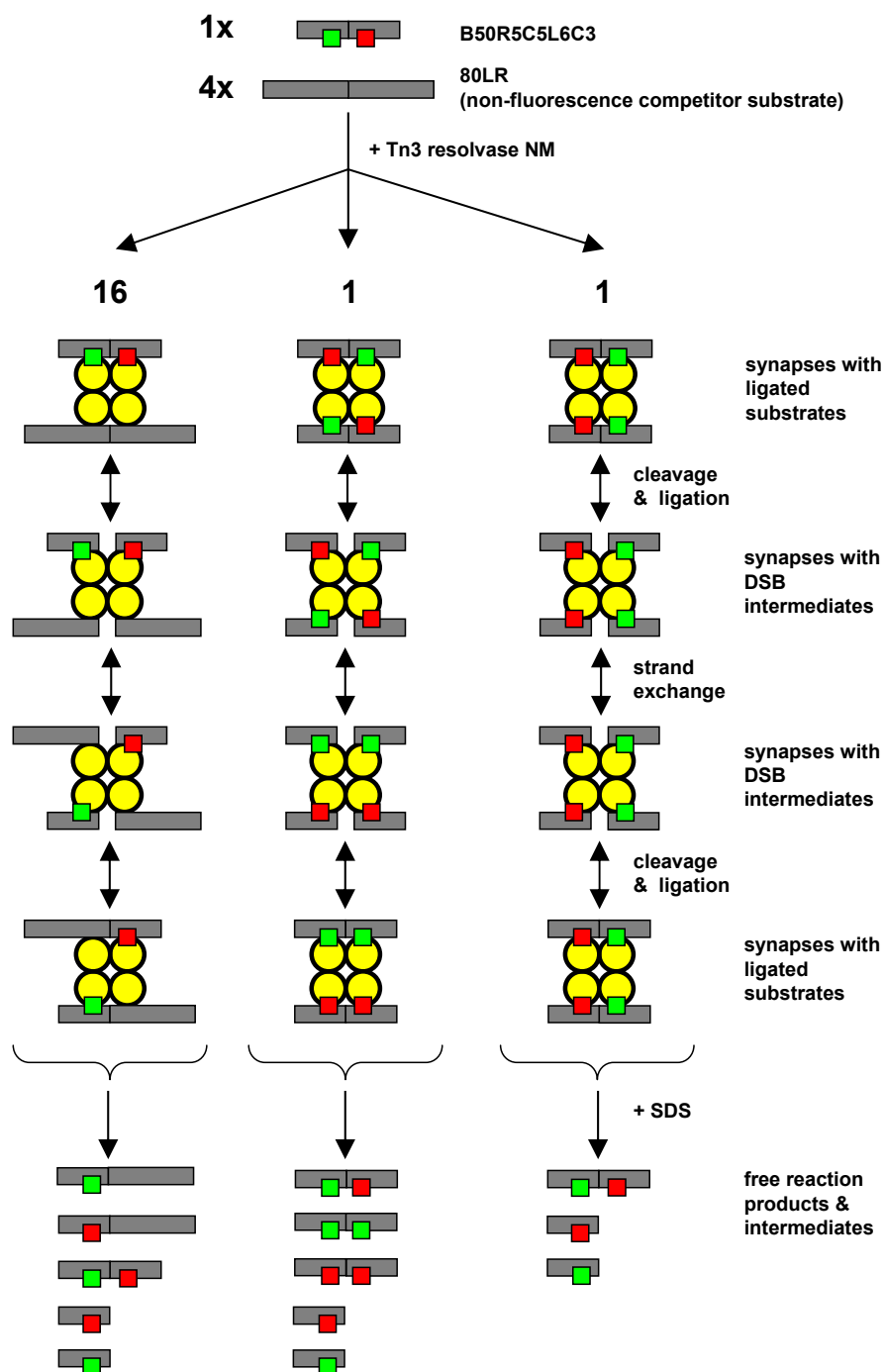


Figure 6.1: Recombination reaction in the first ensemble FRET experiment.

The fluorescent substrate B50R5C5L6C3, containing a Cy5 dye (red square) and a Cy3 dye (green square) was recombined with an excess of the non-fluorescent competitor substrate 80LR using Tn3 resolvase NM (yellow spheres). DNA is represented by grey bars. All possible variations of synapses containing fluorescent substrates are shown. The initial molar ratio of both substrates is given. Further, the relative concentrations of the different synapses were predicted as in chapter 5.

The main reaction in the sample is the recombination of substrate B50R5C5L6C3 with the competitor substrate 80LR resulting in products containing one dye each. However, this reaction cannot proceed to completion since multiple rounds of strand exchange can produce the original substrate.

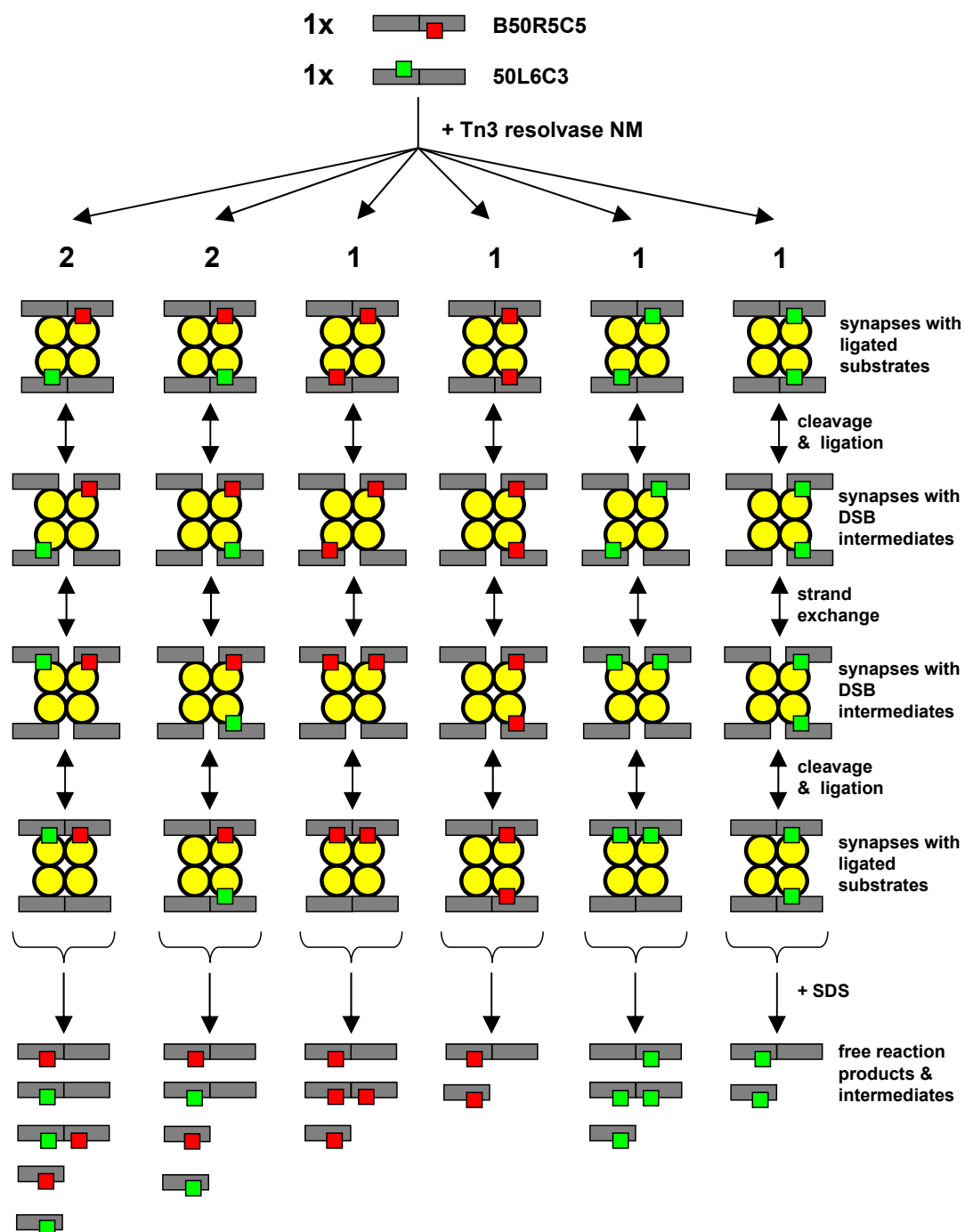


Figure 6.2: Recombination reaction in the second ensemble FRET experiment.

An equimolar mixture of the fluorescent substrates B50R5C5, containing a Cy5 dye (red square), and 50L6C3, containing a Cy3 dye (green square) was recombined by Tn3 resolvase NM (yellow spheres). DNA is represented by grey bars. All possible variations of synapses containing fluorescent substrates are shown. The relative concentrations of the different synapses were predicted as in chapter 5.

One reaction in the sample results in products containing a FRET pair and increases the FRET efficiency in the sample. However, this reaction competes with several other reactions resulting in a smaller increase in FRET efficiency than initially expected. Further, the reaction cannot proceed to completion since multiple rounds of strand exchange can produce the original substrate.

6.1 Results

6.1.1 Recombination of substrate B50R5C5L6C3 with an excess of the competitor substrate 80LR

The first ensemble FRET experiment showed that the FRET pair in substrate B50R5C5L6C3 alone provides a relatively high FRET efficiency of ~ 0.63 under the buffer conditions used for recombination experiments (figure 6.3A). Addition of catalytically inactive Tn3 resolvase NM-S10A produced inactive synapses with the substrates B50R5C5L6C3 and 80LR and quickly increased the FRET efficiency slightly to a stable level of around 0.71. The increased FRET efficiency might have been caused by bound resolvase units changing the environment of the dyes or by synapses bringing the two fluorescent substrates together. However, the majority of fluorescent synapses should contain a combination of the substrate B50R5C5L6C3 and the competitor substrate 80LR due to the fourfold excess of the competitor substrate. Adding SDS to this sample reduced the FRET efficiency back to the level observed with substrate B50R5C5L6C3 alone, which was due to the disruption of all protein-DNA complexes.

Activated Tn3 resolvase NM slowly decreased the FRET efficiency in samples containing substrate B50R5C5L6C3 and an excess of the non-fluorescent competitor substrate 80LR. The reduction of the FRET efficiency results from the separation of the FRET pair of dyes by cleavage of the fluorescent substrate and strand exchange separating the two halves of the substrate which contain one dye of the FRET pair each. During recombination, the synapses can contain the original substrate B50R5C5L6C3, ligated recombinant products or double-strand break intermediates (figure 6.1). Synapses containing the original substrates provide a high FRET efficiency as described above. Synapses containing recombinant products, each with one dye of the FRET pair, are expected to have a lower FRET efficiency than synapses containing substrate B50R5C5L6C3 but a higher FRET efficiency than a mixture of free recombinant products since the products are held in close proximity by the synapse (see second ensemble FRET experiment, figure 6.2). Synapses containing DSB intermediates may have a FRET efficiency similar to synapses containing ligated recombinant products, since both dyes of the FRET pair are located in two distinct DNA molecules within one synapse. The DSB intermediates can move within the synapse either due to strand exchange or conformational changes and it is unclear if this allows the dyes to come closer than in synapses containing ligated recombinant products. In summary, synapses with ligated recombinant products and synapses with DSB intermediates may not show the same FRET efficiency and their exact FRET efficiencies

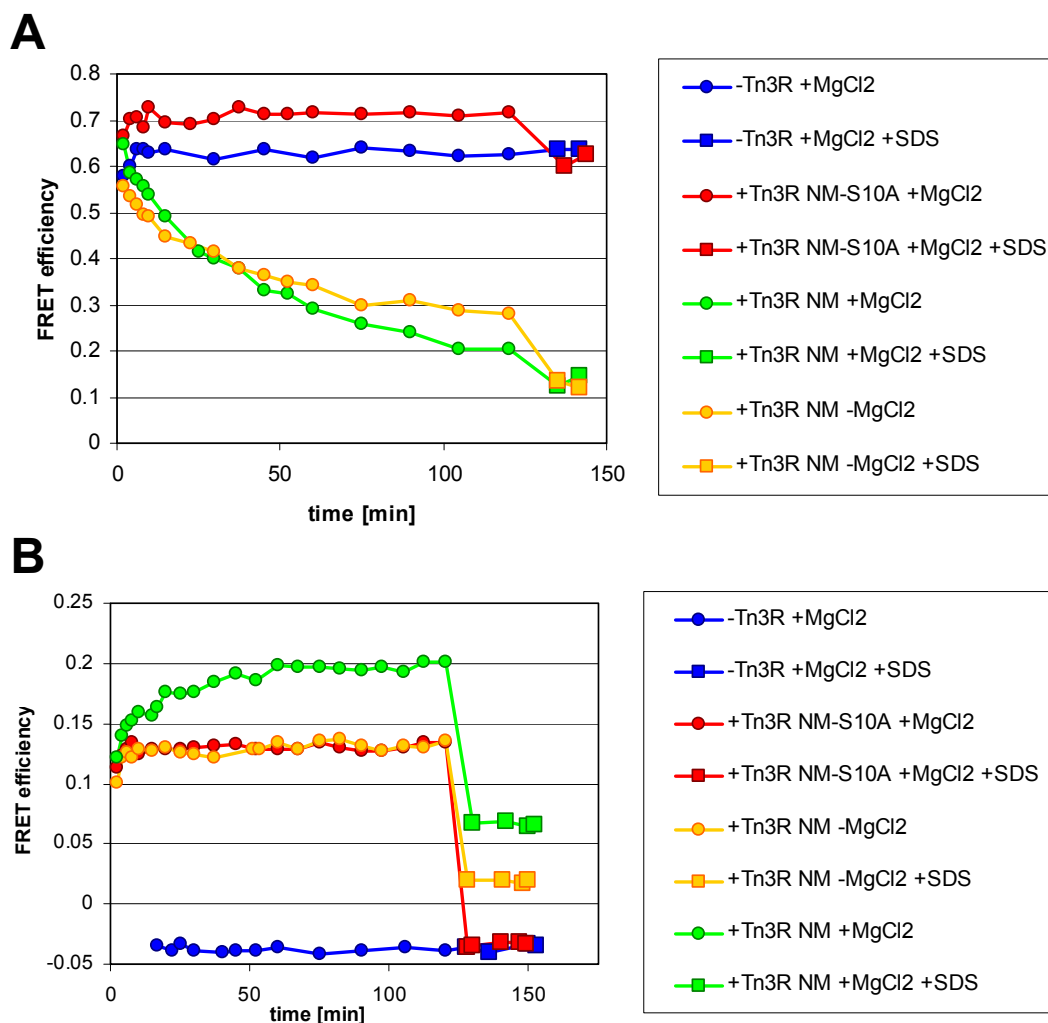


Figure 6.3 Ensemble FRET studies of the recombination of single-site substrates

Samples containing fluorescent single-site substrates were studied in a micro cuvette in a fluorescence spectrometer. The FRET efficiency of the substrate alone, with added inactive Tn3R NM-S10A or added activated Tn3R NM was measured over two hours of incubation at 20 °C after mixing. Tn3R NM was added in presence and absence of MgCl₂ while all other samples contained magnesium chloride. After two hours SDS was added to the samples. **(A)** Substrate B50R5C5L6C3 contains a FRET pair and recombination with an excess of the non-fluorescent competitor substrate 80LR yields products with a single dye each resulting in decreased FRET efficiency. **(B)** A mixture of equal amounts of substrates B50R5C5 and 50L6C3 has a low FRET efficiency but synapsis can bring the dyes of both substrates into one synapse while recombination can bring the dyes into one substrate. Both processes increase the FRET efficiency. The data in **(A)** and **(B)** corresponds to single experiments.

are expected to be between the FRET efficiencies observed with free substrates containing one dye each and those FRET efficiencies observed with synapses containing substrate B50R5C5L6C3.

Shortly after adding hyperactive Tn3 resolvase NM, the decrease in FRET efficiency appeared to be quicker in absence of magnesium but after two hours of incubation the FRET efficiency reached a lower level of ~ 0.26 in the presence of magnesium compared to 0.32 in the absence of magnesium. The faster initial decrease in FRET efficiency in samples without magnesium may due to the increased formation of synapses containing DSB intermediates in absence of magnesium. The samples with magnesium form more ligated recombinant products, but up to 50% of the recombinant products may contain a complete FRET pair after multiple rounds of strand exchange. After prolonged incubation, dissociation and reassembly of synapses may become important in samples with magnesium, allowing the formation of more recombinant products with one dye each and allowing recombinant products with one dye to leave the synapses. Therefore, after prolonged incubation, samples with and without magnesium may produce similar amounts of DNA molecules which lower FRET in synapses, including DSB intermediates and ligated recombinant products with one dye. However, in the presence of magnesium, some recombinant products could leave the synapses, decreasing the FRET efficiency further than in samples not containing magnesium.

After two hours, the addition of SDS reduced the FRET efficiency further to the same level of ~ 0.13 in samples with and without magnesium. This further decrease of the FRET efficiency suggests that samples with and without magnesium contained synapses with DNA intermediates or products which provide a low FRET efficiency when removed from the synapse. Double-strand break intermediates (DSB intermediates) were held in close proximity within the synapses but were separated upon disruption of the synapses by SDS, effectively separating the FRET pair and decreasing the FRET efficiency. The effect was stronger in samples without magnesium which had been shown to accumulate more double-strand break intermediates in gel-based assays. In part, the decrease in FRET efficiency upon addition of SDS may also have resulted from the disruption of synapses containing products from the recombination of substrate B50R5C5L6C3 and the non-fluorescent substrate. These synapses could feature two ligated products, each with only one fluorophore. The synapses probably held both products in close proximity, but upon SDS addition they were separated decreasing the FRET efficiency. It is likely that the separation of double-strand break intermediates plays a more important role in samples without magnesium while the separation of recombinant products plays a more important

role in samples with magnesium, which have been shown to yield higher amounts of ligated recombinant products in gel based assays. After addition of SDS, samples with and without magnesium reach a similar FRET efficiency, indicating that the amount of low FRET species, the sum of DSB intermediates and recombinant products, is similar in both samples.

6.1.2 Recombination of a mixture of the substrates B50R5C5 and 50L6C3

In the second experiment, an equimolar mixture of two substrates with one dye each was analysed (figure 6.2). In the absence of Tn3 resolvase, this mixture of B50R5C5 and 50L6C3 showed a very low FRET efficiency of -0.04 (figure 6.3). The slightly negative value is likely to result from inaccuracies in the calculation of the FRET efficiency. These inaccuracies may include inaccurate literature values of the extinction coefficients of the fluorophores or imperfect matching of the fluorescence peaks due to slightly shifted or broadened fluorescence peaks. Nevertheless, the inaccuracies appear to be consistent in all samples of the experiment and should allow the comparison of FRET efficiencies relative to each other.

The addition of catalytically inactive Tn3 resolvase NM-S10A resulted in a quick and strong increase in FRET efficiency. This increase was too fast to be resolved in the ensemble FRET experiment and a stable but increased FRET efficiency of ~0.13 was observed. To increase the FRET efficiency, the fluorophores of both substrates must have become closer together. Tn3 resolvase NM-S10A cannot recombine the fluorescent substrates but can bring two substrates into close proximity within a synapse. In some combinations, a substrate with a Cy3 dye and a substrate with a Cy5 dye are held together in a synapse, increasing the FRET efficiency (figure 6.2). Further, the binding of resolvase units may also enhance the FRET efficiency of fluorophore pairs which are brought close enough to each other to allow FRET (see first experiment, section 6.1.1). Upon disruption of the synapses by SDS, the substrates were no longer held together by synapses separating the dyes and decreasing the FRET efficiency to the very low base levels seen in the samples not containing resolvase. This confirms that Tn3 resolvase NM-S10A was unable to make recombinant substrates with potentially higher FRET efficiency.

Adding hyperactive Tn3 resolvase NM to the mixture of B50R5C5 and 50L6C3 had different effects in the presence and absence of magnesium. In both cases, the FRET efficiency was quickly raised to ~0.13, which is comparable to the samples containing inactive Tn3 resolvase NM-S10A as discussed above. The initial quick increase in FRET

efficiency is likely to be caused by the quick process of binding and synapse formation as in the samples containing Tn3 resolvase NM-S10A. After the initial increase, the FRET efficiency stayed stable at ~ 0.13 in the absence of magnesium, comparable to the observation with Tn3 resolvase NM-S10A. This may lead one to suspect that Tn3 resolvase NM, just like Tn3 resolvase NM-S10A, did not form any recombinant products which contain two fluorophores increasing the FRET efficiency. However, after disruption of the synapses by SDS, the FRET efficiency in samples with Tn3 resolvase NM in absence of magnesium was decreased to 0.02 compared to the stronger decrease to ~ 0.05 in the sample with Tn3 resolvase NM-S10A. This suggests that a small amount of recombinant products containing a FRET pair was formed resulting in a slightly increased FRET efficiency in presence of SDS. It appears that the small amount of recombinant products with a high FRET efficiency had no detectable effect on the overall FRET efficiency of the sample before the disruption of the synapses. This may be due to the strong effect of bringing the substrates in close proximity within the synapse which masks the effect of the miniscule amount of recombinant products with high FRET. Further, the fact that the sample with Tn3 resolvase NM in absence of magnesium shows a constant FRET efficiency comparable to the FRET efficiency in samples containing catalytically inactive Tn3 resolvase NM-S10A, may have implications for the DSB intermediates in the sample with Tn3 resolvase NM in absence of magnesium. It suggests that the DSB intermediates in the synapse are held in together in one or more conformations that provide a FRET efficiency that is not much higher than simply bringing two substrates with one dye each into close proximity within an inactive synapse. However, this interpretation is speculative because hyperactive Tn3 resolvase NM may form slightly different amounts of synapses compared to Tn3 resolvase NM-S10A.

The addition of hyperactive resolvase had a different effect in the presence of magnesium. After the initial quick increase in FRET efficiency due to synapse formation, the FRET efficiency increased further at a slow rate reaching ~ 0.2 after two hours. The further increase likely results from the formation of a high amount of ligated recombinant products containing a FRET pair. Samples with magnesium have been shown to yield far more ligated products, which may explain the difference between the samples with and without magnesium.

6.1.3 Gel-based analysis of recombination products in the ensemble FRET experiment samples

During the ensemble FRET experiments, samples were taken, treated with SDS to stop the reaction and analysed in a gel-based assay (figure 6.4). In general, the identified reaction products agree with the assumptions made during the interpretation of the FRET data. The samples without magnesium accumulated larger quantities of DSB intermediates while the samples with magnesium yielded larger quantities of ligated recombinant products.

To test if the FRET efficiency provides a good quantitative representation of the recombination process, the FRET efficiency was compared to the quantity of relevant reaction products found in the gel-based assay. However, the second ensemble FRET experiment used a mixture of the substrates B50R5C5 and 50L6C3. This made it hard to distinguish and quantify recombinant and non-recombinant products on the gel since both have a length of 50 base pairs and differ only in the number of attached dyes (figures 6.2, 6.4). Therefore, only quantitative data from the gel-based assays of the samples containing the substrate B50R5C5L6C3 and the competitor substrate 80LR was used for the comparison to the ensemble FRET data of both experiments. The datasets needed to be formatted to compare the FRET efficiency with the quantity of products in the gel based assay.

The FRET efficiency was transformed into $\%E_{\text{FRET}}$, the percentage of the maximum FRET efficiency, according to equation 6.1. The maximum FRET efficiency, $E_{\text{FRET}}(\text{max})$, was defined as the average FRET intensity of the sample containing substrate B50R5C5L6C3 and the competitor substrate 80LR in the presence of inactive Tn3 resolvase NM-S10A. The average FRET efficiency of the sample containing substrates B50R5C5 and 50L6C3 without resolvase used as $E_{\text{FRET}}(\text{min})$ defining 0% FRET efficiency.

$$\%E_{\text{FRET}}(\text{sample}) = \frac{E_{\text{FRET}}(\text{sample}) - E_{\text{FRET}}(\text{min})}{E_{\text{FRET}}(\text{max}) - E_{\text{FRET}}(\text{min})} \cdot 100\% \quad 6.1$$

The band intensities from the gel-based assay were also transformed into $\%E_{\text{FRET}}$ according to equations 6.3 and 6.4. For this purpose, the reaction products were assigned E_{FRET} values. The original substrate B50R5C5L6C3 and its nicked version were assigned with $100\%E_{\text{FRET}}$ while the fluorescent recombinant product with one fluorophore and its nicked versions were assigned $0\%E_{\text{FRET}}$. When comparing band intensities to ensemble FRET samples containing SDS, the DSB intermediate was attributed with $0\%E_{\text{FRET}}$ since the DSB intermediates were not held together in synapses. When comparing to ensemble

FRET samples without SDS, the DSB intermediates were given an arbitrary intermediate value of 50% E_{FRET} since the exact FRET efficiency of synapses holding two DSB intermediates closely together is not known but expected to be between the FRET efficiency of free substrates with one dye each and synapsed substrates containing a FRET pair. For further calculations, the band intensity, I , of each product was expressed as the fraction of all bands:

$$f(\text{reaction product}) = \frac{I(\text{reaction product band})}{I(\text{all bands})} \quad 6.2$$

This fraction was then multiplied with the % E_{FRET} value assigned to the reaction product. The sum of these products yielded % E_{FRET} for the whole sample:

$$\begin{aligned} \%E_{FRET}(\text{sample}) &= f(\text{substrate}) \cdot 100\%E_{FRET} + f(\text{nicked substrate}) \cdot 100\%E_{FRET} \\ &+ f(\text{recombinant}) \cdot 0\%E_{FRET} + f(\text{nicked recombinant}) \cdot 0\%E_{FRET} \\ &+ f(\text{DSB}) \cdot 50\%E_{FRET} \end{aligned} \quad 6.3$$

$$\begin{aligned} \%E_{FRET}(\text{SDS sample}) &= f(\text{substrate}) \cdot 100\%E_{FRET} + f(\text{nicked substrate}) \cdot 100\%E_{FRET} \\ &+ f(\text{recombinant}) \cdot 0\%E_{FRET} + f(\text{nicked recombinant}) \cdot 0\%E_{FRET} \\ &+ f(\text{DSB}) \cdot 0\%E_{FRET} \end{aligned} \quad 6.4$$

The % E_{FRET} values calculated from ensemble FRET measurements and from the band intensities in the gel-based assay are generally in good agreement (figure 6.5). This suggests that the ensemble FRET measurements provide a good quantitative representation of the recombination process. Especially samples containing SDS provided very similar % E_{FRET} values calculated from ensemble FRET measurements and band intensities. This suggests that the % E_{FRET} values assigned to each reaction product are most accurate for samples with SDS which do not contain synapses that can alter the FRET efficiency of reaction products by bringing them into close proximity.

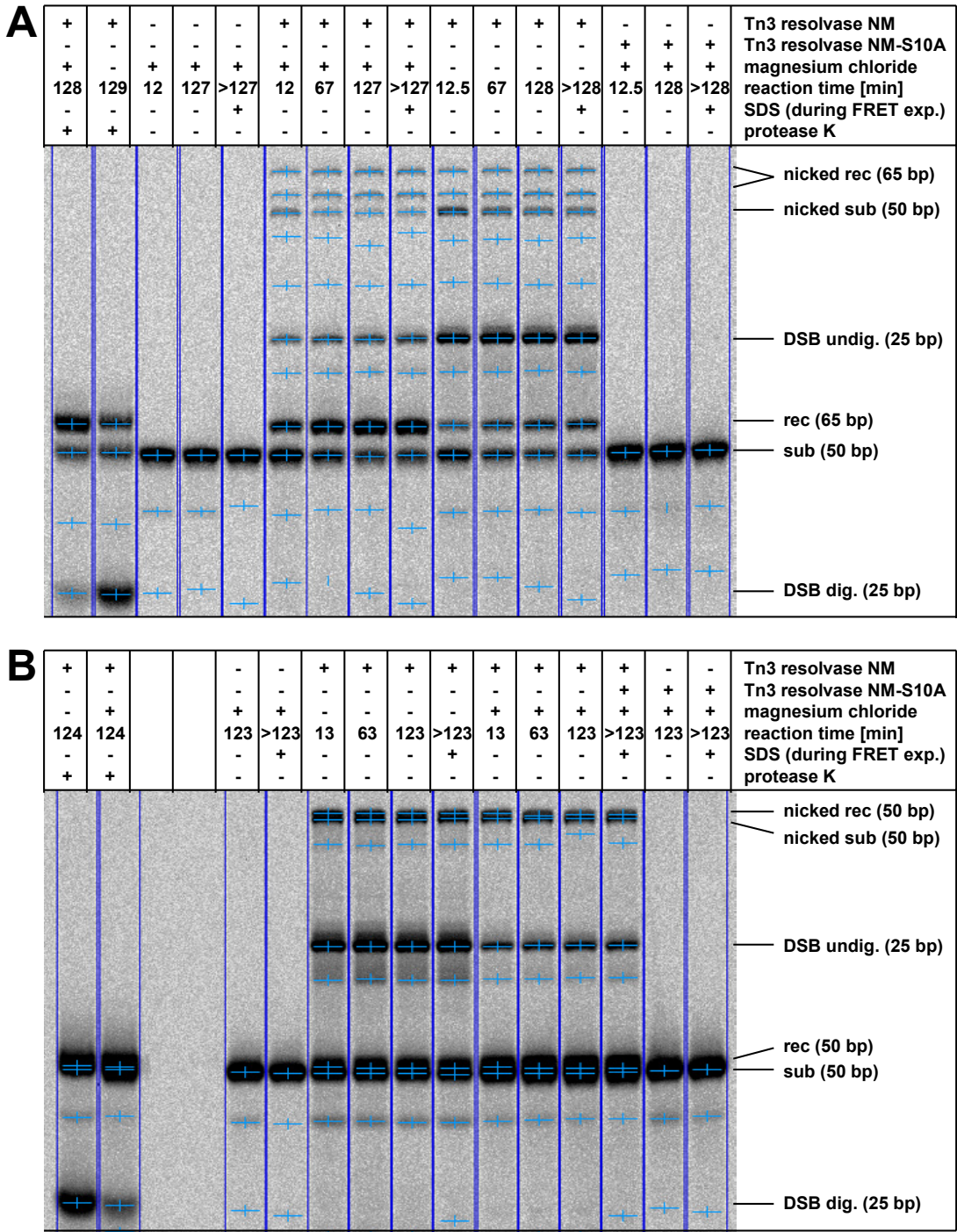


Figure 6.4 Gel-based analysis of the reaction products of ensemble FRET samples

Small samples were taken during the ensemble FRET experiments and treated with SDS to stop the reaction. Selected samples were digested with protease K to remove covalently bound resolvase units. The reaction products were separated on an SDS polyacrylamide gel and visualised using a fluorescence imager. **(A)** Samples of the ensemble FRET experiment using the substrate B50R5C5L6C3 and a fourfold excess of the non-fluorescent competitor substrate 80LR. **(B)** Samples of the ensemble FRET experiment using an equimolar mixture of the substrates B50R5C5 and 50L6C3.

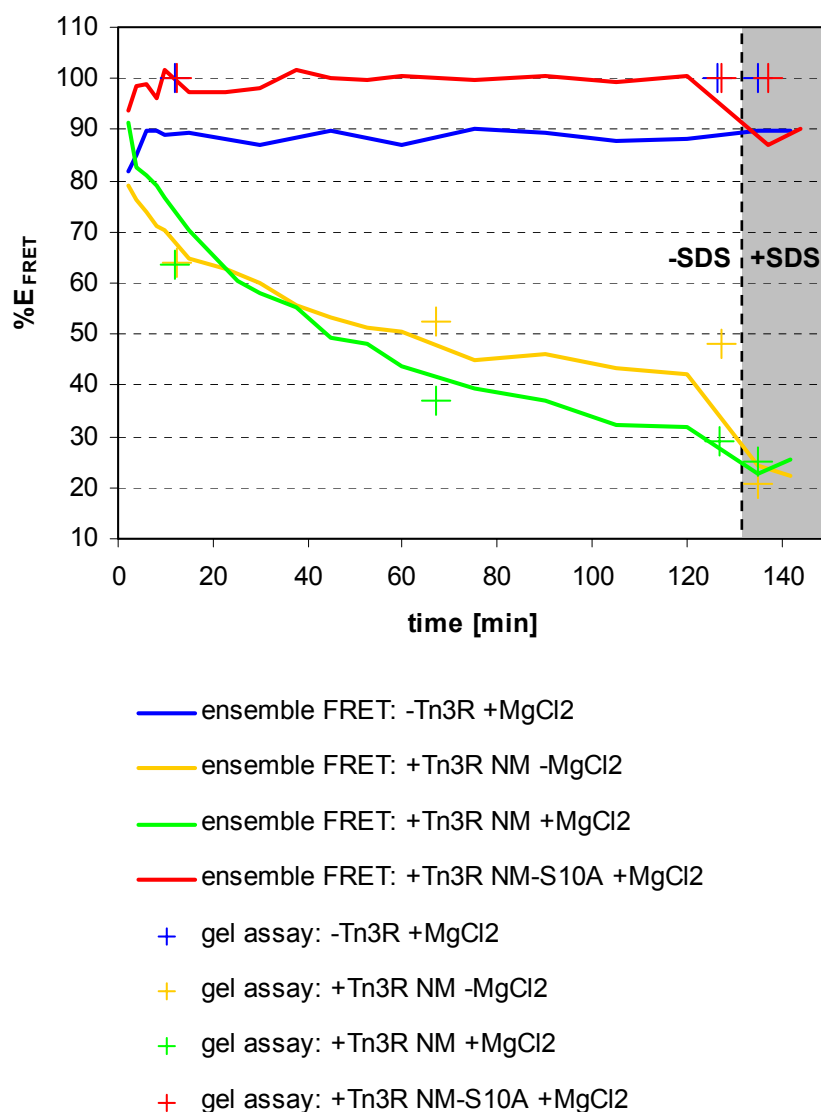


Figure 6.5 Comparison of $\%E_{\text{FRET}}$ calculated from ensemble FRET measurements and from the gel-based assay of the same samples

The FRET efficiency from ensemble FRET measurements was transformed into the percentage of maximum FRET efficiency, $\%E_{\text{FRET}}$ according to equation 6.1. Similarly, the band intensities of reaction products from the gel-based assay were transformed into $\%E_{\text{FRET}}$ by assigning a $\%E_{\text{FRET}}$ value to each reaction product and calculating the overall $\%E_{\text{FRET}}$ of the sample using the fractions of the quantified reaction products according to equations 6.2, 6.3 and 6.4. The data corresponds to single experiments.

The %E_{FRET} values were less accurate for samples containing hyperactive Tn3 resolvase NM in the absence of magnesium before the addition of SDS. These samples contained large amount of DSB intermediates which were held in close proximity within synapses. The FRET efficiency of these synapses had not been established and an arbitrary, intermediate %E_{FRET} value of 50% was assigned to the DSB intermediates. This resulted in an inaccurate calculation of the overall %E_{FRET} of the sample.

Further, the calculation of %E_{FRET} from band intensities did not account for the fact that the substrate B50R5C5L6C3 shows different FRET efficiencies within synapses and as free unbound DNA. Therefore, the same %E_{FRET} value of 100% was calculated from the bands intensities of samples without Tn3 resolvase or with inactive Tn3 resolvase NM-S10A.

There may be another inaccuracy in the calculation of %E_{FRET} from band intensities since the calculations consider recombinant products containing one dye as a low FRET species with 0%E_{FRET}. However, similar to DSB intermediates, these recombinant products can be held in close proximity within synapses. This may explain why lower %E_{FRET} values were calculated from band intensities than from ensemble FRET measurements for early time points of the sample with Tn3 resolvase NM in presence of magnesium. At early time points, considerable quantities of synapses containing two recombinant products, each with one dye of the original FRET pair, are present in the sample. At later time points, the recombinant products were likely to end up in distinct synapses, lowering their FRET efficiency and reducing the effect of the inaccurate calculation of %E_{FRET} from band intensities.

Overall, the ensemble FRET measurements seem to provide a good measure of the processes of cleavage and recombination. However, synapses can hold reaction products and intermediates in close proximity and effectively increase the FRET efficiency of DNA molecules which would show a lower FRET efficiency in free solution.

6.2 Discussion

In free solution, the substrate B50R5C5L6C3 which contains a FRET pair had a FRET efficiency of ~ 0.63 while a mixture of the substrates B50R5C5 and 50L6C3, each containing one dye of a FRET pair, had an extremely low FRET efficiency of ~ 0.04 . Recombination of B50R5C5L6 with an excess of the non-fluorescent competitor substrate 80LR yielded recombinant products with one fluorophore each putting comparable to the mixture of the substrates B50R5C5 and 50L6C3. In the reverse reaction, an equimolar mixture of the substrates B50R5C5 and 50L6C3 yielded small amounts of the recombinant product containing a FRET pair identical to substrate B50R5C5L6C3. Since the substrates with a FRET pair and mixtures of substrates with one dye each had very different FRET efficiencies, it was possible to observe both recombination reactions using ensemble FRET measurements. However, recombination of the equimolar mixture of the substrates B50R5C5 and 50L6C3 resulted only in a very small increase in FRET efficiency (figure 6.3), due to the fact that only 1/8 of all possible recombination reactions yield the recombinant product containing a FRET pair (figure 6.2). The frequencies of all possible synapses were predicted in chapter 5. Only 50% of all synapses bring together one B50R5C5 and one 50L6C3 substrate, 50% of those synapses align both substrates in the correct orientation and up to 50% of synapses may form the original substrates due to multiple rounds of recombination. Comparison of the ensemble FRET measurements and a gel-based assay have shown that ensemble FRET measurements provide a good, quantitative measure of the processes of cleavage and recombination by Tn3 resolvase NM (figure 6.5).

Binding by Tn3 resolvase mutants and synapse formation can also be detected by FRET measurements since the FRET efficiency was found to be increased in the presence of Tn3 resolvase mutants. However, the exact FRET efficiency of synapses and substrates remained unclear since the samples were mixtures of different synapses and presumably unbound substrates. The situation was even more complicated in samples with a mixture of substrates B50R5C5 and 50L6C3, which yield high amounts synapses containing different substrates in different orientation immediately after the start of the reaction (see above and figure 6.3B). It appeared that synapses containing two DSB intermediates, each with one dye of a FRET pair, had an intermediate FRET efficiency somewhere between that of DSB substrates in free solution and ligated substrates in synapses. The FRET efficiency of those intermediates was high enough to mask the small FRET increase resulting from the formation of ligated recombinant products in the sample containing a mixture of the substrates B50R5C5 and 50L6C3 and Tn3 resolvase NM in the absence of magnesium.

Synapses containing ligated substrates, each with one dye of a FRET pair, also appeared to have an intermediate FRET efficiency. This became clear when synapses containing mainly ligated reaction products were disrupted by SDS, leading to a strong decrease in FRET efficiency in the sample containing the substrate B50R5C5L6C3 and the competitor substrate 80LR in presence of Tn3 resolvase NM and magnesium (figure 6.3). It remained unclear, if synapses containing DSB intermediates with one dye each and synapses containing ligated products with one dye each show different FRET efficiencies.

In summary, ensemble FRET experiments provide a good, quantitative method to study recombination, including the formation of synapses, cleavage and formation of recombinant products. To identify the FRET efficiency of different synapses and intermediates, single molecule experiments FRET experiments are required to avoid the mere observation of an average FRET value of a mixed population of different synapses and unbound substrates. Since the exact FRET efficiency of most synapses remained unidentified, it is unclear if it is possible to observe strand-exchange using single molecule FRET with the tested fluorescent substrates. However, synapses containing one non-fluorescent and one ligated product with a FRET pair have a very high FRET efficiency, suggesting that ligation and cleavage can be observed in single-molecule FRET experiments. Single-molecule experiments should be able to detect strand exchange if the DSB intermediates come very close to each other during strand exchange providing a high FRET efficiency close to the FRET efficiency of the ligated substrate. In that case, there would be distinct FRET states during strand exchange since the average FRET efficiency of synapses with DSB products is intermediate while some conformations during strand exchange may provide high FRET efficiencies.

7 Development of U-shaped substrates

7.1 *Limitations of single-site substrates*

The single-site substrates with fluorophores at the positions R5 and L6 had been tested successfully in ensemble FRET experiments. Recombination of the substrate B50R5C5L6C3, containing a FRET pair, with an excess of the non-fluorescent competitor substrate 80LR had given rise to a strong decrease of the FRET efficiency of the sample (figure 6.3). However, the reverse recombination reaction of two fluorescent substrates, each containing one dye of the FRET pair, resulted only in a small increase in the FRET efficiency of the sample. This was mainly due to the fact that only a small fraction of all synapses in the sample contained the desired combination of substrates in the desired orientation (figure 6.2). Therefore, it would be advantageous to develop U-shaped substrates that force the formation of synapses containing two copies of site I in the desired combination and orientation. For example, these substrates could contain two copies of site I to promote intramolecular recombination reactions between these sites with structural restraints favouring the correct orientation of both sites (figure 7.1).

Gel-based assays and ensemble FRET experiments had shown that substrates with dyes at the positions R5 and L6 are promising candidates for single-molecule FRET experiments. There are various approaches to employ single-site substrates with fluorophores at positions R5 and L6 in single-molecule experiments. However, each of the approaches using single-site substrates has its own disadvantages.

Generally, to study any substrate or any synapse in the single-molecule setup, these must be attached to the surface of a reaction chamber via the biotin of the substrates. Samples cannot be mixed within the chamber because the addition of solutions into the chamber pushes out and removes the previous solution. Therefore, sample conditions can only be changed by first binding the molecules of interest to the reaction chamber surface and then passing a different buffer. Furthermore, the final buffer used during data-acquisition must not contain fluorescent substrates to avoid background fluorescence.

Using single-site substrates, this means it is necessary to prepare the synaptic complexes in eppendorf tubes, dilute the complexes strongly, attach the complexes to reaction chamber surface and flush the reaction chamber with a suitable imaging buffer before starting the acquisition of single-molecule FRET data (figure 7.1A-C). This process lasts about 15-20 minutes before data can be recorded. This may be problematic if many complexes

dissociate before they can be observed. Once dissociated, the complexes do not reassemble due to the extremely low substrate concentrations. Further, the complexes may dissociate and reassemble in different combinations before they are diluted and attached to the surface, even though this process should be very slow and negligible in the absence of magnesium. Finally, the fastest period of recombination may be over by the time the samples are ready for data acquisition. To circumvent these problems, U-shaped substrates containing two copies of site I were developed (figure 7.1D). Such substrates could be attached to the reaction chamber surface before adding imaging buffers containing no Tn3 resolvase or Tn3 resolvase NM both in presence and absence of magnesium. The samples could be studied nearly immediately after the start of the recombination reaction through the addition of the imaging buffer. Further, the intramolecular recombination of two sites within one substrate is not affected by the low concentration of the substrate. Therefore, new synapses could be assembled using Tn3 resolvase NM from the imaging buffer during the acquisition of single-molecule data. This makes the relative stability of synapses less of an issue in the single-molecule experiments.

In hindsight, any approach to single-molecule experiments using two single-site substrates, each with one fluorophore of the FRET pair was unlikely to succeed. The second ensemble FRET experiment had shown that only a small fraction of all synapses contained the desired combination of substrates in the desired orientation (see chapter 6). Therefore a very heterogeneous mixture of synapses would be observed in the single-molecule experiment which makes the data interpretation more complicated (figure 7.1C).

Approaches employing samples similar to those in the first ensemble FRET experiment were more promising. Recombination of the substrate B50R5C5L6C3 which contains a FRET pair with an excess of the non-fluorescent competitor substrate 80LR had given rise to a strong decrease of the FRET efficiency of the sample. This was mainly due to the fact that at the start of the reaction, all synapses containing any fluorophores contained in fact a FRET pair which could be separated by cleavage and/or strand exchange. However, the substrate B50R5C5L6C3 features a biotin label at the 5'-end and can bind directly to the reaction chamber surface. Therefore, not only synapses can bind to the surface but also free B50R5C5L6C3 substrates (figure 7.1A). The majority of fluorescent molecules observed in the single-molecule setup could be the free B50R5C5L6C3 substrates, depending on the stability of the synapses. This would require the identification of active synapses amongst large numbers of irrelevant fluorescent molecules increasing the chances of observing artefacts.

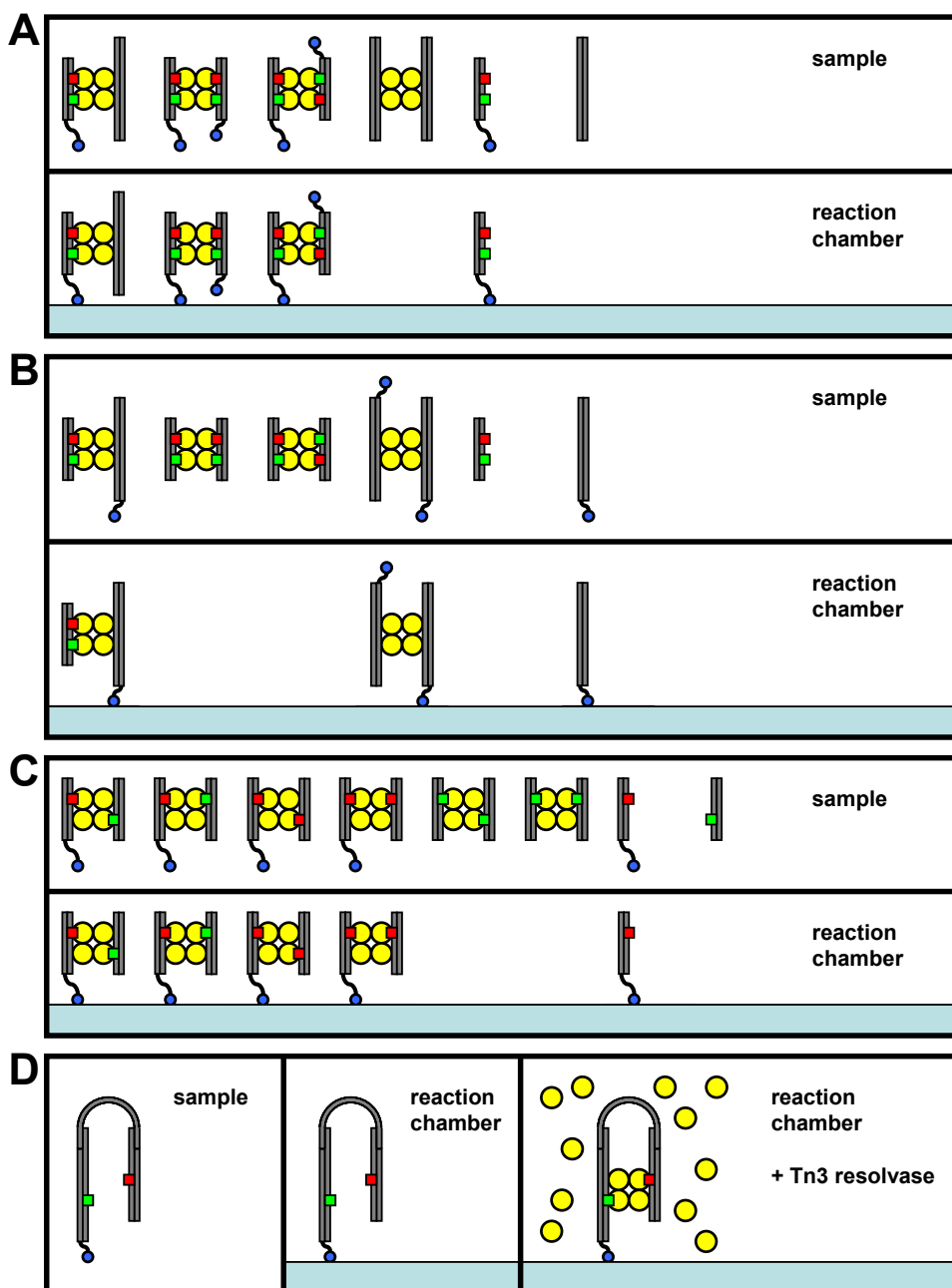


Figure 7.1: Approaches to single-molecule FRET experiments using single-site substrates and U-shaped substrates.

In single-molecule FRET experiments, the molecules and complexes of interest need to be attached to the reaction chamber surface (pale blue block) via the biotin label (blue sphere) of the DNA (DNA single-strands = grey bars) to be observed. Only fluorescent molecules containing a Cy3 dye (green square) or Cy5 dye (red squares) can be observed.

Using single-site substrates, the synapses need to be prepared in an eppendorf tube before attaching them to the surface of the reaction chamber. **(A)** A sample containing a biotinylated fluorescent substrate (B50R5C5L6C3), a non-fluorescent substrate and Tn3 resolvase NM (yellow spheres) forms several fluorescent species which can be attached to the chamber surface. **(B)** A sample containing a non-biotinylated fluorescent substrate (50R5C5L6C3), a biotinylated non-fluorescent substrate and Tn3 resolvase NM forms only one fluorescent species that can attach to the reaction chamber surface: A synapse with the desired substrate configuration **(C)** A sample containing a mixture of the fluorescent substrates B50R5C5 and 50L6C3 and Tn3 resolvase NM forms a large variety of fluorescent species which can attach to the chamber surface.

(D) U-shaped substrates featuring two sites can be bound to the surface before adding Tn3 resolvase to assemble synapses containing the correct combination of fluorescent substrates. The U-shape may restrict recombination to synapses with both sites in the desired orientation.

Instead of using the substrate B50R5C5L6C3, a version without a biotin label, 50R5C5L6C3, could avoid the binding of free fluorescent substrates to the surface (figure 7.1B). To attach the synapses to the reaction chamber surface, Tn3 resolvase NM needs to be added to a mixture of the substrate 50R5C5L6C3 and a non-fluorescent competitor substrate with a biotin label. In that case the only fluorescent molecules bound to the surface would be synapses containing the desired combination of one 50R5C5L6C3 substrate and one non-fluorescent substrate. However, once bound to the surface, the dissociation of any of these complexes would be irreversible due to the low substrate concentrations. At least in the presence of magnesium, synapse dissociation and reassembly seem to be common and would decrease the amount of observable molecules during the single-molecule experiment.

7.2 Design of U-shaped substrates

U-shaped substrates containing two copies of Tn3 *res* site I were designed to address the limitations of single-site substrates. The two sites within the substrate need to be linked in a fashion that allows intramolecular recombination of both sites. Further, it would be beneficial to constrain intramolecular recombination to one orientation of both sites since this allows for more control over the configuration of synapses.

Previously, substrates containing two crossover sites with strict restrictions for their relative orientation had been successfully developed by Leschziner and Grindley (2003). They created a linear, double-stranded DNA molecule (~200 bp) with a copy of $\gamma\delta$ resolvase site I at each end and a binding site for the Integration Host Factor (IHF) at the centre (figure 7.2A). The addition of IHF introduced bend of about 180° bending the linear DNA into a U-shape. This brought both copies of site I into close proximity and allowed recombination only in one orientation of both sites. However, the physical constraints on recombination were extremely strict and intramolecular recombination depended strongly on the exact spacing between the IHF binding site and the copies of site I. A change of the spacing between rotated the crossover sites along the DNA-double-strand and changed the angle between the crossover sites and affected recombination. This effect is very strong due to the high torsional stiffness of the double-stranded DNA.

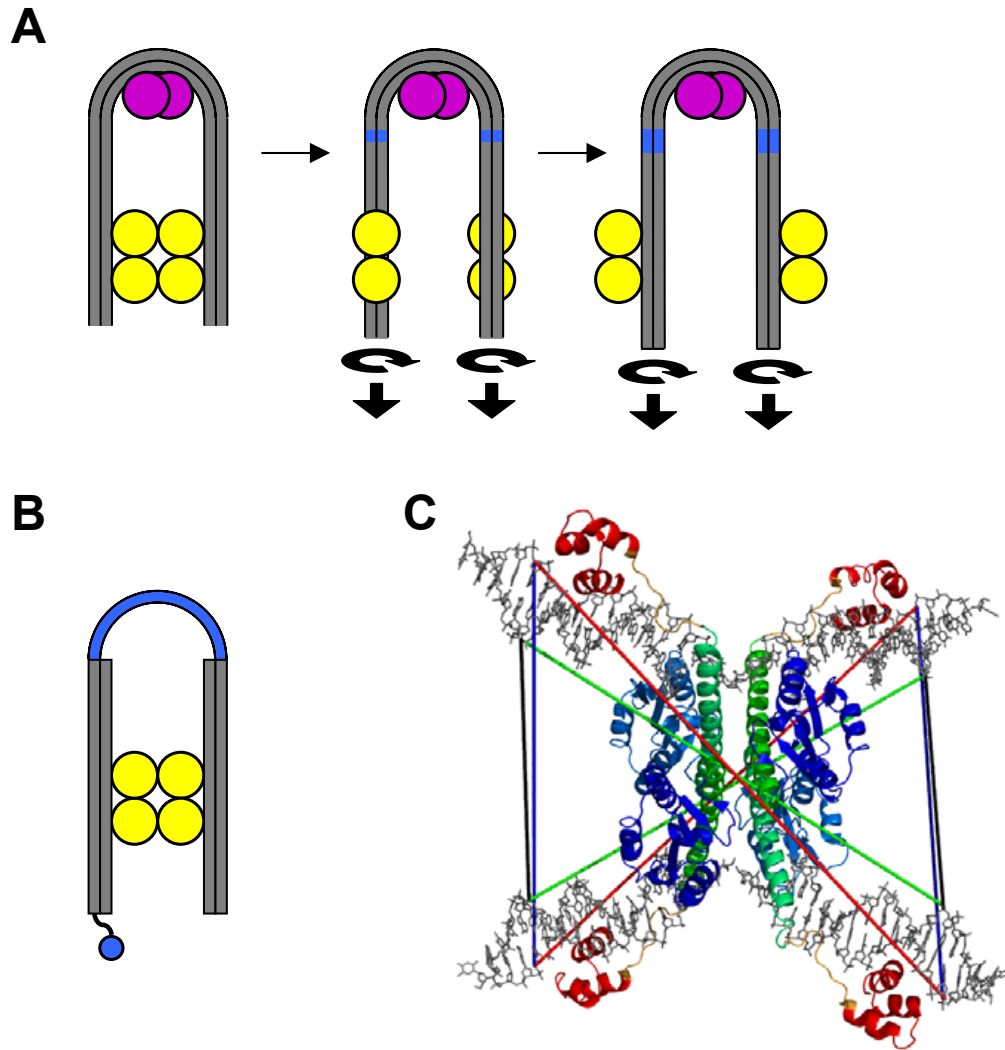


Figure 7.2: Design of the linker in U-shaped substrates

(A) U-shaped substrates developed by Leschziner and Grindley (2003) were formed by binding IHF (purple spheres) to a site at the centre of a double-stranded substrate (grey bars). An increase in the spacing (blue bars) between the IHF binding site and the resolvase crossover sites rotated the crossover sites. Recombination occurred only when the angle between both crossover sites was correct.

(B) The U-shaped substrates used in this project consist of two double-stranded arms (grey bars) connected by a single-stranded poly(dT) linker (blue bars). Each arm contains a crossover site for Tn3 resolvase (yellow spheres). A biotin label (blue sphere) enables the use in single-molecule FRET experiments.

(C) The single-stranded linker of the new U-shaped substrates should provide enough flexibility to allow recombination but should constrain recombination to parallel orientation of both crossover sites. To estimate the required linker length, the distance between the ends of the substrate DNA in the crystal structure of the $\gamma\delta$ resolvase site I synapse (pdb: 1ZR4; Li *et al.* 2005) was measured. In parallel orientation of both sites, the distance was ~ 60 Å between close DNA backbone parts (black lines) and ~ 100 Å between far DNA backbone parts (blue lines). To bring both sites into anti-parallel orientation, the linker needs to stretch diagonally across the whole synapse. In that case, the distance was ~ 110 Å between close DNA backbone parts (green lines) and ~ 130 Å between far DNA backbone parts (red lines).

The development of U-shaped substrates for Tn3 resolvase, similar to those developed by Leschziner and Grindley (2003), was considered to be extremely complicated since the spacing between the IHF sites and the copies of Tn3 *res* site I would need to be exactly correct to allow recombination. Using a flexible, single-stranded poly-thymine linker instead of the IHF binding site was expected to allow the formation of an U-shaped bend as well but without the strong dependence of recombination on the spacing between IHF and the crossover sites (figure 7.2B). The sequence of the linker was chosen to contain only thymines to prevent the formation of secondary structures by base-pairing. The linker should be short enough to favour one orientation of both crossover sites during recombination. At the same time, the linker should be long enough to allow unimpaired synapse formation and recombination. This restriction of the recombination reaction should be possible if the linker is connected to the right half of both copies of site I. In that case, the linker connects two relatively close DNA ends in parallel orientation of both sites (figure 7.2C). In contrast, anti-parallel orientation of the sites affords the linker to stretch further across the whole synapse to connect two ends which are far apart. To estimate the linker length required for recombination in parallel orientation, the distance between two right DNA ends or two left DNA ends was measured in the crystal structure of the $\gamma\delta$ resolvase site I synapse (Li *et al.* 2005). The distance between those DNA ends was ~ 60 Å for the DNA backbone towards the synapse core and ~ 100 Å for the backbone on the outside of the synapse (figure 7.2C). For recombination in anti-parallel orientation, this distance increases to 110-130 Å. However, the crystal structure shows the two halves of each substrate sites at an angle and the substrate ends point outwards. Since the double-stranded arms of the U-shaped are longer than the substrates in the crystal structure, a longer single-stranded linker of about 200 Å may be required. Assuming that single-stranded DNA has a length of ~ 6.3 Å per base (Murphy *et al.* 2004), the required linker length is about 32 bases. However, considering the semi-flexible properties of single-stranded DNA, a 32 base linker has a mean end-to-end length, $\langle l_c \rangle$, of only ~ 100 Å according to equation 7.1, using a persistence length, l_p , of 30 Å (Murphy *et al.* 2004). The contour length, l_c , describes the length of the fully stretched single-stranded DNA and was determined by multiplying the length of a single nucleotide with the number of bases in the linker. However, the mean end-to-end length may not be relevant for the linker length since single-stranded DNA is very flexible (Murphy *et al.* 2004). To find a suitable linker length, substrates with linkers of 30, 40 and 50 bases length were generated.

$$\langle l_c \rangle = \sqrt{2 \cdot l_p \cdot l_c - 2 \cdot l_p^2 \cdot [1 - \exp(-l_c / l_p)]} \quad 7.1$$

To allow the gel-based analysis of reaction products from the recombination of U-shaped substrates by Tn3 resolvase NM, the double-stranded arms of the U-shaped substrates were designed to have different lengths (figure 7.3). The X-arm comprises 69 base pairs while the Y-arm comprises 57 base pairs. In both arms, Tn3 res site I has the same distance from the linker to allow the formation of symmetrical synapses. However, the end of each arm has a different length. Intramolecular recombination swaps the long and short ends of the X- and Y- arms. This alone would not alter the retardation of the U-shaped substrate on a SDS polyacrylamide gel very much. Therefore, each arm contains a different restriction endonuclease site located between site I and the linker (figure 7.3, 7.4). This allows the specific separation of the majority of each arm, including Tn3 res site I, from the rest of the U-shaped substrate by restriction endonuclease digestion. A restriction digest enables the identification of products of intramolecular and intermolecular recombination since the resulting fragments have different lengths in the recombinant and non-recombinant states (figure 7.3C). Further, various fragments can contain different fluorescent dyes and recombination can change the lengths of these fragments. The U-substrate contains a BamHI restriction site in the X-arm and a MluI restriction site in the Y-arm. These restriction endonucleases were chosen since they are capable of cutting within short double-stranded DNA fragments, are commercially available with high activity and work in a range of buffers with high salt content. This allows the quick, direct digestion of the recombination products without changing the reaction buffer.

The final U-shaped substrate had to be assembled from five oligonucleotides due to the overall length of the U-shaped substrate (figure 7.3B, 7.4). Each arm consists of two oligonucleotides leaving an overhang which can be annealed to the complementary ends of the oligonucleotide which forms the poly-T linker. The overhangs were kept as short as possible without lowering the predicted melting temperature, T_m , of the annealed connection below 60 °C to prevent the dissociation of the U-shaped substrate in solution. The melting temperature of the connection was predicted using the DINAMelt server (Markham and Zuker 2005; Markham and Zuker 2008) server and a connecting overhang of 16 bp with a high GC-content ensured the stability of the U-shaped substrate.

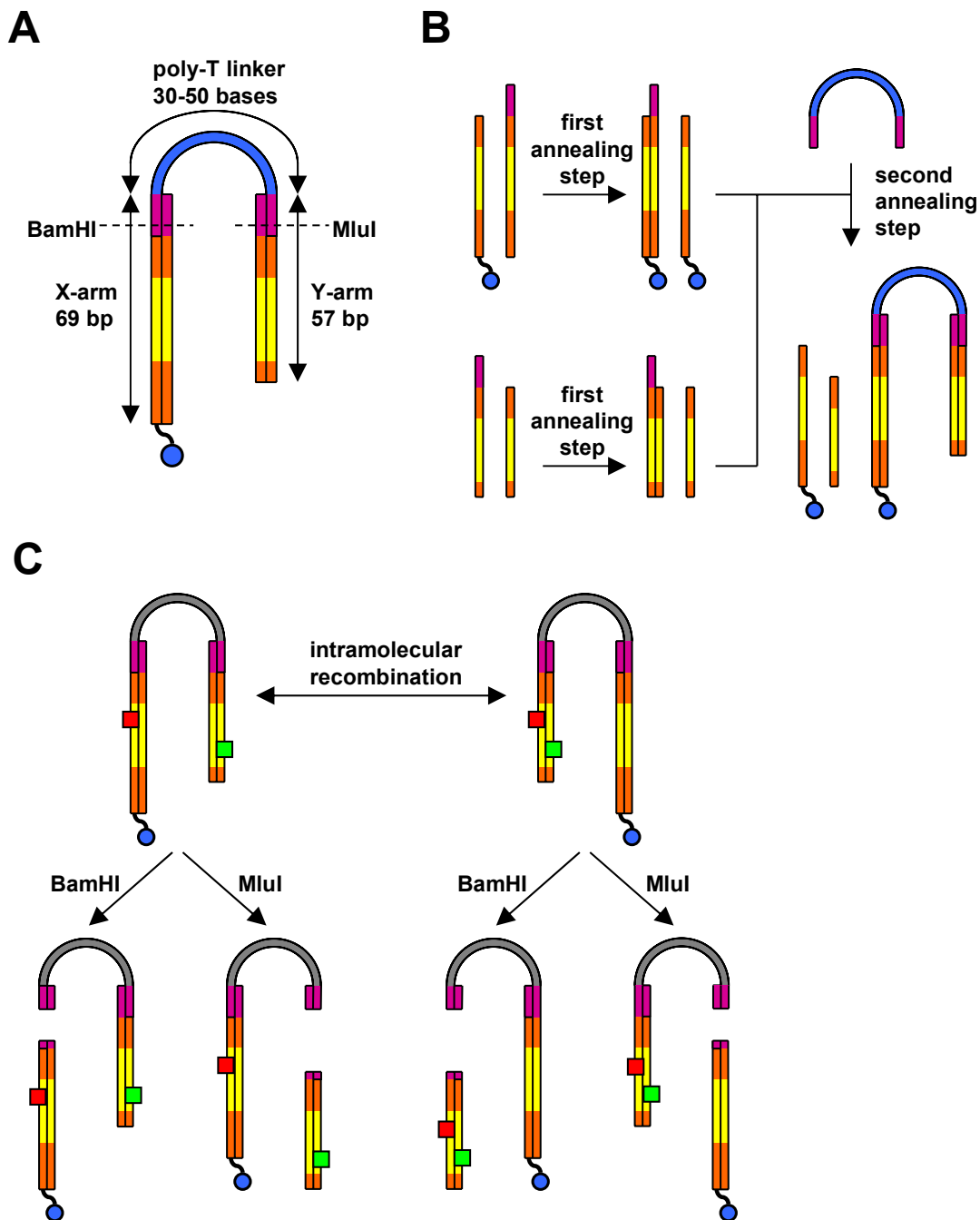


Figure 7.3: Design and assembly of U-shaped substrates

(A) The U-shaped substrates feature two double-stranded arms (orange), each containing one copy of Tn3 res site I (yellow). An overhang (purple) connects the arms to a complementary part in the single-stranded poly(dT) linker (grey). The connecting overhang of the X-arm contains a site for the restriction endonuclease BamHI while the Y-arm contains MluI site. A biotin label (blue sphere) enables the use in single-molecule FRET experiments.

(B) The U-substrates were annealed from five oligonucleotides. In the first annealing step, each arm was annealed separately. Using an excess of the oligonucleotide without the connecting overhang ensured all molecules with an overhang are double-stranded. In the second annealing step, the U-substrate is formed amongst much shorter side-products allowing simple gel purification.

(C) In this example intramolecular recombination occurs in a U-substrate containing a Cy3 dye (green square) and a Cy5 dye (red square). The digestion with different restriction endonucleases produces characteristic fragments for the original substrate and for the recombinant products.

A safe but time-consuming and wasteful method of annealing the U-substrate from five oligonucleotides would have been to anneal each arm separately from two oligonucleotides followed by gel-purification of the double-stranded products. The annealed arms could then be annealed with the linker oligonucleotide to form the U-shaped substrate followed by a further gel purification step. However, material would have been lost in each gel purification step. Another method using one gel purification step was deemed more efficient. In the alternative method, each arm was annealed separately from two oligonucleotides. An optimised annealing process using a 1.5-fold excess of the oligonucleotide without the overhang ensured that all oligonucleotides containing the connecting overhang were annealed to the complementary strand. Subsequently, the two annealed arms were mixed with an equimolar amount of the linker nucleotide and a second annealing step was performed at a low temperature without melting the arms. The optimised first annealing step guaranteed that, in the second annealing step, only fully annealed, double-stranded arms could connect to the linker oligonucleotide to form the U-substrate. The U-substrate was then purified by polyacrylamide gel electrophoresis.

The optimised annealing method required that the sequences of all oligonucleotides were sufficiently different to avoid incorrect annealing of any parts of the U-substrate. Both arms contain the Tn3 *res* site I sequence were flanked by GC-rich sequences to prevent fraying of the annealed arms. Choosing highly different flanking sequences resulted in distinct sequences of both arms.

The connecting overhang also had to be GC-rich to ensure the stability of the U-shaped substrate. At the same time, the sequence of both connecting overhangs needed to differ strongly to avoid annealing two identical arms to the linker oligonucleotide. Only part of the connecting overhang was variable, since the overhang contained the restriction endonuclease sites. The overhang sequence was designed by selecting appropriate overhangs from a large library of sequences assembled from the endonuclease sites and randomised sequence generated with the PHP nucleotide sequence generator (Lind 2003). The overhang sequences were selected after analysis using the DINAMelt server (Markham and Zuker 2005; Markham and Zuker 2008). Sequences were chosen if they provided a high melting temperature above 60 °C when annealed to the correct partner and a low melting temperature when annealed to the wrong partner. Sequences which could form stable, undesirable secondary structures like hairpins were rejected leaving a small number of possible candidates.

The final design of the U-shaped substrates was selected from a library of designs, each combining an overhang candidate and one of several versions of the sequences flanking Tn3 *res* site I in the arms. For this purpose the designs were analysed using the DINAMelt server (Markham and Zuker 2005; Markham and Zuker 2008). Most designs for U-shaped substrates were omitted since their constituent oligonucleotides could form stable, incorrect dimers or stable, undesirable secondary structures like hairpins. The design chosen for all U-shaped substrates met all requirements and should allow the correct assembly employing two annealing steps and only one gel purification step.

7.3 Preparation of U-shaped substrates

To test the assembly and recombination of U-shaped substrates, these were initially prepared without Cy3 or Cy5 dyes to avoid the lengthy conjugation and purification process. Instead, the top-strand of the Y-arm was readily synthesised with a fluorescein label at the 5'-end for detection in gels.

7.3.1 Results

The preparation and purification of U-shaped substrates by a method using only two annealing and one gel purification step was tested. For this purpose, the X-arm was annealed from the bottom strand (XB69) and a 1.5-fold molar excess the biotinylated top-strand (BXT53). The Y-arm was annealed from the fluorescein-labelled top-strand (FYT57) and a 1.5-fold molar excess of the bottom strand (YB41). After the first annealing step, an equimolar mixtures of the annealed X-arm, the annealed Y-arm and a linker oligonucleotide with 30, 40 or 50 thymine bases (L30, L40, L50) was annealed at a low temperature without melting the arms.

Analysis of the annealed products by PAGE showed that the mixture formed mainly one strongly retarded band on the gel (figure 7.5, lanes 9-11). This band potentially contained the annealed U-shaped substrate with a linker with 30, 40 or 50 thymine bases. For comparison, the annealed X-arm and the annealed Y-arm were separated on the same gel (figure 7.5, lanes 1,2) and produced bands which were far less retarded than the potential band of the annealed U-shaped substrate. For further comparison, substrates were annealed using mixtures containing only the X-arm and the linker or only the Y-arm and a linker (L30, L40 or L50). These incomplete mixtures formed a major band which had a higher retardation than the bands of single arms but a lower retardation than the potential band of the complete U-shaped substrate (figure 7.5, lanes 3-8). Therefore, the potential band of the U-shaped substrate contains a species much larger than a single X-arm, a single Y-arm or an incomplete substrate with only one arm connected to the linker. Most likely, this species was the correctly annealed U-shaped substrate.

1	2	3	4	5	6	7	8	9	10	11	12	13	14	15	Lane
-	-	+	+	+	+	+	+	+	+	+	+	+	-	-	linker
-	-	30	30	40	40	50	50	30	40	50	30	30	-	-	linker length
+	-	+	-	+	-	+	-	+	+	+	-	+	-	-	X-arm
-	+	-	+	-	+	-	+	+	+	+	+	-	-	-	Y-arm
-	-	-	-	-	-	-	-	-	-	-	-	-	+	-	incorrect arm: no overhang
-	-	-	-	-	-	-	-	-	-	-	+	+	-	+	incorrect arm: two overhangs

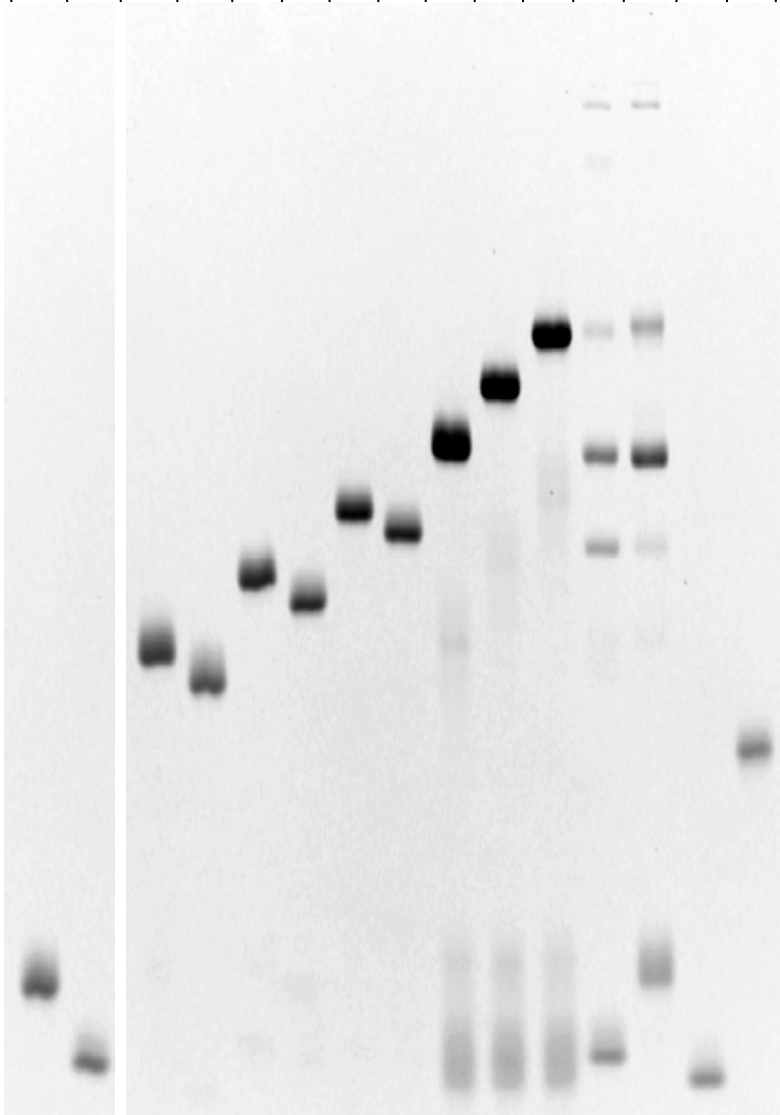


Figure 7.5: Test-annealing of U-shaped substrates.

The products of different annealing reactions were separated by PAGE and visualised by ethidium bromide staining. In the first annealing step, the X-arm and the Y-arm of the U-shaped substrate were annealed separately (lanes 1-2). As a control, the short top-strand of the X-arm and the short bottom-strand of the Y-arm were annealed to form an arm without connecting overhangs (lane 14). The top-strand of the Y-arm and the bottom-strand of the X-arm formed a “sticky” arm with two connecting overhangs (lane 15). Annealing of a linker (30, 40 or 50 thymine bases) and only one arm formed incomplete substrates (lanes 3-8). Complete U-shaped substrates were annealed from the X-arm, the Y-arm and a linker (30, 40 or 50 thymine bases) (lanes 9-11). Annealing of one arm (X-arm or Y-arm), a linker (30 thymine bases) and the “sticky” arm produced multiple fragments (lanes 12-13).

The gel image is representative of similar experiments (data not shown).

To identify incorrectly annealed substrates, several samples were prepared using oligonucleotide mixtures which favour incorrect substrate assembly during annealing. In one of these samples, a mixture of the two short oligonucleotides of both arms (BXT53 and YB41), which do not contain the connecting overhang, was annealed using the complementary sequence of Tn3 *res* site I in both oligonucleotides. This sample produced a single fragment smaller than the Y-arm (figure 7.5, lane 14). In another sample, a mixture of the two long oligonucleotides of both arms (XB69, FYT57), which contain the connecting overhang, was annealed using the complementary sequence of Tn3 *res* site I in both oligonucleotides. This sample produced mainly one strongly retarded band (figure 7.5, lane 15). This band may be formed by a “sticky” arm containing two overhangs. However, the strong retardation of the band indicates that the DNA construct may consist of multiple annealed oligonucleotides. The bands of the incorrectly annealed arms were not found in the sample prepared using the correct annealing mixture and the correct annealing process. This suggests that the U-shaped substrate can be annealed without the formation of incorrectly annealed arms.

Further, the incorrectly annealed “sticky” arm with two connecting overhangs, annealed from XB69 and FYT57, was used to assemble incorrectly annealed U-shaped substrates. In one sample, the incorrectly annealed “sticky” arm was mixed with the short linker oligonucleotide (L30) and the annealed X-arm. A second sample contained a mixture of the incorrectly annealed “sticky” arm, the short linker oligonucleotide (L30) and the Y-arm. After annealing these samples at low temperature, they were also run on the same polyacrylamide gel (figure 7.5, lanes 12, 13). The incorrectly annealed substrates produced multiple bands. One band had nearly the same retardation as the potential band of the correct U-shaped substrate with the short linker (L30). However, the sample of the incorrectly annealed substrates produced multiple other bands, with higher and lower retardation, which were not found in the sample of the correctly annealed substrate. The lack of these additional bands in the sample of the correctly annealed U-shaped substrate suggests that the use of suitable annealing method successfully prevents the formation of incorrectly annealed arms and substrates. Therefore, the main band in the samples containing the correct mixture is most likely the fully annealed U-shaped substrate.

7.3.2 Discussion

It has been shown that the U-shaped substrate can be annealed using two annealing steps. The method results in mainly one product and provides the U-substrate at a high yield. Further, none of the undesirable side-products, which had been produced using altered annealing reactions for comparison, was found in the samples using the correct annealing

method. Finally, the annealed U-shaped substrate had been extracted from the gel bands without dissociation (data not shown) and was ready for in-vitro recombination tests.

7.4 Effect of the linker length on recombination

Three U-shaped substrates with a linker length of 30, 40 and 50 bases were prepared to test the ideal linker length. The substrates contained a fluorescein label at the 5'-end of the top-strand of the Y-arm for visualisation. Recombination of the substrates could proceed in two ways (figure 7.6). Intermolecular recombination occurs when two U-shaped substrates come together and any of their arms are recombined. Intramolecular recombination occurs within one U-shaped substrate between the two arms. Intramolecular recombination includes the recombination of both arms in parallel orientation, resulting in inversion products, and the recombination of both arms in anti-parallel orientation, resulting in deletion products. The U-shaped substrates were developed to promote intramolecular recombination resulting in inversion products.

After recombination of the three different U-shaped by Tn3 resolvase NM for one hour, the reaction products were digested with restriction endonucleases for five minutes before stopping the reaction with SDS. The endonuclease BamHI cuts within the connecting overhang of the X-arm, while the endonuclease MluI cuts within the connecting overhang of the Y-arm. The digest generated characteristic fragments for the products of the different recombination pathways (figures 7.6 and 7.7). Further, the optional digestion of the fragments with protease K removed covalently bound resolvase from recombination intermediates and allowed a more detailed analysis of the recombination products. These fragments were then separated by SDS-PAGE to identify the recombinant products. Only fragments containing the fluorescein label were visualised with a fluorescence imager simplifying the analysis of the recombination products (figure 7.7).

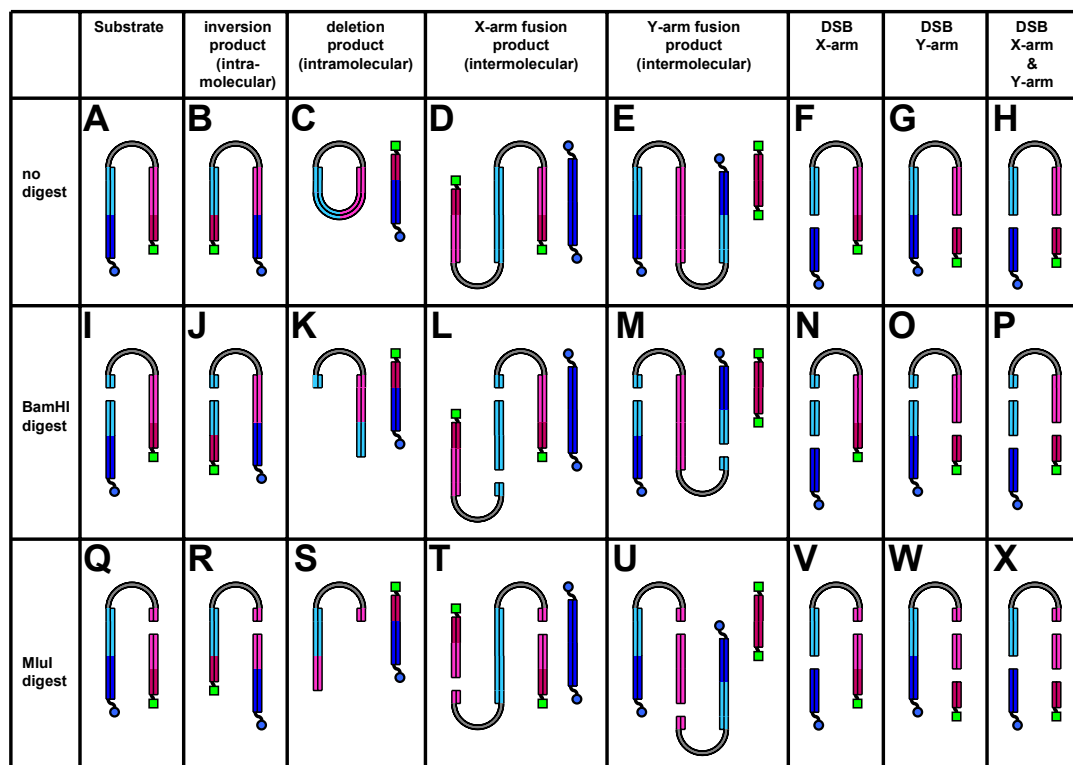


Figure 7.6: Recombination products of fluorescein labelled, U-shaped substrates.

The recombination of U-shaped substrates with a single-stranded linker (grey) can proceed via several different pathways.

Intramolecular recombination of fluorescein labelled (green square) U-shaped substrates occurs within one substrate between the X-arm (dark and pale blue) and the Y-arm (dark and pale pink). Intramolecular recombination of both arms in parallel orientation (dark ends of both arms on the same side) results in inversion products while recombination in anti-parallel orientation (dark ends of both arms on opposite sides) results in deletion products.

Intermolecular recombination of the substrates can occur between any of the arms of two substrates. The intermolecular recombination and fusion of two X-arms or two Y-arms are shown here, since these reactions result in characteristic recombinant products.

Double-strand breaks can result in various recombination intermediates, depending on the cleaved arm.

Digestion of the recombination products and intermediates with restriction endonucleases generates characteristic fragments for each recombination pathway. The endonuclease BamHI cuts within the X-arm while MluI cuts within the Y-arm.

	Substrate	inversion product (intra- molecular)	deletion product (intramolecular)	X-arm fusion product (intermolecular)	Y-arm fusion product (intermolecular)	DSB X-arm	DSB Y-arm	DSB X-arm & Y-arm
no digest	A	B	C	D	E	F	G	H
BamHI digest	I	J	K	L	M	N	O	P
MluI digest	Q	R	S	T	U	V	W	X

Figure 7.7: Detectable recombination products of fluorescein labelled, U-haped substrates.

This figure lists a selection of the reaction products shown in figure 7.6. Only reaction products which contain a fluorescein label for the detection using a fluorescence imager are shown here.

7.4.1 Results

Separation of the recombination products of the three U-shaped substrates resulted in multiple bands (figures 7.8, 7.9, 7.10). The band of the original U-shaped substrate was identified by comparison to samples without Tn3 resolvase NM. However, since the restriction digest does not proceed to completion, this band also includes inversion products which have the same size before the digestion with restriction endonucleases. The bands containing DSB intermediates, covalently bound by resolvase units, were identified by comparing undigested samples with samples which were digested with protease K. There two major DSB intermediates and their length depended on the location of the DSB (figures 7.6, 7.7). The digested version of the shortest DSB intermediate left the bottom of the gel due to its low retardation on a polyacrylamide gel with 8% w/v acrylamide. The size of the intramolecular deletion product is not affected by the restriction digest and could be found at the same position for all samples with Tn3 resolvase NM (figure 7.6). The same is true for the smaller intermolecular recombination product resulting from the recombination and fusion of two Y-arms. The inversion products were identified according to their size and specific occurrence in samples digested with different enzymes. Finally, several strongly retarded bands were found at the top of the gel. Most likely, these bands contain intermolecular reaction products consisting of multiple copies of the U-shaped substrate. Some these strongly retarded bands may have been formed by nicked intermediates of full length substrates. However, the bands of the potential nicked products run at the same position as the protease K resulting in obscured bands. Therefore, the comparison between samples with and without protease K is not possible and the highly retarded bands cannot not be interpreted unambiguously.

All three substrates with different linker lengths allowed inversion, deletion and intermolecular recombination. The bands of the recombination products were quantified (table 7.1) to establish if any of the recombination pathways was favoured and if the linker length affected the formation of specific products. The band of the undigested (restriction endonucleases) original substrate contained not only the substrate but also undigested inversion products. Therefore, the percentage of inversion products in the band of the undigested substrate was assumed to be the identical to the percentage of inversion products amongst all restriction digest fragments in the sample. This allowed a more accurate estimation of the total amount of inversion products.

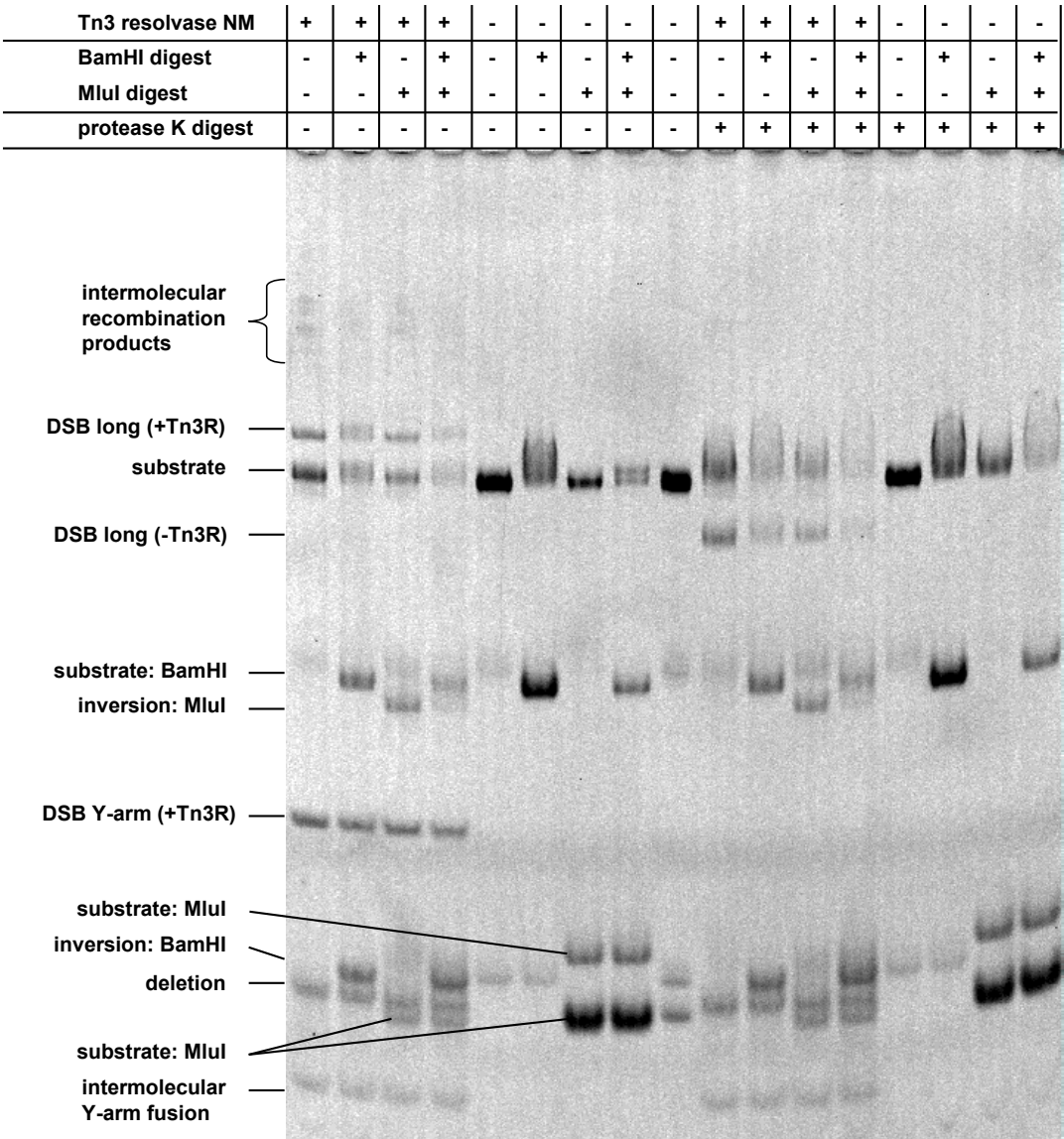


Figure 7.8: Recombination products of U-shaped substrates with a 30 base linker separated by SDS-PAGE.

A fluorescein labelled, U-shaped substrate with a 30 base linker was recombined with Tn3 resolvase NM (1.2 μ M) in presence of magnesium chloride (10 mM) for one hour at 20 °C. The reaction products were digested with the restriction endonucleases BamHI and/or Mlul followed by optional digestion with protease K. The reaction was then stopped by addition of SDS and the reaction products were separated by SDS-PAGE (8% w/v acrylamide). The DNA fragments were visualised with a fluorescence imager using the fluorescein label of the substrate. For a description of the reaction products see figure 7.6 and 7.7. The gel image is in agreement with a partial repeat of the experiment.

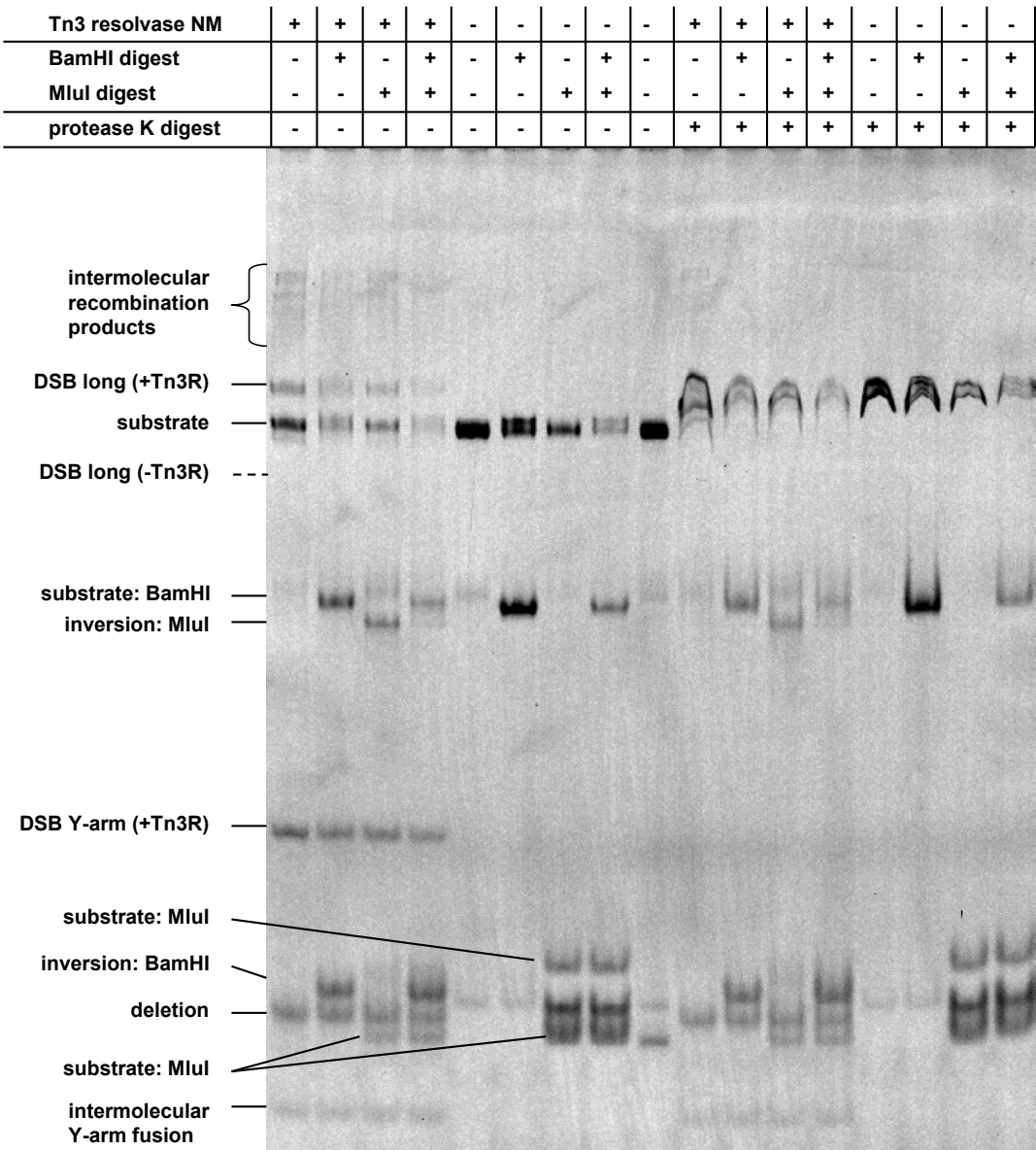


Figure 7.9: Recombination products of U-shaped substrates with a 40 base linker separated by SDS-PAGE.

A fluorescein labelled, U-shaped substrate with a 40 base linker was recombined with Tn3 resolvase NM (1.2 μ M) in presence of magnesium chloride (10 mM) for one hour at 20 $^{\circ}$ C. The reaction products were digested with the restriction endonucleases BamHI and/or MluI followed by optional digestion with protease K. The reaction was then stopped by addition of SDS and the reaction products were separated by SDS-PAGE (8% w/v acrylamide). The DNA fragments were visualised with a fluorescence imager using the fluorescein label of the substrate. For a description of the reaction products see figure 7.6 and 7.7. The gel image is in agreement with a partial repeat of the experiment.

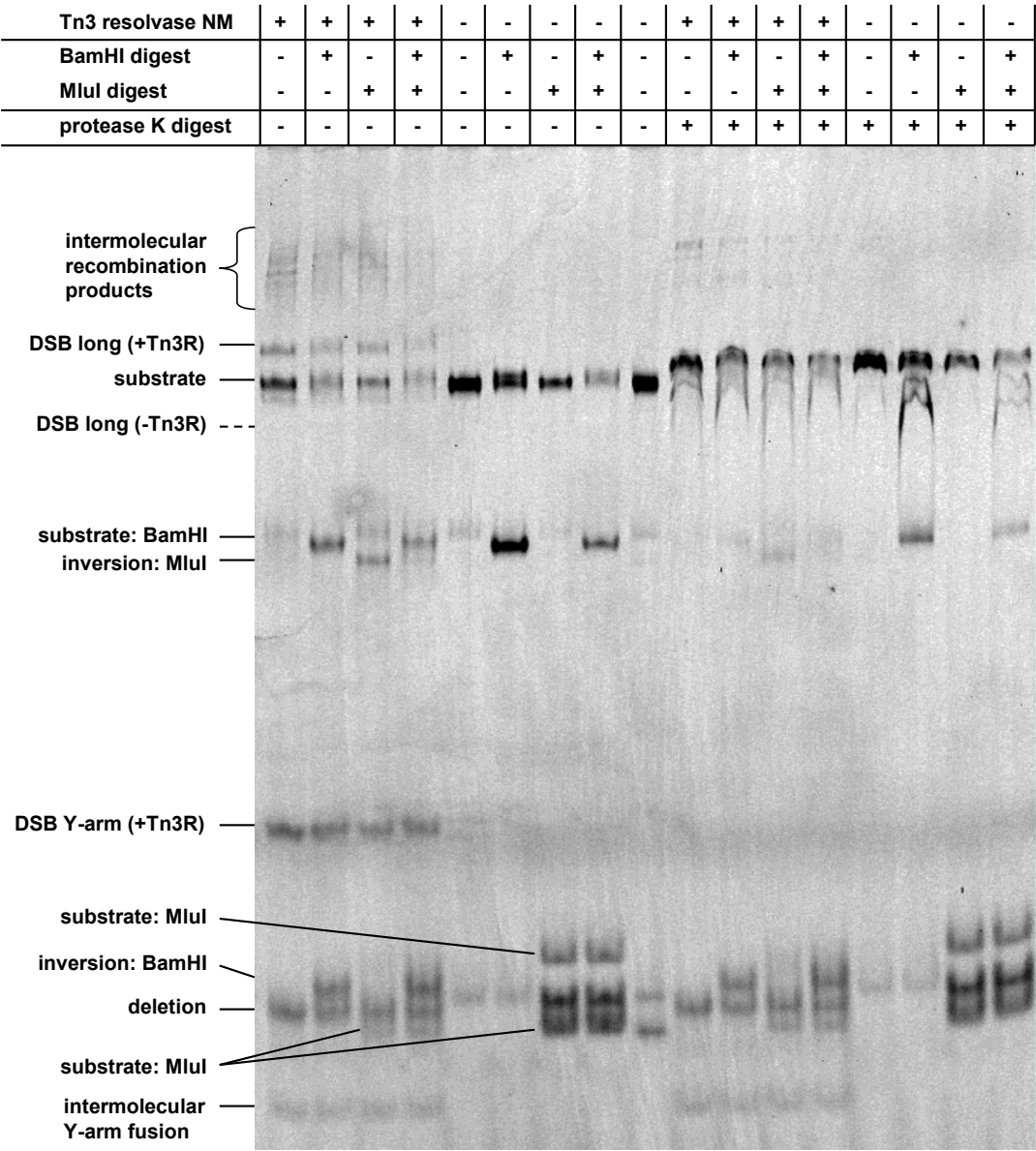


Figure 7.10: Recombination products of U-shaped substrates with a 50 base linker separated by SDS-PAGE.

A fluorescein labelled, U-shaped substrate with a 50 base linker was recombined with Tn3 resolvase NM (1.2 μ M) in presence of magnesium chloride (10 mM) for one hour at 20 $^{\circ}$ C. The reaction products were digested with the restriction endonucleases BamHI and/or MluI followed by optional digestion with protease K. The reaction was then stopped by addition of SDS and the reaction products were separated by SDS-PAGE (8% w/v acrylamide). The DNA fragments were visualised with a fluorescence imager using the fluorescein label of the substrate. For a description of the reaction products see figure 7.6 and 7.7. The gel image is in agreement with a partial repeat of the experiment.

linker length	30	30	40	40	50	50
protease K digest	-	-	-	-	-	-
BamHI digest	+	-	+	-	+	-
MluI digest	-	+	-	+	-	+
% inversion	26	29	26	19	26	15
% substrate	29	23	31	27	19	17
% deletion	10	15	16	24	17	27
% intermolecular Y-arm fusion	6	6	5	6	5	6
% DSB	30	27	23	25	33	35

Table 7.1 Effect of the linker length on the recombination of U-shaped substrates

It was found that all linkers allowed the formation of large amounts of inversion products (table 7.1). The L30 linker may have resulted in slightly higher amounts of inversion products than the L40 and L50 linker but the values varied strongly between individual samples. However, the shortest linker decreased the formation of deletion products compared to the L40 and L50 linker. This suggests that a shorter linker limits, to some degree, intramolecular recombination to the parallel orientation of both arms. The formation of intermolecular products was unaffected by the linker length. This was expected since the linker does not limit the movement of two U-shaped substrates relative to each other.

7.4.2 Discussion

It appears that the shortest linker favours, to some degree, the desired intramolecular inversion reaction. The low amount of unambiguous intermolecular products suggests that intramolecular recombination proceeded faster than intermolecular recombination. This may be due to the fact that both arms of the U-shaped substrate are always in relatively close proximity, allowing intramolecular recombination, while intermolecular recombination requires two substrates to come together by diffusion over larger distances. However, intermolecular recombination can combine any substrate arm in any orientation and may therefore result in products identical to intramolecular recombination products. It remains unclear what percentage of the seemingly intramolecular recombination products stemmed from intermolecular recombination events.

7.5 Timescale of the recombination of U-shaped substrates and the effect of the resolvase concentration

To confirm that the U-shaped substrates allow intramolecular recombination, the recombination products after ten minutes incubation were compared to the recombination products after two hours. Intramolecular recombination is expected to occur faster than intermolecular recombination since the arms within one substrate are readily in close proximity while intermolecular recombination requires the diffusion of two substrates over larger distances. Further, the effect of the resolvase concentration on the formation of recombinant products was tested. For these purposes, the fluorescein labelled, U-shaped substrate with a 30 base linker was incubated with Tn3 resolvase NM at concentrations of 0.6, 1.2 and 2.4 μM . Samples were taken and digested with the restriction endonuclease BamHI after ten minutes and after two hours. The digestions with the restriction endonuclease MluI and with protease K were omitted since the previous experiments had shown that the BamHI digest was already sufficient for the identification of the recombination products.

7.5.1 Results

The recombination products were analysed by SDS-PAGE as in the previous experiment (figure 7.11). The bands containing the intermolecular recombination product from the recombination and fusion of two Y-arms (figure 7.6) were stronger after two hours than after ten minutes for all samples containing Tn3 resolvase NM. The same was true for the bands of the intramolecular deletion product. However, the bands of the desired intramolecular inversion product appeared to have the same intensity after ten minutes and after two hours.

To confirm the trends seen in the image of the SDS-gel, the bands were quantified (table 7.2) as in the previous experiment. It became clear that the samples contain only low amounts of unambiguous intermolecular recombination products (3.8-5%) after ten minutes but the amount increases to 8-8.7% after two hours. The concentration of Tn3 resolvase had no effect on this process.

The amount of intramolecular deletion products increases from 2.4-2.8% after ten minutes incubation to 8.1-16.9% after two hours. However, unlike intermolecular recombination products, the amount of the intramolecular deletion product after two hours increases strongly with increasing concentrations of Tn3 resolvase NM. This suggests that intramolecular deletion proceeds slowly and is dependent on the resolvase concentration.

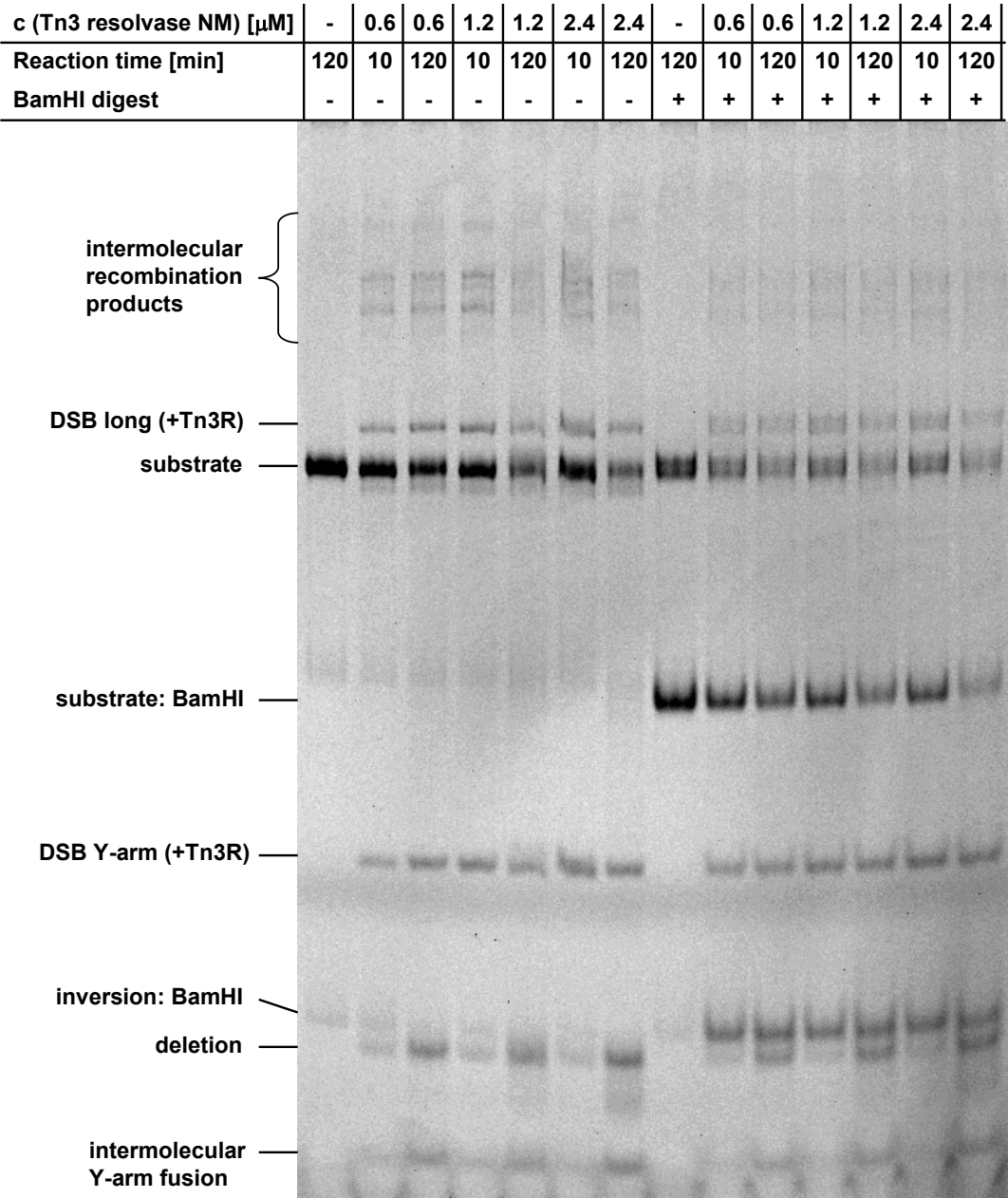


Figure 7.11: SDS-PAGE of recombination products of U-shaped substrates: Effect of the resolvase concentration and of the incubation time on recombination.

A fluorescein labelled, U-shaped substrate with a 30 base linker was recombined with Tn3 resolvase NM in presence of magnesium chloride (20 mM) for ten minutes or two hours at 20 °C. The resolvase concentration varied from 0.6 to 2.4 μ M. Optionally, the reaction products were digested with the restriction endonucleases BamHI. The reaction was then stopped by addition of SDS and the reaction products were separated by SDS-PAGE (8% acrylamide). The DNA fragments were visualised with a fluorescence imager using the fluorescein label of the substrate. For a description of the reaction products see figure 7.6 and 7.7. The gel image corresponds to a single experiment.

c(Tn3R NM) [μ M]	0.6	0.6	1.2	1.2	2.4	2.4
reaction time [min]	10	120	10	120	10	120
% inversion	27.2	27.8	26.5	28.8	26.2	24.3
% deletion	2.6	8.1	2.4	12.6	2.8	16.9
% intermolecular Y-arm fusion	3.8	8.0	3.9	8.7	5.0	8.2
% substrate	44.3	33.2	40.0	25.8	38.4	25.9
% DSB	14.6	15.7	18.4	16.2	19.0	17.5
% large intermol. rec. products	7.5	7.2	8.8	7.8	8.7	7.2

Table 7.2: Kinetics of the recombination of U-shaped substrates and effect of the resolvase concentration

The formation of the desired intramolecular inversion product seemed to be independent from the resolvase concentration. Further, the amount of the inversion product reached a maximum of 24.3-28.8 already after ten minutes, suggesting that this intramolecular recombination reaction is indeed much faster than intermolecular recombination.

7.5.2 Discussion

As expected, intramolecular inversion occurs quicker than the intermolecular fusion of two Y-arms. This confirms that the intramolecular recombination occurs and it was found to proceed at high rates. Both processes, intramolecular inversion and intermolecular Y-arm fusion, seemed to be independent from the concentration of Tn3 resolvase NM.

The intramolecular deletion appeared to depend strongly on the concentration of Tn3 resolvase NM. This could allow the promotion of inversion, rather than deletion, in FRET experiments by simply decreasing the resolvase concentration. Surprisingly, intramolecular deletion proceeded slowly, similar to intermolecular recombination. One possible explanation is that the U-shaped substrate puts structural constraints on intramolecular recombination of both arms in anti-parallel orientation, effectively slowing down this reaction. A second possible explanation is that most of the seemingly intramolecular deletion products are actually produced by intermolecular recombination of arms in suitable combinations and orientations. If the second explanation is correct, intramolecular reaction proceeds mainly via the desired inversion reaction and all other products result mostly from intermolecular recombination. This would be advantageous for future FRET experiments since the arms can be aligned and recombined in any chosen combination and orientation.

7.6 Recombination of U-shaped substrates with Cy dyes attached within Tn3 *res* site I

After it had been established that U-shaped substrates favour the desired inversion reaction, the recombination of U-shaped substrates with Cy dyes attached within Tn3 *res* site I was tested. Previously, it was shown with single-site substrates that fluorescent dyes at positions R5 and L6 have nearly no inhibitory effect on recombination by Tn3 resolvase NM (see chapter 5). At the same time, Cy5 and Cy3 dyes at these positions can form FRET pairs which provide high FRET efficiencies. Therefore, the U-shaped substrate U3 with a 30 base linker (L30) was prepared. The substrate contained a Cy5 dye at position R5 in the X-arm and a Cy3 dye at position L6 in the Y-arm (figure 7.4, 7.12). This substrate should provide a low FRET efficiency in the original state and a high FRET efficiency after intramolecular inversion.

The substrate U3 was recombined by Tn3 resolvase NM in the presence to test if the Cy dyes within Tn3 *res* site I affect recombination and if inversion provides a strong increase in FRET efficiency. After recombination with 1.2 μ M Tn3 resolvase NM in the presence of 20 mM magnesium chloride for ten minutes or for two hours, the recombination products were digested with the restriction endonuclease BamHI or MluI to generate DNA fragments characteristic for each recombination pathway (figure 7.12). The reaction was then stopped by the addition of SDS and the DNA fragments were separated by SDS-PAGE. The digestion of the fragments with protease K was omitted.

The Cy3 and Cy5 dyes of the substrate enabled three different visualisations of the DNA fragments using a Typhoon fluorescence imager. DNA fragments containing the Cy3 dye (figure 7.13) were selectively visualised using a laser matching the excitation wavelength of the Cy3 dye and an optical filter setup permitting mainly the detection of Cy3 fluorescence. However, fragments containing a FRET pair with high FRET efficiency (figure 7.15) would show very weak bands since the Cy3 dye transfers most of its excitation energy to the Cy5 dye. Fragments containing a Cy5 dye (figure 7.14) were selectively visualised using a laser matching the excitation wavelength of the Cy5 dye and an optical filter setup permitting mainly the detection of Cy5 fluorescence. Finally, fragments containing a FRET pair with high FRET efficiency (figure 7.15) were visualised selectively using a laser matching the excitation wavelength of Cy3 while using a filter setup that permits mainly the detection of Cy5 fluorescence.

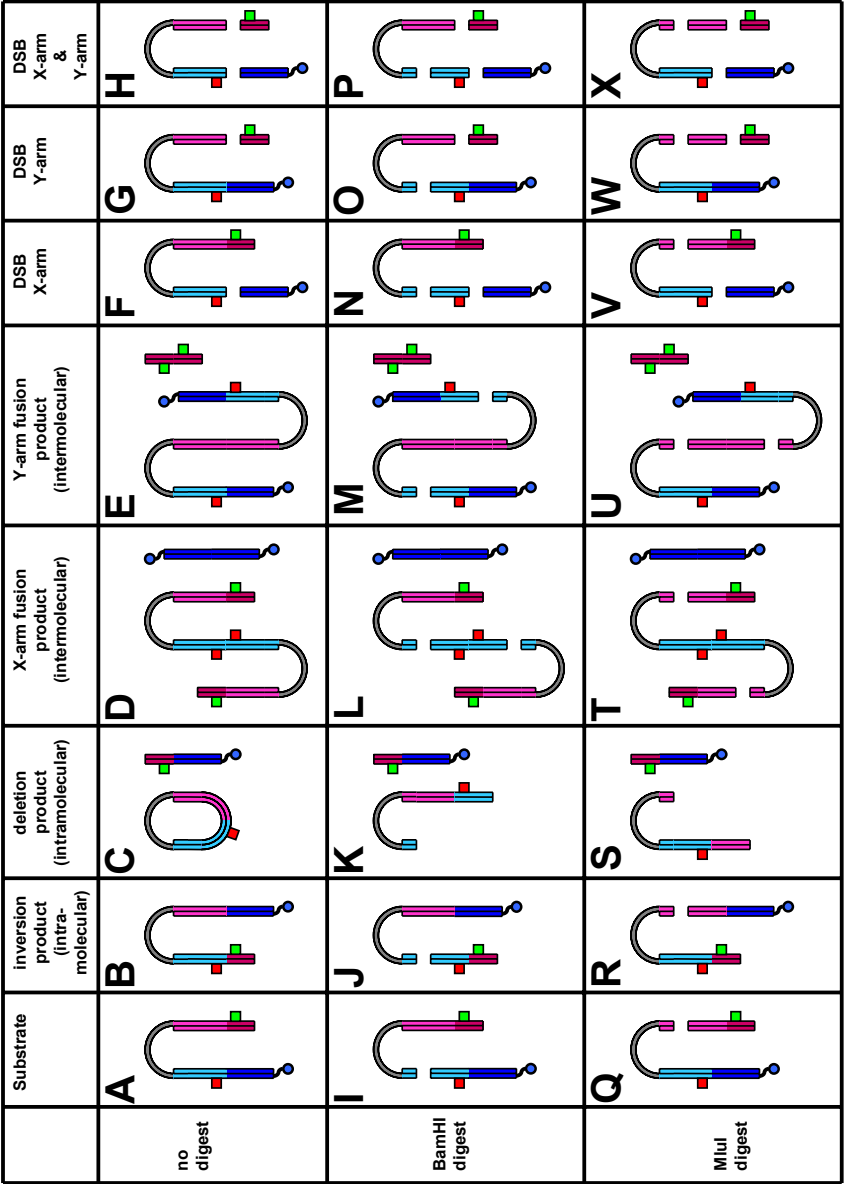


Figure 7.12: Recombination products of the fluorescent U-shaped substrate U3

The fluorescent U-shaped substrate U3 consists of the X-arm (dark and pale blue), with a Cy5 dye (red square) and the Y-arm (dark and pale pink), with a Cy3 dye (green square) at position L6. Both arms are connected by a 30 base single-stranded linker (grey). The recombination of the fluorescent U-shaped substrate U3 can proceed via several different pathways resulting in different products as described in figure 7.6. For each pathway, characteristic DNA fragments are generated by digestion of the products with the restriction endonuclease BamHI or MluI as described in figure 7.6.

	Substrate	inversion product (intra- molecular)	deletion product (intramolecular)	X-arm fusion product (intermolecular)	Y-arm fusion product (intermolecular)	DSB X-arm	DSB Y-arm	DSB X-arm & Y-arm
no digest	A	B	C	D	E	F	G	H
	I	J	K	L	M	N	O	P
	Q	R	S	T	U	V	W	X
BamHI digest	I	J	K	L	M	N	O	P
MluI digest	Q	R	S	T	U	V	W	X

Figure 7.13: Recombination products of the fluorescent U-shaped substrate U3 with high Cy3 fluorescence

This figure lists a selection of the reaction products shown in figure 7.12. Only those reaction products are shown, which contain a Cy3 dye for the detection with a fluorescence imager using a laser and filter setup optimised for Cy3 detection.

	Substrate	inversion product (intra- molecular)	deletion product (intramolecular)	X-arm fusion product (intermolecular)	Y-arm fusion product (intermolecular)	DSB X-arm	DSB Y-arm	DSB X-arm & Y-arm
no digest	A	B	C	D	E	F	G	H
	I	J	K	L	M	N	O	P
	Q	R	S	T	U	V	W	X
BamHI digest								
MluI digest								

Figure 7.14: Recombination products of the fluorescent U-shaped substrate U3 with high Cy5 fluorescence

This figure lists a selection of the reaction products shown in figure 7.12. Only those reaction products are shown, which contain a Cy5 dye for the detection with a fluorescence imager using a laser and filter setup optimised for Cy5 detection.

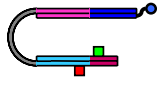

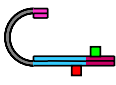
	Substrate	inversion product (intra- molecular)	deletion product (intramolecular)	X-arm fusion product (intermolecular)	Y-arm fusion product (intermolecular)	DSB X-arm	DSB Y-arm	DSB X-arm & Y-arm
no digest	A	B 	C	D	E	F	G	H
	I	J 	K	L	M	N	O	P
BamHI digest								
MluI digest	Q	R 	S	T	U	V	W	X

Figure 7.15: Recombination products of the fluorescent U-shaped substrate U3 with high FRET efficiency

This figure lists a selection of the reaction products shown in figure 7.12. Only those reaction products are shown, which contain a Cy5 dye and a Cy3 dye in close proximity forming a FRET pair with high FRET efficiency. On a gel, these products can be visualised selectively with a fluorescence imager using a laser setup optimised for Cy3 excitation and a filter setup optimised for Cy5 detection.

The laser and filter setups allowed small amounts of crosstalk. For example, strong bands of DNA fragments containing only the Cy5 dye could be visualised as a weak band using the laser and filter setup designed for the detection of fragments containing FRET pairs with high FRET efficiency. However, the different laser and filter setups enabled the characterisation of the DNA fragments in each band by indicating which dyes are present in the DNA fragment.

7.6.1 Results

The products of the recombination of the U-shaped substrates by Tn3 resolvase NM were digested with the endonucleases BamHI or MluI and separated by SDS-PAGE. Selective visualisation of those fragments containing a Cy3 dye (figure 7.16) produced a band pattern similar to the recombination products of the fluorescein labelled U-substrates since the Cy3 dye was located in the same half of the same arm as the fluorescein label previously (figures 7.6 and 7.12). Therefore, when using the Cy3 visualisation, the recombination products of the substrate U3 were identified in the same as the recombination products of the fluorescein labelled substrates. Recombination of the U-shaped substrate U3 resulted in the production of only small quantities of the undesired intramolecular deletion product and only after two hours of incubation with Tn3 resolvase NM. Even less of the product resulting from the intermolecular recombination and fusion of the Y-arm was detected. Only weak bands of the DSB intermediates were found since the samples contained 20 mM magnesium chloride which enhances the ligation efficiency. However, using the selective Cy3 visualisation, only small amounts of the expected intramolecular inversion product were found. This was due to the fact that the inversion product contains a FRET pair with high FRET efficiency and the excited Cy3 fluorophore transferred most of its energy to the Cy5 fluorophore. Therefore, the bands of the inversion product, which were expected in the selective Cy3 visualisation (figure 7.16), were detected more strongly when using the selective visualisation of the Cy5 fluorophore (figure 7.16) and the selective visualisation of fragments containing FRET pairs with high FRET efficiency (figure 7.17).

Using the selective visualisation of the Cy5 fluorescence, a slightly different band pattern emerged (figure 7.16). The bands of fragments resulting from the restriction digestion of the original substrate were identified in the samples without Tn3 resolvase NM. The bands of the digested inversion products were easily identified since they also appear strongly when selectively visualising the fragments containing FRET pairs with high FRET efficiency. Using the selective visualisation of the Cy5 dye, only two weak bands remained to be identified. The intensity of the unidentified band in the BamHI digested sample was

similar to the intensity of the unidentified band in the MluI sample, indicating that both bands contain the same recombination product which differs in length after digestion with different restriction endonucleases. The retardation of the unidentified bands suggests that they contain digested intermediates resulting from a DSB in the X-arm. Most other recombination products could be ruled out since their restriction digest fragments have the wrong size or have the same size as the fragments from other recombination products.

Using the selective visualisation of fragments containing a FRET pair with high FRET efficiency showed mainly the bands of intramolecular inversion products (figure 7.17). However, due to crosstalk, strong bands of fragments containing only Cy5 dyes or only Cy3 dyes produced weak bands when visualising FRET pairs. An overlay of images using different selective visualisations was generated to determine which bands represent fragments with FRET pairs with high FRET efficiency and which bands are artefacts caused by crosstalk. The overlay was generated using the computer program Fireworks (Macromedia). The FRET image, created by visualisation of FRET pairs with high FRET efficiency, was used as the bottom layer of the final image. The Cy3 image, created by selective visualisation of the Cy3 dye, was transformed by conversion into a RGB image followed by the removal of the red and blue channel, leaving only the green channel. The Cy5 image, created by the selective visualisation of the Cy5 dye, was transformed by conversion into a RGB image followed by the removal of the green and blue channel, leaving only the red channel. To produce the final image, the transformed Cy3 image and the transformed Cy5 image were subtracted from the FRET image. The final image showed dark bands for fragments with high FRET efficiency while fragments with only Cy3 dyes were represented as bright, fluorescent green bands and fragments with only Cy5 dyes were represented as bright, fluorescent red bands. It became clear that all bands with high FRET contained inversion products. However, the band of the original substrate U3 appeared to show a high FRET efficiency in some samples. This is in part due to the saturation of the strong band. In addition, the band of the original substrate contained undigested inversion products which have the same retardation on the gel.

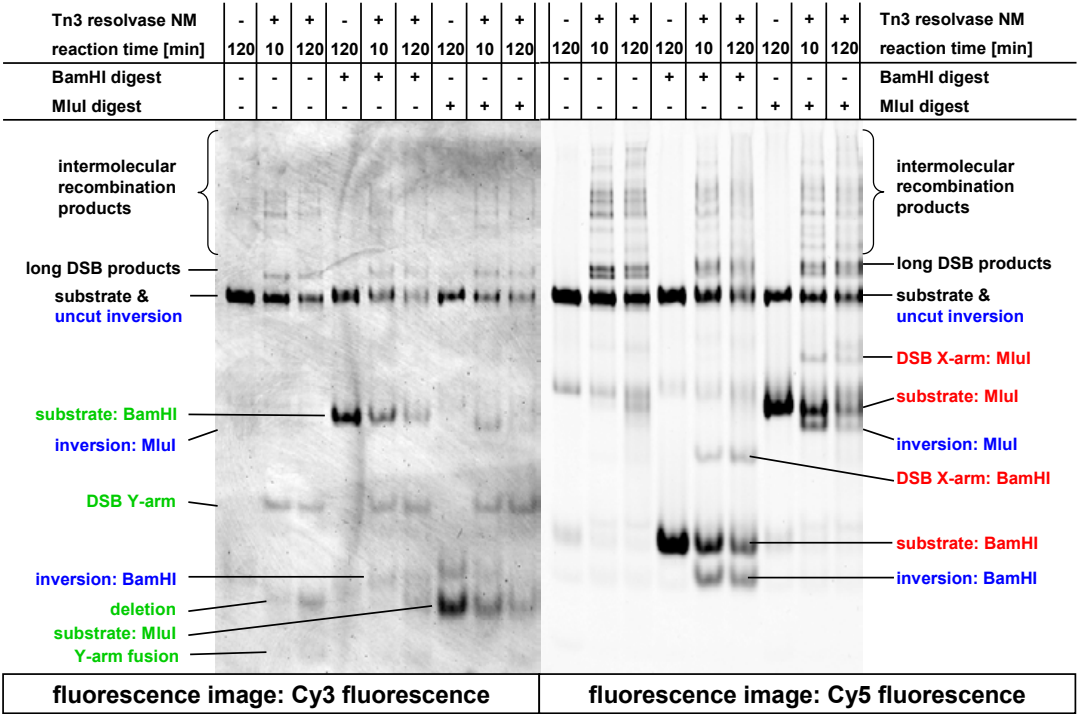


Figure 7.16: SDS-PAGE of recombination products of U-shaped substrates containing a FRET pair: Selective visualisation of the Cy3 dye and of the Cy5 dye.

The U-shaped substrate U3 has a 30 base single-stranded linker and contains a Cy5 dye at position R5 in the X-arm and a Cy3 dye at position L6 in the Y-arm. The substrate U3 was recombined with Tn3 resolvase NM (1.2 μ M) in presence of magnesium chloride (20 mM) for ten minutes or two hours at 20 °C. The reaction products were optionally digested with the restriction endonuclease BamHI. The reaction was then stopped by addition of SDS and the reaction products were separated by SDS-PAGE (8% w/v acrylamide). For a description of the reaction products see figure 7.12-7.15.

The gel images were produced using a fluorescence imager with the laser and filters set up for the selective detection of the Cy3 dye (left image) or the selective detection of the Cy5 dye (right image). When selectively visualising the Cy3 dye, some fragments containing a Cy3 dye produced only weak bands due to the fact the excitation energy is transferred to a close Cy5 dye by FRET. The gel images correspond to a single experiment.

Bands of fragments containing only Cy3 dyes are labelled green, bands of fragments containing only Cy5 are labelled red and bands containing FRET pairs with high FRET efficiency are labelled blue.

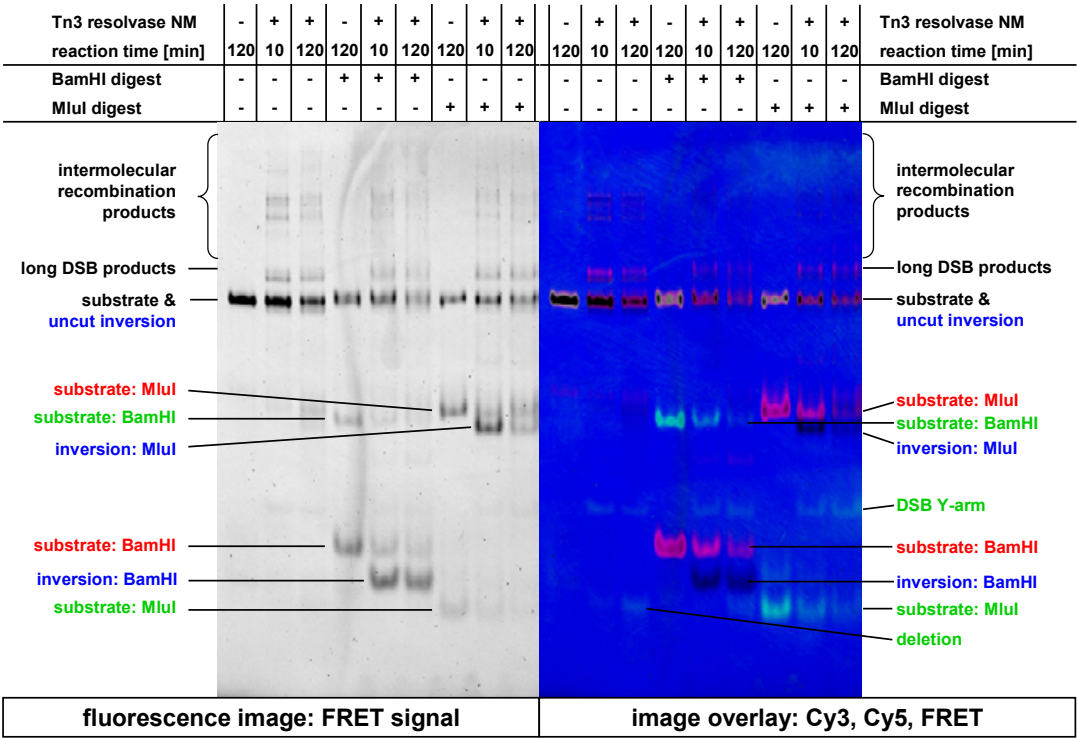


Figure 7.17: SDS-PAGE of recombination products of U-shaped substrates containing a FRET pair: Selective visualisation of FRET pairs with a high FRET efficiency.

The U-shaped substrate U3 has a 30 base single-stranded linker and contains a Cy5 dye at position R5 in the X-arm and a Cy3 dye at position L6 in the Y-arm. The substrate U3 was recombined with Tn3 resolvase NM (1.2 μ M) in presence of magnesium chloride (20 mM) for ten minutes or two hours at 20 °C. The reaction products were optionally digested with the restriction endonuclease BamHI. The reaction was then stopped by addition of SDS and the reaction products were separated by SDS-PAGE (8% w/v acrylamide). For a description of the reaction products see figure 7.12-7.15.

The left gel image was produced using a fluorescence imager with the laser and filters set up for the selective detection of the FRET pairs with a high FRET efficiency. To identify bands caused by crosstalk, an overlay of the selective visualisation of FRET pairs, of the selective visualisation of the Cy3 dye and of the selective visualisation of the Cy5 dye was generated (right image). The overlay image shows dark bands for fragments with high FRET efficiency while fragments with only Cy3 dyes are represented as bright, fluorescent green bands and fragments with only Cy5 dyes are represented as bright, fluorescent red bands. The gel images correspond to a single experiment.

Bands of fragments containing only Cy3 dyes are labelled green, bands of fragments containing only Cy5 are labelled red and bands containing FRET pairs with high FRET efficiency are labelled blue.

7.6.2 Discussion

The Cy dyes within Tn3 *res* site I did not seem to impair the recombination of the U-shaped substrate U3. As observed with fluorescein labelled, U-shaped substrates, the formation of the desired intramolecular inversion product was favoured. The formation of undesired intramolecular deletion products and of intermolecular recombination products proceeded slowly and the bands of these products could were hardly visible on the gel. Using the selective visualisation of different dyes and FRET pairs had shown that the original substrate U3 has a low FRET efficiency while intramolecular recombination could form an inversion product with a high FRET efficiency.

The U-shaped substrate U3 may be useful in future ensemble FRET experiments since it prefers the intramolecular recombination of both arms in one orientation. Using single-site substrates, the recombination of two substrates, each with one dye of a FRET pair, resulted only in a marginal increase in FRET efficiency since the substrates could come together in various combinations and orientations. This problem would be less of an issue using the U-shaped substrate U3.

The U-shaped substrate U3 may be more suitable for single-molecule experiments, since it can be attached to a surface via the biotin label (blue sphere in the figures). It provides two copies of Tn3 *res* site I allowing the attachment of the substrate to the surface followed by the addition of Tn3 resolvase NM in different buffers into the reaction chamber to start the recombination reaction (see figure 7.1). This would allow the observation of active synapses shortly after the start of the reaction and avoids potential problems arising from instable synapses. Single-site substrates do not allow this approach and several limitations of the single-site substrates, as described in chapter 7.1, may be overcome by using the U-shaped substrate U3.

Further, the U-shaped substrates had been shown to favour the recombination of both copies of Tn3 *res* site in parallel orientation producing inversion products. The parallel orientation is required to induce a big change in FRET efficiency during recombination. When synapses are assembled using two copies of Tn3 *res* site I, each with one fluorophore of a FRET pair, the U-shaped substrates provide more control over the orientation of both sites than single-site substrates. In single-molecule experiments, this allows the production of synapses with mainly one configuration, the desired parallel configuration. The interpretation of the single-molecule data was expected to be simpler if most of the observed synapses have only one configuration. However, it has to be

considered that the U-shaped substrates favour recombination of the sites in parallel orientation and that some residual recombination of both sites in anti-parallel orientation may occur.

8 Single-molecule fluorescence experiments with U-shaped substrates

All single-molecule experiments were performed in the laboratory of Prof. David M.J. Lilley FRS at the University of Dundee. I performed the experiments as described in the materials and methods section after training and advice by Prof. David M.J. Lilley FRS, Dr Anne-Cécile Déclais and Dr Jonathan Ouellet.

Ensemble FRET experiments can only show the general progress of the recombination reaction, providing an averaged value for the states of all molecules in the sample. In contrast, single-molecule FRET experiments analyse molecules individually, providing information about the different states molecules can adopt in the sample. The aim of single-molecule FRET experiments was to identify the intermediate states during recombination, especially during strand exchange. The stability of those intermediates could be determined by analysis of the half-life of FRET states in individual molecules. The transitions between those states were of special interest since they provide information about the kinetics of the involved processes. Further, statistical analysis of all recorded transitions may show the order of the reaction steps, which reaction steps occur repeatedly and which steps are irreversible.

8.1 Substrate choice for single-molecule FRET experiments

A library of fluorescent substrates with a FRET pair within Tn3 *res* site I had been developed for the potential use in FRET experiments. Gel based experiments with single-site substrates and U-shaped substrates had shown that the fluorophores can be placed within site I at positions R5 and L6 without major impact on recombination. In ensemble FRET experiments with single-site substrates and gel-based assays with U-shaped substrates, it had been shown that a FRET pair at positions R5 and L6 can provide large FRET changes upon recombination as required for single-molecule experiments,.

In chapter 7.1, the limitations of single-site substrates for ensemble FRET and single-molecule FRET experiments had been discussed. Further gel-based recombination assays with U-shaped substrates had shown that U-shaped substrates promote intramolecular recombination between its two arms, each containing a copy of site I. The intramolecular recombination allows a quicker and simpler approach to single-molecule FRET experiments. The tested U-shaped substrate can readily be attached to the reaction chamber

of the single-molecule setup via the biotin label in the X-arm. After attachment to the surface, different buffers containing Tn3 resolvase NM can be filled into the reaction chamber to start the recombination reaction (see figure 7.1). This would allow the observation of active synapses shortly after the start of the reaction. Further, it avoids potential problems arising from instable synapses since both copies of Tn3 res site I are bound to the surface while the buffer provides resolvase for the reassembly of synapses. Single-site substrates do not allow this approach.

In summary, the U-shaped substrate U3, consisting of a 30 base single-stranded linker, a X-arm with a Cy5 dye at position R5 and a Y-arm with a Cy3 dye at position L6 (figure 7.12) was considered the best candidate for single-molecule FRET experiments. It provides all the advantages over single-site substrates as described above and in chapter 7. In addition, after attachment to the reaction chamber surface, the U-shaped substrate U3 shows a low FRET efficiency in absence of Tn3 resolvase. After the addition of Tn3 resolvase NM, synapses can form bringing both arms into close proximity increasing the FRET efficiency. The increased FRET efficiency of the synapses should help to isolate synapses within a population of free substrates and synapses.

8.2 Conduction of the single molecule experiment

In preparation of the single molecule experiment, the U-shaped substrate U3 was strongly diluted and attached to the quartz surface within the reaction chamber. The attachment was facilitated by coating the quartz surface with biotinylated bovine serum albumin (BSA), binding the protein neutravidin to the biotinylated BSA and finally binding the U-shaped substrate U3 to the neutravidin via the biotin label of the substrate.

The reaction chamber was then flushed with an imaging buffer A which contained no magnesium and no resolvase. Subsequently, single molecule data of the attached U-shaped substrates was recorded for about 45 minutes.

Next, the reaction chamber was flushed with imaging buffer B which contained 0.6 μM Tn3 resolvase NM but no MgCl_2 . In this buffer, Tn3 resolvase NM was expected to form synapses with the U-shaped substrate, to cleave the substrate and perform strand exchange while the ligation of the substrate would be relatively slow. The synapses were expected to be very stable in this buffer since the absence of magnesium slows down synapse reassembly. Single-molecule of the observed substrates was recorded for about 52 minutes.

Finally, the reaction chamber was flushed with imaging buffer C which contained 0.6 μM Tn3 resolvase NM and 20 mM magnesium chloride. Tn3 resolvase was expected to increase the rate of substrate ligation in this buffer and the synapses were expected to be slightly less stable. Single-molecule data of the observed substrates was recorded for about 52 minutes.

8.3 Data acquisition and transformation into hel files

To record single molecule data, the substrates bound to the surface were excited with a green laser which matches the excitation wavelength of the Cy3 fluorophore. The microscope was then focussed on areas of the reaction chamber surface with a high number of attached substrates which appeared as bright spots. However, areas with too high a density of attached substrates were not useful since the fluorescent spots of too many substrate molecules could overlap making the data analysis more complicated. For each suitable surface area, a movie was recorded at different frame rates for 1-3 minutes until photobleaching of the fluorophores occurred. Each frame in the movie file shows two images of the surface side by side. The “green” image shows filtered light which matches the wavelength of the fluorescence emissions of Cy3 (donor). The “red” image shows filtered light matching the wavelength of the fluorescence emissions of Cy5 (acceptor). Therefore, each movie frame consists of an image of the potential Cy3 fluorescence in the observed surface area next to an image of the potential Cy5 fluorescence in the same surface area.

The movie files were then transformed into hel files using a software routine written in IDL by Stephen Chu. This software routine automatically finds bright spots on the surface and matches their position in the “green” and “red” images. Each of these bright spots, often referred to as “molecules” in the following text, might be a fluorescent substrate or a contamination. The hel files contain two intensity values for each detected molecule on the surface at each frame within the recording time of the movie. One intensity value is the intensity of the molecule in the green image; the other intensity value is the intensity of the molecule in the red image. Therefore, the hel files contain the green and red intensity of each molecule over the recording time. Depending on the nature of the molecule, the green and red intensities can correspond to the Cy3 and Cy5 fluorescence of the molecule. The green intensity is therefore referred to as the donor intensity, I_D , and the red intensity is referred to as the acceptor intensity, I_A . The plots of the donor and acceptor intensities versus the recording time are referred to as traces.

In addition, the software routinely generates a picture of the combined red and green images averaged over the complete recording time. The hel files contain the location of the molecule in this image. This allows the quick matching of the trace of each molecule to the corresponding bright spot in the generated image for reference.

8.4 Results

8.4.1 Analysis of single-molecule traces

The hel files were analysed with the software routine UniCon, which runs within the MatLab program (The MathWorks Inc.) and was written by T. Ha, J. Ouellet and C. Penedo in MatLab. UniCon was used to generate plots, referred to as traces, of the donor and acceptor intensities versus the recording time. UniCon was also used to calculate plots of the total intensity, the sum of the donor and acceptor intensity, versus the recording time. Further, UniCon could calculate the apparent FRET efficiency, E_{app} , of the molecule from the donor intensity, I_A , and the acceptor intensity, I_D , according to equation 8.1 (Roy *et al.* 2008). The apparent FRET efficiency was then plotted versus the recording time, producing FRET traces.

$$E_{app} = \frac{I_A}{I_A + I_D} \quad 8.1$$

Analysis of the hel files showed that some of the automatically identified molecules were potentially complete fluorescent substrates with a single FRET pair while other molecules were damaged or incomplete substrates or simply fluorescent contaminations.

Complete substrates containing one functional Cy3 and one functional Cy5 dye show both donor and acceptor intensity. Since both dyes are located within one substrate, their separation is limited resulting in an apparent FRET efficiency above zero. This means the acceptor intensity does not drop to the baseline value unless photobleaching occurs (figure 8.1). Photobleaching is the irreversible inactivation of a fluorophore in the intense light of the laser in the single-molecule setup.

The baseline value of the acceptor and donor intensity can easily be identified towards the end of suitable traces when photobleaching of the Cy3 occurs in a complete molecule, rendering the particular dye non-fluorescent. Photobleaching of the Cy3 dye results in the drop of both donor and acceptor intensity to the baseline since the Cy5 dye can only be excited by energy transfer from the Cy3 dye (figure 8.1A). When the Cy5 dye bleaches, the detected Cy5 intensity drops nearly, but not completely, to the baseline. This is due to the crosstalk between both channels which results in the detection of residual acceptor intensity if the acceptor is bleached while the donor intensity is high (figure 8.1B/C). Commonly, the donor intensity baseline was around -40 to 0 (arbitrary units) and the acceptor intensity baseline was around 0 to 25 (arbitrary units).

If the dyes within the substrate are far apart, the donor intensity is high and the acceptor intensity is low resulting in a low apparent FRET efficiency (figure 8.4). If the dyes within the substrate come into closer proximity, for example in synapses or due to recombination, the acceptor fluorescence is high and the donor fluorescence is low, resulting in a high apparent FRET efficiency. When the FRET efficiency changes, the total intensity stays nearly stable since the total intensity depends only on the amount of energy absorbed by the Cy3 dye. However, at high FRET efficiencies (>0.5), the molecules can show a slightly elevated total intensity due to the properties of the single-molecule setup.

The traces of fluorescent contaminations, of incomplete substrates with only one dye or bleached dyes or of multiple substrates located at the same spot are unsuitable for the interpretation of the biological system of interest. Such traces can be identified by several characteristic properties.

The simplest way to identify unsuitable traces is to check the total intensity of the trace. If the total intensity is much more than twice the total intensity in most other traces, it is likely that multiple more than two fluorophores are present. Multiple stable levels of the total intensity also indicate that more than two fluorophores are present (figure 8.3A/C). Further, very noisy, “spiky” total intensities indicate that fluorescent contamination diffuse through the location of the observed molecule. Noisy traces can also be caused by diffusing contaminations quenching the fluorescence of Cy dyes. A gradual decrease of the total intensity also indicates that the observed molecule is a fluorescent contamination since Cy dyes bleach quickly resulting in an immediate intensity decrease. Finally, the total intensity should change only slightly when the FRET efficiency changes, since the total intensity depends only on the amount of energy absorbed by the Cy3 dye (figure 8.4).

Unsuitable traces can also be identified analysing the donor and acceptor intensities. If the donor or acceptor intensity does not immediately return to the baseline after bleaching of the Cy3 dye, it is likely that a slowly bleaching fluorescent contamination is located at the same spot as the observed molecule (figure 8.3A/B).

The donor and acceptor intensity are correlated in complete molecules with a single FRET pair consisting of a Cy3 and a Cy5 dye. This means, in complete molecules, a decrease in the acceptor intensity coincides with an increase in the donor intensity and vice versa until photobleaching occurs (figure 8.4). This is due to the fact that a fixed amount of energy is absorbed by the Cy3 dye and then emitted as Cy3 fluorescence or as Cy5 fluorescence after FRET occurs. Therefore, independent changes of the donor or acceptor intensity

indicate that a fluorescent contamination diffused into the location of the observed molecule (figure 8.3C). The presence of more than two Cy dyes can also result in independent changes of the donor or acceptor intensity.

Molecules without a Cy5 dye or with a non-fluorescent Cy5 dye cannot support FRET and are therefore unsuitable for interpretation. As discussed above, U-shaped substrates containing one Cy3 dye and one Cy5 have an apparent FRET efficiency above zero and therefore an acceptor intensity above baseline. However, crosstalk between the channels results in residual acceptor intensity if the donor intensity is high (figure 8.1B/C).

Therefore, molecules with an acceptor intensity slightly above baseline may not contain a Cy5 dye. The apparent FRET efficiency can be used to determine if the low acceptor intensity is purely due to crosstalk. If the apparent FRET efficiency is below 0.15, the residual acceptor intensity is likely to be caused by crosstalk. The separation of the FRET pair is limited in the U-shaped substrates and the apparent FRET efficiency is not expected to drop below 0.15. In the U-shaped substrates with a FRET efficiency below 0.15. In most cases, complete molecules with an apparent FRET efficiency below 0.15 and incomplete molecules cannot be distinguished efficiently and should not be considered for interpretation. The classification of molecules with low FRET efficiency is simpler when detectable photobleaching of the Cy5 dye occurs (figure 8.1C). The photobleaching of Cy5 results in a further small drop of the already low acceptor intensity indicating that the molecule initially contained a functional Cy5 dye.

After the identification of traces suitable for the interpretation in context of recombination, it became clear that the collected traces were characteristic for the different conditions during the recording of the data. In the absence of Tn3 resolvase NM and $MgCl_2$, nearly all suitable traces showed an apparent FRET efficiency between 0.2 and 0.3 similar to the trace in figure 8.1C. No major transitions between stable FRET efficiency levels, referred to as FRET states, were observed. This suggests that the apparent FRET efficiency of the free U-shaped substrate was around 0.2 to 0.3. In addition, the substrate alone does not appear to have multiple, stable conformations with different FRET efficiencies. This makes the further interpretation much simpler.

After the addition of Tn3 resolvase NM in the absence of $MgCl_2$, the appearance of the traces changes drastically. Much higher apparent FRET efficiencies (0.5-0.9) were observed, suggesting that the FRET pair in the two arms of the U-shaped substrate was brought into close proximity by synapse formation or recombination. Multiple transitions between different FRET states were found in the traces (figure 8.1A, 8.4A-C), suggesting

that processes like binding of Tn3 resolvase, synapse formation or recombination were taking place.

In the presence of Tn3 resolvase NM and MgCl_2 , the traces were similar to those observed after the addition of Tn3 resolvase NM in absence of MgCl_2 . This indicates that, after the addition of Tn3 resolvase NM, the processes in the sample are similar in the presence and absence of MgCl_2 .

The transitions between FRET states observed in samples with Tn3 resolvase did not occur at fixed rates. The lifetime of the FRET states was found to take any value between one minute and less than a second. Some traces seemed to show transitions that could hardly be resolved at the maximum frame rate used in this experiment (50 ms/frame). To test if there were faster transitions, a confocal single-molecule FRET setup would need to be employed since it has a higher time resolution. There were not enough transitions to calculate the rates of the transitions.

However, there were enough traces to perform a statistical analysis of the observed FRET states which may provide further insight into the processes in the different samples.

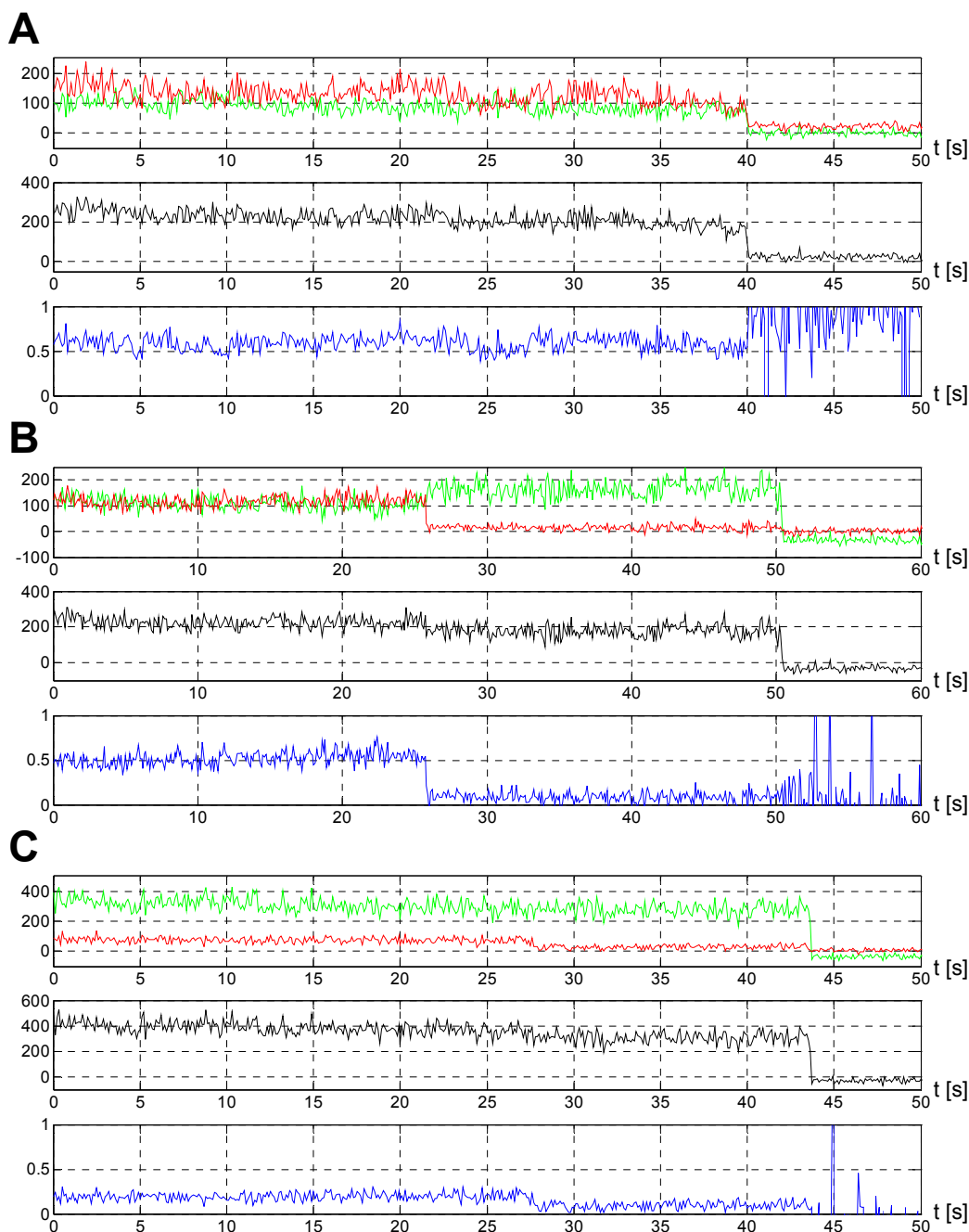


Figure 8.1: Traces of molecules showing photobleaching

The traces of molecules include plots of the donor intensity (green), acceptor intensity (red) and total intensity (black) in arbitrary units versus the recording time in seconds. The FRET traces (blue) plot the apparent FRET efficiency versus the recording time in seconds.

The Cy3 dye (donor) and especially the Cy5 dye (acceptor) dyes can photobleach when exposed to the intense laser light in the single-molecule FRET setup. **(A)** Bleaching of the Cy3 dye immediately decreases the donor and acceptor intensities to the baseline. **(B)** Bleaching of the Cy5 dye causes an immediate decrease of the acceptor intensity to the baseline while the donor intensity increases, keeping the total intensity nearly stable. However, the high donor intensity results in a slightly increased acceptor intensity due to crosstalk between the channels. Towards the end of the recording time, the Cy3 dye bleaches, causing the donor and acceptor intensities to drop to the absolute baseline. **(C)** After bleaching of the Cy5 in molecules with low FRET efficiency, the drop of the acceptor fluorescence is small but indicates that a Cy5 dye was initially present in the molecule.

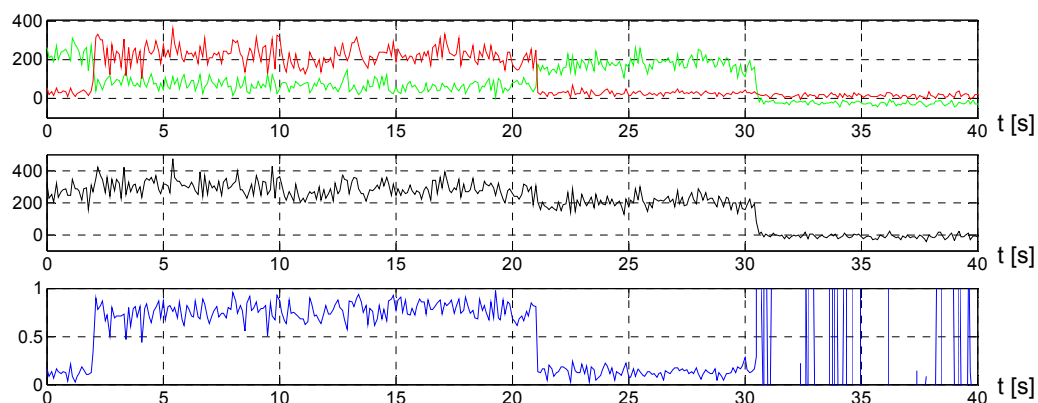


Figure 8.2: Traces of molecules showing blinking

The traces of molecules include plots of the donor intensity (green), acceptor intensity (red) and total intensity (black) in arbitrary units versus the recording time in seconds. The FRET traces (blue) plot the apparent FRET efficiency versus the recording time in seconds.

Blinking of the Cy5 dye (acceptor) describes the reversible transition of the Cy5 dye into a non-fluorescent state. In this example, the acceptor intensity was close to the baseline level at the beginning of the recording time. At the same time the donor intensity was high. This indicates that the Cy5 dye was in a non-fluorescent state. After about two seconds the Cy5 fluorophore is reactivated and the molecule shows a high FRET efficiency. However, after about 21 seconds, the Cy5 dye photobleaches, followed by the Cy3 dye after about 31 seconds.

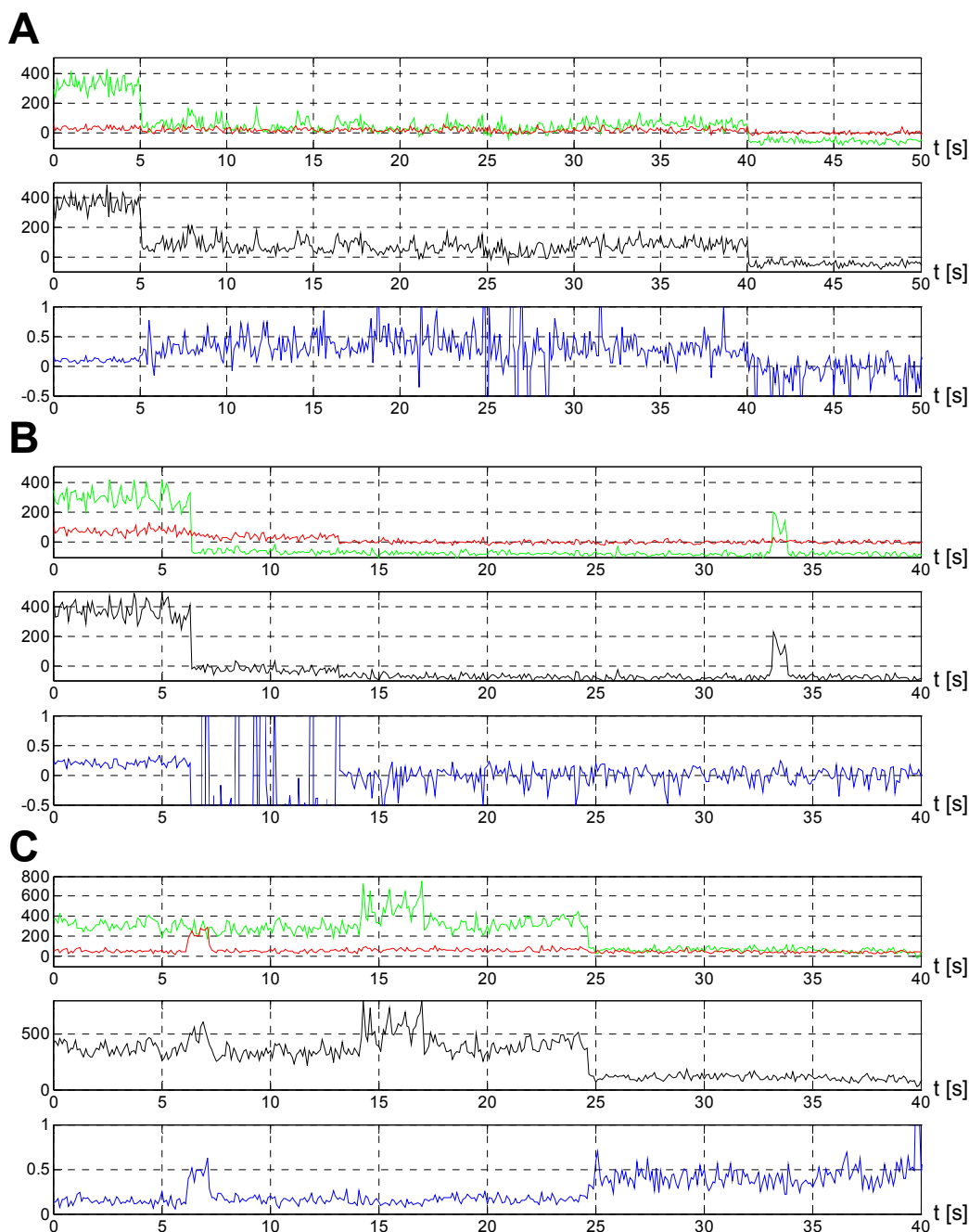


Figure 8.3: Traces of molecules unsuitable for data analysis

The traces of molecules include plots of the donor intensity (green), acceptor intensity (red) and total intensity (black) in arbitrary units versus the recording time in seconds. The FRET traces (blue) plot the apparent FRET efficiency versus the recording time in seconds.

(A) In this example, the donor intensity drops to a level above the baseline value at 5 seconds and then to the baseline level after 40 seconds. This indicates that, apart from a Cy3 dye, a fluorescent contamination was observed which disappears after 40 seconds. **(B)** The donor intensity drops to the baseline after ~7 seconds indicating photobleaching of the Cy3 dye. However, the Cy5 fluorescence does not drop to the baseline level until 13 seconds, indicating a fluorescent contamination. **(C)** In this molecule, the acceptor intensity increased between 6 and 7 seconds without a correlated decrease of the donor intensity. In a molecule with a FRET pair, a strongly increased acceptor intensity always coincides with a decrease of the donor intensity. Therefore, a fluorescent contamination is detected from 6 to 7 seconds in this example. Further, donor intensity levels indicate the presence of more contaminations or of multiple Cy3 dyes.

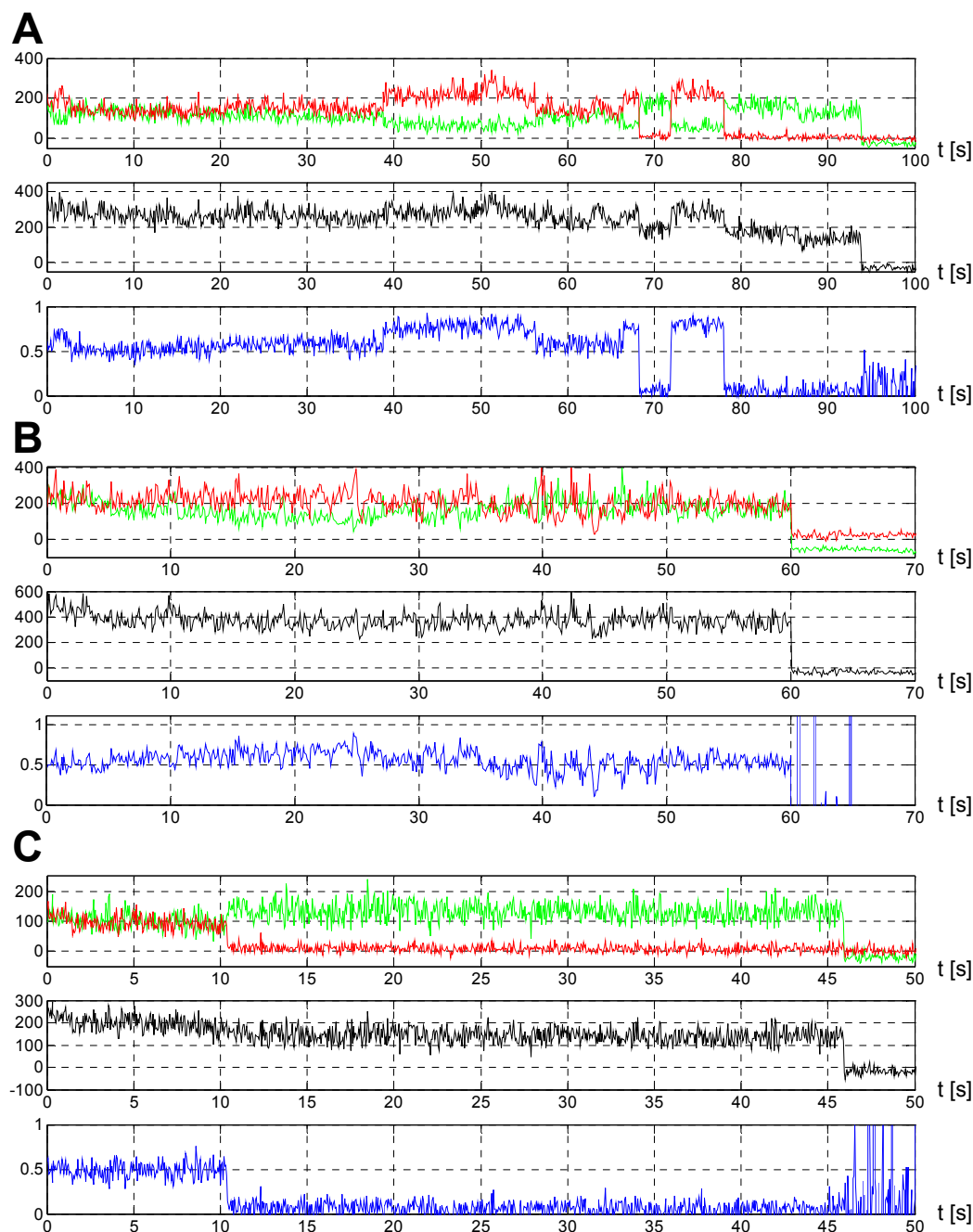


Figure 8.4: Traces of potential U-shaped substrates showing transitions between FRET states

The traces of molecules include plots of the donor intensity (green), acceptor intensity (red) and total intensity (black) in arbitrary units versus the recording time in seconds. The FRET traces (blue) plot the apparent FRET efficiency versus the recording time in seconds. The examples were recorded (**A&B**) in absence of MgCl_2 and (**C**) in presence of MgCl_2 during a single experiment.

In molecules containing a single FRET pair, any changes in the donor and acceptor intensity are correlated keeping the total intensity roughly stable until photobleaching occurs.

(A) In this example, the FRET efficiency switches between intermediate and high levels until about 68 seconds. At 68 seconds the acceptor intensity reversibly drops to the baseline, indicating blinking of the Cy5 dye. At 78 seconds, bleaching of the Cy5 dye occurs, followed by bleaching of the Cy3 dye at 94 seconds. **(B)** In this molecule, the FRET efficiency changes quickly between intermediate levels until photobleaching of the Cy3 dye occurs at 60 seconds. **(C)** The traces of this molecule were recorded at a high rate of 50 ms per frame. However, the quick FRET efficiency changes until 10 seconds are nearly too quick to be resolved. Any quicker FRET efficiency changes cannot be observed with the settings used in this experiment.

8.4.2 Filtering of traces and statistical analysis of the observed FRET states

The traces of the U-shaped substrate showed different FRET states depending on the conditions in the studied sample. Before the frequency of certain FRET states in the traces of identified molecules can be calculated, any unsuitable traces need to be removed.

Unsuitable traces can be identified as described in chapter 8.4.1. The MatLab based software routine UniCon, written by T. Ha, J. Ouellet and C. Penedo, was used to visualise the traces in each hel file and to remove unsuitable traces automatically or manually.

UniCon can automatically identify and remove traces with a total intensity above a chosen limit. This removes traces of highly fluorescent contaminations or of molecules with more than two dyes. Further, UniCon can identify and remove traces with an acceptor intensity below a chosen limit. This removes some of the traces of molecules without a Cy5 dye or with a damaged Cy5 dye. However, UniCon considers only the first ten frames (timepoints) of each trace to identify and remove unsuitable traces. Therefore, UniCon may remove traces due to a low acceptor intensity in the first ten frames even though the acceptor intensity increases in the later frames. This made it necessary to manually keep traces which were falsely removed by UniCon during the automatic filtering. Table 8.1 shows the number of traces in the hel files of each sample before and after the automatic filtering process.

After the removal of large numbers of traces by automatic filtering, more unsuitable traces were removed manually. For this purpose, the traces were visualised using UniCon and unsuitable traces were identified and removed according to the criteria described in chapter 8.4.1. In addition, traces of molecules which overlapped with other molecules on the reaction chamber surface were removed. This was possible since the hel files contain for each trace the location of the corresponding molecule in an image of the observed surface area (see chapter 8.3). The manual filtering was performed in several steps with increasingly strict requirements for suitable traces. The number of traces in each hel file before and after manual filtering is shown in table 8.1.

Automatic filtering removed about 2/3 of all traces while only about 10% of all traces remained after the last manual filtering step. The removal of about 90% of all traces is common (personal communication with J. Ouellet) and much care was taken to avoid biased filtering. “Interesting” traces were filtered according to the same criteria in the strict manual filtering steps to avoid favouring of traces with expected or desired properties.

automatic filter: maximum total intensity				-	500	500	500
automatic filter: minimum Cy5 intensity				-	30	30	30
manual filter: dead Cy5				-	-	+	+
manual filter: unsuitable traces				-	-	+	+
manual filter: overlapping molecules				-	-	+	+
manual filter: remaining overlaps (strict)				-	-	-	+
manual filter: remaining unsuitable traces (strict)				-	-	-	+
file	t/f [sec]	Tn3R NM	MgCl2	n	n	n	n
hel7	0.1	-	-	342	222	40	39
hel8	0.1	-	-	330	224	28	27
hel10	0.1	-	-	307	264	32	29
hel11	0.05	-	-	171	140	26	25
hel13	0.05	-	-	281	190	22	21
hel14	0.02	-	-	119	87	9	9
hel16	0.1	+	-	201	127	14	13
hel17	0.1	+	-	178	131	23	17
hel18	0.1	+	-	158	113	13	8
hel19	0.1	+	-	157	123	14	10
hel21	0.02	+	-	103	62	11	5
hel22	0.1	+	-	210	163	23	18
hel23	0.1	+	-	189	115	15	14
hel24	0.1	+	-	148	97	19	11
hel26	0.1	+	-	121	97	11	5
hel27	0.02	+	-	102	79	15	12
hel29	0.02	+	-	117	77	16	9
hel30	0.02	+	-	141	90	20	16
hel31	0.02	+	-	136	83	18	14
hel32	0.1	+	-	122	85	9	5
hel33	0.1	+	-	130	98	13	8
hel34	0.1	+	-	101	74	13	9
hel35	0.1	+	+	177	139	35	30
hel36	0.1	+	+	149	129	25	19
hel39	0.1	+	+	149	112	26	18
hel40	0.1	+	+	124	108	18	10
hel41	0.05	+	+	102	79	14	9
hel42	0.05	+	+	118	80	20	10
hel43	0.05	+	+	126	109	22	18
hel44	0.05	+	+	137	106	18	16
hel46	0.05	+	+	120	83	14	12
hel48	0.05	+	+	233	160	28	23
hel49	0.05	+	+	232	153	25	22
hel50	0.05	+	+	205	135	29	24
hel51	0.05	+	+	275	171	20	16
hel52	0.05	+	+	215	142	18	17
hel53	0.05	+	+	175	116	22	17
hel57	0.1	+	+	163	113	15	15
sum	all	-	-	1550	1127	157	150
sum	all	+	-	2314	1614	247	174
sum	all	+	+	2700	1935	349	276
sum	all samples			6564	4676	753	600

Table 8.1: Number (n) of single-molecule FRET traces of substrate U3 before and after filtering.

After each filtering step, all traces of each sample were analysed statistically. For this purpose, all traces in all hel files of one sample were merged into one hel file using UniCon after each filtering step. Subsequently, the average apparent FRET efficiency in the first ten frames (time points) was calculated for each trace. This average apparent FRET efficiency will be referred to as “initial FRET efficiency” in the following text. A histogram of all traces of each sample was prepared showing the number of traces (or molecules) with a particular initial FRET efficiency observed in the sample (figure 8.5A).

The distribution of the initial FRET efficiency seemed similar in all samples before filtering. After filtering, it emerged that the samples without Tn3 resolvase NM and MgCl_2 contained only molecules with an initial FRET efficiency between 0.15 and 0.3. In contrast, the samples with Tn3 resolvase NM contained molecules with initial FRET efficiencies up to 0.85-0.9.

As described in chapter 8.4.1, this suggests that the free U-shaped substrate had a basic apparent FRET efficiency of about 0.15 to 0.3. The addition of Tn3 resolvase allowed the formation of molecules with higher FRET efficiency. The increased FRET efficiency shows that the Cy5 in the X-arm and the Cy3 dye in the Y-arm of the substrate could come into closer proximity in the presence of Tn3 resolvase NM. This may be due to the formation of synapses or due to the recombination of the arms in parallel orientation.

Both samples with Tn3 resolvase contained molecules with a slightly increased initial FRET efficiency of up to 0.35-0.4, forming a tail from the main peak in the histogram (after strict filtering). This increase may be due to the binding of Tn3 resolvase NM to its sites, changing the local environment of the dyes providing an only slightly increased FRET efficiency.

Furthermore, both samples contained molecules with an initial FRET efficiency between 0.55 and 0.9. Tn3 resolvase NM can form synapses and perform recombination in absence and presence of MgCl_2 . Therefore, the molecules with a FRET efficiency between 0.55 and 0.9 are likely to be the synapses of the U-shaped substrate in the recombinant or non-recombinant state.

However, the histograms show a difference between the sample with Tn3 resolvase NM in absence of MgCl_2 and the sample with Tn3 resolvase NM in presence of MgCl_2 . The sample without MgCl_2 contained molecules with an intermediate initial FRET efficiency between 0.4 and 0.55. Only very few molecules in the sample with MgCl_2 had an initial

FRET efficiency between 0.4 and 0.55. This suggests that the U-shaped substrate forms synapses with a distinct configuration in the absence of MgCl_2 . One explanation for these synapses with a distinct configuration is that the substrate is observed at an intermediate stage of strand exchange which has a slightly lower FRET efficiency than the finished recombinant or non-recombinant products. The synapses with the distinct FRET efficiency are less abundant in the presence of MgCl_2 , probably because Tn3 resolvase shows a higher rate of ligation in the presence of MgCl_2 fixing the U-shaped substrate in the ligated recombinant or non-recombinant state for most of the time. An alternative explanation is that the synapses, in the recombinant and non-recombinant state, adopt a different conformation in the absence of MgCl_2 . This conformation could be similar to the one seen in the crystal structure of the $\gamma\delta$ resolvase site I synapse (Li *et al.* 2005), showing a large gap between the scissile phosphates of site I in the unligated state. A further, less likely explanation is that Tn3 resolvase might prefer the inversion reaction less strongly in the absence of MgCl_2 compared to the strong preference in the presence of magnesium. Therefore, more synapses with both arms anti-parallel orientation might be formed in the absence of MgCl_2 . This explanation could be ruled or confirmed out using a gel-based assay for the recombination of U-shaped substrates in the absence of MgCl_2 .

After the analysis of the histograms of the initial apparent FRET efficiency (figure 8.5A), slightly different histograms were generated. Each trace can contain several stable FRET states since transitions can occur between different FRET states (or FRET levels). The apparent FRET efficiency of every FRET state found in each trace was determined by eye. A list of all found FRET states was created for each sample. Using this list, histograms of all identified FRET states were generated similar to the histograms of the initial apparent FRET efficiency (figure 8.5B). The number (or count) of FRET states in the new histograms was higher than the number of molecules in the histograms of the initial apparent FRET efficiency since each molecule can adopt several FRET states. The new histograms showed that the identified FRET states have the same distribution as the initial apparent FRET efficiency of the molecules. However, the histograms of all FRET states also showed an increased occurrence of apparent FRET efficiencies below 0.15. This is due to the fact that many molecules with a higher initial apparent FRET efficiency photobleach within the recording time. When photobleaching of the Cy3 dye occurred, the apparent FRET efficiency was chosen to be zero. The apparent FRET efficiency of the bleached state is not included in the histograms of the initial apparent FRET efficiency but is considered in the new histograms of all FRET states.

The comparison of the histograms of the initial apparent FRET efficiency and the histograms of all FRET states confirmed that the FRET states could be identified by eye with sufficient accuracy. Further, it confirmed that the distribution of the initial FRET efficiencies (in the first ten frames of each trace) is representative of the distribution of all FRET states found in the complete FRET traces.

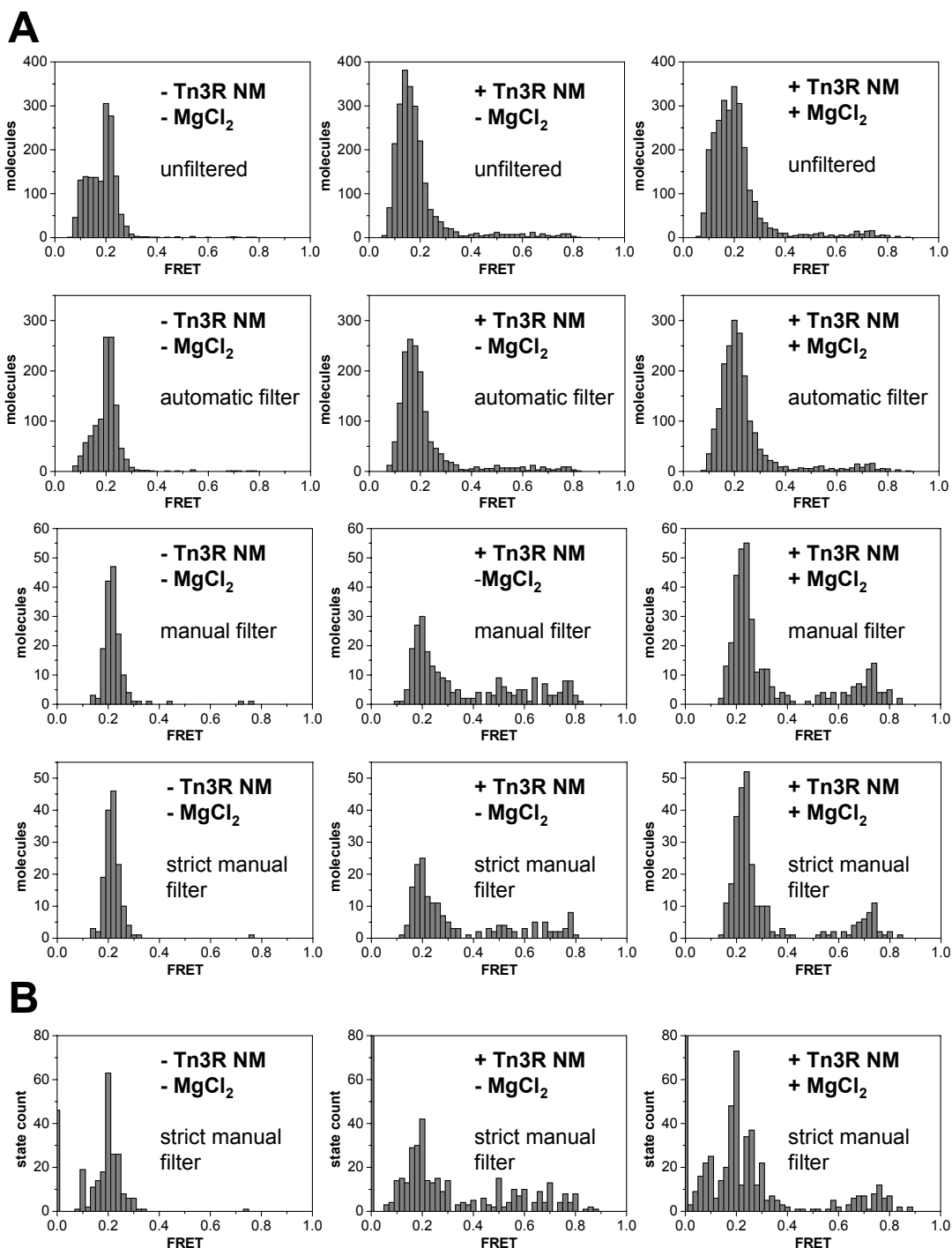


Figure 8.5: FRET Histograms of single-molecule traces of the substrate U3 before and after filtering.

The single-molecule FRET traces of U3 substrates in presence and absence of Tn3R NM and magnesium chloride were filtered by automatic and manual methods (see table 8.1). **(A)** The average FRET value in the first ten frames was calculated for each of each trace and summarised in FRET histograms. The FRET histograms show the distribution of the initial FRET states within the whole population of molecules. **(B)** After strict filtering, all FRET states in each single-molecule FRET trace were identified by eye. The FRET histograms show the distribution of FRET states within the population of molecules over the whole duration of the FRET traces.

All data was collected during a single experiment.

8.4.3 Analysis of the transitions between FRET states

During the preparation of the histograms of FRET states (figure 8.5B), all FRET states in each trace were identified by eye and added to a list of all FRET states found in the traces of one sample. However, this list contained not only the apparent FRET efficiency of each identified FRET state. Some FRET states were followed by a second, different FRET state in the trace. The list of FRET states contained the apparent FRET efficiency the originally identified FRET state (FRET state 1) and, if a second FRET state followed, of the following FRET state (FRET state 2). All pairs of FRET state1 and FRET state 2 were extracted into a new list, the list of FRET transitions. Therefore the new list contained all transitions from one FRET state to another which were observed for the molecules in a sample.

To access the information in the lists of the FRET transitions, the lists were transformed into matrices using the program OriginPro (OriginLab Corporation). Subsequently, the matrices were used to generate two-dimensional histograms (2D-histograms) (figures 8.. The X-axis of the 2D-histograms shows the apparent FRET efficiency of the FRET state 1 while the Y-axis shows the apparent FRET efficiency of the FRET state 2. Each FRET state transition falls into a field in the graph area, depending on the combination of the apparent FRET efficiencies of FRET state 1 and FRET state 2. Every field measures 0.5 apparent FRET efficiency units in the direction of the X-axis and in the direction of the Y-axis. The colour of each field indicates how transitions fall within the field's limits for FRET state 1 and for FRET state 2. Therefore, the 2D-histograms provide a good visual representation of the frequency of different FRET state transitions in the molecules of a sample.

Initially, 2D-histograms were generated using a linear colour representation for the frequency of (i.e. number of) the FRET transitions (figure 8.6A/C/E). White indicated a frequency of zero, black represented the maximum frequency and shades of grey represented the values between zero and the maximum. However, it became clear that this linear representation was unsuitable for the visualisation of FRET transitions with low frequencies. Most FRET transitions describe photobleaching events and the high number of these events resulted in a weak representation of the biologically relevant transitions. Therefore, a linear grey-scale representation with a bin size of 1 was chosen for frequencies below 6 while a colour representation with a larger bin size was used for frequencies ≥ 6 (figure 8.6B/D/F and figure 8.7A/C/E).

It became clear that the frequencies of certain FRET transitions differed greatly between the samples with and without Tn3 resolvase NM and samples with and without MgCl_2 . To allow the description of different FRET transitions or classes of transitions which span several areas in the 2D-histograms, areas of interest were marked with coloured rectangles (figure 8.7B/D/E). The sum of the frequencies of all transitions which fall into an area, marked with a rectangle, is given in table 8.2.

A large number of transitions described photobleaching events. These transitions were marked with a blue rectangle and are located at the bottom of the 2D-histograms since they resulted in a apparent FRET efficiency of FRET state 2 below 0.15-0.2. Similarly, blinking of Cy5 results in an apparent FRET efficiency below 0.15-0.2 and these events are also represented at the bottom of the 2D-histograms. Since blinking is reversible, many transitions from FRET state 1, with an apparent FRET efficiency below 0.15-0.2, to FRET state 2, with any apparent FRET efficiency, were observed. These transitions can be found at the left side of the histograms and were also marked with a blue rectangle. The photobleaching and blinking events have no relevance for the biological system and are therefore not discussed in context of the recombination of the U-shaped substrate.

A 45 ° diagonal across the plot area (black rectangle in figure 8.7B/D/F) covered transitions between nearly identical FRET states. These transitions may be due slight fluctuations in the detection system and may or may not have biological relevance. In fact, very few transitions were covered by this diagonal area because it is hard to identify transitions between two similar states by eye due to the noise in the traces.

After identifying the biologically irrelevant transitions, it became no biologically relevant transitions were found in the sample without Tn3 resolvase NM. This makes it easier to interpret FRET transitions of the U-shaped substrate in presence of Tn3 resolvase, since all biologically relevant transitions were due to the effect of Tn3 resolvase NM.

In the presence of Tn3 resolvase and MgCl_2 , the U-shaped substrate showed nearly exclusively transitions between states with a high or very high apparent FRET efficiency and medium/high FRET efficiency. Particularly the transition between FRET states with an apparent FRET efficiency of 0.75-0.85 and FRET states with an apparent FRET efficiency of 0.55-0.7 (red rectangle) had a high frequency (table 8.2). The frequencies also show that this transition was reversible since it occurred in both directions. This FRET state transition describes changes in the U-shaped substrate which moves the dyes from relatively close proximity towards the closest proximity observed during the whole

experiment. Interestingly, this transition had a much lower frequency in the absence of MgCl_2 . Therefore it is likely that this transition describes a conformational change related to the process of the ligation, which proceeds at much higher rates in the presence of MgCl_2 . The conformational change could be the closing and opening of the gap between the scissile phosphates of site I seen in the crystal structure of the active site I synapse of $\gamma\delta$ resolvase (Li *et al.* 2005). In the case of recombinant inversion products, ligation could bring relatively close fluorophores into very close proximity resulting in the change from high to very high FRET efficiency.

In the presence of magnesium, nearly no FRET states with a medium apparent FRET efficiency were observed (0.4-0.55, see chapter 8.4.2) and none of the observed FRET state transitions involved FRET states with a medium apparent FRET efficiency. However, there are two major versions of the U-shaped substrate present in the population. One version is the original U-shaped substrate which has a low FRET efficiency when it is not synapsed. The other version is the inversion product which contains the FRET pair within one arm resulting in a high FRET efficiency even when it is not synapsed. The question is if both versions have a high FRET efficiency in the synapsed state accounting for the FRET states with high apparent FRET efficiency observed in the presence of MgCl_2 . Otherwise, synapses of the original, non-recombinant U-shaped substrate may account for the observed FRET states with a low/medium (0.3-0.4) apparent FRET efficiency. However, the latter case does not explain the fact that no transitions between the FRET states with low/medium FRET apparent efficiency (corresponding to the inversion reaction) were observed in the presence of MgCl_2 unless strand exchange events are very rare in the presence of MgCl_2 . This might be true, since the substrates might spend most of the time in the ligated state and because the number of observed FRET state transitions was too low to detect rare events. Therefore it is unclear if the original, non-recombinant substrate has an apparent FRET efficiency of 0.3-0.4 or of 0.55-0.85. A control single-molecule FRET experiment using an inactive version of Tn3 resolvase NM, the resolvase mutant NM-S10A could solve this problem since Tn3 resolvase NM can form synapses without cleaving or recombining the substrate.

In samples with Tn3 resolvase NM in the absence of MgCl_2 , the transition between FRET states with a very high apparent FRET efficiency (0.75-0.85) and medium/high FRET efficiency (0.55-0.67) was far less frequent than in samples with MgCl_2 (table 8.2). However, the smaller transition between two FRET states with a medium/high and a high apparent FRET efficiency (0.55-0.65 to 0.65-0.75, purple rectangle) was more common in samples without MgCl_2 than in samples with MgCl_2 . Further transitions were found in the

sample with Tn3 resolvase in absence of MgCl_2 while these transitions were nearly completely absent in the samples with MgCl_2 . These transitions included the transition between FRET states with medium and medium/high apparent FRET efficiency (0.45-0.55 to 0.55-0.7, pink rectangle), the transition between FRET states with low and high FRET efficiency (0.25-0.35 to 0.65-0.75, orange rectangle), the transition between FRET states with low and medium/high apparent FRET efficiency (0.2-0.3 to 0.5-0.6, yellow rectangle) and the transition between FRET states with low and low/medium apparent FRET efficiency (0.2-0.3 to 0.35-0.45, green rectangle). All these transitions were reversible. Since these transitions are found in the absence of MgCl_2 but not in the presence of MgCl_2 , they most likely resulted from conformational changes in the synapses which occur more often in the absence of MgCl_2 . As discussed in section 8.4.2, conformational changes between intermediate states of strand exchange may occur more often in the absence of MgCl_2 since the recombination products are more likely to be locked in the ligated state in the presence of MgCl_2 . There are FRET transitions which lead from relatively low apparent FRET efficiencies directly to high apparent FRET efficiencies and smaller intermediate steps. This suggests that strand exchange may proceed directly in one step or may stop temporarily at intermediate states. Further, the reversibility of all FRET state transitions suggests that all strand exchange steps are reversible as well.

However, some of the FRET states, involved in the transitions observed in the absence of MgCl_2 , had a relatively low apparent FRET efficiency. The low apparent FRET efficiency can easily be explained if the synapse of the original, non-recombinant U-shaped substrate has a low/medium apparent FRET efficiency as discussed above. Then, the FRET state transitions, observed exclusively in the absence of MgCl_2 , are intermediate steps of the strand exchange necessary for the inversion reaction. In this case, the observed transitions agree with the subunit rotation model which could involve intermediate rotation steps.

The situation is more complicated if the synapse of the original, non-recombinant U-shaped substrate has a higher FRET efficiency between 0.55 and 0.85. In this case, the intermediate strand exchange steps involve FRET states with far lower apparent FRET efficiencies than the non-recombinant and the recombinant synapse. This may or may not be in agreement with the proposed subunit-rotation model of strand exchange. An alternative explanation may be that the FRET state transitions involving states with low apparent FRET efficiency are due to conformational changes prior to cleavage of the substrate. In this case, the synapses might rest in an inactive state with a distinct conformation, due to the lack of magnesium ions, before forming a synapse capable of cleavage. This explanation is contradicted by the fact that gel based assays showed no

decrease of DNA cleavage rate in the absence of MgCl_2 . A further alternative explanation is that the U-substrates may have a lower preference for the inversion reaction in the absence of MgCl_2 . In this case, some, if not all transitions exclusive to samples without MgCl_2 are due to conformational changes during the recombination of both arms of the U-shaped substrates in anti-parallel orientation. Intermolecular reactions cannot be involved since single U-shaped substrates are fixed to the reaction chamber surface.

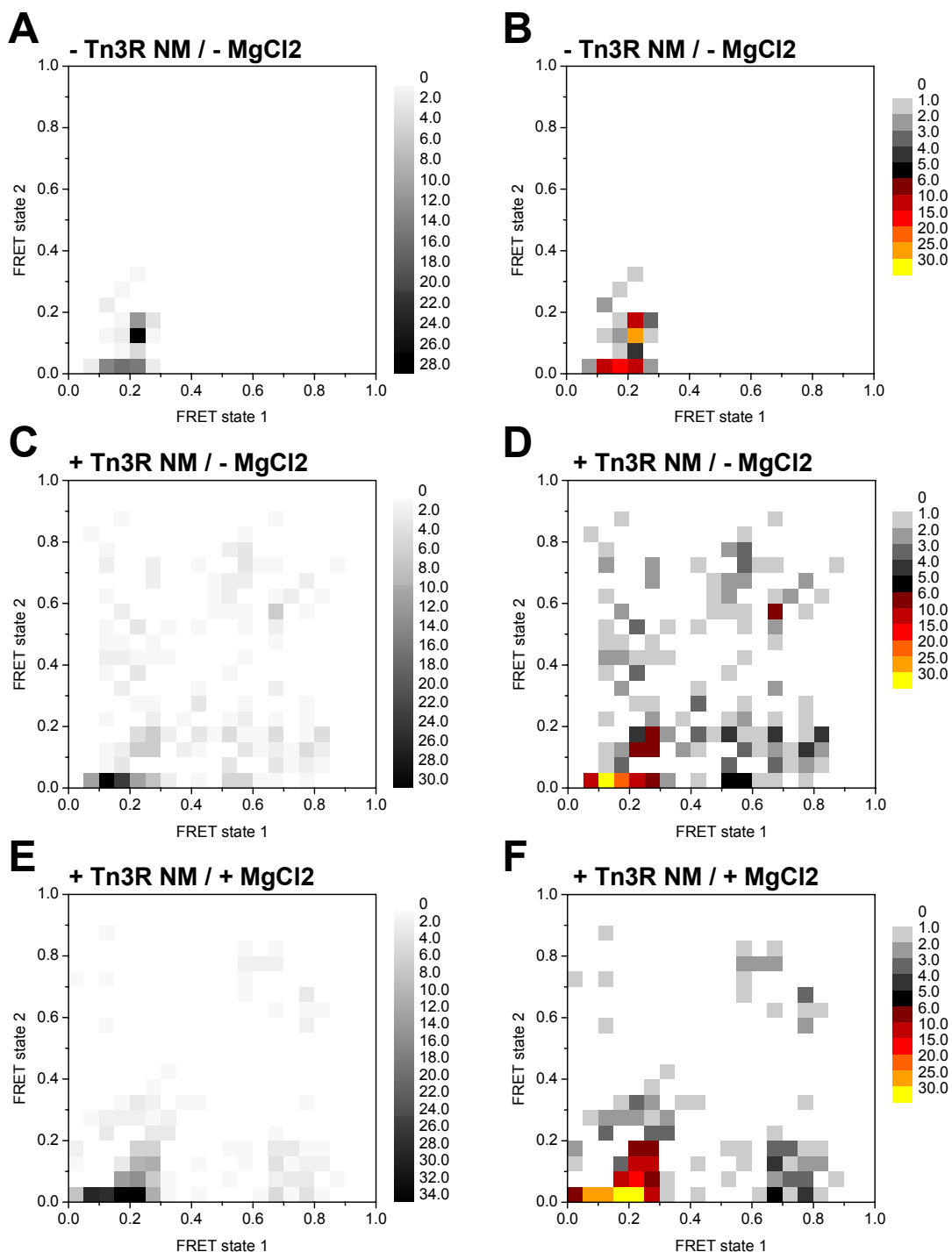


Figure 8.6: 2D-histograms of FRET state transitions of U3 substrates.

After strict filtering (see table 8.1), the single-molecule traces of U3 substrates in the presence and absence of Tn3R NM and magnesium chloride were analysed. All FRET states in the complete FRET traces of the U3 substrates were identified by eye. The transitions from one FRET state (FRET state 1) to the next (FRET state 2) were identified and listed. These lists of transitions are represented in 2D- histograms with a binning of 0.05 (apparent FRET efficiency) for the FRET states 1 and 2. The frequency of each transition is represented by a colour. The colour represents all frequencies equal or greater than the lower FRET limit and smaller than the upper FRET limit indicated in the legends. A non-linear colour representation of the frequencies (B, D, F) reveals transitions with lower frequencies which are hardly visible in histograms with a linear colour representation of frequencies (A, C, E).

All data was collected during a single experiment.

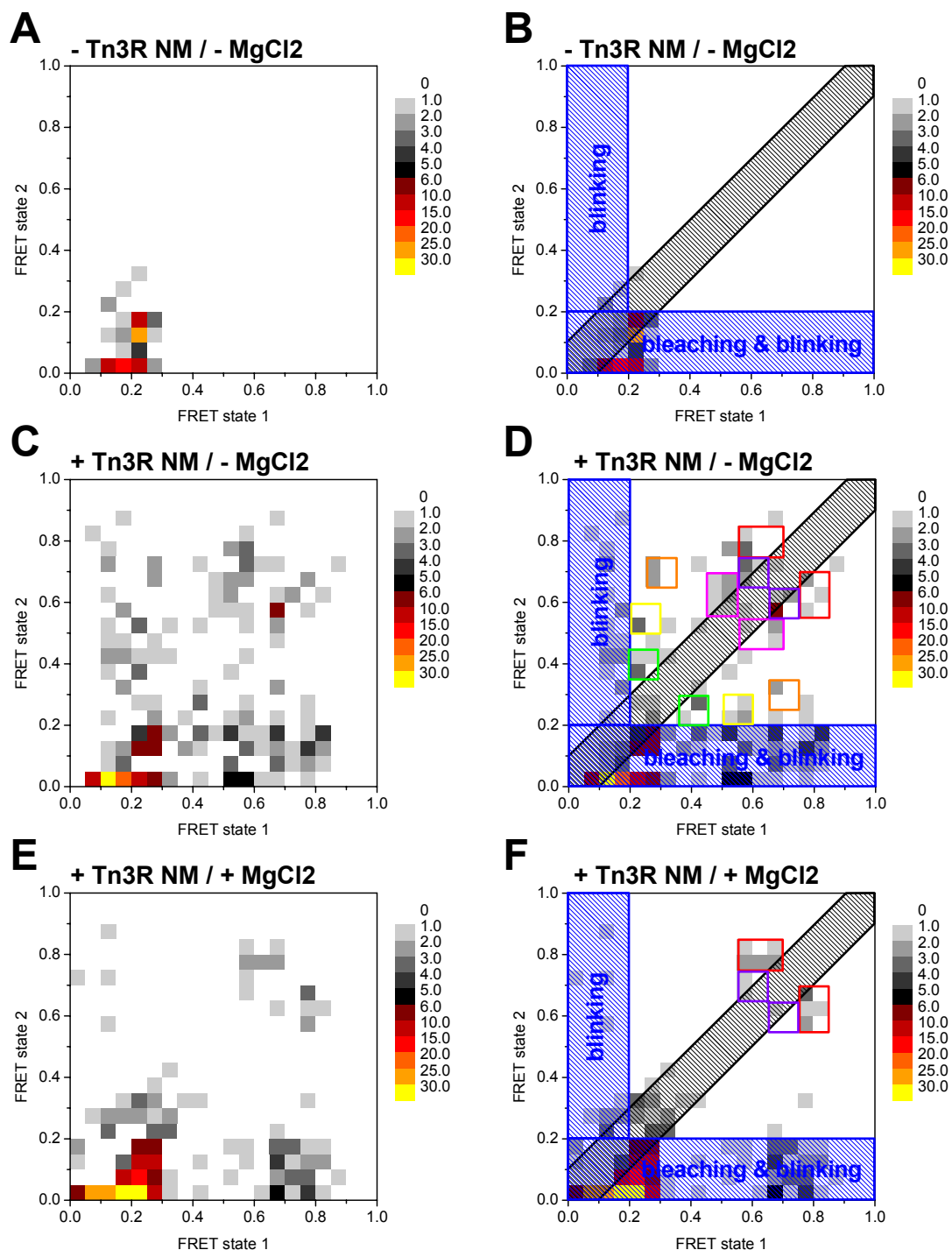


Figure 8.7: Marked transitions in 2D-histograms of FRET state transitions of U3 substrates.

The 2D-histograms show the frequencies of transitions from one FRET state (FRET state 1) to the next (FRET state 2) observed in the complete single-molecule FRET traces of U3 substrates in the presence and absence of Tn3R and magnesium chloride. The construction of the 2D-histograms is described in figure 8.6 in more detail.

The FRET transitions found in the original 2D-histograms (A, C, E) are annotated with coloured markers (B, D, F). Photobleaching and blinking (blue areas) account for most transitions. A black area indicates all small FRET transitions between nearly identical states. Coloured rectangles are used to mark common FRET transitions. Each marked FRET transition spans several bins and the overall frequency of the marked transition is the sum of the frequencies of the individual bins. The frequencies of the marked transitions differ between the samples and are summarised in table 8.2.

All data was collected during a single experiment.

marker colour in 2D FRET histogram	state 1	state 1	state 2	state 2	# of	# of	# of
	lower	upper	lower	upper	transitions	transitions	transitions
	FRET	FRET	FRET	FRET	-Tn3R NM	+Tn3R NM	+Tn3R NM
	limit	limit	limit	limit	-MgCl ₂	-MgCl ₂	+MgCl ₂
	0.55	0.7	0.75	0.85	0	4	11
	0.75	0.85	0.55	0.7	0	4	7
	0.55	0.65	0.65	0.75	0	6	2
	0.65	0.75	0.55	0.65	0	9	1
	0.45	0.55	0.55	0.7	0	8	0
	0.55	0.7	0.45	0.55	0	4	0
	0.25	0.35	0.65	0.75	0	4	0
	0.65	0.75	0.25	0.35	0	2	0
	0.2	0.3	0.5	0.6	0	3	0
	0.5	0.6	0.2	0.3	0	4	0
	0.2	0.3	0.35	0.45	0	5	1
	0.35	0.45	0.2	0.3	0	4	0

Table 8.2: Transitions between FRET states in U3 substrates in presence and absence of Tn3R and magnesium chloride

8.5 Discussion

The single-molecule experiment was conducted with the U-shaped substrate U3, which features a Cy5 dye in its X-arm and a Cy3 dye in the Y-arm. This substrate prefers recombination forming the inversion product which features both dyes in close proximity within the same arm.

The single-molecule FRET experiment had shown that the U-shaped substrate alone had a low apparent FRET efficiency between 0.15 and 0.3. Further, it was shown that the U-shaped substrate can provide large changes in the FRET efficiency upon recombination. In the presence of Tn3 resolvase NM, several specific FRET states and transitions between FRET states had been identified and these FRET states and transitions differed in the presence and absence of MgCl_2 .

The simplest interpretation of the FRET states and FRET state transitions involved synapses which had a low apparent FRET efficiency between 0.3 and 0.4 when they contained the original, non-recombinant substrate and had a high apparent FRET efficiency between 0.55 and 0.85 when they contained the recombinant inversion product. One transition between FRET states with medium/high and high apparent FRET efficiency (0.55-0.7 to 0.75-0.85) was far more prominent in the presence of MgCl_2 . According to the simplest interpretation, this transition corresponded to the conformational changes involved in the process of ligation which is more prominent in the presence of MgCl_2 . This conformational change may be the opening and closing of the gap between the scissile phosphates of site I which is seen in the crystal structure of the $\gamma\delta$ resolvase site I synapse. Most other transitions between FRET states with low, medium or high apparent FRET efficiency were exclusive to the samples without MgCl_2 . According to the simplest interpretation, these transitions were intermediate steps in the strand exchange process which is necessary to transform the original substrate into the inversion product by recombination. These intermediate strand exchange steps are in agreement with the subunit rotation model and could describe steps of partial rotation. Nearly none of the intermediate strand exchange steps were observed in the presence of MgCl_2 , presumably because the substrate was fixed in the ligated state most of the time. Therefore strand exchange events could be relatively rare and the low amount of analysed FRET state transitions may not be sufficient to allow the observation of rare events.

All FRET state transitions could occur in both directions suggesting that all intermediate steps of the cleavage process, the ligation process and the process of strand exchange are

reversible. Further, multiple repeats of FRET state transitions were observed within the traces of the molecules. This suggests that, in the absence of MgCl_2 , multiple strand exchange steps may occur before ligation takes place. Vice versa, in the presence of MgCl_2 , multiple repeats of the cleavage and ligation process may occur before strand exchange takes place.

However, there were alternative interpretations of the observed FRET states and FRET state transitions. One alternative interpretation assumes that the synapses have a relatively high apparent FRET efficiency (0.55-0.85) when they contain the original, non-recombinant substrate. This alternative interpretation could be confirmed or ruled out with a further single-molecule FRET experiment using an inactive version of Tn3 resolvase NM which forms synapses but does not cleave or recombine the substrate. Another alternative explanation assumes that the U-shaped substrate has a lowered preference for the inversion reaction in the absence of MgCl_2 . This interpretation could be confirmed or ruled out with a gel-based assay of the recombination of the U-shaped substrate in the absence of MgCl_2 .

Generally, the involvement of the deletion reaction in the recombination of the U-shaped substrate could be analysed by performing single-molecule FRET experiments with different versions of the U-shaped substrate. One version could feature the dyes at positions which result in a FRET pair, located in one substrate-arm, after the deletion reaction. Another version could feature both dyes within one substrate-arm in the non-recombinant state. With these substrates, recombination would result in the separation of FRET pair both by the inversion reaction and by the deletion reaction.

In future single-molecule FRET experiments, a confocal microscope setup could be used to reveal potential fast FRET state transitions which could not be resolved with the current single-molecule setup.

9 Conclusions and general discussion

In chapter 5 the development of fluorescent substrates for FRET based studies of the mechanism of strand exchange by Tn3 resolvase has been described. Further, different single-site substrate had been tested and, in chapter 6, suitable candidates had been used in ensemble FRET experiments. Several limitations of the single-site substrates became clear and U-shaped substrates had been developed in chapter 7 to overcome these limitations. In chapter 8, a single-molecule FRET experiment was performed with a U-shaped substrate with optimised linker length and a FRET pair at positions which worked well in single-site substrates. Several characteristic FRET states and transitions were observed during the single-molecule FRET experiment. In the following sections, I will discuss the conclusions of the performed experiments, the greater biological and methodological context as well as possible future experiments with the developed fluorescent substrates.

9.1 Development and testing of suitable fluorescent substrates

The aim of this project was to study the mechanism of strand exchange by Tn3 resolvase using FRET spectroscopy. The current model for the strand exchange is supported by several lines of evidence, but direct proof was still required and the potential intermediate steps of the strand exchange process were unknown. To learn more about the mechanism of strand exchange, a Cy3 dye and a Cy5 dye were attached to modified thymines within Tn3 *res* site I, the DNA substrate of Tn3 resolvase. The dyes can form a FRET pair and follow the movements of the substrates, resulting in changes of the distance between both dyes and therefore changes in the FRET efficiency of the FRET pair which can be monitored using fluorescence spectroscopy.

Before using any fluorescent substrates, the general reaction conditions were optimised in chapter 5. It was found that DNA cleavage took place at normal rates in absence of magnesium ions but ligation of cleaved intermediates is slowed down considerably in absence of magnesium ions. This also had an effect on the stability of individual complexes. In absence of magnesium, synapses remained stable in an intermediate state with cleaved sites. In presence of magnesium, synapses could finish the recombination reaction and reassemble. This was promising in context of single-molecule FRET experiments since it was likely that the synapses, trapped in an intermediate state with cleaved substrates, could perform multiple rounds of recombination in the absence of magnesium. The probability of detecting conformational changes related to strand-

exchange, rather than synapse formation, would increase in that case. If single-site substrates would be used in single-molecule experiments, the synapses might remain intact at the reaction chamber surface for a longer time in the absence of magnesium ions. This generally constitutes a weakness of single-site substrates since the dissociation of synapses is irreversible in the extremely dilute solutions used in single-molecule FRET experiments.

Later in chapter 5, potential positions for the dyes within Tn3 res site I were explored. Considering the crystal structure of the $\gamma\delta$ resolvase site I synapse (Li *et al.* 2005) and the subunit rotation model, positions towards the centre of Tn3 res site I were expected to provide a large changes in the FRET efficiency during strand exchange. Furthermore, potential inhibitory effects of the dyes on the formation of synapses and on recombination were also considered for the choice of the positions of the dyes. A library of short, double-stranded substrates containing one copy of Tn3 *res* site I with one or two attached fluorophores, termed single-site substrates, was generated.

First, the impact of the fluorescent dyes, attached to positions near the centre of Tn3 res site I, on the formation of synapses was tested using the activated Tn3 resolvase mutant NM. No inhibition of the synapse formation was found in a gel-based assay, despite the importance of the central positions for recombination. This is in agreement with work showing that DNA-binding is mainly mediated by the C-terminal domain of resolvase, which binds at the edges of site I (Rimphanitchayakit *et al.* 1989). It would be interesting to test the influence of all possible dye positions on binding and synapsis, even though the following recombination assays provide no reason to suspect that synapsis could be inhibited by dyes in other positions. In the context of assays for other DNA-protein interactions, it was promising to see that dyes could be introduced without inhibition of binding and complex formation. Therefore, FRET-based assays can provide a good alternative for binding assays using fluorescence anisotropy and could offer increased sensitivity for internal conformational changes which have little effect on the overall shape of the complex.

Next, the effect of the dyes on the recombination of the short double-stranded substrates by Tn3 resolvase NM was tested in a gel based assay. This assay was performed with substrates containing one or two dyes within Tn3 *res* site I, testing every potential position of the library and every combination of these positions. It was found that dyes attached close to the centre of site I inhibited the recombination, especially the ligation step. This provided some information about the catalytical steps of cleavage and ligation. Either the ligation step is more selective for the correct substrate than the cleavage step or the dyes

interfere sterically with the closing of the gap between the scissile phosphates in the DSB intermediate as proposed by Li *et al.* (2005). Substrates with dyes attached to the central bases of Tn3 res site I might still be useful for future FRET experiments, since they may trap the synapses in a state of continued strand exchange without ligation and therefore increase the chances of observing strand exchange in single-molecule FRET experiments. Dyes further to the outside of site I had less or no inhibitory effect on the recombination of the substrates. A combination of dyes attached to positions R5 and L6 within site I or attached to positions L5 and R4 allowed recombination of the substrates comparable to substrates without modifications within site I. These positions were separated by 8-10 bases but were located in the same helical phase and the dyes protruded from the double-helix in the same direction. Therefore, dyes attached to these positions were still expected to be in relatively close proximity and to provide the high FRET efficiency required for FRET experiments.

9.2 Ensemble FRET experiments

In chapter 6, the best candidates from the gel based assays were tested in ensemble FRET experiments. These substrates had dyes attached within site I at positions R5 and L6. Since positions R5 and L6 are relatively close to each other and within the same helical phase, the substrate containing a FRET pair within site I showed a high FRET efficiency of ~0.63 in solution. In contrast, a mixture of two substrates, each containing one dye of the FRET pair, had a very low FRET efficiency around zero. In the first FRET experiment, Tn3 resolvase NM recombined the substrate containing a FRET pair with an excess of a non-fluorescent competitor substrate forming recombinant products with one dye each. This resulted in a strong drop of the FRET efficiency showing that FRET based methods can be used to study DNA cleavage and possibly recombination. Many commercial FRET-based assays detect cleavage or dissociation of DNA molecules, including the Taqman probes (Applied Biosystems) for real-time PCR. These probes are cleaved during PCR, separating a fluorescent dye on one end and a quencher on the other end of the probe, thereby reporting the progress of the PCR reaction.

However, it was possible that the FRET efficiency drop was mainly caused by DSB products, not recombinant products. To test this, the reverse experiment was performed. Tn3 resolvase NM recombined two fluorescent substrates, each containing one dye, forming recombinant products containing a complete FRET pair. The FRET efficiency increased slightly showing that the dyes of the FRET pair were brought into close proximity within one recombinant product. This proved that not only DNA cleavage but also recombination can be studied by FRET based methods. FRET based methods used

before to study enzymes that move DNA to bring together different DNA molecules or DNA regions, such as DNA looping restriction enzymes (Bellamy *et al.* 2009).

The small FRET efficiency increase in the reverse FRET experiment showed that only a small fraction of the substrates were recombined to form the desired recombinant product with a FRET pair. This was due to the fact that the correct combination of substrates comes together only in 50% of all synapses. Further, the correct substrates can come together in parallel orientation, enabling the formation of the desired recombinant product, or in anti-parallel orientation resulting in undesired recombinant products. This showed that the pre-equilibrium state of the sample has to be designed carefully to develop a sensitive ensemble FRET assay. Ideally, all molecules are in a state of very high or low FRET efficiency before the reaction starts and can be converted to the opposite state quantitatively.

The reverse experiment also revealed that binding by Tn3 resolvase NM and/or synapse formation can result in a considerable increase in FRET efficiency when working with two substrates, each containing one dye of a FRET pair. This needs to be considered in single-molecule FRET experiments and makes it necessary to perform control experiments which show the exact effect of binding and synapse formation. For that purpose, catalytically inactive resolvase mutants may be used. On the other hand, this shows that FRET could be employed for binding assays as an alternative to fluorescence anisotropy. When the binding reaction does not alter the fluorescence anisotropy of the labelled molecule, FRET may even offer higher sensitivity.

The reverse experiment also highlighted a weakness of the single-site substrates relevant to single-molecule FRET experiments. Single-site substrates do not allow control over the orientation of both sites within a synapse when using a mixture of substrates with a single dye each. The orientation of both sites determines if the recombination reaction can result in recombinant products with high or low FRET efficiency. However, single-molecule FRET experiments require a homogenous population of synapses to allow the unambiguous interpretation of different FRET states.

9.3 U-shaped substrates

Due to the limitations of single-site substrates observed in the ensemble FRET experiments, it was considered advantageous to develop substrates which contain two copies of site I and prefer the intramolecular recombination of both sites in one orientation. A strong preference for recombination of sites in parallel, not in anti-parallel orientation, is

important to create a homogenous synapse population to simplify the interpretation of single-molecule FRET data. Further, substrates containing two sites were expected to avoid potential problems in single-molecule FRET experiments arising from the irreversible dissociation of synapses due to extremely low substrate concentrations.

Therefore, in Chapter 7, U-shaped substrates were developed, consisting of two double-stranded arms, each containing one copy of Tn3 *res* site I, and a single-stranded poly(T) linker. Gel-based assays were employed to find the ideal length of the single-stranded linker for the selective promotion of the intramolecular recombination of both arms in parallel orientation resulting in the desired inversion products. A linker with a length of 30 bases constrained recombination mainly to the parallel orientation of both arms.

Decreasing the linker length slowed down the intramolecular recombination of both arms in anti-parallel orientation but not in parallel orientation. This suggests that even shorter linkers could be tested for the future development of U-shaped substrates with a high or complete selectivity for intramolecular recombination in parallel orientation. In general, it was shown that intra-molecular recombination was much faster than intermolecular recombination and should be observable in single-molecule experiments.

Finally, the U-shaped substrate U3 with a Cy5 dye at position R5 within site I in one arm and a Cy3 fluorophore at position L6 within site I in the other arm was prepared and shown to allow recombination comparable to the non-fluorescent U-shaped substrates in a gel-based assay. The gel-based assay allowed the use of in-gel FRET analysis and showed that the original U-shaped substrate had a low FRET efficiency since both dyes were located in distinct arms while the inversion product had a high FRET efficiency since both dyes were located in one arm. Therefore, the U-shaped substrate U3 promised to allow the observation of strand-exchange in FRET experiments.

The use of in-gel FRET could be useful to study other DNA binding proteins that break or join DNA, such as other recombination enzymes, transposases, restriction enzymes or DNA repair enzymes. In-gel FRET could allow the analysis of the binding behaviour, complex and catalytic activity in one step using native PAGE. The fluorophores could enable the detection of the protein/DNA complexes and in-gel FRET can be used to determine status of the substrate DNA. Without in-gel FRET, a second step is often necessary to determine the status of the substrate DNA, e.g. a restriction digest of the substrate DNA or a second electrophoresis step of the same gel in presence of SDS (Rowland *et al.* 2009). Placing the fluorophores at different positions could also allow direct testing of the conformation / orientation of the DNA within the complex. In-gel

FRET might also help to study the structure of the synaptosome, including the accessory sites. In case of the Sin system, a model of the synaptosome was prepared from the X-ray structures of all constituent parts (Rowland *et al.* 2009; Rice *et al.* 2010) and could be tested after labelling specific parts with FRET pairs.

9.4 Single-molecule FRET experiments

The initial ensemble fluorescence experiment had shown that dyes attached to the positions R5 and L6 within Tn3 res site one allow observation of synapse formation and recombination by Tn3 resolvase NM using FRET-based methods. The U-shaped substrate U3 contained dyes at exactly these positions and had been shown to promote the formation of synapses in mainly one configuration in gel-based assays. In chapter 8, the U-shaped substrate U3 was attached to the surface of a reaction chamber and single-molecule FRET experiments were performed without Tn3 resolvase NM and with Tn3 resolvase in the presence and absence of MgCl_2 .

The U-shaped substrate alone had a low apparent FRET efficiency between 0.15 and 0.3 in solution. This was higher than the ensemble FRET efficiency of a mixture of two single-site substrates with one dye each and could be explained with a decreased average distance between the fluorophores when both sites are covalently connected through a linker. An ensemble FRET experiment with the U-shaped substrate U3 would be necessary to test if this is the case or if single-molecule and ensemble measurements produce different FRET efficiency values.

The addition of Tn3 resolvase induced strong changes in the observed FRET efficiencies. In the presence of Tn3 resolvase NM, several specific FRET states and transitions between FRET states had been identified and these FRET states and transitions differed in the presence and absence of MgCl_2 . In the simplest interpretation of the FRET states and FRET state transitions, synapses containing the recombinant inversion product have a high apparent FRET efficiency (0.55-0.85) while synapses containing the original, non-recombinant substrate have a low apparent FRET efficiency (0.3-0.4).

Comparing the sample in presence and absence of MgCl_2 , it became clear that one transition between FRET states with the highest observed apparent FRET efficiencies was far more prominent in the presence of MgCl_2 . This suggested that the transition could be related to the ligation step which was faster in the presence of MgCl_2 . The transition might correspond to the conformational changes described by Li *et al.* (2005) which may be necessary to open and close the gap between the scissile phosphates of site I seen in the

crystal structure of the $\gamma\delta$ resolvase site I synapse (Li *et al.* 2005). In this crystal structure, both halves of the cleaved site are separated by ~ 17 Å and the positions R5 and L6 are separated by ~ 52 Å. Assuming a Förster Radius of ~ 60 Å for a Cy3/Cy5 FRET and using equation 2.2, the transition between the ligated and cleaved state would result in a transition between FRET efficiencies of 0.96 and 0.7. This is in agreement with the observed transitions which are prominent in presence of magnesium and may therefore correspond to the ligation step. In contrast, assuming a Förster Radius of ~ 50 Å, a transition between FRET efficiencies of 0.89 and 0.45 would be observed. This is more similar to FRET state transitions observed in absence of magnesium. However, the correct calculation of absolute FRET efficiencies requires exact determination of many parameters and is hard to apply in this case.

Most other transitions between FRET states with low, medium or high apparent FRET efficiency were observed exclusively in the absence of MgCl_2 . Most likely, these transitions represented intermediate strand exchange steps of the inversion reaction. The subunit rotation model agrees with the apparent FRET efficiencies during these FRET state transitions and strand exchange might proceed through intermediate steps of partial subunit rotation. In the presence of MgCl_2 , these intermediate strand exchange steps were nearly absent. This could be caused by the domination of a fixed, ligated state of the substrate DNA limiting the frequency of strand exchange events. Therefore it is likely that strand exchange steps were not observed in the presence of magnesium due to the low number of analysed FRET transitions.

All intermediate steps of the recombination step appeared to be reversible since all observed FRET state transitions occurred in both directions. Further, multiple repeats of FRET state transitions were observed within the traces of the molecules. This suggests that, in the absence of MgCl_2 , multiple strand exchange steps may occur before ligation takes place. Similarly, in the presence of MgCl_2 , multiple repeats of the cleavage and ligation process may occur before strand exchange takes place. In the future, more data should be collected and statistical analysis of the transitions could be used to test for a preferred order of strand exchange steps, similar to the order of rotational steps observed in single-molecule FRET experiments with the F0F1-ATP synthase (Diez *et al.* 2004). However, it is unlikely that there is a preferred direction of subunit rotation in U-shaped substrates since the directionality in the wildtype system is driven by DNA supercoiling. This role of DNA supercoiling has been shown *in vitro* (Stark *et al.* 1989; McIlwraith *et al.* 1996; McIlwraith *et al.* 1997) and *in vivo* supercoiling is generally available as a driving

force in bacterial plasmids. Magnetic or optical tweezers could be used to study the rotational process further, similar to work on DNA topoisomerases (Koster *et al.* 2005).

In the future, single-molecule experiments with different mutants of Tn3 resolvase as well as different substrates are necessary to assign the observed FRET states and transitions to more to specific recombination processes more confidently. The use of wildtype Tn3 resolvase could single out transitions corresponding to resolvase binding. The catalytically inactive mutant Tn3 resolvase NM-S10A can form tetramers and could be used to identify the transitions related to synapse association and dissociation. Readily available U-shaped substrates containing both fluorophores within one arm could help to distinguish between transitions occurring during inversion and the rarer deletion reaction. For this purpose, a U-shaped substrate with both dyes located in the same half of site I could also be used since the FRET state corresponding to inversion and deletion steps would be swapped between both reaction pathways. Most importantly, more single-molecule FRET data needs to be collected to improve the statistical analysis. This would allow the identification of rarer transitions as well as the determination of rates for all transitions. Further, a confocal microscope setup could be used to reveal potential fast FRET state transitions which could not be resolved with the current single-molecule setup. Finally, simple gel-based experiments could be employed to rule out alternative interpretations which assume a decreased preference of the U-shaped for the inversion reaction in the absence of MgCl_2 .

Overall, the single-molecule FRET experiment promises to reveal more about the mechanism and kinetics of strand exchange by Tn3 resolvase. However, this approach could be used to study a wide range of protein/DNA systems. FRET-based assays (Bellamy *et al.* 2009) and single-molecule FRET experiments (Morgan *et al.* 2005) have been used before to study the mechanism of DNA-rearranging enzymes such as restriction enzymes that induce DNA looping. However, simpler approaches like tethered particle motion dominate this research area (Laurens *et al.* 2009; Ramanathan *et al.* 2009). Single-molecule FRET approaches have been used mainly for research on DNA or RNA constructs like ribozymes (Tan *et al.* 2003) and holiday junctions (McKinney *et al.* 2005) or enzymes working on holiday junctions. I hope this thesis contributes to establish single-molecule FRET as an approach to studying DNA-rearranging enzymes. Particularly the emerging field of structural research on the organisation of bacterial chromatin could benefit from tools, such as the FRET based assay developed here, to analyse proteins involved in DNA bending, looping and bridging (Wiggins *et al.* 2009).

10 Bibliography

1. Abraham, J. M., Freitag, C. S., Clements, J. R. and Eisenstein, B. I. (1985). "An invertible element of DNA controls phase variation of type 1 fimbriae of *Escherichia coli*." *Proc Natl Acad Sci U S A* **82**(17): 5724-5727.
2. Ackroyd, A. J., Avila, P., Parker, C. N. and Halford, S. E. (1990). "Site-specific recombination by mutants of Tn21 resolvase with DNA recognition functions from Tn3 resolvase." *J Mol Biol* **216**(3): 633-643.
3. Aitken, C. E., Marshall, R. A. and Puglisi, J. D. (2008). "An oxygen scavenging system for improvement of dye stability in single-molecule fluorescence experiments." *Biophys J* **94**(5): 1826-1835.
4. Akopian, A., He, J., Boocock, M. R. and Stark, W. M. (2003). "Chimeric recombinases with designed DNA sequence recognition." *Proc Natl Acad Sci U S A* **100**(15): 8688-8691.
5. Arnold, P. H., Blake, D. G., Grindley, N. D., Boocock, M. R. and Stark, W. M. (1999). "Mutants of Tn3 resolvase which do not require accessory binding sites for recombination activity." *Embo J* **18**(5): 1407-1414.
6. Arthur, A. and Sherratt, D. (1979). "Dissection of the transposition process: a transposon-encoded site-specific recombination system." *Mol Gen Genet* **175**(3): 267-274.
7. Azaro, M. A. and Landy, A. (2002). λ integrase and the λ Int family. *Mobile DNA II*. N. L. Craig, R. Cragie, M. Gellert and A. M. Lambowitz. Washington, DC, American Society for Microbiology (ASM): 118-148.
8. Barre, F.-X. and Sherratt, D. J. (2002). Xer site-specific recombination: Promoting chromosome segregation. *Mobile DNA II*. N. L. Craig, R. Cragie, M. Gellert and A. M. Lambowitz. Washington, DC, American Society for Microbiology (ASM): 149-161.
9. Bellamy, S. R., Kovacheva, Y. S., Zulkipili, I. H. and Halford, S. E. (2009). "Differences between Ca^{2+} and Mg^{2+} in DNA binding and release by the SfiI restriction endonuclease: implications for DNA looping." *Nucleic Acids Res* **37**(16): 5443-5453.
10. Blake, D. G., Boocock, M. R., Sherratt, D. J. and Stark, W. M. (1995). "Cooperative binding of Tn3 resolvase monomers to a functionally asymmetric binding site." *Curr Biol* **5**(9): 1036-1046.
11. Boocock, M. R., Zhu, X. and Grindley, N. D. (1995). "Catalytic residues of gamma delta resolvase act in cis." *Embo J* **14**(20): 5129-5140.
12. Brown, J. L., He, J., Sherratt, D. J., Stark, W. M., Boocock, M. R., Brown, J. L., He, J., Sherratt, D. J., Stark, W. M. and Boocock, M. R. (2002). "Interactions of protein complexes on supercoiled DNA: the mechanism of selective synapsis by Tn3 resolvase." *J Mol Biol* **319**(2): 371-383.
13. Burke, M. E., Arnold, P. H., He, J., Wenwieser, S. V. C. T., Rowland, S.-J., Boocock, M. R. and Stark, W. M. (2004). "Activating mutations of Tn3 resolvase marking interfaces important in recombination catalysis and its regulation." *Mol Microbiol* **51**(4): 937-948.
14. Burke, M. E. and Stark, W. M., DNase I footprinting assay of synapsed Tn3 res sites (unpublished work), University of Glasgow, Glasgow
15. Burke, M. E. and Stark, W. M., Mutagenesis of Tn3 res site I, (unpublished work), University of Glasgow, Glasgow
16. Chou, J., Casadaban, M. J., Lemaux, P. G. and Cohen, S. N. (1979). "Identification and characterization of a self-regulated repressor of translocation of the Tn3 element." *Proc Natl Acad Sci U S A* **76**(8): 4020-4024.
17. Clegg, R. M., Murchie, A. I., Zechel, A., Carlberg, C., Diekmann, S. and Lilley, D. M. (1992). "Fluorescence resonance energy transfer analysis of the structure of the four-way DNA junction." *Biochemistry* **31**(20): 4846-4856.
18. Curcio, M. J. and Derbyshire, K. M. (2003). "The outs and ins of transposition: from mu to kangaroo." *Nat Rev Mol Cell Biol* **4**(11): 865-877.
19. DeLano, W. L. (2006). The PyMOL Molecular Graphics System, *DeLano Scientific LLC*, Palo Alto, CA, USA., www.pymol.org
20. Dhar, G., Sanders, E. R. and Johnson, R. C. (2004). "Architecture of the hin synaptic complex during recombination: the recombinase subunits translocate with the DNA strands." *Cell* **119**(1): 33-45.
21. Diez, M., Zimmermann, B., Borsch, M., Konig, M., Schweinberger, E., Steigmiller, S., Reuter, R., Felekyan, S., Kudryavtsev, V., Seidel, C. A. M. and Graber, P. (2004). "Proton-powered subunit rotation in single membrane-bound F0F1-ATP synthase.[see comment]." *Nat Struct Mol Biol* **11**(2): 135-141.
22. Droge, P., Hatfull, G. F., Grindley, N. D. and Cozzarelli, N. R. (1990). "The two functional domains of gamma delta resolvase act on the same recombination site: implications for the mechanism of strand exchange." *Proc Natl Acad Sci U S A* **87**(14): 5336-5340.

23. Eggeling, C., Fries, J. R., Brand, L., Gunther, R. and Seidel, C. A. (1998). "Monitoring conformational dynamics of a single molecule by selective fluorescence spectroscopy." *Proc Natl Acad Sci U S A* **95**(4): 1556-1561.
24. Elrod-Erickson, M. and Pabo, C. O. (1999). "Binding studies with mutants of Zif268. Contribution of individual side chains to binding affinity and specificity in the Zif268 zinc finger-DNA complex." *J Biol Chem* **274**(27): 19281-19285.
25. Elrod-Erickson, M., Rould, M. A., Neklodova, L. and Pabo, C. O. (1996). "Zif268 protein-DNA complex refined at 1.6 Å: a model system for understanding zinc finger-DNA interactions." *Structure (Camb)* **4**(10): 1171-1180.
26. Falvey, E., Hatfull, G. F. and Grindley, N. D. (1988). "Uncoupling of the recombination and topoisomerase activities of the gamma delta resolvase by a mutation at the crossover point." *Nature* **332**(6167): 861-863.
27. Gasteiger, E., Hoogland, C., Gattiker, A., Duvaud, S., Wilkins, M. R., Appel, R. D. and Bairoch, A. (2005). Protein identification and analysis tools on the ExPASy Server. *The proteomics protocols handbook*. J. M. Walker. Totowa, New Jersey, Humana Press. **1**: 571-607.
28. Gersbach, C. A., Gaj, T., Gordley, R. M. and Barbas, C. F., 3rd (2010). "Directed evolution of recombinase specificity by split gene reassembly." *Nucleic Acids Res.*
29. Gill, R., Heffron, F., Dougan, G. and Falkow, S. (1978). "Analysis of sequences transposed by complementation of two classes of transposition-deficient mutants of Tn3." *J Bacteriol* **136**(2): 742-756.
30. Gill, R. E., Heffron, F. and Falkow, S. (1979). "Identification of the protein encoded by the transposable element Tn3 which is required for its transposition." *Nature* **282**(5741): 797-801.
31. Gordley, R. M., Gersbach, C. A. and Barbas, C. F., 3rd (2009). "Synthesis of programmable integrases." *Proc Natl Acad Sci U S A* **106**(13): 5053-5058.
32. Gordley, R. M., Smith, J. D., Graslund, T. and Barbas, C. F., 3rd (2007). "Evolution of programmable zinc finger-recombinases with activity in human cells." *J Mol Biol* **367**(3): 802-813.
33. Grindley, N. D., Lauth, M. R., Wells, R. G., Wityk, R. J., Salvo, J. J. and Reed, R. R. (1982). "Transposon-mediated site-specific recombination: identification of three binding sites for resolvase at the res sites of gamma delta and Tn3." *Cell* **30**(1): 19-27.
34. Grindley, N. D., Whiteson, K. L. and Rice, P. A. (2006). "Mechanisms of site-specific recombination." *Annu Rev Biochem* **75**: 567-605.
35. Grindley, N. D. F. (2002). The movement of Tn3-like elements: Transposition and Cointegrate resolution. *Mobile DNA II*. N. L. Craig, R. Cragie, M. Gellert and A. M. Lambowitz. Washington, DC, American Society for Microbiology (ASM): 272-302.
36. Haffter, P. and Bickle, T. A. (1988). "Enhancer-independent mutants of the Cin recombinase have a relaxed topological specificity." *Embo J* **7**(12): 3991-3996.
37. Hatfull, G. F. and Grindley, N. D. (1986). "Analysis of gamma delta resolvase mutants in vitro: evidence for an interaction between serine-10 of resolvase and site I of res." *Proc Natl Acad Sci U S A* **83**(15): 5429-5433.
38. Haykinson, M. J., Johnson, L. M., Soong, J. and Johnson, R. C. (1996). "The Hin dimer interface is critical for Fis-mediated activation of the catalytic steps of site-specific DNA inversion." *Curr Biol* **6**(2): 163-177.
39. He, J., McIlwraith, M. J., Burke, M. E., Boocock, M. R., Stark, W. M., He, J., McIlwraith, M. J., Burke, M. E., Boocock, M. R. and Stark, W. M. (2002). "Synapsis of Tn3 recombination sites: unpaired sites destabilize synapses by a partner exchange mechanism." *J Mol Biol* **319**(2): 385-393.
40. Heffron, F., McCarthy, B. J., Ohtsubo, H. and Ohtsubo, E. (1979). "DNA sequence analysis of the transposon Tn3: three genes and three sites involved in transposition of Tn3." *Cell* **18**(4): 1153-1163.
41. Hickman, A. B., Chandler, M. and Dyda, F. (2010). "Integrating prokaryotes and eukaryotes: DNA transposases in light of structure." *Crit Rev Biochem Mol Biol* **45**(1): 50-69.
42. Holden, N., Blomfield, I. C., Uhlin, B. E., Totsika, M., Kulasekara, D. H. and Gally, D. L. (2007). "Comparative analysis of FimB and FimE recombinase activity." *Microbiology* **153**(Pt 12): 4138-4149.
43. Hughes, R. E., Hatfull, G. F., Rice, P., Steitz, T. A. and Grindley, N. D. (1990). "Cooperativity mutants of the gamma delta resolvase identify an essential interdimer interaction." *Cell* **63**(6): 1331-1338.
44. Jayaram, M., Mehta, S., Uzri, D., Voziyanov, Y. and Velmurugan, S. (2004). "Site-specific recombination and partitioning systems in the stable high copy propagation of the 2-micron yeast plasmid." *Prog Nucleic Acid Res Mol Biol* **77**: 127-172.

45. Johnson, R. C. (2002). Bacterial site-specific DNA inversion systems. *Mobile DNA II*. N. L. Craig, R. Cragie, M. Gellert and A. M. Lambowitz. Washington, DC, American Society for Microbiology (ASM): 230-271.
46. Johnson, R. C., Bruist, M. F. and Simon, M. I. (1986). "Host protein requirements for in vitro site-specific DNA inversion." *Cell* **46**(4): 531-539.
47. Kamtekar, S., Ho, R. S., Cocco, M. J., Li, W., Wenwieser, S. V., Boocock, M. R., Grindley, N. D. and Steitz, T. A. (2006). "Implications of structures of synaptic tetramers of gamma delta resolvase for the mechanism of recombination." *Proc Natl Acad Sci U S A* **103**(28): 10642-10647.
48. Kibbe, W. A. (2007). "OligoCalc: An online oligonucleotide properties calculator." *Nucleic Acids Res* **35**(webserver issue): W43-W46.
49. Kilbride, E., Boocock, M. R. and Stark, W. M. (1999). "Topological selectivity of a hybrid site-specific recombination system with elements from Tn3 res/resolvase and bacteriophage P1 loxP/Cre." *J Mol Biol* **289**(5): 1219-1230.
50. Kitts, P. A., Symington, L. S., Dyson, P. and Sherratt, D. J. (1983). "Transposon-encoded site-specific recombination: nature of the Tn3 DNA sequences which constitute the recombination site res." *Embo J* **2**(7): 1055-1060.
51. Klippel, A., Cloppenborg, K. and Kahmann, R. (1988). "Isolation and characterization of unusual gin mutants." *Embo J* **7**(12): 3983-3989.
52. Komano, T. (1999). "Shufflons: multiple inversion systems and integrons." *Annu Rev Genet* **33**: 171-191.
53. Koster, D. A., Croquette, V., Dekker, C., Shuman, S. and Dekker, N. H. (2005). "Friction and torque govern the relaxation of DNA supercoils by eukaryotic topoisomerase IB." *Nature* **434**(7033): 671-674.
54. Krasnow, M. A. and Cozzarelli, N. R. (1983). "Site-specific relaxation and recombination by the Tn3 resolvase: recognition of the DNA path between oriented res sites." *Cell* **32**(4): 1313-1324.
55. Laemmli, U. K. (1970). "Cleavage of structural proteins during the assembly of the head of bacteriophage T4." *Nature* **227**: 680-685.
56. Laurens, N., Bellamy, S. R., Harms, A. F., Kovacheva, Y. S., Halford, S. E. and Wuite, G. J. (2009). "Dissecting protein-induced DNA looping dynamics in real time." *Nucleic Acids Res* **37**(16): 5454-5464.
57. Leschziner, A. E. and Grindley, N. D. F. (2003). "The architecture of the $\gamma\delta$ resolvase crossover site synaptic complex revealed by using constrained DNA substrates." *Mol Cell* **12**: 775-781.
58. Li, W., Kamtekar, S., Xiong, Y., Sarkis, G. J., Grindley, N. D. F. and Steitz, T. A. (2005). "Structure of a synaptic gammadelta resolvase tetramer covalently linked to two cleaved DNAs." *Science* **309**(5738): 1210-1215.
59. Lieber, M. R. (2010). "The mechanism of double-strand DNA break repair by the nonhomologous DNA end-joining pathway." *Annu Rev Biochem* **79**: 181-211.
60. Lilley, D. M. (1997). "Site-specific recombination caught in the act." *Chem Biol* **4**(10): 717-720.
61. Lilley, D. M. and Wilson, T. J. (2000). "Fluorescence resonance energy transfer as a structural tool for nucleic acids." *Curr Opin Chem Biol* **4**(5): 507-517.
62. Lind, G. R. (2003). PHP Nucleotide Sequence Generator, www.llamastar.com/phptest/dna.php
63. Liu, P., Jenkins, N. A. and Copeland, N. G. (2003). "A highly efficient recombineering-based method for generating conditional knockout mutations." *Genome Res* **13**(3): 476-484.
64. Longhese, M. P., Bonetti, D., Guerini, I., Manfrini, N. and Clerici, M. (2009). "DNA double-strand breaks in meiosis: checking their formation, processing and repair." *DNA Repair (Amst)* **8**(9): 1127-1138.
65. Mahaney, B. L., Meek, K. and Lees-Miller, S. P. (2009). "Repair of ionizing radiation-induced DNA double-strand breaks by non-homologous end-joining." *Biochem J* **417**(3): 639-650.
66. Mahillon, J. and Lereclus, D. (1988). "Structural and functional analysis of Tn4430: identification of an integrase-like protein involved in the co-integrate-resolution process." *Embo J* **7**(5): 1515-1526.
67. Markham, N. R. and Zuker, M. (2005). "DINAMelt web server for nucleic acid melting prediction." *Nucleic Acids Res* **33**: 577-581.
68. Markham, N. R. and Zuker, M. (2008). UNAFold: Software for nucleic acid folding and hybridization. *Bioinformatics: Structure, function and applications*. J. M. Keith. Totowa, Humana Press. **2**: 3-31.
69. McClintock, B. (1950). "The origin and behavior of mutable loci in maize." *Proc Natl Acad Sci U S A* **36**(6): 344-355.

70. McIlwraith, M. J., Boocock, M. R. and Stark, W. M. (1996). "Site-specific recombination by Tn3 resolvase, photocrosslinked to its supercoiled DNA substrate." *J Mol Biol* **260**(3): 299-303.
71. McIlwraith, M. J., Boocock, M. R. and Stark, W. M. (1997). "Tn3 resolvase catalyses multiple recombination events without intermediate rejoining of DNA ends." *J Mol Biol* **266**(1): 108-121.
72. McKinney, S. A., Freeman, A. D., Lilley, D. M. and Ha, T. (2005). "Observing spontaneous branch migration of Holliday junctions one step at a time." *Proc Natl Acad Sci U S A* **102**(16): 5715-5720.
73. Moore, M., Ullman, C., Moore, M. and Ullman, C. (2003). "Recent developments in the engineering of zinc finger proteins." *Brief* **1**(4): 342-355.
74. Morgan, M. A., Okamoto, K., Kahn, J. D. and English, D. S. (2005). "Single-molecule spectroscopic determination of lac repressor-DNA loop conformation." *Biophys J* **89**(4): 2588-2596.
75. Mouw, K. W., Rowland, S. J., Gajjar, M. M., Boocock, M. R., Stark, W. M. and Rice, P. A. (2008). "Architecture of a serine recombinase-DNA regulatory complex." *Mol Cell* **30**(2): 145-155.
76. Murphy, M. C., Rasnik, I., Cheng, W., Lohman, T. M. and Ha, T. (2004). "Probing single-stranded DNA conformational flexibility using fluorescence spectroscopy." *Biophys J* **86**(4): 2530-2537.
77. Nagy, A. (2000). "Cre recombinase: the universal reagent for genome tailoring." *Genesis* **26**(2): 99-109.
78. Nagy, A., Perrimon, N., Sandmeyer, S. and Plasterk, R. (2003). "Tailoring the genome: the power of genetic approaches." *Nat Genet* **33 Suppl**: 276-284.
79. Nollmann, M., He, J., Byron, O., Stark, W. M., Nollmann, M., He, J., Byron, O. and Stark, W. M. (2004). "Solution structure of the Tn3 resolvase-crossover site synaptic complex." *Mol Cell* **16**(1): 127-137.
80. Olorunniji, F. J. (2006) Tn3 resolvase-catalysed recombination: Assembly and activation of the site I synapse. Department of Molecular and Cellular Biology, University of Glasgow, Glasgow
81. Olorunniji, F. J., He, J., Wenwieser, S. V., Boocock, M. R. and Stark, W. M. (2008). "Synapsis and catalysis by activated Tn3 resolvase mutants." *Nucleic Acids Res* **36**(22): 7181-7191.
82. Oram, M., Marko, J. F. and Halford, S. E. (1997). "Communications between distant sites on supercoiled DNA from non-exponential kinetics for DNA synapsis by resolvase." *J Mol Biol* **270**(3): 396-412.
83. Parker, C. N. and Halford, S. E. (1991). "Dynamics of long-range interactions on DNA: the speed of synapsis during site-specific recombination by resolvase." *Cell* **66**(4): 781-791.
84. Pavletich, N. P. and Pabo, C. O. (1991). "Zinc finger-DNA recognition: crystal structure of a Zif268-DNA complex at 2.1 Å." *Science* **252**(5007): 809-817.
85. Pitcher, R. S., Brissett, N. C. and Doherty, A. J. (2007). "Nonhomologous end-joining in bacteria: a microbial perspective." *Annu Rev Microbiol* **61**: 259-282.
86. Prorocic, M. M. (2009) Sequence selectivity of the resolvase catalytic domain: Implications for Z-resolvase design. Department of Molecular and Cellular Biology, University of Glasgow, Glasgow
87. Rajeev, L., Malanowska, K. and Gardner, J. F. (2009). "Challenging a paradigm: the role of DNA homology in tyrosine recombinase reactions." *Microbiol Mol Biol Rev* **73**(2): 300-309.
88. Ramanathan, S. P., van Aelst, K., Sears, A., Peakman, L. J., Diffin, F. M., Szczelkun, M. D. and Seidel, R. (2009). "Type III restriction enzymes communicate in 1D without looping between their target sites." *Proc Natl Acad Sci U S A* **106**(6): 1748-1753.
89. Reed, R. R. (1981a). "Resolution of cointegrates between transposons gamma delta and Tn3 defines the recombination site." *Proc Natl Acad Sci U S A* **78**(6): 3428-3432.
90. Reed, R. R. (1981b). "Transposon-mediated site-specific recombination: a defined in vitro system." *Cell* **25**(3): 713-719.
91. Reed, R. R. and Grindley, N. D. (1981). "Transposon-mediated site-specific recombination in vitro: DNA cleavage and protein-DNA linkage at the recombination site." *Cell* **25**(3): 721-728.
92. Rice, P. A., Mouw, K. W., Montano, S. P., Boocock, M. R., Rowland, S. J. and Stark, W. M. (2010). "Orchestrating serine resolvases." *Biochem Soc Trans* **38**(2): 384-387.
93. Rice, P. A. and Steitz, T. A. (1994a). "Model for a DNA-mediated synaptic complex suggested by crystal packing of gamma delta resolvase subunits." *Embo J* **13**(7): 1514-1524.
94. Rice, P. A. and Steitz, T. A. (1994b). "Refinement of gamma delta resolvase reveals a strikingly flexible molecule." *Structure (Camb)* **2**(5): 371-384.

95. Rice, P. A., Yang, S., Mizuuchi, K. and Nash, H. A. (1996). "Crystal structure of an IHF-DNA complex: a protein-induced DNA U-turn." *Cell* **87**(7): 1295-1306.
96. Riha, K., Heacock, M. L. and Shippen, D. E. (2006). "The role of the nonhomologous end-joining DNA double-strand break repair pathway in telomere biology." *Annu Rev Genet* **40**: 237-277.
97. Rimphanitchayakit, V. and Grindley, N. D. (1990). "Saturation mutagenesis of the DNA site bound by the small carboxy-terminal domain of gamma delta resolvase." *Embo J* **9**(3): 719-725.
98. Rimphanitchayakit, V., Hatfull, G. F. and Grindley, N. D. (1989). "The 43 residue DNA binding domain of gamma delta resolvase binds adjacent major and minor grooves of DNA." *Nucleic Acids Res* **17**(3): 1035-1050.
99. Rowland, S. J., Boocock, M. R., McPherson, A. L., Mouw, K. W., Rice, P. A. and Stark, W. M. (2009). "Regulatory mutations in Sin recombinase support a structure-based model of the synaptosome." *Mol Microbiol* **74**(2): 282-298.
100. Rowland, S. J., Boocock, M. R. and Stark, W. M. (2005). "Regulation of Sin recombinase by accessory proteins." *Mol Microbiol* **56**(2): 371-382.
101. Rowland, S. J., Boocock, M. R. and Stark, W. M. (2006). "DNA bending in the Sin recombination synapse: functional replacement of HU by IHF." *Mol Microbiol* **59**(6): 1730-1743.
102. Rowland, S. J., Stark, W. M. and Boocock, M. R. (2002). "Sin recombinase from *Staphylococcus aureus*: synaptic complex architecture and transposon targeting." *Mol Microbiol* **44**(3): 607-619.
103. Roy, R., Hohng, S. and Ha, T. (2008). "A practical guide to single-molecule FRET." *Nat Methods* **5**(6): 507-516.
104. Sadowski, J., Gasteiger, J. and Klebe, G. (1994). "Comparison of Automatic Three-Dimensional Model Builders Using 639 X-ray Structures." *Journal of Chemical Information and Computer Sciences* **34**(4): 1000-1008.
105. Sadowski, J., Gasteiger, J. and Klebe, G. (2008). 3D Structure Generator CORINA (Demo), *Molecular Networks GmbH Computerchemie*, Erlangen, Germany, www.molecular-networks.com/online_demos/corina_demo.html
106. Sambrook, J. and Russell, D. (2001). *Molecular Cloning*. New York, Cold Spring Harbor Laboratory Press.
107. Santoro, S. W., Schultz, P. G., Santoro, S. W. and Schultz, P. G. (2002). "Directed evolution of the site specificity of Cre recombinase." *Proc Natl Acad Sci U S A* **99**(7): 4185-4190.
108. Saraf-Levy, T., Santoro, S. W., Volpin, H., Kushnirsky, T., Eyal, Y., Schultz, P. G., Gidoni, D., Carmi, N., Saraf-Levy, T., Santoro, S. W., Volpin, H., Kushnirsky, T., Eyal, Y., Schultz, P. G., Gidoni, D. and Carmi, N. (2006). "Site-specific recombination of asymmetric lox sites mediated by a heterotetrameric Cre recombinase complex." *Bioorg Med Chem* **14**(9): 3081-3089.
109. Sarkis, G. J., Murley, L. L., Leschziner, A. E., Boocock, M. R., Stark, W. M. and Grindley, N. D. (2001). "A model for the gamma delta resolvase synaptic complex." *Mol Cell* **8**(3): 623-631.
110. Shapiro, J. A. (1979). "Molecular model for the transposition and replication of bacteriophage Mu and other transposable elements." *Proc Natl Acad Sci U S A* **76**(4): 1933-1937.
111. Sherratt, D., Arthur, A. and Burke, M. (1981). "Transposon-specified, site-specific recombination systems." *Cold Spring Harb Symp Quant Biol* **45 Pt 1**: 275-281.
112. Shuman, S. and Glickman, M. S. (2007). "Bacterial DNA repair by non-homologous end joining." *Nat Rev Microbiol* **5**(11): 852-861.
113. Stark, W. M. and Boocock, M. R. (1994). "The linkage change of a knotting reaction catalysed by Tn3 resolvase." *J Mol Biol* **239**(1): 25-36.
114. Stark, W. M. and Boocock, M. R. (1995). "Gatecrashers at the catalytic party.[see comment]." *Trends Genet* **11**(4): 121-123.
115. Stark, W. M., Grindley, N. D., Hatfull, G. F. and Boocock, M. R. (1991). "Resolvase-catalysed reactions between res sites differing in the central dinucleotide of subsite I." *Embo J* **10**(11): 3541-3548.
116. Stark, W. M., Sherratt, D. J. and Boocock, M. R. (1989). "Site-specific recombination by Tn3 resolvase: topological changes in the forward and reverse reactions." *Cell* **58**(4): 779-790.
117. Stryer, L. (1978). "Fluorescence energy transfer as a spectroscopic ruler." *Annu Rev Biochem* **47**: 819-846.
118. Studier, F. W., Rosenberg, A. H., Dunn, J. J. and Dubendorf, J. W. (1990). "Use of T7 RNA polymerase to direct expression of cloned genes." *Methods Enzymol* **185**: 60-89.

119. Tan, E., Wilson, T. J., Nahas, M. K., Clegg, R. M., Lilley, D. M. and Ha, T. (2003). "A four-way junction accelerates hairpin ribozyme folding via a discrete intermediate." *Proc Natl Acad Sci U S A* **100**(16): 9308-9313.
120. van de Putte, P. and Goosen, N. (1992). "DNA inversions in phages and bacteria." *Trends Genet* **8**(12): 457-462.
121. Van Duyne, G. D. (2001). "A structural view of cre-loxp site-specific recombination." *Annu Rev Biophys Biomol Struct* **30**: 87-104.
122. Wasserman, S. A. and Cozzarelli, N. R. (1985). "Determination of the stereostructure of the product of Tn3 resolvase by a general method." *Proc Natl Acad Sci U S A* **82**(4): 1079-1083.
123. Wasserman, S. A., Dungan, J. M. and Cozzarelli, N. R. (1985). "Discovery of a predicted DNA knot substantiates a model for site-specific recombination." *Science* **229**(4709): 171-174.
124. Weterings, E. and Chen, D. J. (2008). "The endless tale of non-homologous end-joining." *Cell Res* **18**(1): 114-124.
125. Wiggins, P. A., Dame, R. T., Noom, M. C. and Wuite, G. J. (2009). "Protein-mediated molecular bridging: a key mechanism in biopolymer organization." *Biophys J* **97**(7): 1997-2003.
126. Yang, W. and Steitz, T. A. (1995). "Crystal structure of the site-specific recombinase gamma delta resolvase complexed with a 34 bp cleavage site." *Cell* **82**(2): 193-207.
127. Zhang, Y., Buchholz, F., Muirers, J. P. and Stewart, A. F. (1998). "A new logic for DNA engineering using recombination in Escherichia coli." *Nat Genet* **20**(2): 123-128.